

GEOTECHNICAL, GEOLOGICAL AND EARTHQUAKE ENGINEERING

**GEOTECHNICS AND  
EARTHQUAKE GEOTECHNICS  
TOWARDS  
GLOBAL SUSTAINABILITY**

SUSUMU IAI  
EDITOR

 Springer

GEOTECHNICS AND EARTHQUAKE GEOTECHNICS  
TOWARDS GLOBAL SUSTAINABILITY

# GEOTECHNICAL, GEOLOGICAL AND EARTHQUAKE ENGINEERING

---

Volume 15

---

## *Series Editor*

Atila Ansal, *Kandilli Observatory and Earthquake Research Institute,  
Boğaziçi University, Istanbul, Turkey*

## *Editorial Advisory Board*

Julian Bommer, *Imperial College London, U.K.*

Jonathan D. Bray, *University of California, Berkeley, U.S.A.*

Kyriazis Pitilakis, *Aristotle University of Thessaloniki, Greece*

Susumu Yasuda, *Tokyo Denki University, Japan*

For further volumes:

<http://www.springer.com/series/6011>

# Geotechnics and Earthquake Geotechnics Towards Global Sustainability

*Edited by*

SUSUMU IAI

*Kyoto University, Kyoto, Japan*

Prologue by Michael J. Pender

 Springer

*Editor*  
Susumu Iai  
Disaster Prevention Research Institute  
Kyoto University  
Gokasho, Uji  
611-0011 Kyoto  
Japan  
iai@geotech.dpri.kyoto-u.ac.jp

ISSN 1573-6059

ISBN 978-94-007-0469-5

e-ISBN 978-94-007-0470-1

DOI 10.1007/978-94-007-0470-1

Springer Dordrecht Heidelberg London New York

Library of Congress Control Number: 2011922129

© Springer Science+Business Media B.V. 2011

No part of this work may be reproduced, stored in a retrieval system, or transmitted in any form or by any means, electronic, mechanical, photocopying, microfilming, recording or otherwise, without written permission from the Publisher, with the exception of any material supplied specifically for the purpose of being entered and executed on a computer system, for exclusive use by the purchaser of the work.

Printed on acid-free paper

Springer is part of Springer Science+Business Media ([www.springer.com](http://www.springer.com))

# Preface

Global sustainability is the greatest long term challenge of our time. The breadth of disciplines that need to work together and the long duration over which action must be coordinated is unprecedented in the history of engineering. In geotechnical engineering and earthquake geotechnics in particular, we are unused to the challenge of working with other disciplines to address such problems, which have been far removed from our daily practice to date.

This book is the result of a new initiative: it is intended to be an initial, bold step towards approaching this challenging subject from the discipline of geotechnical engineering and earthquake geotechnics through the contributions of thirteen world leading experts. A special seminar was held in Kyoto, Japan, hosted by the Kyoto Sustainability Initiative, from January 12–14, 2010, which brought a number of experts together to discuss the opportunities for geotechnical engineering and earthquake geotechnics as we face up to this global challenge. The seminar generated intensive and stimulating discussions on a wide range of topics from the purely technical to government policy. Following the seminar, each of the experts was invited to set down their thoughts, from which this book has been prepared.

Soil in one form or another covers most of the surface of the planet, and yet soil mechanics as such does not seem to be a big factor in global sustainability. The subjects covered by the international experts in this book include an overview of global sustainability, geotechnical challenges in counteracting natural hazards, the role of geotechnical engineering in creating a low carbon society, world heritage, lifelines in megacities, coastal protection, exploring non-gravity geotechnics, designing for sustainability and more. We hope that these contributions from the Kyoto Seminar 2010 will stimulate debate over the role of geotechnics in achieving a more sustainable future for the world.

The compilation and editing of this book coincided with the initial phase of activities of Technical Committee 303 (TC303) “Coastal and River Disaster Mitigation and Rehabilitation” (short name “Floods”), a new Technical Committee (TC) of the ISSMGE created for the period 2009–2013 under the wider theme of “Impact on Society”. TC303 continues the work of the former TC39 “Geotechnical Engineering for Coastal Disaster Mitigation and Rehabilitation”, which was focused on tsunami

risk following the 2004 Sumatra earthquake in Indonesia. The editing of this book reflects the activities of TC303.

In compiling the manuscripts, the assistance by Ms. Waka Yuyama, Kyoto University, is gratefully acknowledged.

Uji, Kyoto

Susumu Iai

# Prologue: Designing for Sustainability

## From the Big Picture to the Geotechnical Contribution

Michael J. Pender

### 1 Introduction

Many of the contributions to this volume make clear that sustainability is a broad concept embracing multiple distinct facets. In this prologue some of the wider aspects are discussed briefly, particularly in relation to earthquake geotechnical engineering. This is preceded with comments on the motivation for the drive towards sustainability both from an aesthetic viewpoint and a practical one.

### 2 Natural Beauty of Our World – One Motivation for Sustainable Development

A few days before travelling to Kyoto, one sunny summer afternoon at my home in Auckland, whilst I was preparing my presentation for the seminar, I looked out the window and saw a kingfisher (a small brightly coloured bird) perched on a stake that had been driven into the ground to support the tomatoes growing in our vegetable garden (Fig. 1). A few haiku-like lines popped into my mind. With a bit of polishing these became:

Kingfisher perched on garden stake,  
plumage iridescent in sunlight.  
Oh, the joys of summer!

This seriously infringes the haiku 17 syllable rule, but I hope it expresses the delight we all experience when, unawares, we are suddenly struck by some facet of the marvellous beauty of the world we inhabit. The mention of summer probably reflected my subconscious realisation that going to Kyoto, an invitation which I accepted with much delight, meant forgoing part of the peak summer holiday season in

---

M.J. Pender (✉)

Department of Civil and Environmental Engineering and Geotechnical Engineering,  
University of Auckland, Auckland 1142, New Zealand  
e-mail: m.pender@auckland.ac.nz



**Fig. 1** One sunny summer afternoon in the vegetable garden at my home in Auckland

New Zealand. Often in January my wife and I enjoy camping at a seaside location. This involves putting the bright lights of Auckland far behind us. On a clear moonless night I like to leave our tent at 2 or 3 am to gaze at the myriad stars overhead in the Milky Way. This awe inspiring view is not available to city dwellers, thus the few occasions a year that I can be so amazed are very memorable. Another enjoyable aspect of camping near the seaside is walking along the beach on the firm wet sand exposed at low tide, noting the dilatant response of the sand with every footfall, enjoying the crash of the breaking waves in the surf on one side, and wondering at the green forest-clad rolling hills on the other. After some days of these delights one returns to the city refreshed.

Many striking photographic images have come to define aspects of the twentieth century, some, of course, quite horrible. One that has rightly achieved iconic status is the view of the earth first obtained from within the lunar orbit during the Apollo programme of the 1960s. Ever since the time of Galileo people have gazed at the planets through telescopes and wondered about conditions there and the possibility of life existing in these distant worlds. But compared with the view of the earth from near space these planets look quite uninteresting. The great surprise was the realisation that our planet is very beautiful and yet seems to be so delicate (Fig. 2). At the time of the first moon landing Norman Cousins, a columnist in the *New York Saturday Review*, made an important observation:

What was most significant about the lunar voyage  
was not that men set foot on the moon,  
but that they set eye on the earth.

The beauty of this image must surely have been a formative influence in the ever strengthening realisation in the final 3 or 4 decades of the twentieth century that our

**Fig. 2** The earth as seen from within the lunar orbit



planet is finite and could be damaged irreparably by rapacious human exploitation. This is not to say that prior to the 1960s people had not realised that environmental matters were a vital concern. In the late nineteenth century John Muir championed the natural beauty of the Yosemite region of California; many students of English poetry have been captivated by Wordsworth's eighteenth century feeling for the beauty of nature expressed in his poem "Daffodils"; and about a century earlier than Wordsworth, Basho, during his wanderings around Japan, was able to capture in so few syllables the endless fascination of nature. Perhaps one could use the insights of these prescient individuals as a pointer to an innate human appreciation of the beauty of our world. Even so, the realisation that the resilience of our planet could not be taken for granted slowly dawned for large numbers of people only during the second half of the twentieth century. The image of earth from space has become a visual expression of this understanding.

Thus it is very clear that the major driver in our present concern about sustainability is the widely perceived worry about the ability of our planet to survive the demands placed on it by humanity. I think the first reason for our concern about the future of the earth is an aesthetic one: With our knowledge of the beauty of the earth, how could we be so negligent as not to commit ourselves to preservation? The second is a moral reason: Who are we to destroy what we have inherited or to pass on to future generations a seriously depleted planet? Finally, there is a practical reason: If we do not protect the earth there is a very real possibility that life on our planet will be snuffed out.

### **3 Sustainability**

As stated above sustainability is an all-embracing concept, and consequently it is often dismissed as being too vague. Although a universally accepted definition might be difficult to reach, the following are important components of sustainability. First, the earth's resources need to be used wisely and with particular attention to avoiding waste. Second, energy supply and use has become a critical question along with the accompanying threat of global warming. Third, sustainability must also encompass the idea of equitable sharing of the earth's resources. Clearly, there are issues of justice involved if some parts of the human population consume far more than their fair share of what our planet can produce whilst others are deprived.

### **4 Global Warming**

The question of energy production and global warming is currently very important. The big issue is whether or not there is a link between energy produced by burning fossil fuels and global warming. The sceptics say that the scientific evidence produced so far is not convincing. But it is undeniable that the amount of carbon dioxide being spewed into the atmosphere has been increasing at an accelerating rate since the beginnings of the Industrial Revolution. An aspect of engineering thinking is the making of decisions with imperfect or incomplete information, thus it requires judgement. Consequently an engineering approach to global warming is to admit that, although we may not have certain evidence at present, the risk of deferring action until definite evidence comes to hand is too great. This means that it is simply a matter of prudence to take action now to control the outputs that are thought to be contributing to global warming.

### **5 Transport Fuels**

Worldwide there is much interest in renewable energy sources. Wind, wave and solar generation of electricity are undergoing accelerated development. These and other approaches are thought to have considerable potential in leading to better ways of producing electricity for homes, offices and factories. Much interesting information about the energy question is given in MacKay (2009).

More problematic are transport fuels. Some think the electric car, recharged from mains electricity overnight, has potential to fulfil needs for short distance travel in cities and towns in a way that is much more satisfactory than the present use of fossil fuels. Challenges with longer distance travel remain. Even more challenging is the question of air travel. Air travel has about the same energy consumption per passenger kilometre as car travel (McKay, 2009), but the great distances people travel by air means that vast quantities of combustion products are released at locations where the atmosphere is easily damaged. At present it is not clear what alternative fuels are possible for this transport medium.

More than half the presenters at the seminar travelled considerable distances by air to reach Kyoto. We could be asked, given the electronic media available today, if this was justified. Coming from a remote part of the globe I wish to emphasise the importance of air travel. When young people of my parents' generation wanted to travel to Europe or North America from New Zealand they had to spend weeks onboard ship. Now I can complete the journey to Europe in not much more than a day. Travel to North America or Asia is accomplished in half a day or less. In my professional life I have enjoyed the privilege of participating in international meetings and visiting colleagues in most parts of the world. I am sure that this mobility contributes to the effectiveness of our profession, to the growth of knowledge, and to improvements in engineering practice. Even more it has developed an international community able to pool knowledge and insight; with the advantage that rapid implementation becomes possible. Perhaps even more important though, is the way air travel has made people from all corners of the globe aware that our shared humanity is much more significant than our differences. I think this has produced a remarkable sense of belonging to the human family, in this way one can even defend air travel as a means of tourist transport to say nothing of the contribution tourism makes to local economies around the globe.

## **6 Geotechnical Engineering – Big Contributions to Sustainability**

A perusal of the Table of Contents of this volume illustrates that many facets of the application of geotechnical understanding to sustainability issues are covered by the contributors. Clearly advancing understanding of earthquakes and other natural disasters is a fertile field for contributions by the geotechnical profession to sustainable development.

Yet there is more that could be done. Last year the University of Auckland had a visit from Martin Fisher, a Stanford PhD graduate in mechanical engineering, who had spent time in Kenya on a Fulbright scholarship. While in Kenya he realised that water for irrigation of crops was the great need. He developed a simple human-powered water pump that can draw well water from depth. This can be manufactured at modest cost and has transformed the lives of many families giving them economic independence (Fig. 3). The website of this group – [www.kickstart.org](http://www.kickstart.org) – tells the story. From water pumps they have moved onto other products. One of these is a human-powered press for the formation of building blocks from soil. With one bag of cement about 100 blocks can be produced in a day. This means that with simple equipment construction of dwellings is possible with local materials. However, with further geotechnical work it might even be possible to develop processes for making building blocks that require no cement, which will clearly be a contribution to sustainability given that the manufacture of cement requires a high energy input. This development would require understanding of the properties of soil, containing at least some clay, at very low water content. This is a potential joint research topic between a sophisticated geotechnical laboratory somewhere in the developed world with field workers in the developing world. About one third of the world population



**Fig. 3** Human-powered irrigation pump from *Kick Start*

live in houses constructed of mud bricks, or adobe, so the comments just made relate to what is already a well established process in many parts of the world. However, we know that dwellings constructed from unreinforced adobe and bricks perform extremely poorly in earthquakes. Examples are the Bam earthquake in Iran in 2003 and the earthquake in Peru in 2007 in which 80% of the housing in the town of Pisco was destroyed. We also know that the application of relatively simple engineering is able to greatly improve the performance of these structures. Building dwellings that can survive earthquakes must be high on the list of priorities that could contribute to a sustainable world. In many cases it appears that the barrier to the implementation of improved building practices is sociological rather than technical. Poverty levels are often such that people cannot afford the small additional cost of incorporating some reinforcing into their buildings or to construct roofing of lightweight materials. Here we have a challenge presented to the world community that has great bearing on sustainability but which is not a technical problem. We as geotechnical engineers can do our part, though, by endeavouring to influence decision makers in Governmental and non-Governmental organisations charged with improving the lot of those in relatively undeveloped parts of the world. A particular role we and our colleagues can fulfil is to quantify the improvements in sustainability that could be achieved from modest expenditure.

## **7 Recycling and Use of Natural Materials**

In discussing the Kyoto sustainability seminar with colleagues at the University of Auckland, I learnt of several initiatives to recycle materials or to use natural materials in new ways. Apparently water based paint has a composition not much different from the additives used in concrete making. One paint company in New

Zealand offers a disposal service for left-over paint and one of my colleagues is investigating the effectiveness of this as a concrete additive and the properties of the resulting paint-crete. Another similar project is based on the use of crushed glass as a substitute for sand in concrete, so producing glass-crete. Auckland is an area with an impending shortage of concrete aggregate so work is being done on the recovery of aggregate from demolition concrete. Other colleagues are looking at the use of natural fibres as concrete reinforcing and another is investigating the effect of reinforced adobe in shaking table tests. Finally, another group is investigating the performance of natural fibre as reinforcing for rammed earth construction, a technique that may provide an inexpensive means of improving the earthquake resistance of adobe construction and so offer a solution to the problem discussed above.

These applications are not geotechnical as such but they point to ways of improving the sustainability that will be utilised alongside geotechnical work. So I conclude this prologue by emphasising that although geotechnical insight can make an important contribution to world-wide sustainable development, as demonstrated by the contributions to this volume, the way forward requires the marshalling of insights from many different disciplines, engineering and otherwise, and these groups, in turn, working together with the wider community.

## Reference

MacKay DJC (2009) Sustainable energy – without the hot air. UIT Cambridge Ltd., Cambridge

# Contents

<b>1 Introduction</b> . . . . .	1
Susumu Iai	
<b>2 Seismic Hazards</b> . . . . .	21
W.D. Liam Finn	
<b>3 Lifelines in Megacities</b> . . . . .	37
Craig A. Davis and J.P. Bardet	
<b>4 Infrastructure</b> . . . . .	59
Kenichi Soga	
<b>5 Geotechnics and Society</b> . . . . .	75
R. Scott Steedman	
<b>6 World Heritage in Asia</b> . . . . .	89
Yoshinori Iwasaki	
<b>7 Coastal Protection</b> . . . . .	115
Jian Chu and Shuwang Yan	
<b>8 Combined Hazards</b> . . . . .	131
Masyhur Irsyam, H. Hendriyawan, M. Asrurifak, Hamzah Latif, Nazili Razali, and Anita Firmanti	
<b>9 Urban Microzonation</b> . . . . .	151
Atilla Ansal, Gökçe Tönük, and Aslı Kurtuluş	
<b>10 Slope Failure</b> . . . . .	169
Michele Maugeri and Ernesto Motta	
<b>11 Geo-Hazards</b> . . . . .	191
Wei F. Lee, Kenji Ishihara, and C.H. Chen	
<b>12 Exploring Non-gravity Geotechnics</b> . . . . .	215
Ikuo Towhata, Thi Lan Anh Trinh, and Suguru Yamada	

**13 Soil Mechanics** . . . . . 231  
Hideki Ohta, Atsushi Iizuka, and Shintaro Ohno

**Index** . . . . . 251

# Contributors

**Atilla Ansal** Kandilli Observatory and Earthquake Research Institute, Boğaziçi University, Istanbul 34684, Turkey, ansal@boun.edu.tr

**M. Asrurifak** Faculty of Civil and Environmental Engineering, Institut Teknologi Bandung, Bandung 40132, Indonesia, m\_asrurifak@yahoo.com

**J.P. Bardet** Department of Civil and Environmental Engineering, University of Southern California, Los Angeles, CA 90089-2531, USA; Center on Megacities, University of Southern California, Los Angeles, CA 90089-2531, USA, bardet@usc.edu

**C.H. Chen** National Taiwan University, Taipei, Taiwan, chchen2@ntu.edu.tw

**Jian Chu** School of Civil and Environmental Engineering, Nanyang Technological University, Singapore, Singapore 639798, cjchu@ntu.edu.sg

**Craig A. Davis** Geotechnical Engineering, Los Angeles Department of Water and Power, Los Angeles, CA 90012, USA, craig.davis@ladwp.com

**W.D. Liam Finn** Department of CE, University of British Columbia, Vancouver, BC, Canada V6T 1Z4, finn@civil.ubc.ca

**Anita Firmanti** Research Institute for Human Settlements, Indonesia Ministry of Public Works, Indonesia, anitafirmanti@yahoo.com

**H. Hendriyawan** Faculty of Civil and Environmental Engineering, Institut Teknologi Bandung, Bandung 40132, Indonesia, hendriyawan@ocean.itb.ac.id

**Susumu Iai** Disaster Prevention Research Institute, Kyoto University, Uji, Kyoto 611-0011, Japan; Kyoto Sustainability Initiative (KSI), Kyoto University, Uji, Kyoto 611-0011, Japan, iai@geotech.dpri.kyoto-u.ac.jp

**Atsushi Iizuka** Research Center of Urban Safety and Security, Kobe University, Nada-ku, Kobe 657-8501, Japan, iizuka@kobe-u.ac.jp

**Masyhur Irsyam** Faculty of Civil and Environmental Engineering, Institut Teknologi Bandung, Bandung 40132, Indonesia, masyhur.irsyam@yahoo.co.id

**Kenji Ishihara** Chuo University, Tokyo, Japan, kenji-ishihara@e-mail.jp

**Yoshinori Iwasaki** Cyber University, Fukuoka, Japan; Geo Research Institute, Osaka 550-0012, Japan, yoshi-iw@geor.or.jp

**Ash Kurtuluş** Kandilli Observatory and Earthquake Research Institute, Boğaziçi University, Istanbul 34684, Turkey, asli.kurtulus@boun.edu.tr

**Hamzah Latif** Center for Marine and Coastal Development, Institut Teknologi Bandung, Bandung 40132, Indonesia, hamzah@ppk.itb.ac.id

**Wei F. Lee** Facilities and Assets Management Center for Infrastructures, National Taiwan University of Science and Technology, Taipei, Taiwan, weilee@mail.ntust.edu.tw

**Michele Maugeri** Department of Civil and Environmental Engineering, University of Catania, 95125 Catania, Italy, mmaugeri@dica.unict.it

**Ernesto Motta** Department of Civil and Environmental Engineering, University of Catania, 95125 Catania, Italy

**Shintaro Ohno** Advanced Analysis Group, Engineering Development Department, Civil Engineering Design Division, Kajima Corporation, Minatoku, Tokyo 107-8502, Japan, onosi@kajima.com

**Hideki Ohta** Research and Development Initiative, Chuo University, Bunkyo, Tokyo 112-8551, Japan, ohta@tamacc.chuo-u.ac.jp

**Michael J. Pender** Department of Civil and Environmental Engineering and Geotechnical Engineering, University of Auckland, Auckland 1142, New Zealand, m.pender@auckland.ac.nz

**Nazili Razali** Research Group on Eco-Hydraulic, Engineering Center for Industry, Institut Teknologi Bandung, Bandung 40132, Indonesia, nazili70@yahoo.com

**Kenichi Soga** Department of Engineering, University of Cambridge, CB2 1PZ Cambridge, UK, ks207@cam.ac.uk

**R. Scott Steedman** Steedman & Associates Ltd., W8 7ST London, UK, contact@scottstedman.com

**Gökçe Tönük** Kandilli Observatory and Earthquake Research Institute, Boğaziçi University, Istanbul 34684, Turkey, gokce.tonuk@boun.edu.tr

**Ikuo Towhata** Department of Civil Engineering, University of Tokyo, Tokyo 113-8656, Japan, towhata@geot.t.u-tokyo.ac.jp

**Thi Lan Anh Trinh** Electricity of Vietnam, Dong Da District, Hanoi, Vietnam

**Suguru Yamada** Department of Civil Engineering, University of Tokyo,  
Tokyo 113-8656, Japan, suguru@geot.t.u-tokyo.ac.jp

**Shuwang Yan** Geotechnical Research Institute, Tianjin University, Tianjin,  
China, yanshuwang@tju.edu.cn

# Chapter 1

## Introduction

### Towards Global Sustainability

Susumu Iai

**Abstract** As an introduction of Geotechnics and Earthquake Geotechnics towards Global Sustainability, this chapter reviews the fundamentals of global sustainability, including the status of climate change and the concepts of growth limits, strong and weak sustainabilities, and an ecological footprint. Based on this review, a conceptual framework of global sustainability is proposed as follows. Because humanity's burden has already exceeded Earth's biological capacity, an increasing number of regional systems may face critical conditions. Thus, studying the vulnerability and robustness of social networks and ecosystems is crucial in establishing a strategy to achieve sustainable development. The risk assessment approach combining the uncertainties in fragility and hazards is readily applicable to form a reasonable strategy in the adaptation and the risk management to the global climate and environmental change. In conventional design, construction of a good geotechnical work was the sole objective of design. In the merging trends in design for sustainability, providing appropriate function and service rather than the construction of a solid structure becomes the final objective of design. A new challenge is combined hazards, such as the combination of earthquake motions and tsunamis observed during 2004 Sumatra, Indonesia earthquake. Thus, radically new approaches and technologies must be developed in the near future.

#### 1.1 Introduction

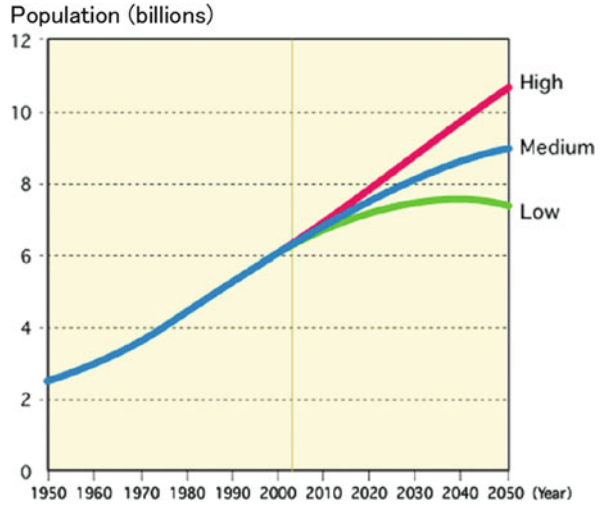
After the Earth was created 4.6 billion years ago, chemical reactions produced organic molecules. These molecules led to a crude form of a life. Four million years ago, human beings evolved, and their population grew to 5 million due to

---

S. Iai (✉)

Disaster Prevention Research Institute, Kyoto University, Uji, Kyoto 611-0011, Japan;  
Kyoto Sustainability Initiative (KSI), Kyoto University, Uji, Kyoto 611-0011, Japan  
e-mail: iai@geotech.dpri.kyoto-u.ac.jp

**Fig. 1.1** World population projections, 1950–2050 (United\_Nations, 2003)



the innovation of stone implements. The development of agriculture expanded this population to 500 million. During the ensuing 10,000 years, which was a period of little technological innovation, the population remained stable. Then the industrial revolution about 200 years ago triggered a population explosion, and the population reached 6 billion. In 50 years the population will reach 10 billion due to the technological revolution of the twentieth century (Fig. 1.1). This growth has consequently created an excessive burden on Earth’s limited resources, which poses threats to human sustainability. The future of the Earth and humans depends on mankind’s approach to solve these problems.

The objective of this chapter is to review the fundamentals of sustainability science as well as to provide a basic conceptual framework for the various approaches of geotechnics and earthquake geotechnics towards global sustainability. Although limited and minimal, this review includes sufficient materials to suggest specific approaches required for sustainability science.

## 1.2 Sustainable Development

The term sustainable development was defined by the Brudtland Commission of the United Nations (World Commission on Environment and Development, 1987) as “development that meets the needs of the present without compromising the ability of future generations to meet their own needs.” This is the most quoted definition in the literature. The underlying notion behind this definition is the awareness that our planet has limited resources, and consequently unlimited development is impossible. A few decades ago, the Club of Rome commissioned an MIT research team to run a series of computer simulations on human growth for our planet. This culminated in the publication of “The Limits to Growth”, which raised key questions about

the sustainability of modern society. The primary findings are as follows (Meadows et al., 1972):

- (1) If the present growth trends in the world population, industrialization, pollution, food production, and resource depletion continue unchanged, the limits of growth on this planet will be reached within the next 100 years. The most probable result will be a rather sudden and uncontrollable decline in both population and industrial capacity.
- (2) These growth trends can be altered. Ecological and economic conditions, which are stable and sustainable, are possible. The state of global equilibrium can be designed so that the basic material needs of each person on Earth are satisfied, and each person has an equal opportunity to realize his or her individual human potential.
- (3) If humanity decides to strive for this second outcome, the sooner this becomes a priority, the greater the chance of success.

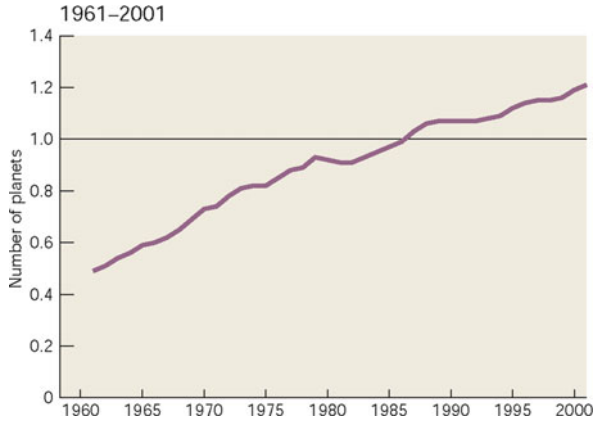
The most significant implication among these findings is even before reaching the physical limits of Earth's resources, society will suddenly and uncontrollably change. Thus, a core aspect of sustainability is to protect natural capital, including the ability of Earth to renew or regenerate itself. Strong (narrow) sustainability will maintain natural capital independent of human-made forms of capital. In contrast to focusing on maintaining natural capital, weak (broad) sustainability aims at preserving the value of all combined assets, including substitutes for lost ecological services produced by technology (Pearce et al., 1989).

Whether society pursues weak or strong sustainability, both paths need metrics to monitor various forms of capital. Thus, the concept of an Ecological Footprint has received much attention in both academic and political societies. An ecological footprint is a measure of the global ecosystem's capacity to reproduce natural (biomass) resources and to provide waste absorbing functions (Wackernagel et al., 2005). The ecological footprint is calculated based on the following seven areas using equivalence factors, whose 2001 values are denoted in parentheses (global hectares/ha):

- (1) Cropland (overall = 2.1; primary = 2.2; marginal = 1.8)
- (2) Pasture (= 0.5)
- (3) Forest (= 1.4)
- (4) Fisheries (= 0.4)
- (5) Built-up area (= 2.2) (A built-up area is assumed to be located mostly on prime agricultural land; hence, a built-up area has the same equivalence factor as primary cropland.)
- (6) Hydropower area (= 1.0)
- (7) Fossil fuels (forest) (= 1.4)

Figure 1.2 shows the ecological footprint calculated for our planet from 1961 to 2001 (WWF, 2004). In 2001, the human burden on the global ecosystem was 2.5 times of that in 1961, and exceeded the Earth's biological capacity by 20%.

**Fig. 1.2** Ecological footprint, 1961–2001 (WWF, 2004)



Although this dramatic increase does not imply an imminent collapse of our planet’s sustainability, it does send an alarming signal related to our ability to achieve sustainable development.

Figure 1.3 shows the global temperature change predicted by IPCC. Even if the CO<sub>2</sub> emission is reduced to certain target levels in 50 years using appropriate mechanisms, such as the Kyoto Protocol, the CO<sub>2</sub> concentrations and related temperature

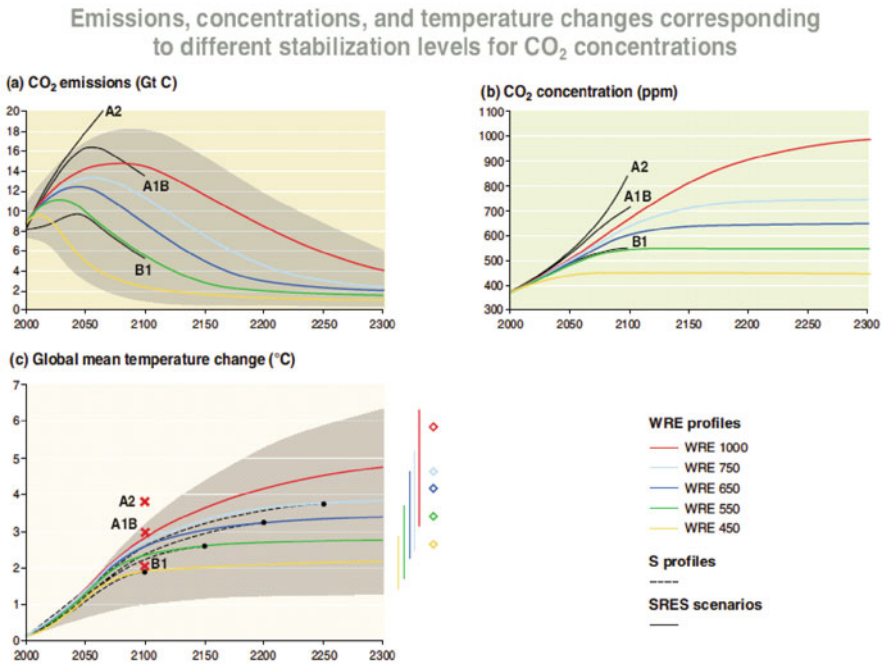


**Fig. 1.3** CO<sub>2</sub> emissions and global temperature change (IPCC, 2001)

increases will continue for more than 100 years. More alarming is the sea level rise due to ice melting, which will continue over several millennia (IPCC, 2001).

### 1.3 From Global Sustainability to Regional Development

The current status of global sustainability reviewed in the previous section is the global average. The underlying mechanisms of these trends are functions of regional activities. For example, the ecological footprint is not uniformly distributed and varies drastically by region (Fig. 1.4). However, this type of map does not indicate the dynamics. Enormous amounts of natural resources are being transferred around our planet through imports and exports. As an example, Fig. 1.5 shows the exports from China in 2001. With rapid economic development in Asia, these flows of biocapacity will drastically change in the near future.

An awareness of these dynamics on the global scale is necessary to study regional sustainable development because regional systems are not closed. The impacts of inputs and outputs from regional systems may be significant for regional sustainability. Thus, trends and changes in the dynamics on the global scale may be closely related to regional sustainability. Ultimately, a study on the interaction between global and regional systems may be required. However, if carefully applied, geoinformatics can be a powerful tool for uncovering the relationships between these systems.

With the aid of satellite and other remote sensing techniques, data is available from various sources on a global scale. For example, Fig. 1.6 depicts natural resources in an animation format from NASA. Moreover, human statistics are available from the United Nations. A general global view of the Earth is available through free software such as Google Earth. With the aid of the Internet, considerable amounts of information on sustainability on the global scale are available.

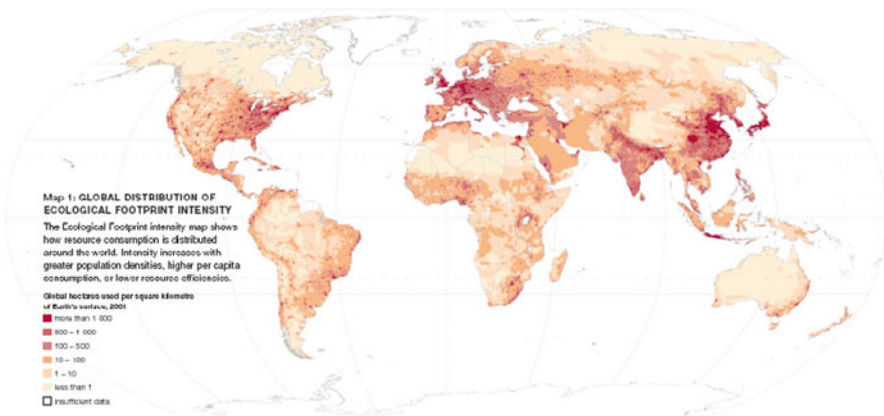


Fig. 1.4 Distribution of ecological footprint (WWF, 2005)

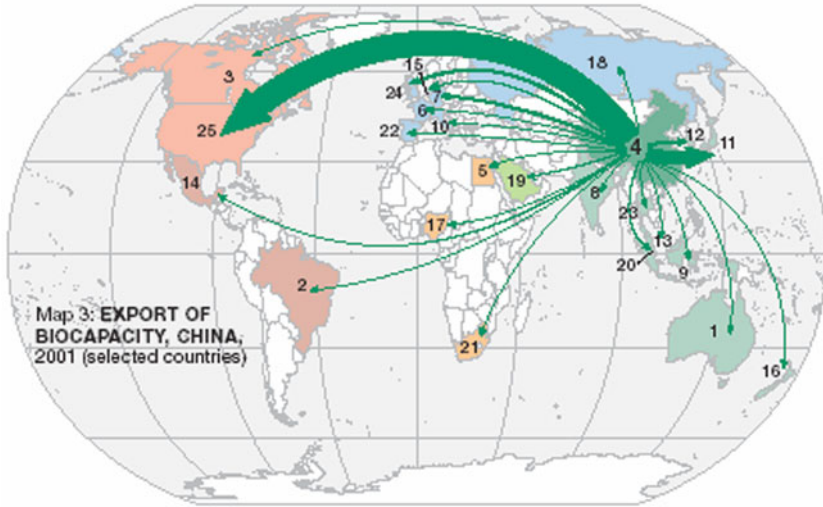


Fig. 1.5 Export of biocapacity, China (WWF, 2005)

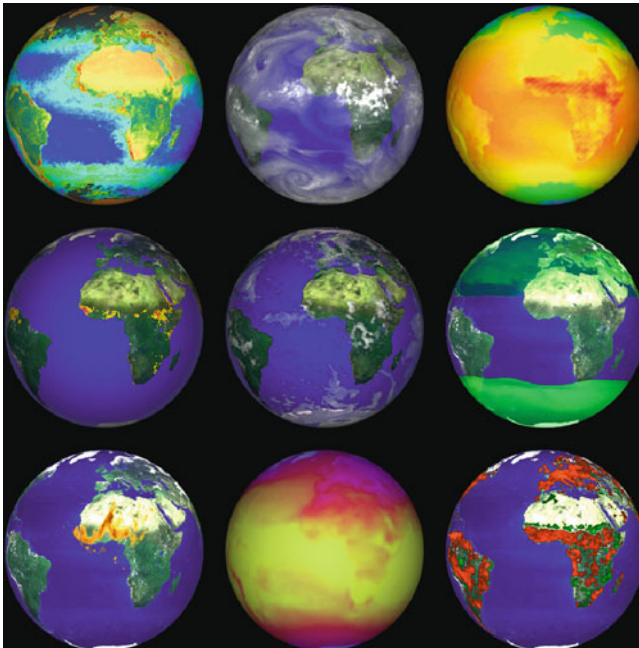


Fig. 1.6 (left to right, top to bottom) Biosphere, water vapor, temperature, fires, clouds, methane, aerosols, radiant energy, vegetation index anomalies (NASA/Goddard Space Flight Center, The SeaWiFS Project and ORBIMAGE, Scientific Visualization Studio)

These useful data sources have recently become available and are intended to be shared. At least in the initial phase, readily available data on the global scale can be useful to determine the general direction of a sustainability study.

## 1.4 Identifying Dynamics

Due to recent industrialization and economic growth, Asia will soon face huge increases in energy demands, especially for petroleum and natural gas. Infrastructure such as lifeline facilities will be rapidly constructed to accommodate these demands, and these rapid changes in social and urban systems will pose a threat to natural environments surrounding urban areas as well as the global environment. As a whole, social and urban systems will face a critical phase of vulnerability against external impacts such as natural disasters.

Indices such as temperature changes used to discuss global sustainability (Fig. 1.3) include both spatially and temporally averaged data. In addition to excluding annual, monthly, or daily variations, this data does not show anomalies or extreme highs or lows. Furthermore, extreme climatic events such as storms, typhoons, and high tides are missing. Thus, to achieve sustainability in a system currently progressing through a critical stage, a systematic response and vulnerability assessment to extreme events should be studied because such extremes often trigger threshold responses (i.e. natural disasters).

Identifying event sequences often leads to a reasonable understanding of the dynamics of social and natural systems. For example, a negative spiraling sequence of events can be recognized in natural disasters and poverty in society due to rapid industrialization and urbanization. Population growth in rural areas will push people to areas, which have yet to be cultivated and are vulnerable to natural disasters. Disasters and the ensuing poverty will force people to even more isolated and vulnerable areas. This rapid industrial growth requires cheap labor; thus, pushing younger generations towards urban areas. Then the population declines in rural areas as only older generations remain.

A positive spiral of events is also possible. For example, poverty in rural areas has been a major social problem in Brazil. Since new technology to efficiently produce ethanol from sugar cane has been developed and implemented, people in these areas are finding new jobs related to ethanol production. The produced ethanol is then put into use as part of the biomass energy, offsetting the human burden on the environment in these areas.

The above discussions can be summarized as follows. Differentiating positive and negative sequences may lead to a strategy to achieve a sustainable society. Identifying the dynamics of the concentration and dispersion of social systems and natural resources is essential for establishing harmonic societies. Moreover, elucidating the relationships between social systems and technological strategies is important. As humanity's burden has already exceeded Earth's biological capacity, an increasing number of regional systems may face critical conditions. Studying the

vulnerability and robustness of social networks and ecosystems will aid in realizing a sustainable development strategy.

## 1.5 Dealing with Uncertainty

When evaluating uncertainty in the geotechnical structures for seismic hazard evaluation, the uncertainties in the fragility of a system and the hazard level the system is exposed are formally treated as follows. In this assessment, “failure” is defined by the state that does not satisfy the prescribed limit states typically defined by an acceptable displacement, deformation, or stress. If a peak ground motion input to the bottom boundary of soil structure systems is used as a primary index of earthquake ground motions, probability of failure  $F_F(a)$  at peak ground motion  $a$  is computed considering uncertainty in geotechnical and structural conditions. A curve described by a function  $F_F(a)$  is called a fragility curve (Fig. 1.7a). Probability of occurrence of earthquake ground motions is typically defined by a slope (or differentiation) of a function  $F_H(a)$  that gives annual probability of exceedance of a peak ground acceleration  $a$ . A curve described by a function  $F_H(a)$  is called a seismic hazard curve (Fig. 1.7b).

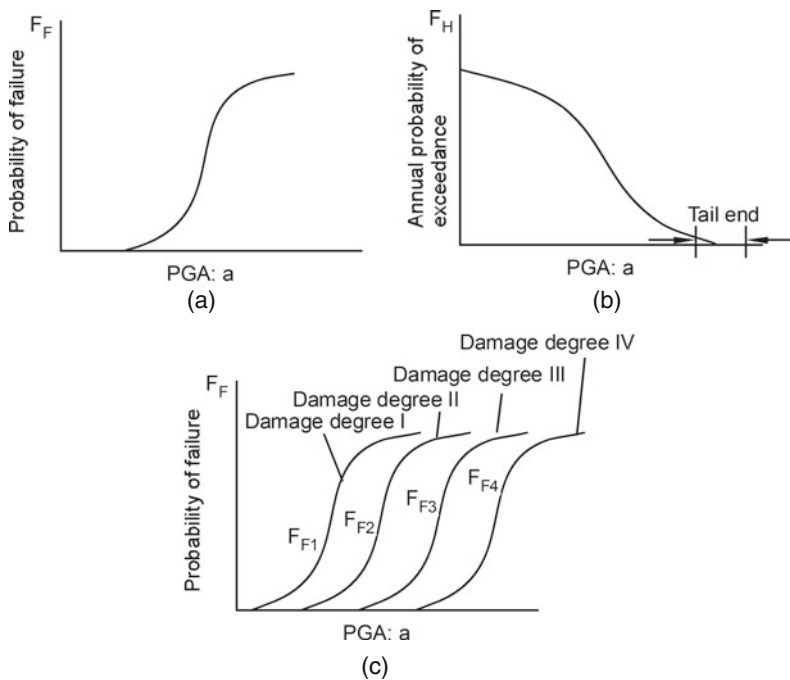


**Fig. 1.7** Schematic figures of a fragility curve (a), a seismic hazard curve (b), and a group of fragility curves for multiple limit states (c)

Given the fragility and seismic hazard curves for a geotechnical structure, annual probability of failure of the structure  $P_1$  is computed as follows:

$$P_1 = \int_0^{\infty} \left( -\frac{dF_H(a)}{da} \right) F_{Fi}(a) da \quad (1)$$

If a design working life is  $T$  years, probability of failure of the structure over the design working life is given by

$$P_T = 1 - (1 - P_1)^T \quad (2)$$

If loss due to earthquake induced damage associated with the prescribed limit state is designated by  $c_D$ , expected loss over the design working life of a structures  $C_D$  is given by

$$C_D = P_T c_D \quad (3)$$

Thus, the life-cycle cost  $C_{LC}$  is given by adding initial construction cost  $C_I$ , maintenance cost  $C_M$  and demolishing cost  $C_{END}$  as

$$C_{LC} = C_I + C_D + C_M + C_{END} \quad (4)$$

This is generalized further by introducing more than one serviceability limit state. Given the fragility curve defined for the  $i$  th limit state as  $F_{Fi}(a)$  (Fig. 1.7c), Eqs. (1) through (4) are generalized as follows:

$$P_{1i} = \int_0^{\infty} \left( -\frac{dF_H(a)}{da} \right) F_{Fi}(a) da \quad (5)$$

$$P_{Ti} = 1 - (1 - P_{1i})^T \quad (6)$$

$$C_{Di} = P_{Ti} c_{Di} \quad (7)$$

$$C_{LC} = C_I + \sum_i C_{Di} + C_M + C_{END} \quad (8)$$

As demonstrated for liquefaction hazard evaluation by Kramer et al. (2006), the probability evaluated by Eqs. (1) and (2) is a consistent index of hazard and the conventional approach based on the return period prescribed in design provisions and codes can be either too conservative or unconservative depending on the site. Expected loss evaluated by Eq. (3) is an index that reflects the consequence of failure. Life-cycle cost evaluated by Eq. (4) is an index that properly reflects the trade-off between initial cost and expected loss. The design option that gives the minimum life-cycle cost is the optimum in terms of overall economy as shown in

**Fig. 1.8** Principle of minimum life-cycle cost

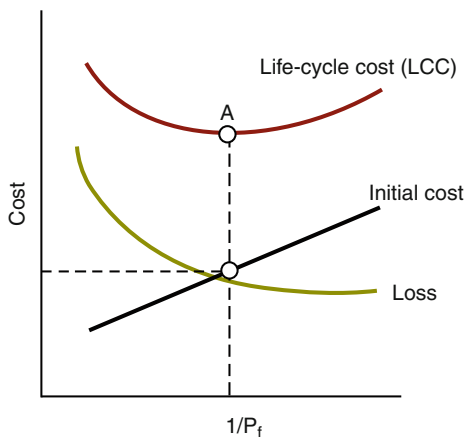
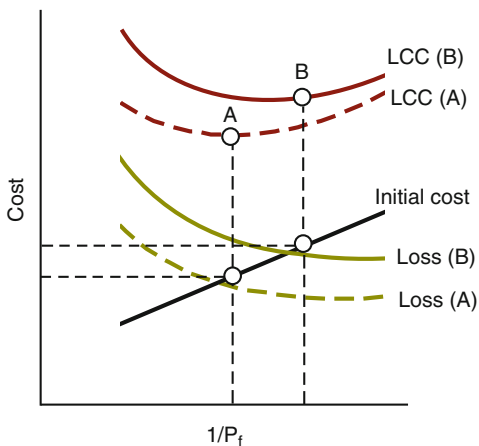


Fig. 1.8. Thus, the optimum design has a certain probability of failure given by Eq. (2).

This probability is not prescribed by an authority (such as 10% over 50 years) but rather determined as a result of the minimum life-cycle cost procedure. The probability of failure can be large if a consequence of failure in meeting the performance criteria, as measured by seismic loss  $c_D$ , is minor. The probability can be small, however, if a consequence of failure, as measured by  $c_D$ , is significant as shown in Fig. 1.9. Thus, the minimum life-cycle cost procedure reflects the possible consequences of failure.



**Fig. 1.9** Effect of the consequence of failure on the minimum life-cycle cost

## 1.6 Adaptation to Global Climate Change

The risk assessment approach for seismic hazard mitigation reviewed in the previous section is readily applicable to form a reasonable strategy in the adaptation to the global climate change. The first step to achieve this application is to generalize the concepts of the urban structures facing the seismic risk in terms of a generalized system subject to an input that poses a certain risk as shown in Fig. 1.10.

In the adaptation to global climate change, the input to the system can be an event in weather, including extremely hot and extremely cold events. The system can be a natural environment or a regional human society. Just like in the risk assessment for seismic hazard mitigation, the input to the system has uncertainty as represented by the hazard curve, posing a risk to the system. The system also has uncertainty as represented by the fragility curve. To evaluate the total risk to the system following the methodology of life-cycle cost approach reviewed in the previous section forms the basis for establishing a best strategy in adaptation to the global climate change.

As shown earlier in Fig. 1.9, the strategy with larger initial cost (investment) will decrease the risks and consequently the expected loss due to the global climate change. The best strategy is chosen where the life-cycle cost becomes the minimum. As shown in Fig. 1.9, if the consequence of the failure is significant, then the strategy with larger initial cost (investment) becomes the best strategy.

When the global climate change is discussed, it is commonly explained in terms of global average of temperature and similar indexes as shown in Fig. 1.11. This type of results does not show extremely hot weather, heavy rain, drought, cold weather, cold summer, storm, typhoon, high tide, all of which are the key factors that governs the critical threshold limit of the system facing the global climate change.

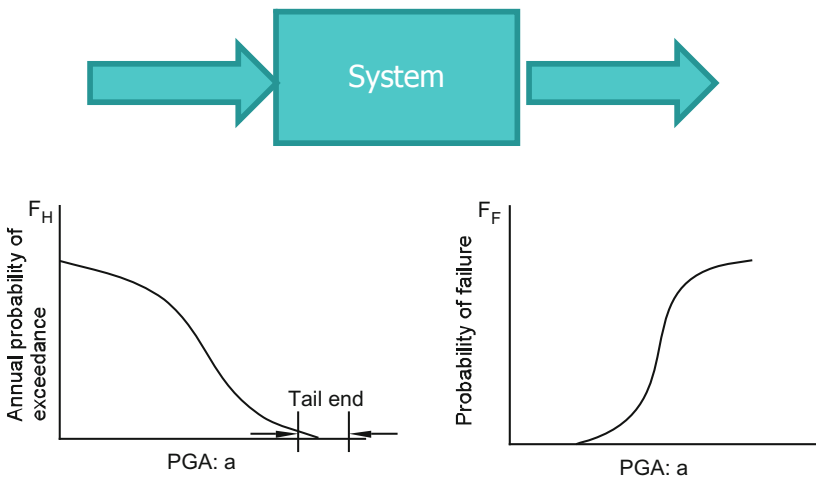


**Fig. 1.10** Hazard and fragility associated with uncertainties in input and response of an idealized system for adaptation to global climate change

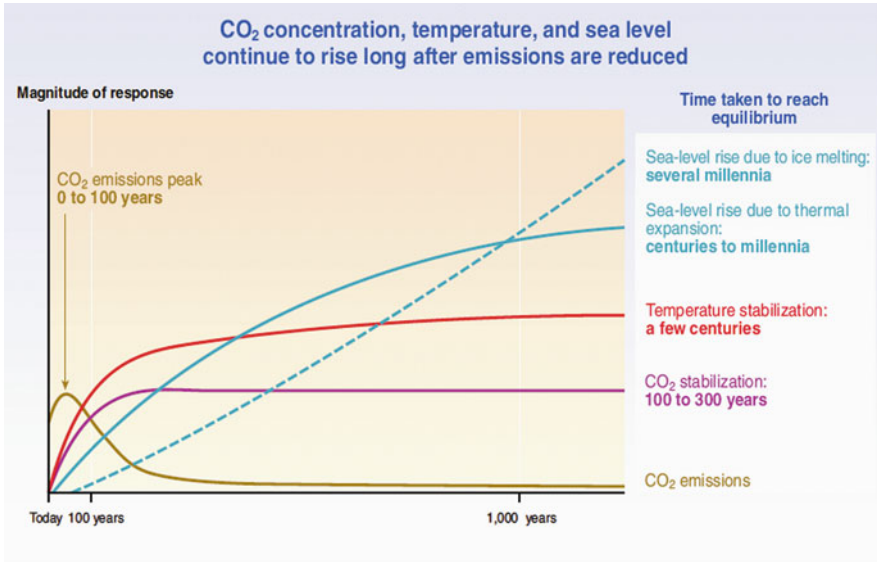


**Fig. 1.11** Average temperature rise and other indexes associated with the global climate change (IPCC, 2001)

Uncertainties associated with the average climate change can be explained through Fig. 1.12. When the average temperature rises associated with the global climate change, extreme hot days increases and cold days decreases as shown in the left in Fig. 1.12. This is the pattern of the change of the events most of the people implicitly expect when they hear the term global warming. Actually, this can be wrong. Even if there is no change in the average, there is a case that the variation becomes larger as shown in the middle in Fig. 1.12. In this case, the extreme hot days as well as extreme cold days increase. Both the average as well as variation can increase as shown in the right in Fig. 1.12. In this case, extreme hot days increases

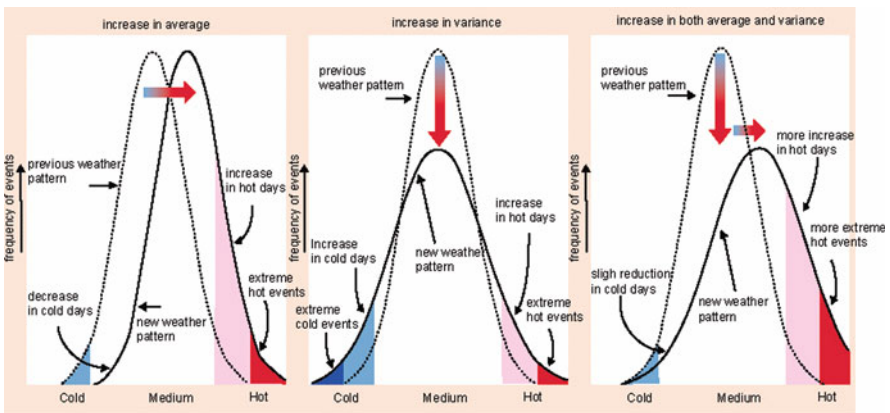


**Fig. 1.12** Uncertainties in the weather associated with the global climate change

but the extreme cold days can also persistent. Unexpected heavy snow falls despite the average temperature rise can be categorized in this patten. Although there is not a definite consensus formed among the experts on which patten of the three should be expected in future, the importance of differentiating these patterns with respect to the variation may be understood from these figures.

Once these uncertainties associated with the input to the system are idealized in terms of a hazard curve, then the best strategy of adaptation can be established based on the minimum life-cycle cost principle described earlier.

Adaptation is associated with the case when the rate of change is relatively slow. Disaster mitigation may be required when the rate of change is too fast to adapt or when the people are too slow to act for the global climate change.

## **1.7 Emerging Trends in Design**

Emerging trends in design may be summarized as follows.

### ***1.7.1 From Design-for-Construction to Design-for-Performance***

The concept of operational damage introduced in the performance based design plays a significant role in emerging trends in design. In conventional design, construction of a good geotechnical work was the sole objective of design. In the emerging trends in design, providing appropriate function and service rather than a physical construction becomes the final objective of design. There is an important paradigm shift from structure-oriented to performance-oriented approach.

### ***1.7.2 From Standardized-Design to Site-Specific-Design***

Conventional design relied on the standardized earthquake loads such as those specified by design spectra and seismic coefficient. If needed, variability of these loads was considered in a framework such as reliability design methodology but the loads were standardized. In the merging trends in design, site-specific earthquake motions are used for achieving the optimum design best suited for the construction site.

### ***1.7.3 From Analysis-of-Structural/Foundation Parts to Analysis-of-Soil-Structure-System***

Conventional design was based on the analysis of structural or soil part idealized to fit to the simplified methodologies. In the emerging trends in design, analysis of whole soil-structure system and identification of failure modes are the bases.

In fact, these emerging trends in design are incorporated in the International Standard (ISO) on seismic actions for designing geotechnical works (Iai, 2005).

## 1.8 Applications to Sustainable Civil Construction

The discussions on these emerging trends in design can be extended further to the applications to sustainable civil construction. By expanding the concept of performance-oriented approach, a new horizon of design will become apparent. In stead of trying to reduce the cost for construction, the new objective of design will be to increase the service produced by the designing process. In stead of constructing buildings and producing things based on the concept of production efficiency through mass production process and ending up producing unnecessary products and infrastructures, the new objective of design will be to offer performance and service required by the society and human.

The concept of offering performance and service further triggers us to have a new look at civil engineering structures. In stead of trying to optimize individual structures for construction, we can define a system consisting of a group of structures and try to optimize it. The structural system can be as large as an entire urban system. In this case, we can look at this system as built environment rather than social infrastructure. Once we establish the function and objective of the built environment, then we can further expand our design approach for natural environment and the interaction between the built and natural environments. In stead of using conventional materials such as steel and concrete, new materials and intelligent technologies may offer a completely new performance and service. In stead of trying to maintain the old infrastructure based on life-cycle management, we can renovate and redevelop those infrastructures to achieve required and enhanced performance and service. Based on these merging trends, objective of the seismic design may be transformed into the new objective to create a space of safety and security in the decade to come.

The approaches and new concepts in design discussed above will be useful for designing new and large geotechnical works that have to meet the rapidly growing social and economic demands in Asia.

## 1.9 New Challenge: Combined Hazards

State-of-the-art geotechnical earthquake engineering is typically based on site-by-site detailed analysis. However, directly applying cutting-edge earthquake engineering is difficult for a long coastal protection line. Thus, a new methodology should be developed; an example, which has been developed via the collective efforts of the author and their associates, has been adopted for coastal areas in Japan and is briefly reviewed below.

The seismic performance of geotechnical structures, which extend over 70 km of coastline along the Osaka Bay area, is evaluated (Fig. 1.13). The northern part of

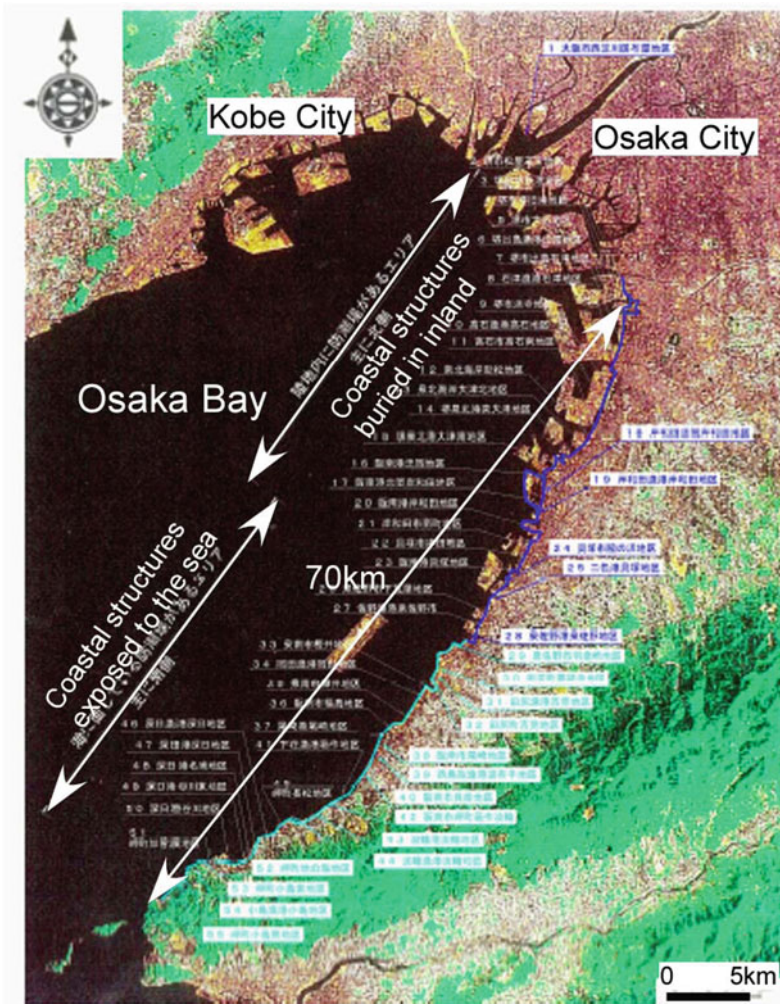


Fig. 1.13 Investigated coastal protection line for Osaka Bay Area, Japan

the coastal protection line is slightly inland from the sea, whereas the southern part of the coastal protection line is directly exposed to the sea. Geotechnical conditions along the coastal protection line were compiled based on boring data, which was originally obtained at 100–500 m intervals for the construction of the Hanshin Bay Area Highway.

The primary objective of this assessment was to avoid combined hazards such as those that occurred during the 2004 Sumatra, Indonesia, earthquake (Fig. 1.14). The performance grades of the coastal structures reflect the consequences of failure and were based on importance categorized by land use and the elevation of



**Fig. 1.14** Coastal area of Banda Aceh, Indonesia, before (*above*) and after (*below*) the Indian Ocean-Sumatra earthquake of 2004 (after Quickbird)

the ground relative to the sea level. Highly industrialized zones with low ground water level are assigned the highest performance requirements for protection of the coastal zone.

Instead of performing effective stress analysis on a site-by-site basis, a set of design charts has been developed based on a comprehensive set of parametric studies on embankments and gravity structures, which are idealized in Fig. 1.15. The design charts are incorporated into a spreadsheet format. Required input

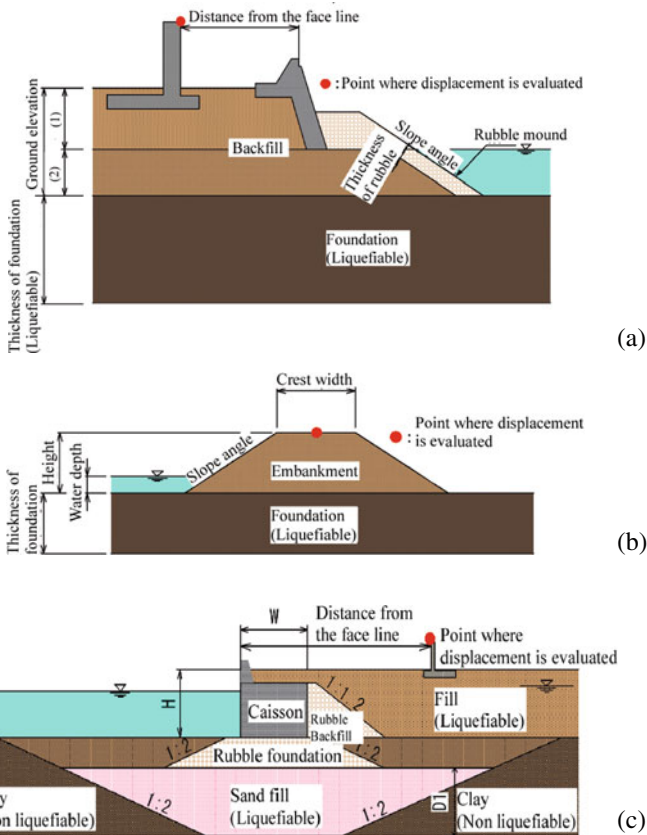


**Fig. 1.15** Cross sections and primary parameters used for the simplified design charts stress analysis. (a) Leaning bulkhead; (b) embankment type; (c) gravity type

data are (1) the basic parameters defining the cross section of the structures, (2) geotechnical conditions as represented by the SPT N-values, and (3) earthquake data represented by the wave form, peak ground acceleration, or distance and magnitude from the seismic source. These design charts can conveniently and efficiently assess the vulnerability of coastal geotechnical structures that extend a long distance such as tens of kilometers over variable geotechnical and structural conditions.

Figure 1.16 shows the results of the seismic assessment of the coastal protection line in the Osaka Bay Area. The settlements of the coastal protection facilities due to earthquake shaking ranged from 0.2 to 1.2 m (Fig. 1.16a), and areas with smaller margin to the acceptable level of settlements are not robust. Figure 1.16c denotes areas less likely to protect the land from a tsunami and must be strengthened or improved in preparation.

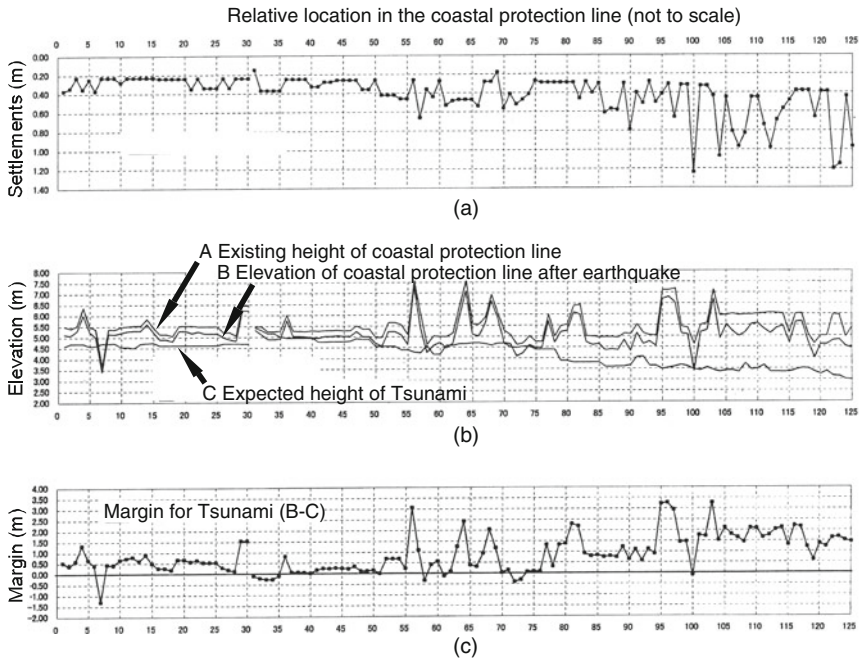


**Fig. 1.16** Results of the seismic assessment of coastal protection line. (a) Settlements of coastal structures; (b) elevations of coastal protection line before and after earthquakes and expected height of tsunami; (c) margin for tsunami

## 1.10 Conclusions

Herein the fundamentals of global sustainability, including the concepts of growth limits, strong and weak sustainabilities, the index called an ecological footprint, and the status of climate change, are reviewed. The following conclusions may serve as a conceptual framework of “the big picture” to discuss global sustainability from geotechnics and earthquake geotechnics towards the big picture:

1. Differentiating positive and negative sequences could lead to a strategy to achieve a sustainable society. Because humanity’s burden has already exceeded Earth’s biological capacity, an increasing number of regional systems may face critical conditions, especially in vulnerable areas with rapid growth and social change. Thus, studying the vulnerability and robustness of social networks and ecosystems is important to find a strategy for sustainable development. Regional systems are not closed. The impacts of inputs and outputs from regional systems may be related to regional sustainability. Moreover, the dynamics on the global scale may be closely related to regional sustainability.
2. The risk assessment approach for seismic hazard mitigation is readily applicable to form a reasonable strategy in the adaptation to the global climate change. The first step to achieve this application is to generalize the concepts of the urban structures facing the seismic risk in terms of a generalized system subject to

an input that poses a certain risk. In the adaptation to global climate change, the input to the system can be an event in weather, including extremely hot and extremely cold events. The system can be a natural environment or a regional human society. Just like in the risk assessment for seismic hazard mitigation, the input to the system has uncertainty as represented by the hazard curve, posing a risk to the system. The system also has uncertainty as represented by the fragility curve. To evaluate the total risk to the system following the methodology of life-cycle cost approach forms the basis for establishing a best strategy in adaptation to the global climate change.

3. In conventional design, construction of a good geotechnical work was the sole objective of design. In the emerging trends in design, providing appropriate function and service rather than a physical construction becomes the final objective of design. There is an important paradigm shift from structure-oriented to performance-oriented approach. By expanding the concept of performance-oriented approach, a new horizon of design will become apparent. In stead of trying to reduce the cost for construction, the new objective of design will be to increase the service produced by the designing process. In stead of constructing buildings and producing things based on the concept of production efficiency through mass production process and ending up producing unnecessary products and infrastructures, the new objective of design will be to offer performance and service required by the society and human.
4. A new challenge is combined hazards, such as the combination of earthquake motions and tsunamis observed during 2004 Sumatra, Indonesia earthquake. Thus, radically new approaches and technologies must be developed in the near future.

## References

- Iai S (2005) International Standard (ISO) on seismic actions for designing geotechnical works – an overview. *Soil Dynamics Earthquake Eng* 25:605–615
- IPCC (2001) IPCC third assessment report – Climate change 2001. <http://www.ipcc.ch/>
- Kramer SL, Mayfield RT, Anderson DG (2006) Performance-based liquefaction hazard evaluation: implications for codes and standards. Proceedings of the 8th U.S. National conference on earthquake engineering, San Francisco, Paper No. 888
- Meadows DH, Meadows LM, Randers J, Behrens WW III (1972) *The limits to growth*. Universe Books, New York, NY
- Pearce D, Markandya A, Barbier E (1989) *Blueprint for a green economy*. Earthscan Publications Ltd, London
- United\_Nations (2003) *World population prospects: the 2002 revision*. United Nations, New York, NY
- Wackernagel M, Monfreda C, Moran D, Wermer P, Goldfinger S, Deumling D, Murray M (2005) National footprint and biocapacity accounts 2005: the underlying calculation method. Global Footprint Network, Oakland, CA. <http://www.footprintnetwork.org/en/index.php/GFN/>
- World Commission on Environment and Development (1987) *Our common future*. Oxford University Press, Oxford
- WWF (2004) *Living planet report 2004*. WWF International, Gland, Switzerland
- WWF (2005) *Ecological footprint and natural wealth Asia-Pacific 2005*. Living planet. <http://wwf.panda.org/>

# Chapter 2

## Seismic Hazards

### Mitigating Seismic Threats to Sustainability

W.D. Liam Finn

**Abstract** Sustainability is a vague all-encompassing concept that increasingly influences industrial and social actions and is a controlling element in many major engineering projects. This chapter focuses on the mitigation of threats to sustainability by earthquakes. There are two components to mitigation; providing structures by appropriate resistance to earthquake shaking and minimization of deaths and suffering by cost effective emergency response. Both aspects of mitigation will be illustrated by recent innovative engineering developments in the context of major projects; retrofit of 800 schools within a 15 year period, and the development and application of a real time post-earthquake decision model for dealing with national emergencies. This model is currently being employed to evaluate various threats from a natural disaster to a terrorist act during the 2010 Olympic Winter Games in Vancouver.

#### 2.1 Introduction

Sustainability is an all-encompassing concept that increasingly influences industrial and social actions and is a controlling element in many major engineering projects. Stephen Toope, President of the University of British Columbia, in a recent article gave a lucid and illuminating description of the concept. “Sustainability has become one of our society’s most compelling- if somewhat imprecise – ideas. From climate change and resource management to social equality and cultural diversity, this concept drives us to examine how we can live in harmony with the world around us, and insists that we make choices that will have a positive impact on generations to come. As individuals, each of us has an opportunity and a responsibility to apply the filter of sustainability to our activities.”

---

W.D.L. Finn (✉)

Department of CE, University of British Columbia, Vancouver, BC, Canada V6T 1Z4  
e-mail: finn@civil.ubc.ca

Natural disasters pose major threats to the sustainability of existing life style and the progress to better conditions for all in a region affected by a natural disaster. This was clearly illustrated by the consequences of Hurricane Katrina in the USA, the 1995 Kobe earthquake in Japan and the 2010 Haiti earthquake. Mitigating a seismic threat has two significant components; reducing damage to the physical systems of society such as buildings and infrastructure and effective, post-earthquake emergency response. Effective emergency response is crucial in saving lives and speeding recovery as has been clearly demonstrated in the aftermath of the January 2010 earthquake in Haiti. Truly effective emergency response requires adequate assets, both trained responders and necessary equipment, but another equally important factor is the effective deployment of those assets in action. Effective deployment of assets in emergency response requires real time simulation of the changing post-earthquake situation.

Damage to the physical system can be mitigated by retrofitting the system to resist a reasonable earthquake threat. However retrofits are very expensive, especially when they are conducted in accordance with current building code regulations developed for new buildings (CCBFC, 2005). Therefore much research is being conducted to develop cost effective retrofit strategies to make retrofitting a more sustainable option.

In this chapter, the development of innovative cost effective retrofit strategies will be illustrated by examining the way that the seismic mitigation of 800 schools is being conducted in the Province of British Columbia. This is planned to be a sustained effort over 15 years with an initial commitment of 1.5 billion dollars. Sustainability of this project is a major concern because, over the 15 years, it will be impacted by changing economic conditions, labor costs, changing demographics, and obsolescence of existing schools. A risk management plan is being developed to handle these threats to sustainability of the project. Retrofits are based on performance based design (PBEE) with life safety as the only standard of satisfactory performance.

The federal government of Canada is concerned about the national capability for responding effectively to disasters both natural and man-made, such as terrorist activities. The award of the 2010 Winter Olympics to Vancouver sharply focused the government's concerns. A major research project called the Joint Infrastructures Interdependencies Research Project (JIIRP or JI2RP) was funded at 6 universities, through the federal agency Public Safety Canada, to develop various aspects of effective response to disasters. The University of British Columbia was given the project to develop a simulator, I2SIM, to model the interdependencies between critical lifelines such as oil, water and gas distribution systems, electrical systems, the structures supporting these systems such as pumping stations, reservoirs and electrical sub-stations and roads and bridges. The real time impacts of damaged systems on the entities served by them such as hospitals, transportation modes and residential areas is made available on line by the simulator and provide the basis for optimum decisions on emergency actions, particularly the deployment of resources. The use of I2SIM will be illustrated by pilot study of post-earthquake operations

at the University of British Columbia after an  $M=6.5$  earthquake used in the initial validation of the simulator.

The simulator is now being used to model potential responses to threats to the Winter Olympic Games to ensure that effective emergency plans are in place to sustain the most harmonious environment possible for the games and limit any deleterious effects of adverse actions. One example of an Olympic scenario will be shown to illustrate how the simulator facilitates making effective post-disaster decisions on how to handle casualties.

## **2.2 An Innovative Cost-Effective Retrofit Process**

In 2004, the British Columbia Ministry of Education initiated a \$1.5 billion seismic mitigation program to make all public elementary and secondary school buildings safe. This seismic safety program is being implemented by the BC Ministry of Education (MOE) in collaboration with the Association of Professional Engineers and Geoscientists of British Columbia (APEGBC). APEGBC has been contracted by MOE to develop a set of state-of-the-art performance-based technical guidelines for structural engineers to use in the seismic risk assessment and retrofit design of low-rise school buildings. In undertaking this technical development program, APEGBC contracted the University of British Columbia (UBC) to draft the performance-based technical guidelines based on an extensive applied research program (APEGBC, 2006). Each draft of these technical guidelines has been peer-reviewed by a BC peer review committee of experienced local consulting engineers and by an external peer review committee comprised of prominent California consulting engineers and researchers. Research on innovative retrofit methods is still being conducted and technical guidelines are issued to keep current with research developments.

The three overall objectives of the guidelines are enhanced life safety, cost effective retrofits and user-friendly technical guidelines. The life safety philosophy of these guidelines is enhanced life safety through minimizing the probability of structural collapse by the use of rational performance-based engineering (PBEE) methods of earthquake damage estimation. The performance criterion of life safety is defined by acceptable drift ratios specified for each generic school building type. The process for evaluating critical drift ratios and establishing the probability of collapse is described below.

### ***2.2.1 Design Ground Motions***

The seismic hazard data to schools is deaggregated by considering the seismic hazard posed by subduction, deep (sub-crustal) and crustal earthquake sources affecting British Columbia separately. The sources are shown in Fig. 2.1. Seismic hazard data

## Cascadia earthquake sources

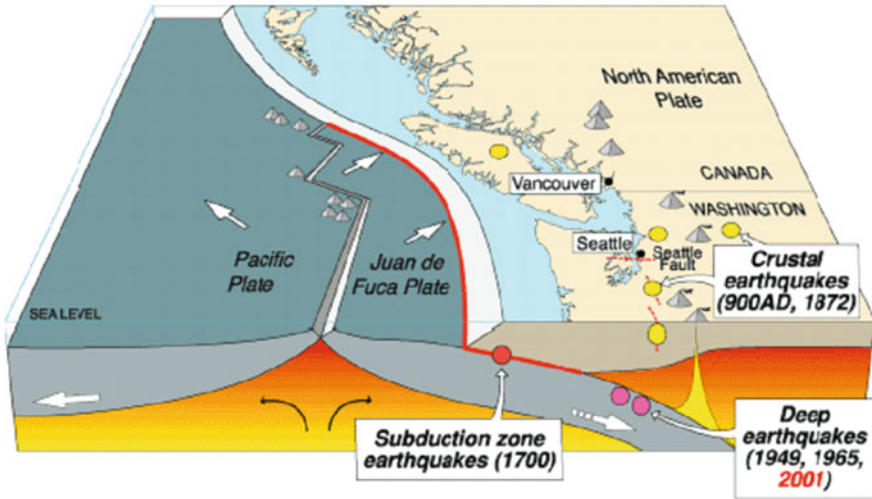


**Fig. 2.1** Subduction, deep (sub-crustal) and crustal earthquakes affecting British Columbia

for each type of earthquake was generated using the commercially available computer program EZ-RISK (Risk Engineering, 2008). The analysis results have been verified with reference to the open source data provided by the Geological Survey of Canada, GSC (Adams and Halchuk, 2003).

Ground motion at any geographic location is modeled by three ground motion suites of ten ground motions per suite – one suite for each of crustal, sub-crustal and subduction earthquakes (Pina et al., 2010a, c). These records were selected on the basis of tectonic setting and appropriate magnitude, distance and site conditions. The crustal and sub-crustal suites of ground motion spectra have been scaled linearly in the period range of interest,  $T = 1-2$  s, for Vancouver's benchmark 100% level of shaking with a 2% exceedance rate in 50 years. The subduction suite of ground motion spectra have been scaled to Victoria's 100% level of shaking because of the larger cities, it is the one most affected by the subduction earthquake. Since structural velocity is considered as the best indicator of severe structural damage to a structure, as opposed to peak ground acceleration or displacement, the associated ground shaking intensity is defined by the average spectral pseudo velocity (PSV) spectrum for each geographic location. The selected ground motion suites are scaled linearly so that on average each suite matches the associated PSV design spectrum in the period range of interest. The scaled design ground motions for the suite of crustal earthquakes are shown in Fig. 2.2 together with their average spectrum and the target PSV design spectrum. Note that the comparison between the average and the design spectrum in the period range of interest,  $T = 1-2$  s, is quite good. There is an additional requirement that no spectrum should fall below 70% of the target spectrum.

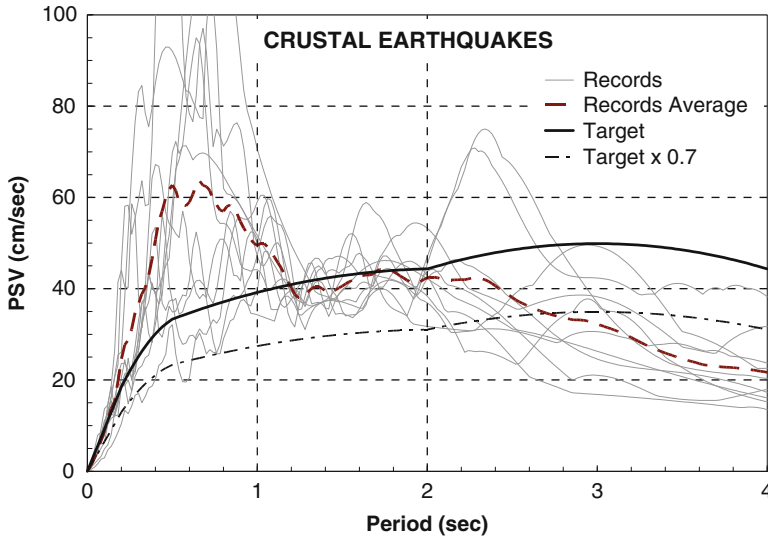


**Fig. 2.2** Design ground motions for crustal earthquakes scaled on average to the period range of interest of 1–2 s (Pina et al., 2010a, c)

The full range of possible ground shaking by the selected ground motions is divided into a series of ground shaking increments. All levels of shaking are expressed as a percentage of a benchmark level of shaking. The “100%” intensity level is taken as the benchmark level, and it corresponds to a level of shaking with a 2% probability of exceedance in 50 years. Each ground shaking increment has a range of 10%. For example, the ground shaking increment immediately below the benchmark level of shaking has a level of shaking that ranges from 90 to 100%. For any geographic location, the full range of ground shaking varies from the 30 to 250% level of benchmark shaking for each selected input motion in order to cover a wide range of intensities in potential input motions in exploring the response of school structures.

Site Class C (firm ground – very dense sand or soft rock) is the reference site classification used in the national building code and was adopted as the reference site for the retrofit program. All soils softer than firm ground amplify/de-amplify the level of shaking at the underside of the building foundations relative to the response at Site Class C. The effects of these soils are introduced in the analysis through the use of an Equivalent Intensity Factor (EIF) that exceeds unity for building sites in the Site Class D/E category (Pina et al., 2010a, c). The equivalent intensity factor, *EIF*, is the ratio of the intensity in the actual or soft site to the intensity at the rock or reference site calculated at the same structural response level.

Figure 2.3 shows a scheme of the EIF calculation process. In this example, the reference and specific sites correspond to Site Class C and Site Class D, respectively. Incremental Dynamic Analysis (IDA) curves (structural damage measure versus input motion Intensity) are first obtained from the combined site response

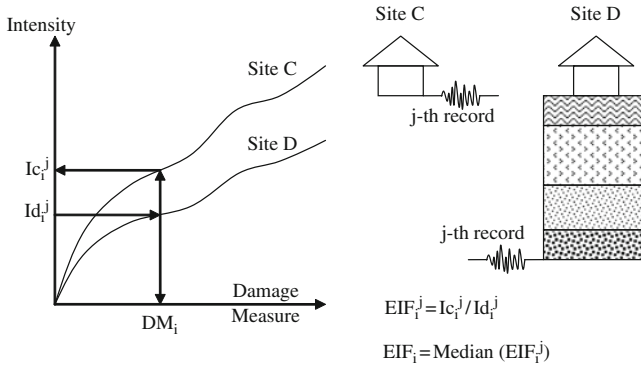


**Fig. 2.3** Calculation process of the equivalent intensity factor,  $EIF$ , for a specific site (Site D), for a given  $i$ -th intensity of the  $j$ -th record (Pina et al., 2010b)

and structural analyses. Figure 2.3 shows the incremental responses of a structural system under the  $j$ -th input motion for the two sites – note that for a given intensity level the IDA curve for Site D has a larger damage measure value, which is equivalent to amplification of the structural response.

## 2.2.2 Incremental Dynamic Analysis

The retrofit methodology is based on an incremental probabilistic non-linear dynamic analysis (IPNLDA) or incremental dynamic analysis (IDA) as it is more commonly called (Vamvatsikos and Cornell, 2001). Common types of low-rise school buildings have been analyzed for the full range of ground shaking in all regions of the province to generate a large database of analysis results. These results are made available to engineers assessing and retrofitting school buildings through the use of an electronic interface called the Seismic Performance Calculator.

The basic steps in the IPNLDA for the seismic risk assessment or retrofit design of a particular school building in a given geographic location are as follows:

- Step 1 – Scaling of Ground Motions for Seismicity.* The three suites of ground selected motions (one suite for each earthquake type) are scaled for the local seismicity.
- Step 2 – Site Class C Analysis.* The building prototype is analyzed for each earthquake type and for each level of shaking in 10% level of shaking increments from 30% level of shaking to 250% level of the 2% in 50 years shaking.
- Step 3 – Soil Amplification Effects.* The results from structural analyses results on Site Class C sites are modified by an Equivalent Intensity Factor (EIF), where applicable, for a site that falls into the Site Class D/E/F category.

Step 4 – There are Two Constraints on Acceptable Drift Performance for a School. The absolute probability of exceeding the tolerable drift (PDE) for the specified type of school structure and the conditional probability of drift exceedance (RDE) if a specified level of excitation occurs. The PDE value is determined by the Seismic Performance Calculator, described below for a given building and geographic location by the cumulative risk calculation process for each level of shaking increment. The Calculator also determines the RDE value at the 100% level of shaking for a retrofit design check.

Step 5 – Risk Assessment or Retrofit Decision Making. The above PDE and RDE values are used to assess an existing building or check a proposed retrofit design.

### 2.2.3 Seismic Performance Calculator

The Calculator in Fig. 2.4 is the principal analytical tool of this methodology. The tool gives the engineer access to a highly advanced, peer-reviewed analytical database without requiring the engineer to be experienced in the use of nonlinear dynamic analysis techniques.

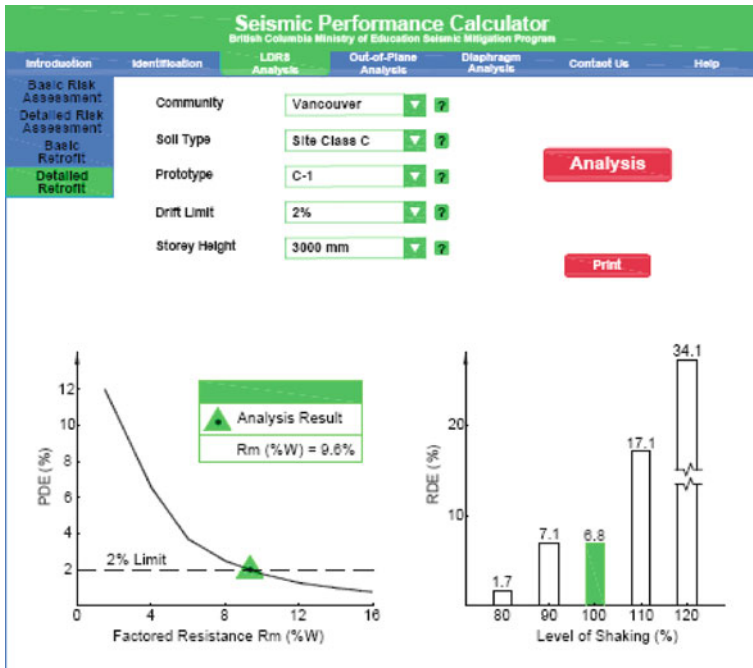


Fig. 2.4 The seismic performance calculator

The calculator permits the engineer to quickly analyze the three principal building elements that have analytically complex behavior. These are LDRSs, walls rocking out-of-plane and diaphragms. For each of these three building elements, the Calculator performs a risk assessment or a retrofit design (either basic or detailed). After making the basic parametric selections (input data), the engineer clicks on the Analysis button and the analysis results are instantly displayed. For acceptable performance the PDE must be less than 2%. Tolerable values of RDE are at present taken to be 10% but this limit is still under review.

### ***2.2.4 Toolbox of Retrofits***

The Toolbox is one of the unique features of the retrofit methodology. The Toolbox permits the engineer to combine the contributions from different LDRSs in performing either a risk assessment or a retrofit design. The Toolbox Method is the generation of LDRS lateral resistance in a drift-compatible manner. For a group of LDRSs, the drift limit for the assembly of LDRSs is the lowest drift limit of the participating LDRSs of the structure being considered. This approach permits the engineer to use all materials, new and existing, in formulating a cost-effective risk assessment or retrofit design (White et al., 2007).

### ***2.2.5 Comments on Retrofit Process***

The methodology described in this chapter represents a major advance in seismic engineering practice in British Columbia. The principal features of this methodology are:

- insight into the mechanics of earthquake damage;
- ability to mitigate earthquake damage to the performance requirements of the owner;
- ability of quantify benefit/cost comparisons easily and quickly for a range of seismic upgrading options;
- deaggregated tri-hazard risk estimation;
- rational quantitative method of assigning risk for ranking schools for retrofit;
- full range of levels of shaking considered (probable damage methodology);
- probabilistic measurement of risk and performance;
- incremental probabilistic non-linear dynamic analysis;
- large electronic database of analysis results for the use of structural engineers engaged to seismically upgrade school buildings, accessible through a web-based calculator; and
- ability to combine lateral resistance contributions for a range of new and existing LDRSs.

## 2.3 Emergency Response Measures

Inadequate coordination among infrastructure systems and among hierarchical decision levels has been a major cause of failures in the response of the systems in emergency situations and it has been responsible for unnecessary losses in human lives, property, and economic activity. The Joint Infrastructure Interdependencies Research Program (JIIRP) is part of an effort by the Government of Canada, through the Natural Sciences and Engineering Research Council (NSERC) and Public Safety Canada, to fund research to develop innovative ways to mitigate large disaster situations. Six universities across Canada were involved in the project including the University of British Columbia (UBC) studied decision support for critical linkages in infrastructure networks.

The JIIRP Project at the University of British Columbia, entitled Decision Coordination for Critical Linkages in a National Network of Infrastructures, is an effort to assess the impact of physical and temporal interdependencies among multiple infrastructure systems, during the evolution of large disaster events. The UBC-JIIRP group, is a team of researchers, graduate students, post doctoral fellows and research engineers from multiple disciplines: Electrical and Computer Engineering, Civil Engineering, Computer Science, Geography, Psychology, and Commerce. The group has developed a “system of systems” simulator I2SIM that can model the interactions between infrastructures, and how the loss of functionality in one system affects all other infrastructures and the overall wellness of the total system.

UBC-JIIRP simulator I2SIM models the real time effects of a disaster and identifies the interdependencies among critical infrastructure networks. There are at least five components of the project’s architecture: the study space with physical and human layers, the hazard (event or scenario), the damage assessment (I2DAM), database (I2DB), and the infrastructure interdependencies simulator (I2SIM) as shown in Fig. 2.5. The arrows indicate the flow of information from each component to the data base that feeds data to the simulator. The simulator then evaluates the consequences of any given scenario event, while taking into account the interdependencies between any interacting systems. The basic structure of the process for coping with interdependency was developed by Juarez Garcia (2009). He also carried out the analyses of the examples reported in this chapter.

Different infrastructures use different terminology to model their operations because of their different characteristics. I2SIM uses a common terminology to describe the same types of functions in different environments. There are four key parameters used in I2SIM to model operations of all kinds: cells, channels, tokens and controls. Cells represent functional units and are modeled as input–output units. A hospital is a cell (a production unit) that requires such inputs (tokens) as doctors, nurses, medicines, water and electricity to perform its function of treating patients at an acceptable rate in an emergency. Channels are transportation units for transporting tokens from a source cell to a consumption cell; cables for conducting electricity, pipes for water and transportation links for delivering medical personnel, food and

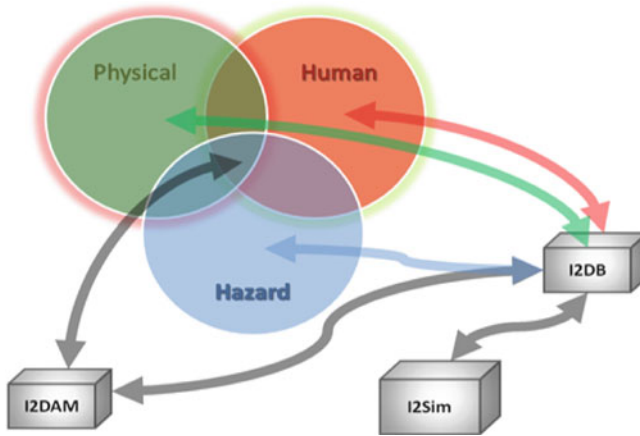


Fig. 2.5 Components of the architecture of the project

medical supplies. Tokens are the input and outputs of cells such as water, electricity, doctors or phone calls. Controls are distributor or aggregator units. These interface the physical layers of the simulator with the decision making layer to formulate effective response. Damage to the infrastructures during the disaster and greater demand for resources creates a situation where decisions need to be made as to the optimum allocation of the available resources. The simulator supports look-ahead and rewind functions to predict the evolution of the system dynamics in order to assess in real time the effect of suggested decisions before they are actually applied to the real system.

## 2.4 UBC Test Case (Juarez Garcia, 2009)

The simulator was initially tested by applying it to the Point Grey Campus of the University of British Columbia. The study space is shown in Fig. 2.6. Area A12 contains the University Hospital and the test of I2SIM was to predict the functionality of this hospital after various intensities of earthquake shaking from low to high. For this study, the functionality of the hospital was considered to be controlled by damage to the hospital itself and its contents and damage to the power and water systems supplying the hospital.

Figure 2.7 shows the loss of functionality of the water system in Zone A12, which includes the hospital, due to losses in the four components of the water supply system; reservoir, transmission line (TL 01), pumping station and local distribution line (DL A12). It is interesting to note that for this case the losses in the reservoir and the pumping station have the greatest effect on the overall loss of water for Zone A12. The pumping station is the most critical asset in this system.

It is now possible to evaluate the functionality of the hospital. The effects of damage to the structure of the hospital, the non-structural items and contents on

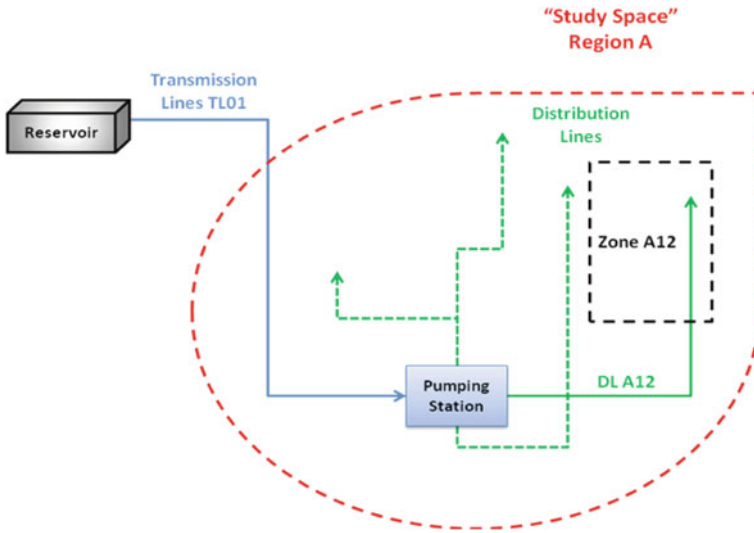


Fig. 2.6 Water system with four components supplying zone A12

functionality are shown by the dotted red line in Fig. 2.8. Then the integrated effect of the interdependencies between the different infrastructure components is evaluated using an interaction matrix. The cumulative effects of all contributions to loss of functionality of the hospital are shown by the solid red line in Fig. 2.8. The difference between the solid and dotted red lines shows the cumulative impact of the infrastructure system on the post-earthquake functionality of the hospital.

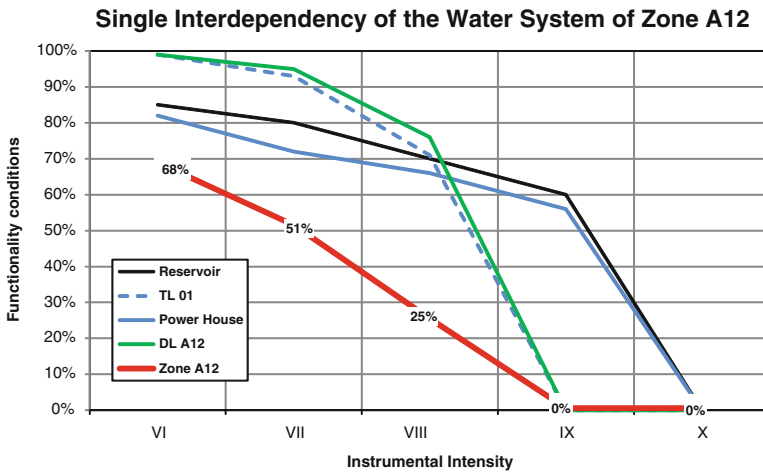


Fig. 2.7 Dependency of the water available in A12 on its infrastructure components

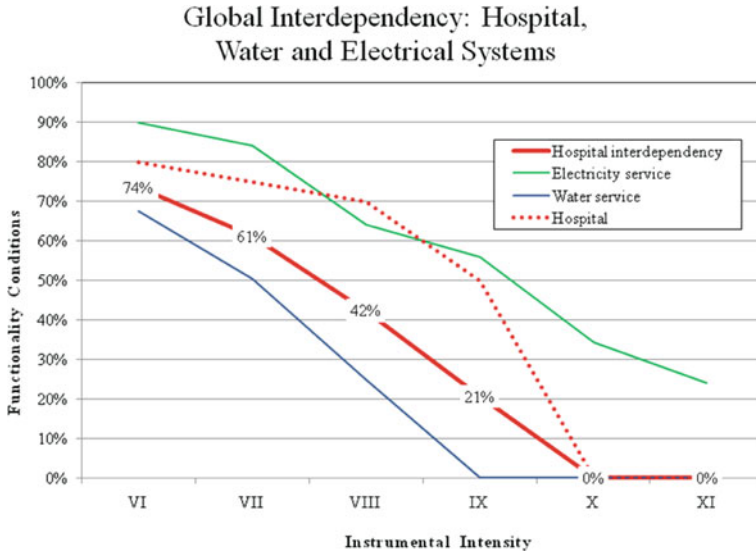


Fig. 2.8 Functionality of the hospital taking its dependency on infrastructure into account

### 2.5 Use of I2SIM for Post-disaster Response

I2SIM has been used to simulate response to potential disaster events during the 2010 Olympic Games in Vancouver. One such event and its aftermath are described below. Only the simulated response to treating casualties is considered here.

Time (min)	Event
00	An explosion occurs in downtown Murrin Electrical Substation
00	Traffic lights are out of service in major streets
05	A stage collapses on top of spectators near BC place
06	A multitude starts an uncontrolled egress from BC place
10	Trapped people and casualties are reported in BC place after the collapse of the stage
19	Casualties are reported in BC place due to egress of spectators

A controlling factor in formulating response to casualties is the speed of response. Serious injuries must be treated within rather short frame to minimize deaths as illustrated by the mortality chart in Fig. 2.9.

The simulator knows the resources available to move casualties, hospital locations and capacities and can examine travel times by various routes taking into

**Fig. 2.9** Mortality rates as a function of time to treatment



account best current information on conditions along these routes by means of an embedded traffic model. Table 2.1 shows the results of the simulation for a low number of casualties – 30. DRR in the table designates special reserved Olympic routes.

The simulator sends all casualties to the two major hospitals, St. Paul’s and Vancouver General, which happen to be reasonably close to BC Stadium. None the less the time to stabilize all patients is close to the 2 h limit where mortality rates begin to climb. The output of I2SIM for a large number of casualties (864) is shown in Table 2.2. Now the simulator brings in all available hospitals and the time to stabilization of all casualties is measured in hours, not minutes. When time to stabilization becomes so long that mortality rates become serious, the alternative procedures must be invoked such as field hospitals. Realistic simulations can provide clear pictures of potential occurrences and demands and allows the prior organization and preparation of reasonable responses.

## 2.6 Final Comments

The mitigation of seismic risk to the well-being of a community and the sustainability of a life style can be achieved by retrofitting buildings and infrastructure to resist the effects of earthquake shaking and by the implementation of effective post-earthquake emergency measures. This chapter describes two new approaches for dealing with both of these procedures.

The procedures for retrofit were developed following the principles of performance based design which reduced costs by 30–40% below conventional procedures based on building code regulations. The new design procedures were approved as good practice by the Association of Professional Engineers and Geologists of British Columbia and have been mandated for school retrofits by the government.

Table 2.1 Statistics on handling a small number of casualties – 30

	Road conditions		Road conditions		Road conditions		Road conditions		
	BCP – VGH (1)	BCP – SPH (1)	BCP – VGH (2)	BCP – SPH (2)	BCP – VGH (3)	BCP – SPH (3)	BCP – SPH (3)	Road conditions	
No of casualties	15	15	15	15	15	15	15	15	
Red-coded casualties	5	5	5	5	5	5	5	5	
Yellow-coded casualties	10	10	10	10	10	10	10	10	
Initial assessment time (min)	2	2	2	2	2	2	2	2	
Rescue time (min)	8	8	8	8	8	8	8	8	
Egress time (min)	16	16	16	16	16	16	16	16	
Triage time (min)	5	5	5	5	5	5	5	5	
Route (streets and avenues)	Pacific Blvd Quebec St 2nd Av Laurel St	Smithe St Burrard St	Pacific Blvd Cambie St 12th Av	Pacific Blvd Nelson St	Pacific Blvd Quebec St 2nd Av Laurel St	Pacific Blvd Quebec St 2nd Av Laurel St	Pacific Blvd Quebec St 2nd Av Laurel St	Smithe St Burrard St	
Distance of route (km)	4.4	2.2	3.8	2.1	4.4	4.4	4.4	2.2	
No of ambulances	30	30	30	30	30	30	30	30	
Patients per ambulance	1	1	1	1	1	1	1	1	
Road conditions	Normal roads	Normal roads	DRR	DRR	DRR	DRR	DRR	Normal roads	
Transportation time	21	9	9	7	15	15	15	No pedestrians	
Total transportation time	42	34	31	31	36	36	36	7	
Time for red-coded patients to arrive at ER	37	21	24	22	28	28	28	30	
Time for red-coded patients to be assessed and stabilized in ER	61	49	50	48	56	56	56	21	
Time after all patients have been assessed and stabilized in ER	121	109	110	108	116	116	116	108	

**Table 2.2** Statistics on handling a large number of casualties – 864

Hospital	VGH	SPH	Women's and children's	Mount St. Joseph's	UBC	Burnaby general	Richmond general
No of casualties	328	242	86	78	43	43	43
Initial assessment time (min)	2	2	2	2	2	2	2
Rescue time (min)	3	3	3	3	3	3	3
Egress time (min)	16	16	16	16	16	16	16
Triage time (min)	5	5	5	5	5	5	5
Route (streets and avenues)	Pacific Blvd Cambie 12th Av	Pacific Blvd Nelson St	Pacific Blvd Cambie King Edward Oak St	Pacific Blvd Cambie Broadway Kingsway	Pacific Blvd Cambie Broadway University Wesbrook	Pacific Blvd Main St Hastings St HWY1 Boundary Kincaid St.	Pacific Blvd Cambie Broadway Granville Marine Dr Russ Baker Way Gilbert Rd Westminster Hwy
Distance of route (km)	3.8	2.9	5.7	3	13	9.3	15.3
No of ambulances	10	7	3	2	2	2	4
Patients per ambulance	2	2	2	2	2	2	2
Route conditions	DRR	DRR	DRR	DRR	DRR	DRR	DRR
Transportation time	5	3	7	4	13	11	15
Total transportation time (h)	4	3	5	4	7	6	4
Time after all patients have been assessed and stabilized in ER (h)	16	15	18	15	17	16	15

A post-disaster simulator developed by UBC for the national government has been described. It can be used to direct in real time the deployment of resources after a disaster and to develop pre-disaster scenarios to permit effective pre-event planning. A simulation conducted for the 2010 Winter Olympic Games was presented to illustrate the utility of real time simulations in devising effective response.

**Acknowledgments** The development of the unique retrofit methodology described in this chapter is the result of a highly supportive and collaborative partnership of the following contributors: the British Columbia Ministry of Education; the Association of Professional Engineers and Geoscientists of British Columbia (APEGBC); the University of British Columbia; the APEGBC Structural Peer Review Committee (BC engineers); and the APEGBC External Peer Review committee (California engineers). The Canadian members of the project team wish to acknowledge the contribution of their California colleagues. Farzad Naeim, Michael Mehrain and Robert Hanson have provided invaluable guidance to this project in their capacity as members of the External Peer Review Committee. Hugon Juarez Garcia developed the seismic aspects of the I2SIM simulator and the concept of the interaction matrix for taking interdependencies into account.

## References

- Adams J, Halchuk S (2003) Fourth generation seismic hazard maps of Canada: values for over 650 Canadian localities intended for the 2005 National Building Code of Canada. Geological Survey of Canada, Ottawa, ON, Open File 4459. [http://earthquakescanada.nrcan.gc.ca/hazard/OF4459/index\\_e.php](http://earthquakescanada.nrcan.gc.ca/hazard/OF4459/index_e.php)
- APEGBC (2006) Bridging guidelines for the performance-based seismic retrofit of BC schools, 2nd edn. Association of Professional Engineers and Geoscientists of British Columbia, Burnaby, BC, Canada
- Canadian Commission on Building and Fire Codes (2005) National building code of Canada. National Research Council of Canada, Ottawa, ON, Canada
- Juarez Garcia H (2009) Multihazard risk assessment: an interdependency approach. PhD thesis, University of British Columbia, Vancouver, BC, Canada
- Pina F, Taylor G, Ventura CE, Finn WDL (2010a) Seismic risk assessment tool for seismic mitigation of schools in British Columbia. Proceedings of the 9th U.S. National and 10th Canadian conference on earthquake engineering, Toronto, ON, Canada
- Pina F, Taylor G, Ventura CE, Finn WDL (2010b) Site response analysis for the seismic risk assessment of schools in British Columbia, Canada. Proceedings of the 9th U.S. National and 10th Canadian conference on earthquake engineering, Toronto, ON, Canada
- Pina F, Ventura CE, Taylor G, Finn WDL (2010c) Selection of ground motions for the seismic risk assessment of low-rise buildings in South-Western British Columbia, Canada. Proceedings of the 9th U.S. National and 10th Canadian conference on earthquake engineering, Toronto, ON, Canada
- Risk Engineering (2008) EZ-FRISK, Software for earthquake ground motion estimation. Risk Engineering Inc., Boulder, CO
- Vamvatsikos D, Cornell CA (2001) Incremental dynamic analysis. *Earthquake Eng & Struct Dyn* 31(3):491–514
- White T, Ventura C, Taylor G (2007) Overview of the Bridging guidelines for the seismic retrofit of BC schools. Proceedings of the 9th Canadian conference on earthquake engineering, June, Ottawa, ON, Canada

# Chapter 3

## Lifelines in Megacities

### Future Directions of Lifeline Systems for Sustainable Megacities

Craig A. Davis and J.P. Bardet

**Abstract** The sustainability of megacities and the ecosystems they influence are critical for ensuring quality of life and environment throughout the world. This sustainability requires infrastructure systems that provide a good and equitable quality of life, and a balance between consumption, disposal, and environmental capacity. Megacities must be strengthened and prepared to resist all hazards that may threaten them. Megacities function as a mega-system made up of many independent subsystems that have been developed in silos. However, the operations of each system depend upon other subsystems within the mega-system, under both extreme and usual circumstances. Lifeline systems are the basic infrastructure that supports all other systems needed for a megacity to function properly. The resiliency of lifeline systems is critical to the sustainability of megacities. Future directions in lifeline systems require improved interactions between the interdependent systems and improved inter-agency coordination. Megacities are extremely vulnerable to risks from natural and man made hazards. Transformative research is needed to better understand how interdependent systems interact and to develop decision support tools that help to understand the performances of complex systems under normal and extreme events. Examples from the Los Angeles megacity region are presented to show the makeup of megacities and mega-systems, and to illustrate their vulnerabilities to extreme events. The simulated performance of water supply and distribution systems in Southern California during a great earthquake scenario are summarized to show how advanced decision support tools may be used for improving the functionality of critical infrastructure systems under normal and extreme circumstances. This study indicates that resilience can be enhanced through multi-system integration and the risks and vulnerabilities to hazards can be overcome through integration of existing infrastructure.

---

C.A. Davis (✉)

Geotechnical Engineering, Los Angeles Department of Water and Power, Los Angeles,  
CA 90012, USA

e-mail: craig.davis@ladwp.com

### 3.1 Introduction

Megacities are characterized by high concentrations of people, values, and infrastructure. Critical to the global economy, they act as gateways interconnecting nations and continents through the flow of information and goods. Megacities are agglomerations of many different cities, usually named after a city among them, which function as a mega-system made up of many interdependent subsystems that have been conceived separately. These large urban areas provide a flurry of opportunities to people not available elsewhere, including better access to employment, education, entertainment and health care (Sadowski et al., 2000). Megacities have very large ecological footprints consuming large volumes of resources that are transported into the urban region through vast infrastructure networks extending over hundreds to thousands of kilometers. Very little of the waste generated by a megacity remains in the megacity.

There is an ongoing worldwide trend toward urbanization as people seek to improve their quality of life. In view of their large population, megacities exemplify the phenomenon of world urbanization and have become natural laboratories for understanding urban sustainability and the resilience of ecosystems they influence. Sustainability is defined by Brundtland (1987) as “development that meets the needs of the present without compromising the ability of future generations to meet their own needs.” In order to do this, megacities must have the following sustainable characteristics:

- Their political, legal, social, economic, and environmental systems must be compatible with the local culture and values,
- They cannot consume more resources than what the ecosystems can replenish,
- They cannot dispose of more waste than the ecosystems can safely absorb,
- They must be prepared to resist all hazards that may threaten them.

The political, legal, social, economic, environmental, and built systems that make up the megacity infrastructure must be sufficient to provide a good and equitable quality of life. Like other urban and rural environments, megacities must coexist with the ecosystems they depend on and must find a balance between their consumption, disposal, and environmental capacity. The natural ecosystems of megacities may also be influenced by natural hazards such as hurricanes, earthquakes, and volcanic eruptions. As a result, megacities must face hazards from the natural environment and consequences of potential disasters. Among all potential hazards, earthquakes pose the greatest natural risks to megacities (Munich Re, 2004). To be truly sustainable, megacities must be prepared to resist all hazards, including manmade hazards, that aim at degrading urban quality of life.

In order to be sustainable, megacities must be resilient to hazards. Resiliency is the ability to recover from an event, such as the strike of a natural or manmade hazard, with the minimum amount of negative impacts. Lifeline systems, such as water, energy, communication, and transportation systems, provide the basic infrastructure that supports all other systems required for a city to function properly. The

resiliency of various lifeline systems is critical to the overall resiliency of a megacity. For instance, many, if not all, industrialized urban regions worldwide can only be resilient to a major event such as an earthquake when their water systems are themselves resilient (Davis, 2008). Therefore, water systems are critical to overall megacity sustainability.

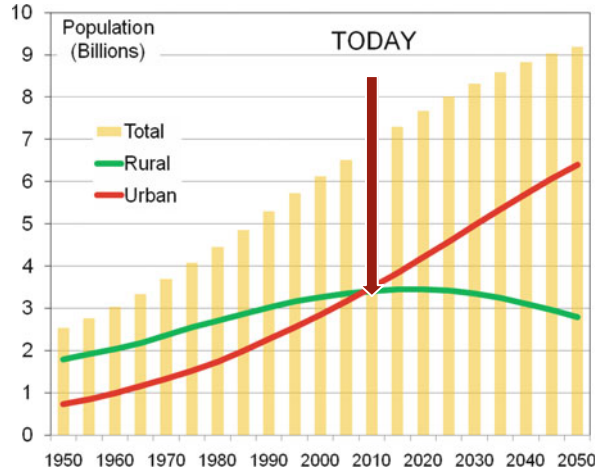
Each city making up the megacity has a set of lifeline infrastructure systems that are operated by different agencies, controlled or influenced by different local governments and laws, retain a legacy of working independently, but yet have numerous interdependencies with other systems. Some lifeline systems service multiple cities within the agglomeration. Megacities are dependent upon all systems to function properly. Future directions in lifeline systems require improved interactions between the interdependent systems and improved inter-agency coordination. Transformative research is needed to make needed improvements, to better understand how interdependent systems interact, and to develop decision support tools that explain how different complex systems perform under normal and extreme events.

This chapter reviews the performance of critical lifeline systems for megacity sustainability under threats from extreme natural hazards, with a primary focus on water systems subjected to earthquakes. An overview of world urbanization and megacity growth, related ecological footprint, and associated risks are described to provide the context for studying lifeline systems within the mega-systems of megacities. Examples from the Los Angeles megacity are presented to show the makeup of megacities, mega-systems, and their vulnerabilities to extreme events. A distinction is made herein between the City of Los Angeles and the Los Angeles megacity, which consists of an agglomeration of cities including the City of Los Angeles. Water systems are critical to maintaining systemic operation of any city and earthquake exposure has the greatest influence on risks to megacities. Earthquake hazards and their ensuing risks to water supply are symbolic of the Los Angeles megacity, as demonstrated through studies on water system performance during a large regional earthquake scenario. Results from the study are used to identify representative needs for megacities and define future directions for lifelines.

## 3.2 Megacities

Megacities exemplify extreme trends in a century of worldwide urbanization. As shown in Fig. 3.1, approximately 50% of the world's populations currently live in cities; this urbanization is projected to continue and concentrate two thirds of the planet population in cities by 2050. The United Nations defines a megacity as an urban agglomeration having at least ten million inhabitants (United Nations, 2008). Made up of an agglomeration of multiple cities, the megacity is usually named after one of its main cities. Table 3.1 lists the 19 megacities currently existing in the world, where approximately 9% of the world population lives. The number of megacities is growing; in 1975 there were only three and there are expected to be at least 23 by 2025. Many more urban areas of several million inhabitants have

**Fig. 3.1** World population (total, rural, and urban) from 1950 to present and projected to 2050 (United Nations, 2008)



common and similar problems as megacities, some of which may soon grow to acquire a megacity status. In addition, the actual sizes of megacities are often inconsistently determined due to imprecise spatial census boundaries in urban regions. For example Table 3.1 identifies the Los Angeles megacity with a population of 12.5 million people within the Los Angeles, Long Beach and Santa Anna areas. However,

**Table 3.1** World megacities – population in millions (United Nations, 2008)

Megacity, Country	Population (millions)		
	1975	2007	2025
Tokyo, Japan	26.6	35.7	36.4
New York-Newark, USA	15.9	19.0	20.6
Mexico City, Mexico	10.7	19.0	21.0
Mumbai (Bombay), India	7.1	19.0	26.4
São Paulo, Brazil	9.6	18.8	21.4
Delhi, India	4.4	15.9	22.5
Shanghai, China	7.3	15.0	19.4
Kolkata (Calcutta), India	7.9	14.8	20.6
Dhaka, Bangladesh	2.2	13.5	22.0
Buenos Aires, Argentina	8.7	12.8	13.8
Los Angeles-Long Beach-Santa Ana, USA	8.9	12.5	13.7
Karachi, Pakistan	4.0	12.1	19.1
Al-Qahirah (Cairo), Egypt	6.4	11.9	15.6
Rio de Janeiro, Brazil	7.6	11.7	13.4
Osaka-Kobe, Japan	9.8	11.3	11.4
Beijing, China	6.0	11.1	14.5
Manila, Philippines	5.0	11.1	14.8
Moskva (Moscow), Russian Federation	7.6	10.5	10.5
Istanbul, Turkey	3.6	10.1	12.1

as shown in Fig. 3.2 there is a very high population density extending inland and the megacity could include more cities toward San Bernardino and Riverside as part of the agglomeration, increasing the population to approximately 16.5 million (SCAG, 2009). Figure 3.2 also shows a nearly continuous urbanization, as bounded by the dashed line, extending along the Pacific coast from north of Los Angeles to south of San Diego, even across the international boarder into Tijuana, Mexico. Including this entire area extending across six counties and two countries would increase the megacity population to about 20 million. This example from Los Angeles is representative of many other megacities and indicates that a simple definition based solely on population count may not be adequate to define a megacity.

Megacities can also be characterized by their global influence on economic, political, and cultural activity and their influential position within a global system of nodal connectivity. Furthermore, megacities encompass large urban sprawl inter-connecting many smaller cities of prior central settlement resulting in an urbanized region having multiple metropolitan centers. Haynes (2006) describes megacities as vast continua of inter-connected urban space having several metropolitan cores. Others expand the concept of megacities using the broader concept of mega regions with large connected networks of metropolitan areas, which may include decentralized metropolitan centers having common environmental, cultural, infrastructural, economical, and functional characteristics (Pisano, 2006; Dewar and Epstein, 2007). It is beyond the scope of this chapter to propose a definition applicable to all megacities. This chapter characterizes megacities as national and international economic, political, and cultural centers encompassing vast continua of highly populated inter-connected urban and suburban space, which may have several metropolitan cores, with a total population of ten million people or more.

As major economic centers, megacities serve as major points of national and international trade, industrial manufacturing, and commerce. As a result, they

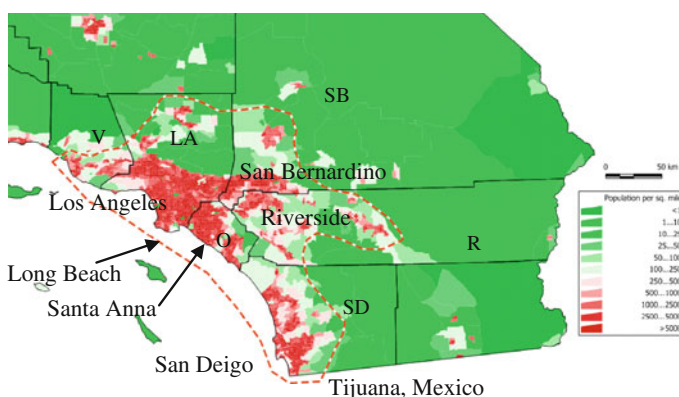


**Fig. 3.2** Southern California population density (modified from US Census Bureau, 2000). Cities are identified by name. Counties are identified by letters: V = Ventura; LA = Los Angeles; O = Orange; SB = San Bernardino; R = Riverside; SD = San Diego

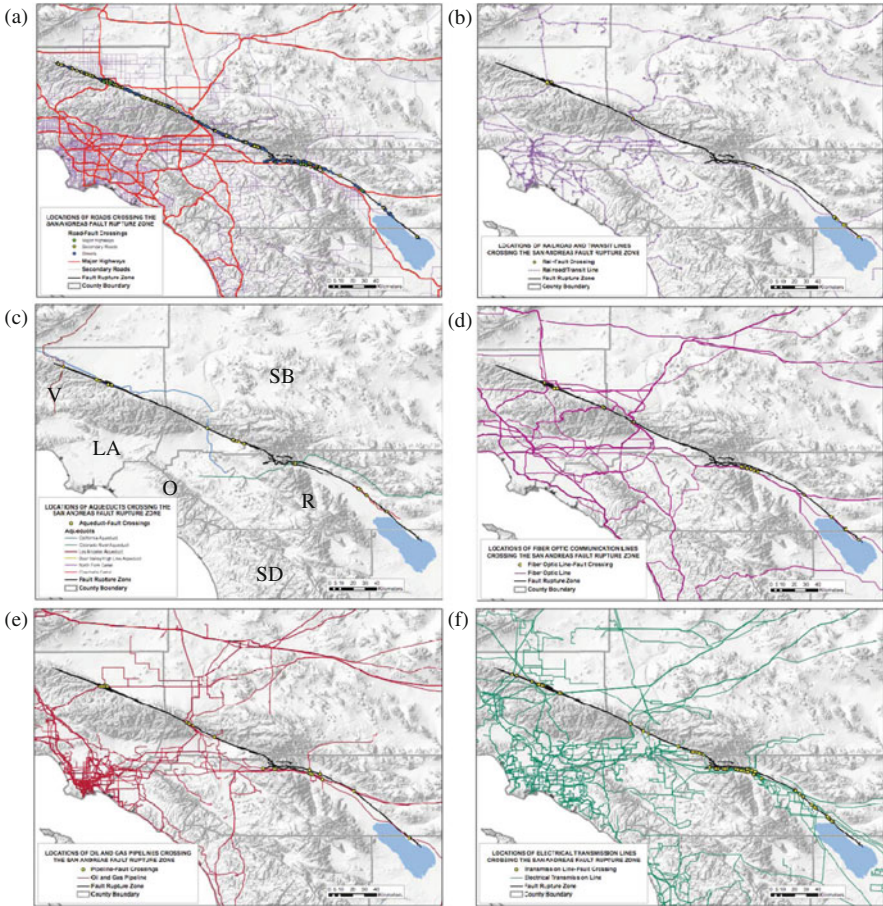


**Fig. 3.3** Major infrastructure systems needed to support the Los Angeles megacity: (a) highway transportation, (b) rail transportation, (c) water aqueducts, (d) fiber optic communication, (e) oil and gas, and (f) electrical transmission. Counties are identified in (c) as defined in Fig. 3.2. The San Andreas Fault is identified by *dark line* running from *lower right* to *upper left* in each map (modified from Jones et al., 2008)

provide job opportunities to people not available elsewhere, resulting in large migration to urbanized regions. Urban areas generally offer better access to employment, education, entertainment, and health care (Sadowski et al., 2000). Megacities need adequate infrastructure to support the congregation of people, goods, and industry.

Megacities apply tremendous pressures to the environment. A megacity consumes enormous amounts of food, water, energy, and other resources; and releases production, exports, ordinary and toxic wastes, and greenhouse gases. Very little that feeds and builds a megacity comes from the city itself and even less of the waste stays there. Thousands of square kilometers are required outside the city limits

to feed a megacity and absorb its discards. Thus, megacities have large ecological footprints that threaten not only their own sustainability but that of many other areas.

Figure 3.3 provides examples of urban infrastructures from the Los Angeles area. These include major highway transportation, rail transportation, water supply aqueducts, fiber optic communication, oil and gas, and electrical transmission lifeline infrastructure systems. The major systems shown in Fig. 3.3 are used for transporting resources, supplies, and information. Some of these systems extend over hundreds of kilometers. In addition to the systems shown in Fig. 3.3, extensive distribution systems exist within the metropolitan areas. For example, there are approximately 12,000 km of underground water distribution pipes within the City of Los Angeles boundary and an estimated 370,000 km of water distribution pipes in the Southern California region. Many more local distribution transportation, communication, and energy related networks exist in relation to the other systems shown in Fig. 3.3. The Southern California region making up the Los Angeles megacity is highly dependent upon the import of resources and export of goods, making the major supply and transport systems shown in Fig. 3.3, and their associated distribution networks, lifeline systems.

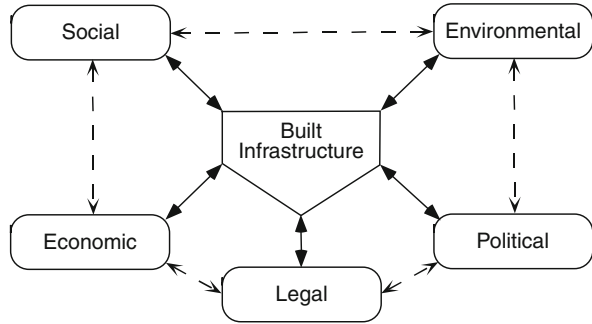
### 3.3 Mega-Systems

Megacities are an agglomeration of multiple cities, each of which evolved independently and expanded geographically until they merged with no visible boundaries. As a result, megacities are collections of cities that have fused together after having been built piece by piece by many designers who at best guessed how their new components would interact with the overall larger urban mega-system. For this and other reasons, megacities have gradually degenerated into complex, interdependent, and sometimes unreliable and uncontrollable systems in the face of population surges or stressors from natural or manmade hazards.

Megacities face tremendous challenges with increasingly complex lifeline systems, environmental impacts, and risks from natural and manmade hazards. The lifeline systems include those described in relation to Fig. 3.3 with the addition of storm and sewerage disposal systems. Also, there are unprecedented pressures from population growth, including homelessness, poverty, and the spread of disease. Megacities function through complex interactions between people and social systems, infrastructure systems, business and industry, and the environment. Today these complex interdependencies are so poorly understood that urban systems may respond unpredictably to extreme events, such as earthquakes, fires, droughts, floods, pandemics, and terrorist attacks.

Lifeline systems provide the basic infrastructure needed to sustain and improve the social, political, economic, legal, and environmental systems within urban settings. At the same time, as shown in Fig. 3.4, these systems interact together and support each other for their continuance, growth, and improvement. The failure of any one system may lead to dysfunction or even collapse of other systems.

**Fig. 3.4** Diagram showing interaction and interdependence of different infrastructure systems, focused around built infrastructure. Lifelines are a subset of built infrastructure



The geographic merging of multiple cities into one boundless megacity results in adjoining different sub-systems (each sub-system may be exemplified by Fig. 3.4) within the larger mega-system, each retaining a legacy of functioning independently. Additionally, the different lifeline systems developed relatively independent of each other, but become increasingly interdependent as the systems grow. Future development of megacity lifeline systems must provide more efficient multi-system integration of services.

Figure 3.5 demonstrates the merging of multiple cities into a boundless urbanized megacity. Figure 3.5a shows neighborhoods and districts within the City of Los Angeles. Many of the different neighborhoods, communities, and districts within the City of Los Angeles started as separate cities or unincorporated communities that were eventually annexed or incorporated to become a part of the City of Los Angeles. The annexation process merged the different infrastructure systems

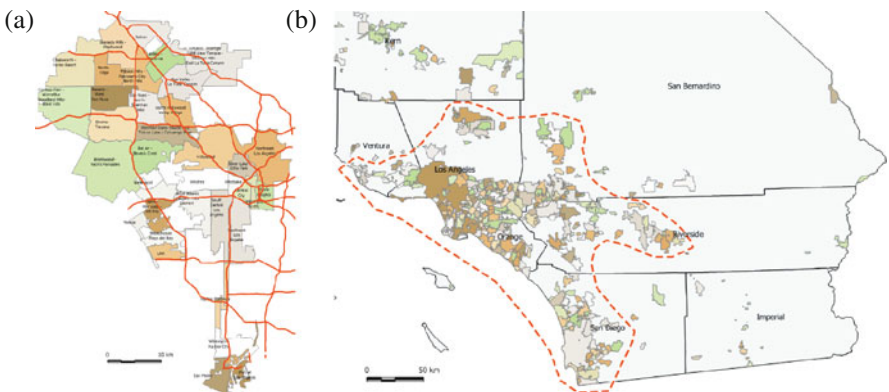


**Fig. 3.5** (a) Neighborhood and district boundaries within the Los Angeles City boundary (Planning Department, 2010), linear features are highways, (b) cities making up the Los Angeles megacity (within dashed boundary). The City of Los Angeles makes up only a portion of the Los Angeles megacity shown in Fig. 3.5b. County boundaries are shown and labeled (modified from US Census Bureau, 2000)

**Table 3.2** Makeup of the Los Angeles megacity (from US Census Bureau, 2000)

County	Within Los Angeles megacity		Overall	
	Number of cities	Population	Number of cities	Population
Los Angeles	127	9,339,404	128	9,342,531
Orange	42	2,794,234	42	2,794,234
Riverside	52	1,315,503	54	1,333,060
San Bernardino	32	1,434,062	43	1,514,655
San Diego	43	2,661,849	46	2,667,506
Ventura	10	754,268	18	921,609
Total	306	18,299,320	331	18,573,595

shown in Fig. 3.4 into a larger unit with consistent governance within the City of Los Angeles. Over time Los Angeles City continued to grow within its boundaries until the intervening space was completely filled, making one large urbanized City shown in Fig. 3.5a. Many of the original cities have become districts and neighborhoods and serve as centers within the main Los Angeles City boundary. There are currently 35 different districts in the City of Los Angeles shown in Fig. 3.5a, holding a population of over 4 million people (Planning Department, 2010). Similarly, Fig. 3.5b shows how the Los Angeles megacity is made up of 306 different cities, each of which initiated as independent municipalities with intervening open space, but evolved and grew in size until their boundaries merged. Figure 3.2 shows a continuum of population spread, indicating that the spaces between cities in Fig. 3.5b are unincorporated communities governed by the counties. Figure 3.5b shows how the Los Angeles megacity agglomeration is governed by many city and county jurisdictions (other megacities may cross state and national boundaries). Table 3.2 presents by county the distribution of cities located within the dashed boundary shown in Fig. 3.5b, showing the megacity incorporates about 92% of all cities and 99% of the entire population of Southern California. The 306 cities and six counties support a population reaching about 20 million people, each having a different set of the infrastructure systems (Fig. 3.4). Figure 3.5 and Table 3.2 show how the Los Angeles megacity is a conglomeration of thousands of different infrastructure systems, which have been developed independently, but are increasingly becoming more dependent upon each other as urbanization proceeds under demographic pressure.

### 3.4 Lifeline Systems in Megacities

Of all the major lifeline systems, water supply raises the most daunting challenges facing megacities. As a result, the remainder of this chapter will focus on water lifeline systems. Water is essential for life and well-being. Our ability to acquire and distribute water, however, is threatened by accelerating watershed shortages and unprecedented competition for water resources. Studies by the United Nations and

numerous other organizations identify the depletion of supplies and mismanagement of water distribution as contributing to the most serious crises of the twenty-first century. Almost all of the megacities face major fresh water challenges. More than a billion people, 20% of the world's population, live without regular access to clean running water. The population of cities is expected to increase to approximately 5 billion by 2025, which will result in an exponential increase in demand for urban water (Abhat et al., 2005). Any solution to the water crisis is therefore closely linked to sustainable megacities.

Water delivery systems are central to the interdependencies of critical infrastructure, and are crucially important for essential services such as fire protection, hospitals, regional businesses, and even electric power networks. Because water and interdependent infrastructure systems face challenges that exceed the capabilities of our current engineering, management, and planning procedures, truly transformative research is needed to initiate the changes required for effective decision making and policy formulation in the future.

Water systems play an important role in the sustainability of megacities. Increasing demands for water resource management requires improved conservation, water recycling/reclamation, and urban storm water management. Currently water and sewerage systems operate completely separate. Increased reclamation will change the cycle of urban water distribution, blurring the future boundaries between water and sewerage systems. Additionally, increased use of storm water runoff will require better integration of water collection, treatment, and distribution with building, paving, and open space.

### **3.5 Risks from Natural Hazards**

Megacities face inherently higher risks from natural hazards than smaller cities with similar hazard exposure. This results from the enormous concentration of people and assets, many being vulnerable to hazards, which may lead to large losses in case of a disaster. Prior to megacities, initial urban settlements were mostly confined to safe areas wherever possible, but their subsequent growth spread them into highly exposed areas (Munich Re, 2004), putting people and assets, including the lifeline networks, at a higher risk to landslides, floods, ground settlements and other hazards or hazard related effects. Growth of the City of New Orleans in the United States is a good example of this urban growth into more vulnerable locations. Although New Orleans is not large enough to qualify as a megacity, it grew similarly to most megacities as it spread from originally relatively safe locations on high ground into highly vulnerable locations in low swamps. The hurricane Katrina disaster exposed the New Orleans' vulnerability to flooding.

Additionally, economic centers sometimes relocate to positions of higher exposure within the cities. For example, in London a new business and commercial center built in the former docklands area is now at greater risk from storm surges (Munich Re, 2004). Los Angeles, San Francisco, Tokyo, Osaka and other megacities continue to grow in size and population despite being exposed to earthquakes; the exposure

level of cities located in highly seismically active areas tends to increase much faster than the engineering knowledge that is supposed to protect them.

Losses from natural disasters have steadily increased around the world since 1950 as a result of increased urbanization, which is epitomized in megacities. As a result, Munich Re (2003, 2004) developed a natural hazard risk index for megacities based on parameters of hazard, vulnerability, and exposure and considering earthquake, volcanic, tsunami, wind storm, flood, brush fire, and frost related hazards. They studied 50 amalgamated mega-urban regions similar to the megacity characterization described herein. Of the 50 cities studied by Munich Re (2004), approximately half have medium or high exposure to earthquake hazards (12 medium and 12 high). The study results show that those megacities having the highest risk index have a high exposure of their valued assets to earthquake hazards. The four cities having the highest risk factors are in California and Japan (Tokyo, Los Angeles, San Francisco, and Osaka). The index is influenced mostly by exposed values, and the total exposure to earthquake plays a dominant role. The study concluded that megacities having exposure to earthquakes warrant more detailed examination (Munich Re, 2004).

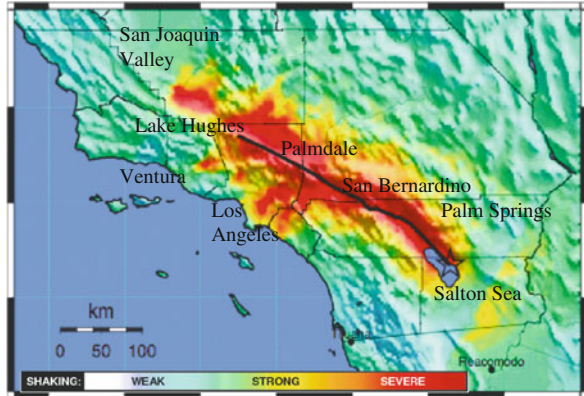
Some of the most complex risks in megacities involve lifeline utility and transportation systems. As shown in Fig. 3.3, major supply and transport lifeline systems extend well beyond the urban region and connect with infrastructure networks on national and global scales. This makes megacities vulnerable to hazards located at great distances. In fact, megacities often are affected by hazards such as drought, earthquake, flood, fires, etc. that do not directly strike their immediate urban region. For instance, droughts in northern California severely impact Los Angeles in Southern California because the majority of water supply is collected from the north. As another example, a great earthquake in Tokyo is projected to cause a worldwide recession (Munich Re, 2004). The hazards directly threatening urban regions can lead to disasters greater than anticipated as they impact the complex interdependencies of the lifeline systems. For example, the lack of potable water following a major earthquake can significantly reduce or even halt air and shipping transport, resulting in worldwide economic impacts.

As previously stated, water systems are critical to maintaining systemic operation of a megacity and earthquakes pose the greatest risks to megacities. The following section summarizes studies of the Los Angeles megacity on the impacts to water supply and distribution from a great moment magnitude ( $M_w$ ) 7.8 San Andreas Fault earthquake in Southern California.

### **3.6 San Andreas Fault Earthquake Impacts to Los Angeles Megacity Water Systems**

A  $M_w$  7.8 earthquake scenario on the southern San Andreas Fault was recently developed for use in the Great Southern California ShakeOut (Jones et al., 2008). Hereafter, this scenario will be referred to as the ShakeOut Scenario. The scenario development was based on a plausible event and resulting impacts, not a worst

**Fig. 3.6** Southern California region showing the epicenter (*star*), fault rupture (*heavy line*), and shaking intensity for the  $M_w$  7.8 San Andreas Fault scenario (modified from Jones et al., 2008)



case scenario. Figure 3.6 shows the Southern California region, ruptured portion of the San Andreas Fault, and shaking intensity for this scenario. The scenario event and resulting impacts are summarized herein to help provide a more complete understanding of impacts to water supply, more detailed reports are presented in Jones et al. (2008) and EERI (2011). Fault rupture displacements exceed 9 m and large ground motions result. Intense shaking is experienced over a large area of Southern California affecting nine counties and over 22 million people. Ground failures from landslides, lurching, liquefaction and lateral spreading result in many locations of the severely shaken areas. Earthquake induced shaking from the main shock causes significant damage and disruption throughout Southern California. Millions of buildings are unusable from structural and non-structural damage.

Figure 3.3 shows the ShakeOut Scenario fault displacements that disrupt many critical lifelines including major highways, railroads, power transmission, oil and natural gas, fiber optic communication, and water supply crossing the fault. Shaking and other ground failures cause additional widespread damage to lifelines throughout Southern California. Transportation corridors and water supplies are severely disrupted for long periods of time. Hundreds of water systems, large and small, are damaged by the earthquake disrupting the supply and distribution to customers and the ability to fight fires. Water lifelines take the longest to restore following damage from the ShakeOut Scenario, as a result water systems are the most critical component to the resiliency of the Los Angeles megacity. An estimated 1.5 million people are without potable water immediately after the earthquake, and after 90 days over 180,000 households are still without potable water due to distribution system damages. Approximately 1,600 ignitions are estimated, some resulting in large fires causing extensive damage after burning for a week in highly urbanized and populated areas.

Figures 3.3c and 3.7 show the three aqueducts that provide over 70% of the annual average water supply for domestic and industrial use to the Los Angeles megacity. Davis (2010) estimated the damage sustained to these aqueducts from fault rupture and shaking induced damages result in a complete disruption of all imported water supplies for approximately 4 months, at which time the California



**Fig. 3.7** California map showing Los Angeles megacity water supply sources from the Los Angeles Aqueduct, Colorado River Aqueduct, and California Aqueduct. EB and WB are the California Aqueduct East and West Branches, respectively. The San Andreas Fault is shown to pass nearly the entire length of the state. The City of Los Angeles is shown matching that area presented in Fig. 3.5a; the Los Angeles megacity area is presented in Figs. 3.2 and 3.5b

Aqueduct West Branch may return to service. The remaining lines will take at least a year to return to service. There is an estimated 6 months of emergency water storage if 25% conservation from pre-earthquake usage is implemented (Jones et al., 2008; Davis, 2010). The longer aqueduct restoration period requires the megacity to implement more extensive conservation measures than currently planned. Restoration of the California Aqueduct West Branch will help the City of Los Angeles and other nearby cities, but will not help all of the megacity population due to limited ability to transmit West Branch water throughout the urban areas. Even those receiving West Branch water must continue to be rationed for many months to stretch this limited supply as far as possible.

Romero et al. (2009, 2010) simulated damage from the ShakeOut Scenario to the City of Los Angeles Department of Water and Power (LADWP) water pipeline network using a recently developed decision support system (O'Rourke et al., 2008). The decision support system works in conjunction with EPANET (EPA, 2007) and a special program for damaged network flow modeling, known as Graphical Iterative Response Analysis for Flow Following Earthquakes (GIRAFFE). The simulation accounts for all 11,691 km of LADWP pipes and the effects of seismic ground waves and ground deformations associated with liquefaction, lurching, and oscillations. The simulation identified nearly 2,700 LADWP pipeline repair locations. Figure 3.8 presents GIRAFFE simulation results at 0 and 24 h after the earthquake showing locations on the trunk line system where pipes are unpressurized and there is insufficient water flow to satisfy demand, prior to utilizing emergency raw water storage reservoirs located within the LADWP system. System serviceability, the ratio of water flow after to water flow before the earthquake, is approximately 76% immediately after the earthquake (at 0 h) and drops to 34% after 24 h. Severe deterioration

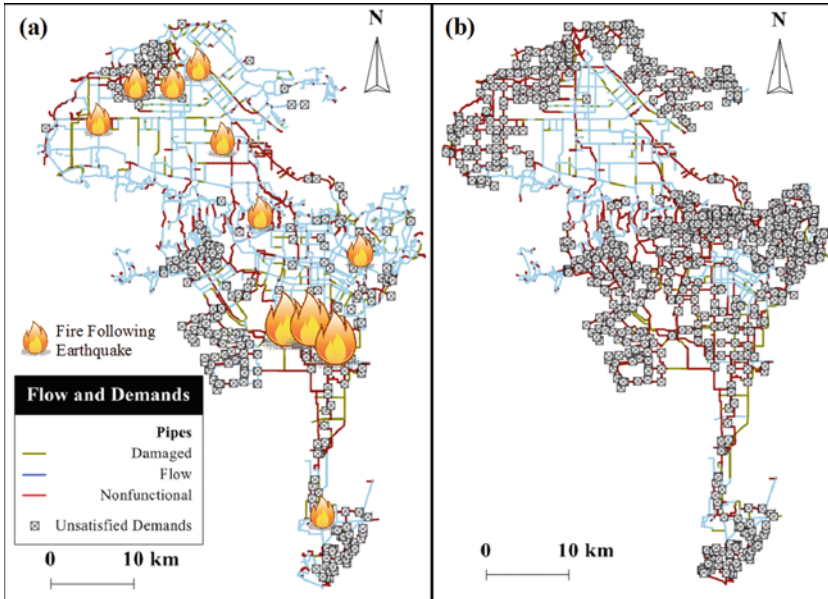


**Fig. 3.8** LADWP water system flow state and unsatisfied demands for: (a) 0 and (b) 24 h after the earthquake (modified from Romero et al., 2009). Predicted fire following earthquake locations, large fires and super conflagrations, are identified based on Scawthorn (2008)

in the ability to deliver water results over a 24 h period due to damaged and leaking pipelines. A 34% system serviceability means that 66% of the normal water demand, throughout the entire system, is not met 1 day after the earthquake. Some areas within the system will have higher or lower serviceability. The simulation results account for service line leakage and damage to interior piping of buildings, which draw more water from the system, but not for fire fighting demand. Leaking pipelines draw down tanks and reservoirs, causing some portions of the system to lose pressure and in some areas all local sources of stored water. Following such a large event, it will take approximately 24 h to mobilize the initial response to isolate and repair leaking pipelines. Thus, Fig. 3.8b represents a likely flow state within 1 day following the earthquake, in the absence of fire demands.

Figure 3.8a identifies locations of potential ignitions as generally described by Scawthorn (2008), overlaying the Romero et al. (2009) estimated water system flow state within the City of Los Angeles. The large flames in Fig. 3.8a locate the area where Scawthorn (2008) predicts super conflagrations in the Los Angeles Central City area. Figure 3.8b shows that trunk lines are unable to provide adequate water supply to this area within 24 h after the earthquake, a potential fire-fighting problem. Romero et al. (2009) found the Central City water service area to have relatively low serviceability (31–45%), without firefighting demand. Inclusion of the large fire demand needed for a super conflagration 1 or more days after the earthquake could potentially degrade service to nearly zero. Although alternate means of fire fighting exist, the loss of water supply in central Los Angeles and other areas inhibits fire

fighting capability and contributes to the overall mortality, injury, and economic losses in this disaster.

Davis (2009) describes the LADWP restoration processes and Davis and O'Rourke (2011) describes impacts from water system restorations throughout the megacity region, which are only summarized here. Water system restorations after a ShakeOut Scenario event will be lengthy because of: damage state, time to discover damage, the number of crews that report and when, travel times, available water supply, (in)ability to isolate damaged pipes, and (in)ability to use redundancy in the trunk/transmission system. In addition to the main shock shown in Fig. 3.6, large aftershocks in the range of  $M_w$  6.4– $M_w$  7.7 will occur throughout the Southern California region causing additional damage, further compounding the disaster and increasing impacts to water supply and distribution.

Approximately 1,300 water supply and distribution systems are impacted by the ShakeOut Scenario; some are outside the Los Angeles megacity. Approximately 375 systems serve a population of 1,000 people and 215 systems serve a population of over 10,000 people, most of which make up portions of the Los Angeles megacity as depicted in Figs. 3.2 and 3.5b. Each of the cities making up the Los Angeles megacity are serviced by one or more water systems. An estimated 370,000 km of water pipe is shaken by the ShakeOut Scenario resulting in approximately 50,000 repairs (Jones et al., 2008) distributed throughout the various water systems. Thus, there are many independent water systems within the Los Angeles megacity impacted by this scenario, the largest being the LADWP system which is a representative system for understanding overall water system performance throughout the megacity region (Davis and O'Rourke, 2011).

Davis and O'Rourke (2011) and Jones et al. (2008) present regional impacts to water systems, which are summarized as follows:

- The domestic emergency water storage is limited, extending the length of this emergency to possibly a year or more, and requiring rationing of 25–75% after services are restored;
- Pre-earthquake serviceability will not be restored to much of the megacity region for well over 6 months;
- Pipe repairs will take up to several months to complete in areas subjected to large ground motions and permanent ground movements;
- Not all customers in areas shaken with severe intensities will lose water service;
- About 50% of customers shaken with Modified Mercalli Intensity (MMI) VIII or greater will be out of service soon after the earthquake and it will take about 1 week to begin restoring services;
- Many customers will be restricted with water purification and conservation announcements;
- Serviceability will continue to decline for several days following the earthquake, after which serviceability will improve and restoration will be achieved in steps as entire blocks are returned to service;
- Within 2 weeks all customers shaken by MMI VII or less have water;
- It takes about 6 weeks for 90% of customers shaken with MMI VIII or greater to receive service and 6 months for the last 5% of customers to have water service;

- An estimated 185,000 households, approximately 500,000–700,000 people, are without potable water for at least 90 days;
- Damage to water supply and distribution systems contribute to post-earthquake conflagrations;
- Mutual aid and assistance will be problematic because of limited local resources.

The rate of service restoration is dependent upon the level of damage and time to restore flow in the regional supply transmission systems. The regional transmission systems have limited to no redundancy, which inhibits the ability to rapidly transmit emergency supplies to the local distribution systems. This combined with the rapid loss of system serviceability will significantly impact the capabilities to fight the estimated 1,200 large fires throughout the Los Angeles megacity. Some areas of the regional transmission system may sustain extensive damage from ground failures, taking months to make repairs. Restoration of the local distribution systems is dependent upon their access to resources and supplies. Most water distribution systems have limited capabilities and resources for such extensive repairs, requiring a widespread coordinated effort for all water systems to restore services. Service is not fully restored until pre-earthquake demands are supplied, which may take a year or more before all the major water supply aqueducts shown in Fig. 3.7 return to service. Thus, the Los Angeles megacity region must undertake significant rationing efforts for long durations in the course of this disaster.

Jones et al. (2008) estimates \$213.3 billion in total losses from the ShakeOut Scenario, approximately two thirds coming from the combination of fire (41%) and water (25%); assuming the three major aqueducts are fully returned to service within 6 months. However, as previously described Davis (2010) indicates the major water supply aqueducts may not return to service for longer than 6 months. The limited emergency water storage will have a significant impact on the regional economy; the \$53 billion in business interruption losses due to reduced water supply (Jones et al., 2008) may have been greatly underestimated for this event (Davis and O'Rourke, 2011). Considering the relation between fire damage and water system damage, the earthquake effects to water supply and distribution systems has possibly the greatest impact of all aspects considered in the ShakeOut Scenario. The regional economy is intertwined with all the Cities impacted by the ShakeOut Scenario. Therefore, the regional economy is affected primarily through the accumulated impacts to all water suppliers and distributors in Southern California. As a result, it is critical for all water agencies to prepare for a great San Andreas Fault earthquake to help make the Los Angeles megacity more resilient to such a disaster.

### **3.7 Results of Water System Impacts from the ShakeOut Scenario**

The study on water system impacts from the ShakeOut Scenario concludes that additional work is needed to make water systems more resilient, including: assess seismic vulnerabilities, post-earthquake serviceability, and restoration time estimates for all major aqueducts, water transmission, and distribution systems;

perform more detailed estimates of the regional emergency storage; evaluate the interaction between water system serviceability and fire following earthquake; and re-evaluate potential socio-economic impacts due to water system damages. From these studies, mitigation alternatives can be identified, prioritized, and implemented.

Most importantly, the study has findings relevant to megacity sustainability. It stresses the need for critical lifeline water systems to improve interactions between the interdependent systems and improve inter-agency coordination within the megacity. Examples for interagency coordination involve: water and fire departments; the major water supply aqueduct operators; public health departments and the water distribution agencies (Davis and O'Rourke, 2011).

One of the most critical aspects is to restore the major water supply and transmission systems. Improved performance and restoration times may be achieved by developing a water supply agency coordination team that consists of the agencies operating the aqueduct systems shown in Fig. 3.7 to coordinate post-earthquake response and recovery and pre-earthquake mitigation efforts. The reliability of transmitting water supplies throughout the region can be improved through developing an intersystem transmission network to create redundancy to the existing regional water transmission capability for use in emergency situations. Redundancy is critical to ensuring community resiliency. This will require some level of regional coordination, with consideration of water quality and other effects such as fire fighting. A regionally reliable water supply source for fighting fires is needed and may be achievable by incorporating seismic design principles in select transmission facilities and pipelines having spatial coverage to enhance firefighting, provisions to isolate damaged portions of the network, storage tanks and cisterns to draw from, and reliable water sources that include reclaimed/recycled water and sea water.

Furthermore, better resource and infrastructure management will contribute to the megacity resiliency. For example, better management of water resources can increase local ground and surface water storage, augment usage of local storm water runoff, and improve water recycling. These and other water resource aspects, which usually make the megacity more resilient to drought hazards, are equally important for seismic resiliency. Improved infrastructure management can extend the life of system assets (e.g., reduced pipe corrosion), render them less vulnerable to seismic damage, and efficiently replace the assets that are more vulnerable to normal and seismic demands. Asset management programs need to be risk-based (Bardet et al., 2010) and consider the total impacts to the megacity, which may include local, regional, national, international, and global impacts.

This study highlights systemic vulnerabilities and provides an example of how systemic performance under extreme events may influence megacity functionality. Many independent yet adjacent water systems have little interconnection and redundancies. Improvement can be realized by considering the needs of the megacity as a whole, similar to viewing one large water system in the City of Los Angeles that was developed through the integration of many different systems over time (e.g., Fig. 3.5a), rather than looking at each system separately. The example above is limited to the interaction of different water systems serving the Los Angeles megacity and the direct impacts to public service and overall recovery

from disasters. However, the impacts go much deeper when considering the dependency of other critical facilities and lifelines on water distribution, such as hospitals. Maintaining a reliable water supply is critical for the Los Angeles megacity, which faces one of its greatest threats from earthquakes.

The systemic vulnerability does not originate from the independency of the organizations operating the systems; in the long term this independency may benefit the needs of local populations. Instead, the vulnerabilities lie in the apparent lack of preparation to plausible disastrous events such as the ShakeOut Scenario, which results in a relatively low level resiliency for the megacity. A more coordinated effort is needed to overcome the aggregate effects from damage to so many independent systems. It is very unlikely that the response and ability to supply water will self organize after a disaster. As a result, there must be a coordinated effort to prepare in advance of an event for the benefit of the entire megacity.

### 3.8 Sustainable Megacities

Megacities have expanded as important global centers, in part, by attracting people seeking a better life. In order to become sustainable, megacities must continuously improve, or at least maintain lifestyles within the expectations of the local customs and values. This requires the infrastructure systems to support a good and equitable quality of life, which is only achievable through a balance between consumption, disposal, and environmental capacity. Additionally, megacities must be fortified to resist all hazards that may threaten them. Resiliency to events, such as earthquakes, is a necessary characteristic of a sustainable megacity. As indicated from the ShakeOut Scenario in the Los Angeles megacity, lifeline system resiliency is critical for the overall megacity resiliency.

Figure 3.9 depicts the concept of resiliency in terms of economic activity. When an earthquake or other hazardous event impacts a megacity, there is an immediate drop in its economic activity. The resiliency is measured by the amount of loss and the time it takes to recover back to the normal activity, projected as the line at the top of Fig. 3.9. The smaller the loss and shorter the duration (upper curve in Fig. 3.9), the more resilient is a megacity. The economy may take years to recover after disastrous events. In some exceptionally large events and/or where high vulnerabilities exist, economic activity may not recover for several decades resulting in a catastrophe (Jones et al., 2008, p. 14). In more extreme cases, economic activity may never recover, continuing to decline and disabling a safe and equitable lifestyle for its residents. In such a case, the megacity is not resilient or sustainable. The evaluation of resiliency must account for all infrastructure systems within the megacity. The concept of resiliency depicted in Fig. 3.9 can be applied to the recovery of various infrastructure systems and business making up a megacity. In the ShakeOut Scenario water system resiliencies are the most critical for the Los Angeles megacity, dictating the shape of the overall economic restoration curve, because they take the longest to recover and have the greatest influence on economic activity.

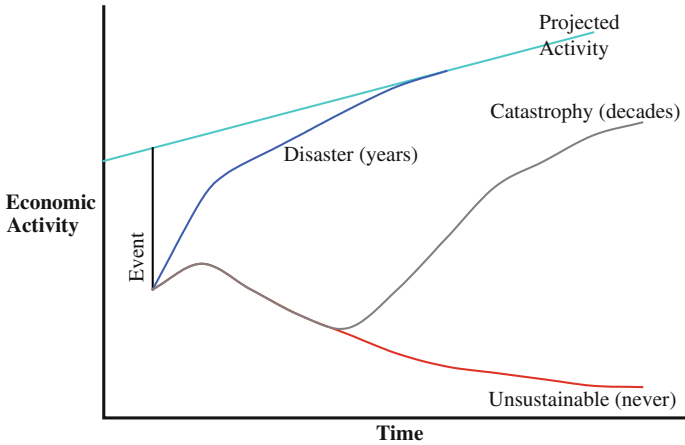


**Fig. 3.9** Megacity resiliency presented in terms of economic activity over time. Recovery time is a function of all urban systems

### 3.9 Future Directions of Lifeline Systems for Sustainable Megacities

As indicated in Fig. 3.9, a sustainable megacity is resilient. Megacities depend upon all its systems to function. The failure of a single system can trigger a cascading effect on all systems, potentially leading to unsustainability. Preparedness requires developing resilient lifeline systems by understanding their complex interdependencies and by integrating multiple systems. Additionally, the risks and vulnerabilities to hazards can be overcome through improvement and better use of the existing infrastructure systems.

Studies such as the ShakeOut Scenario in the Los Angeles megacity expose the complex interdependencies of lifeline systems that have evolved independently. These and other studies reveal vulnerabilities that megacities may have to extreme regional events. Lifelines of the future must be resilient to anticipated hazards and instrumental to the recovery of disaster stricken communities. This requires developing smart infrastructure with advanced modeling systems, real-time monitoring, and improved instrumentation with inter- and intra-system communications. Smart systems must be reliable under normal and extreme conditions and will need to assist managers in making critical decisions for daily operation and maintenance activities and during emergency response. The management of infrastructure assets, under normal or extreme conditions, must be risk based; anticipated system failure, from a simple component to system wide collapse, must account for casualties, total cost of damage, direct and indirect impacts from loss of supply, and regional economic impacts. The systems within the megacities must be viewed from multiple scales ranging from local, regional, national, international, to global.

Future directions in lifeline systems require improved interactions between the interdependent systems and improved inter-agency coordination. In order to make needed improvements, transformative research is needed to better understand how interdependent systems interact and to develop decision support tools to aid in understanding how different complex systems perform under normal and especially extreme events. Future infrastructure systems should reduce hazards created by mega-systems (e.g. ecological and carbon footprint) with smarter infrastructure and improved resource management systems (e.g., water recycling and storm water capture).

Lifelines are only a part of the framework of infrastructure systems (Fig. 3.4). Using the example of Los Angeles water system performance during the ShakeOut Scenario, and only considering the interaction between water system serviceability and fire following earthquake, the subsequent legal, political, social, and economic aspects and consequences can be contemplated:

- Who is legally responsible for providing water for firefighting under such a disaster? Water systems typically supply fire hydrants to fire departments for fighting fires, which may not be serviceable following a major earthquake.
- Following the super conflagrations as described in the ShakeOut Scenario, the political leaders need to answer questions about why such large fires occurred and why they were difficult to put out. The water and fire department leaders likewise need to inform the impacted communities and political leaders.
- Social unrest may likely arise in the form of looting, riots, and violence in different parts of the city. The central Los Angeles area having the super conflagration shown in Fig. 3.9 has a history of civil unrest in 1965, 1992, 2000, and 2009, which should rematerialize following a major earthquake, further compounding the disaster. It will also inhibit the water system from being repaired and keep the firemen from fighting fires.
- The economic consequences from fire following earthquakes were addressed as part of the ShakeOut Scenario (Jones et al., 2008), but did not consider effects from potential social unrest or the political and legal consequences from major fires without a serviceable water system.

The use of advanced technologies to better understand complicated interactions between lifeline systems and other infrastructure systems will lead to new and innovative methods for developing, managing, and operating infrastructure systems in the future.

### 3.10 Conclusion

Sustainable megacities must: (1) have infrastructure systems compatible with the local culture and values; (2) not consume more resources than what the ecosystems can replenish; (3) not dispose of more waste than the ecosystems can safely

absorb; and (4) be strengthened and prepared to resist all hazards threatening them. The concept of sustainability includes surviving potential disasters that may strike. In order to survive a disaster a megacity needs critical infrastructure systems that are resilient to hazards. Earthquakes pose the greatest natural risks to megacities (Munich Re, 2004), and the resiliency of megacities is directly related to the resiliency of their water systems (Davis, 2008). Megacities function as a mega-system made up of multiple subsystems developed separately. Examples of conglomerated megacity infrastructure systems were provided for Los Angeles. The simulated performance of water supply systems in Los Angeles following a great earthquake show the need for resilient lifeline systems and the complicated interactions between critical infrastructure systems. Future directions of lifeline systems include smart infrastructure with advanced modeling systems, improved interactions between interdependent systems, and improved inter-agency coordination. Transformative research is needed to develop a better understanding of the complicated systemic interactions caused by various hazards and reinvent future lifeline systems in megacities. The general conclusions regarding water systems performance during earthquakes in Los Angeles are applicable to other megacities, lifeline systems, and hazards.

## References

- Abhat D, Dineen S, Jones T, Motavalli J, Sanborn R, Slomkowski K (2005) Cities of the future, today's mega-cities are overcrowded and environmentally stressed. *Emagazine.com*, vol XVI, no 5, <http://www.emagazine.com/view/?2849>
- Bardet JP, Ballantyne D, Bell GEC, Donnellan A, Foster S, Fu TS, List J, Little RG, O'Rourke TD, Palmer MC (2010) Expert review of water system pipeline breaks in the City of Los Angeles during summer 2009. Report to the Steering Committee on water pipeline breaks of the City of Los Angeles, 9 Apr
- Brundtland GH (1987) *Our common future*. World commission on environment and development. Oxford University Press, Oxford, Great Britain
- Davis CA (2008) Seismic practices to improve water system resilience. Proceedings of the 14th world conference on earthquake engineering, Paper No. S21-015, Beijing, China, 12–17 Oct
- Davis CA (2009) Scenario response and restoration of Los Angeles water system to a magnitude 7.8 San Andreas fault earthquake. Proceedings of the 7th U.S. conference on lifeline earthquake engineering, ASCE, Oakland, CA, 28 June–1 July, Paper 232
- Davis CA (2010) Los Angeles water supply impacts from a M7.8 San Andreas fault earthquake scenario. International Water Association, *J Water Supply: Res Technol – AQUA* 59(6–7): 408–417
- Davis CA, O'Rourke TD (2011) ShakeOut Scenario: water system impacts from A M7.8 San Andreas earthquake. *EERI Spectra* 27(2)
- Dewar M, Epstein D (2007) Planning for “Megaregions” in the United States. *J Planning Literature* 22:108, <http://jpl.sagepub.com/cgi/content/abstract/22/2/108>
- Earthquake Engineering Research Institute (EERI) (2011) “Shakeout,” Special edition on Shakeout Scenario, *Spectra* 27(2)
- Environmental Protection Agency (EPA) (2007) “EPANET”. <http://www.epa.gov/nrmrl/wswrd/dw/epanet.html>
- Haynes KE (2006) Infrastructure: the glue of megacities. Proceedings of the 9th lecture megacities foundation, The Netherlands. <http://www.megacities.nl/>, 3 Jan 2010

- Jones LM, Bernknopf R, Cox D, Goltz J, Hudnut K, Mileti D, Perry S, Ponti D, Porter K, Reichle M, Seligson H, Shoaf K, Treiman J, Wein A (2008) The ShakeOut Scenario. U.S. Geological Survey OFR 2008-1150 and California Geological Survey Preliminary Report 25
- Munich Re (2003) A natural hazard index for megacities. Topics, Annual review: natural hazards of 2002, 10th year, Münchener Rückversicherungs-Gesellschaft, Georisks Research Department, Germany, [http://www.munichre.co.jp/public/PDF/Topics\\_2002\\_NaturalHazardIndex.pdf](http://www.munichre.co.jp/public/PDF/Topics_2002_NaturalHazardIndex.pdf), 7 Jan 2010
- Munich Re (2004) Megacities – megarisks: trends and challenges for insurance and risk management. Knowledge series, Münchener Rückversicherungs-Gesellschaft, Georisks Research Department, Germany, [http://www.munichre.com/publications/302-04271\\_en.pdf](http://www.munichre.com/publications/302-04271_en.pdf), 3 Jan, 2010
- O'Rourke TD, Jezerski JM, Olson NA, Bonneau AL, Palmer MC, Stewart HE, O'Rourke MJ (2008) Geotechnics of pipeline system response to earthquakes. Geotechnical Earthquake Engineering and Soil Dynamics IV (GEESD), Sacramento, CA, May
- Pisano MA (2006) The Southwest mega region. Presentation from the 2006 MegaRegions symposium on 30 Jan 2006, Atlanta, GA, <http://hdl.handle.net/1853/21302>
- Planning Department, City of Los Angeles (2010) City of Los Angeles community planning areas map. <http://cityplanning.lacity.org/>, 7 Jan 2010
- Romero N, O'Rourke TD, Nozick LK, Davis CA (2009) Los Angeles water supply response to 7.8 Mw earthquake. Proceedings of the 7th U.S. conference on lifeline earthquake engineering, ASCE, Oakland, CA, 28 June–1 July, Paper 220
- Romero N, O'Rourke TD, Nozick LK, Davis CA (2010) Seismic hazards and water supply performance. *J Earthquake Eng*, Taylor and Francis, 14(7):1022–1043
- Sadowski A, Lau SSY, Mahtab-uz-Zaman QM (2000) Megacities: trends and issues towards sustainable urban development. Megacities Background Paper, <http://mc2000.arch.hku.hk/Megacities2000.pdf>, 3 Jan 2010
- Scawthorn CR (2008) Fire following earthquake. ShakeOut Scenario supplement study prepared for United States Geologic Survey and California Geologic Survey, <http://www.colorado.edu/hazards/shakeout/fire.pdf>
- Southern California Association of Governments (2009) Census data, <http://scag.ca.gov/census/index.htm>, 3 Jan 2010
- United Nations (2008) World urbanization prospects. The 2007 revision, New York, NY
- United States Census Bureau (2000), United States Census 2000, <http://www.census.gov/main/www/cen2000.html>

# Chapter 4

## Infrastructure

### Embodied Energy and Gas Emission of Geotechnical Infrastructure

Kenichi Soga

**Abstract** Construction of geotechnical structures produces various environmental impacts. These include depletion of limited natural resources, generation of wastes and harmful substances during material productions and construction, ineffective usage of energy during processing of raw materials into construction materials, and emissions of unwanted gasses during transportation of materials and usage of equipments. With increasing interests in sustainability at the global scale, there is a need to develop a methodology that can assess environmental impacts at such scale for geotechnical construction. Using embodied energy and gas emission, quantitative measures of environmental impact are evaluated using a case study of a new high speed railway line construction in the UK. Based on the results, the keys to energy savings are (a) to optimise the usage of materials with high embodied energy intensity value (b) to optimise the transportation network and logistics for processes using primarily low embodied energy intensity materials and (c) to reuse as much materials on-site as possible to minimise the quantity of spoils or distance to disposal sites. The evaluated embodied energy and embodied carbon values are compared to those of other types of structures and of other activities and carbon tax values. Such comparisons can be used to discuss among various interested parties (clients, contractors, consultants, policy makers, etc) to make the construction industry more energy efficient.

#### 4.1 Introduction

Construction of geotechnical structures produces various environmental impacts. These include depletion of limited natural resources, generation of wastes and harmful substances during material productions and construction, ineffective usage

---

K. Soga (✉)

Department of Engineering, University of Cambridge, CB2 1PZ, Cambridge, UK  
e-mail: ks207@cam.ac.uk

of energy during processing of raw materials into construction materials, transportation of materials and construction, and emissions of unwanted gasses during transportation of materials and usage of equipments. Although the assessment of environmental impacts to the local environment/surrounding is a standard practice when there is an infrastructure development, it is less common to consider impacts to the global environment (such as energy resource depletion and global warming). With increasing interests in sustainability at the global scale, there is a need to develop a methodology that assesses environmental impacts at such scale for civil engineering construction.

Past research on the global scale environmental impact in the area of civil engineering focused on the optimisation of residential building design (e.g. Suzuki and Oka, 1998; Guggemos and Horvath, 2006). The environmental impacts considered were the life cycle energy usage of materials, the emission of gases with global warming potential, ozone depletion potential and acidification potential. However, similar studies for geotechnical structures are yet to be conducted. Perhaps it is because such studies appear to be more complicated and less meaningful than ones for the buildings for the following reasons; (1) the design option is strongly site-specific, (2) less design varieties are available, (3) installation processes described at the design stage often does not reflect what actually happens on sites, partly due to complicated geotechnical profiles and/or conditions around the site; and (4) their service lives are long compared to buildings, and relatively negligible amount of operational energy is required, i.e. much more energy consumed for lighting and heating of buildings than painting of walls.

Another difficulty in assessing the global scale environmental impacts of a large civil engineering construction project is that a full life cycle analysis, which is traditionally used to analyse the environmental performance of products and services, requires substantial amount of time and resources. In order to encourage efforts by practicing engineers to reduce the environmental impacts as the industry, it is necessary to develop a simple methodology that allows optimisation of geotechnical engineering design with an objective to reduce certain environmental impacts.

This chapter describes the results of case studies that examined the embodied energy and the CO<sub>2</sub> emission associated with the construction of geotechnical structures, which were part of a new high speed railway line construction in the UK (Chau et al., 2011). The significance of the engineering work in terms of energy savings and gas emission reduction is discussed.

## 4.2 Channel Tunnel Rail Link (CTRL)

The Channel Tunnel Rail Link (CTRL) is a new high speed railway line running for 108 km between the Channel Tunnel and St. Pancras Station in London and includes over 40 km of tunnel under the streets of London. Upon completion, it halved the Eurostar train journey time to the Channel Tunnel. Figure 4.1 shows the sections of the CTRL near the London area.

### Case 1 – Twin-Bored Tunnel – Contract 220

The first case study focuses on the section of the London tunnel running from Stratford to London St. Pancras, also known as Contract 220 (see Fig. 4.1). It is a twin bore tunnel with two 7.15 m diameter tunnels, each 7.5 km in length, running side by side each carrying a single rail track. The construction required the excavation of a 1 km long subsurface diaphragm “box” at Stratford (as a separate contract), from which the tunnel drive began towards St. Pancras using two 1100 tonne shield machines.

A typical cross-section is shown in Fig. 4.2. The tunnel lining segments are made of reinforced concrete of 1.5 m long and 350 mm thick; 9 segments and a key were grouted together to compose each ring. Spoil from the tunnels was re-used to raise the Stratford railway lands around the “box” by an average of 6–7 m.

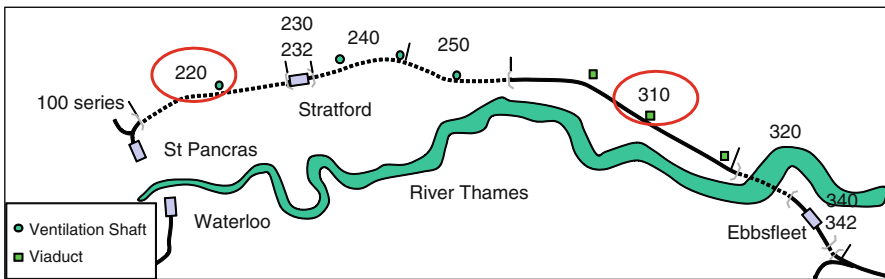
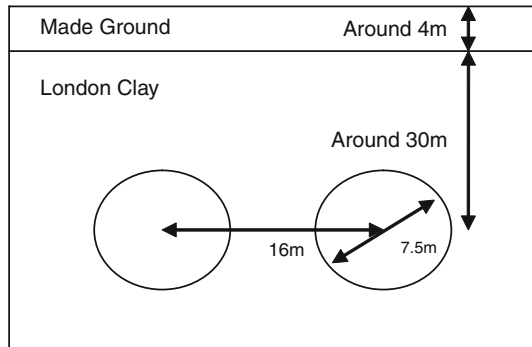


Fig. 4.1 The locations of Contract 220 and 310

Fig. 4.2 Typical tunnel section



### Case 2 – Pile-Slab – Contract 310

The second case study evaluates 7.3 km of the 11.4 km section running between West Thames Ripple Lane and Thurrock Tunnels known as Contract 310 (see Fig. 4.1). This section entails several types of constructions such as pile slab

structures, three types of ground improvements, a bridge, viaducts, a ventilation shaft and embankments. This study examined only in the designs over the alluvium section and therefore excluded approximately 4 km of bridges and viaducts.

The ground profiles along Contract 310 consist primarily of soft alluvium, which is problematic for its susceptibility to the large dynamic loads from the high speed rail. The chosen pile-slab design inserts rows of piles of 10–20 m to the underlying layer which is overlain by concrete slabs, then ballasts, sleepers and rail. Figure 4.3 is a schematic of a typical pile slab structure adopted.

The pile types included continuous flight auger (CFA) piles, contiguous modulus columns (CMC) and driven concrete piles (DCP). The pile types were chosen according to the strength of the local soil. In the weakest marshy areas, CMC piles of 360 mm diameter were installed and overlain with a reinforced soil embankment. Each row of CMC had an average of 13 columns of spacing approximately 2 m to accommodate for the width of the embankment. The distance between each row was around 2 m, the length of section that required CMC was 510 m.

Rows of 4–7 CFA piles or DCPs of 600 or 750 mm diameter were used at locations that the subsoil was stronger than the marshy areas. DCPs were used when piles of up to 15 m were required, while CFA piles were used for depths of 15–25 m. The spacing between each row of piles was approximately 5 m and the lengths of sections that required CFA piles or DCPs were 2.5 and 2.4 km respectively. Concrete slabs were constructed on top of the CFA piles and DCPs; this was the most common configuration for Contract 310. On the straight sections, the slabs were constructed in sections of 60 m in lengths, with widths of 11.6 m and they overlaid rows of 4 or 5 piles. Wider slabs were used at junctions where more piles were required. A layer of sub-grade and ballast, each of 200 mm thick were laid, then sleepers and rails

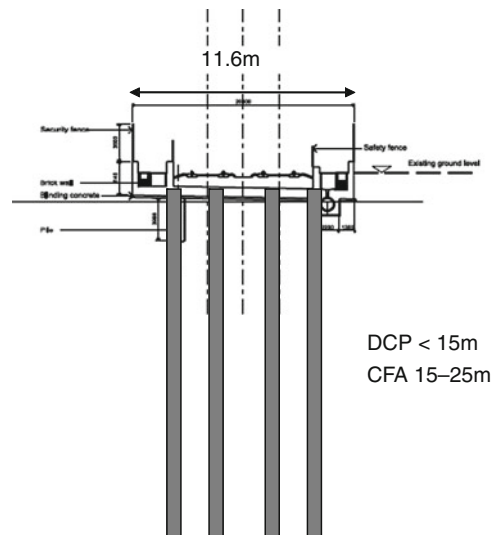


**Fig. 4.3** Typical cross section of pile slab

were constructed on top of the pile-slabs. At noise sensitive areas, a sound barrier was also built.

For areas with chalk as the main ground profile, where it is strong enough to support the load alone, no piles were added. A soil embankment was built to adjust for the rail's vertical alignment, on top of which the ballast and sub-grades were found.

### ***Case 3 – Alternative Hypothetical Embankment Design for Contract 310***

At the design stage, an alternative design using a soil embankment was proposed as shown in Fig. 4.4. In this study, a set of calculations was carried out where all the piled slabs in contract 310 were replaced with an embankment. The design would require a 4.5 m high soil embankment; the thickness of embankment was derived from a dynamic analysis conducted by Arup. The embankment would be made of general fill, with 1 in 2 side slopes and a crest width equal to that of the piled slab.

Assuming that the total settlement of the embankment over the 60 years of earth-work design life (note that the design life for the piled slab system is 120 years) is 1 m; the minimum height for noise barriers terminating at 1 m above rail level is thus about 4.5 m, which is higher than that required for the piled slab.

During construction, the embankment would require ground treatment/surcharge. As a benchmark, a 1 m surcharge thickness during the construction period was assumed (i.e. around 5.5 m general fill thickness, of which about 1.5 m would be removed prior to placement of sub-ballast and ballast). To ensure minimal differential consolidation movements over the long term, a ground treatment in the form of vertical 100 mm wick drains at 1 m triangular centres with an average depth of 10 m into the alluvial/fluvial deposits was assumed. Identical ballast and sub-ballast allowance is taken to be the same as for the pile slab.

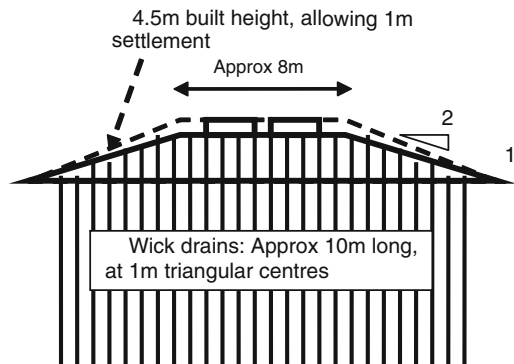


**Fig. 4.4** Alternative embankment design

### 4.3 Calculation Methodology

This study is a retrospective evaluation of the embodied energy of the built structures. The unit of embodied energy (EE) is joules. By definition, it is the total energy that attributes to bringing a particular item to its existing state. This metric can be used in a LCA approach. The advantage is the simple metric allowing comparison among a range of construction methodologies with similar performance criteria. There are also known relationships between EE and carbon dioxide emissions.

In this study, the boundary of the embodied energy calculation starts from the extraction of raw materials and ends at the point when the constructions are completed. Once the goals and study boundaries are established, it is followed by a systematic examination of all the stages involved in the construction. Then detailed data acquisition is required to assess the quantities of materials or machineries used, transportation distances, construction processes and duration of machineries usages for each process stage; followed by the EE evaluation for each process stage.

For the ease of analysis, this study categorises the processes into three types: (a) materials, (b) transportation and (c) installation. An extra type of manufacturing of dedicated shield machines is explored for the tunnel case.

The basic calculation rationale is as follows:

- Material energy is found by the total volume of each material used, hence the weights and multiplying them by their respective Embodied Energy Intensity (EEI) value.
- Transportation energy includes the moving of the machineries and the materials used, thus it is calculated using the litres of fuel consumed by the vehicles multiplied by the EEI of fuel. Alternatively, some EEI are presented as simple MJ/tonne-km values. Calculations are based on returned journey for means of transport except shipping, which is seldom returned empty; this represents the conservation estimation.
- Installation energy is the amount of energy consumed on site to operate the machineries such as the shield machines; this is evaluated as the product of the amount of fuel and/or electricity consumed and their EEI value.
- Manufacturing energy includes the manufacturing of pre-cast piles and tunnel segments. This is evaluated in similar ways to the installation energy.
- The sum of the material, transportation, manufacturing and installation energy would give the total embodied energy.

#### 4.3.1 Embodied Energy Intensity and Fuel Consumption Factors

This study calculates the embodied energy using published Embodied Energy Intensity (EEI) values. EEI indicates the amount of embodied energy required in producing 1 kg of construction material from the point of resource extraction to the end product; its units are MJ/kg for solids or MJ/l for liquids.

There has been research into EEI values since late 1970s from both the public and private domains. However, there is sometimes a wide range of values found

for certain materials such as steel and aggregates. The varying in value can be due to the different types of material specification in question, the assumptions and/or the study boundaries drawn for the EEI evaluations. For example, notable difference is observed between steel produced via the Electric Arc Furnace (EAF) route compared to the integrated steel making route that is based on the Blast Furnace (BF) or Basic Oxygen Furnace (BOF). The former uses primarily recycled scrap iron and steel and electricity, while the latter uses raw materials including iron ore, coal, limestone and some recycled steels. The average typical EEI values of steel via these routes are roughly 10 and 24 GJ/t, with ranges of 10–19 GJ/t and 20–60 GJ/t, respectively. The construction steel one purchases in the form of rebar or sheet piles would generally consist of a variable steel mix produced via both routes depending on availability. Therefore an adopted EEI value for steel is often a subject of discussion in any study.

Fuel consumption rates suffer from similar uncertainties, as these rates are functions of vehicle specifications, speed (including acceleration and breaking), loading and even road gradients etc. Three sources are used in an attempt to eliminate possible biasness from any one source.

The materials EEI and fuel consumption adopted comes from the following five publications:

- Hammond and Jones (2006) deduced a set of recommended ranges of EEI values for the most commonly used building materials suitable for the UK condition from a summary of publications from around the world.
- Kiani (2006) performed a similar exercise with fewer sources, more types of materials and does not have a recommended range. This study discards values which are more than two standard deviations from the mean and then adopts the mean value from the remainders.
- Howard et al. (2000) published guidance for conducting EE LCA with some EEI.
- Highways Agency (2007) Design Manual for Roads and Bridges, Vol. 11, Section 3, Part 1 gives fuel consumptions rates in l/km as a function of speed for seven types of vehicles.
- The Ministry of Land, Infrastructure and Transport in Japan (2008) published a detailed construction machinery models and specification manual which includes detailed fuel consumption rates for most individual machineries used in construction.

Table 4.1 lists the mean and the range of the materials EEI values adopted. The mean values are used for the main EE calculation; the ranges are used for sensitivity analyses.

### ***4.3.2 Data Collection and Uncertainties***

Data was obtained directly from the tunnelling contractor, Nishimatsu Construction, and the shield manufacturer, Kawasaki Heavy Industries, for Section 220 and the archives of the Rail Link Engineering (RLE) for Section 310. The amount of

**Table 4.1** Examples of EEI values used in this study

	EEI (MJ/kg or MJ/l)		
	Mean	Min	Max
Aggregate	0.15	0.05	1
Adhesive	87	60.9	113.1
Cement	4.8	2.8	6.8
Copper	50	44	100
Fiberglass	77.2	95.1	67.5
Fibrin 23	64	44.8	83.2
Low density polyethylene (LDPE)	78.1	67.8	103
Grease	49.6	34.72	64.48
Paint	80	54	98.1
Pulverised fuel ash	0.22	0.154	0.286
Rubber	101	90	120
Steel	24	9	35
Steel frame	27	12	38
Water 799 l/m <sup>3</sup>	0.00078	0.00055	0.00101
Diesel	37.2	–	–

materials consumed was estimated through the structural drawings and concrete records. The transportation routes and distances were evaluated with road journey planning software, port distance calculations and the National Rail Route Map. For other unknown materials and machineries suppliers, the nearest suppliers by distance were assumed to be used. The rates of construction were estimated from the method statements and the weekly piling records. The electricity and fuel consumption were based on companies' electricity bills and the sum of the products of the period of time when the machineries were use and their rate of fuel consumption.

The quantities of materials used were generally assumed to be accurate as they were based from final built versions of the drawings. However, for transportations and installations, estimations had to be made for some transportation distances and duration and/or efficiencies of installation, together with the known-unknown uncertainties in the fuel consumption factors; it was decided that sets of defined multipliers of 90 and 200% or 80 and 200% were used on the mean values to model the uncertainties from transportation and installations respectively. Although crude, this should reasonably represent the possible ranges these energy.

Further details of the calculation methodology as well as some other examples can be found in Chau et al. (2006, 2008, 2011) and Inui et al. (2011).

## 4.4 Results and Discussion

Figure 4.5 shows the total embodied energy of the three cases in TJ. For analysis purposes, the different shadings indicate the breakdown of the energy consumption by materials, transportation, manufacturing or installation. The error bars are strictly

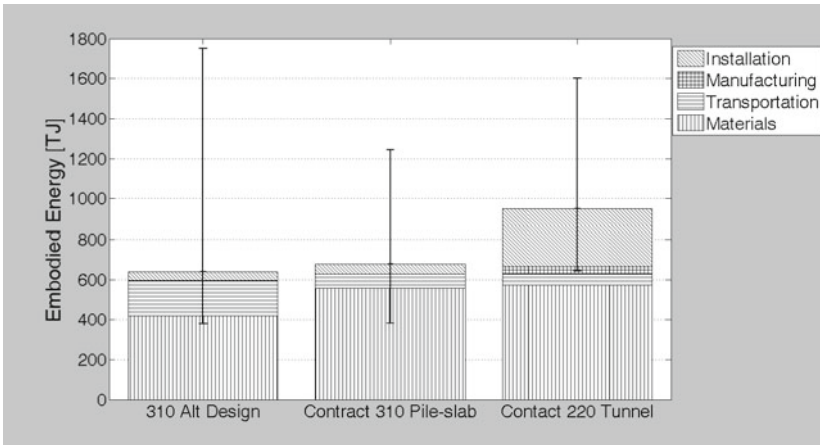


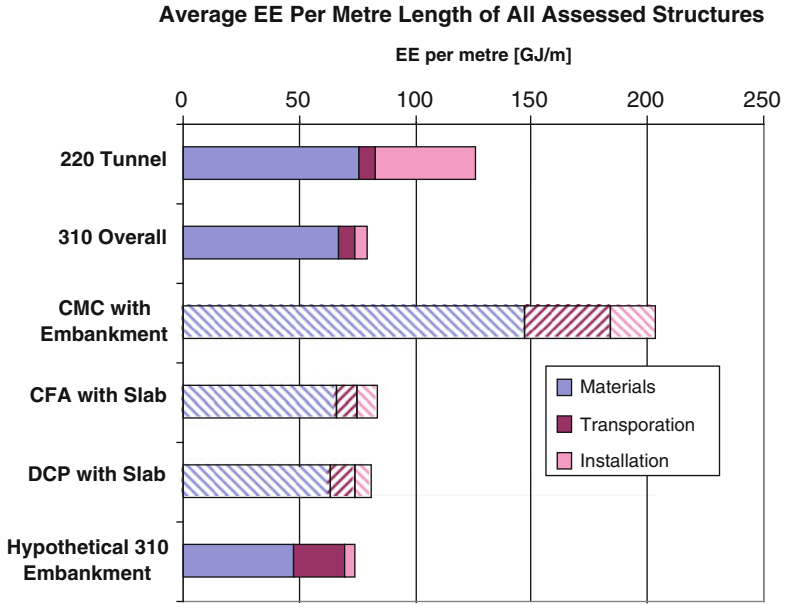
Fig. 4.5 Total embodied energy of Contract 220, 310 and a 310 alternative design

not errors, but they indicate the possible ranges of energy due to the uncertainties explained above. Figure 4.6 shows (a) the embodied energy values per metre for each construction type and (b) percentage contributions of materials, transportation and installation for each construction type. Further details of the results are given in Chau et al. (2011).

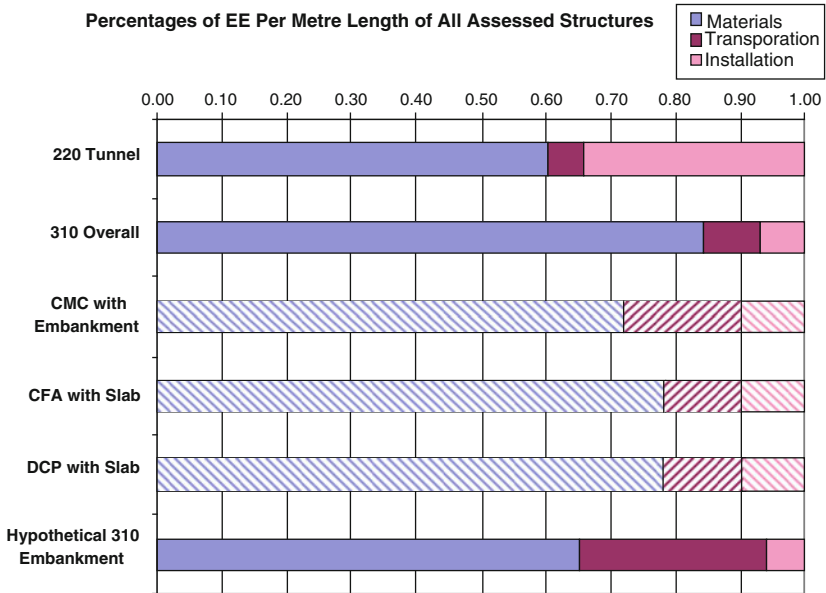
### Case 1 – Twin-Bored Tunnel – Contract 220

The total initial embodied energy of the C220 tunnel construction is estimated to be 949 TJ or 126 GJ/m of the 7.5 km twin bored tunnel. The embodied energy of the construction materials contributes the majority with 573 TJ (61% of the tunnel’s total energy). The energy used in transportation involved with comes to 54 TJ (6%), while the energy in manufacturing the shield machines and the tunnel lining segments is 40 TJ (5%). Another large consumer is the energy during installation which employs 283 TJ (30%), which was used to run the TBM. As shown in Fig. 4.6b, such a large installation energy value is unique for tunnel construction; material energy usually dominates in other geotechnical construction.

Table 4.2 lists energy efficiency values of different excavation processes (tunnel boring machines, hand-digging by human and ants). The energy efficiency is expressed as the energy used to excavate 1 m<sup>3</sup> of soil or rock material. The CTRL tunnelling case shows that  $4.4 \times 10^8$  J was needed to excavate 1 m<sup>3</sup> of soils under London. This is at least one order greater than the energy used by hand digging or two to four orders greater than the energy used to build an ant nest by ants. It appears more energy savings could be made by improving the efficiency of tunnel boring machines.



(a)



(b)

**Fig. 4.6** Embodied energy contributions. (a) Embodied energy value per metre; (b) percentages of EE per metre length

**Table 4.2** Energy efficiencies of various excavation process (after Santamarina, 2007, personal communication)

	Efficiency J/m <sup>3</sup>	Soil/rock	Location	Source
TBM	$4.4 \times 10^8$	London, Lambeth	London, EPB	This study
	$3.0 \times 10^8$	Rock	San Manuel Mine, Arizona	Cigla et al.
	$1.5 \times 10^7$	Sand	Yellow River, China	Robbins Company
Human	$1.0 \times 10^7$	Silt	Backyard	Santamarina/Soga
Ant	$1.2 \times 10^4$	Sand	Florida, USA	Tschinkel
	$7.9 \times 10^5$	Sand	Florida, USA	Mikheyev and Tschinkel

The construction process that gives the largest embodied energy is the raw materials of lining segments (37%) mainly because of its large volume. Results reveal that aggregates and the category “others, mainly water” together account for 94% of the mass while only consumes 21% of the embodied energy. This is due to their low embodied energy intensity values and conveys the point that not only is the quantity of materials used important but also their embodied energy intensities are even more so.

Some 1.4 Mt of spoil was reused at Stratford, which is located at one end of the tunnel. Tunnelling spoil was allowed to stockpile under the discharge and was dumped and compacted at a convenient time at its point of origin raising the railway lands by around 7 m. In a hypothetical scenario where this did not happen, and that the spoils had to be moved to a landfill elsewhere, Fig. 4.7 shows the extra transportation energy that would have required to move all the spoil to varying distances from the site using 25t trucks or trains. Assumptions are made for return journeys where they are fully loaded on one way and empty on their returns. The results reveal that, if the spoils were removed by truck, movement of the spoil a distance of 150 km in this way would see an increase of 283 TJ (30%) to the total energy while by train would generate a 64 TJ (7%) increase.

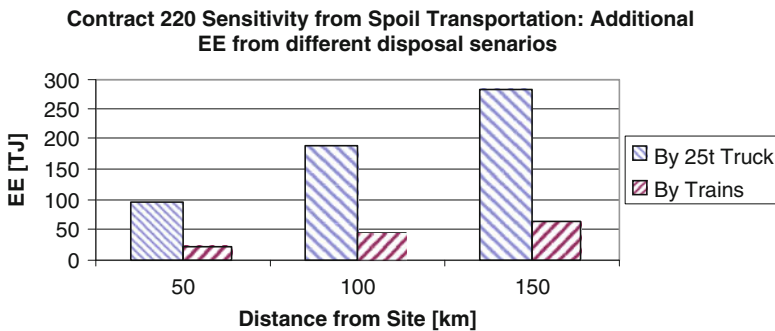


**Fig. 4.7** Extra transportation energy if all the spoil were removed

## ***Case 2 – Pile-Slab – Contract 310***

The embodied energy of Contract 310 sums to 678 TJ. Taking into account only the sections included in this study, 7,295 m of structure is evaluated; this equates to 79 GJ/m of structure. The embodied energy of construction materials contributes to the majority of the overall energy: 557 TJ (82%). The rest is shared by the transportation and installation energy occupying 69 TJ (10%) and 52 TJ (8%) respectively. All the transportation energy is spent on the moving of the materials with less than 1% consumed in the moving of the machineries to and from work-sites. The specifications of the vehicles were obtained from the hiring/transport companies. The installation procedures for each type of pile were found on separate method statements for each sector. All manufacturers that produced the equipment and machinery used for installing piles were contacted to obtain the machine specifications. The pile installation rates were estimated from the construction Gantt chart and the weekly progress reports.

As shown in Fig. 4.6a, the embodied energy value of CMC includes the energy of the embankment that is founded on top; similarly, for CFA and DCP, the values for the slabs are included. For comparison purpose, the energy of rail, sleepers and ballasts is excluded. Comparing the three types of piles used in Contract 310, CMC per metre consumes over 140% more energy than CFA or DCP; due to the amount of materials placed into the ground. The embodied energy per metre of CMC gives the highest values of 189 GJ/m, followed by those of CFA and DCP with similar values of around 75 GJ/m. It seems reasonable as the CMC system was used to improve the weakest marshy grounds.

It is noted here that, at the construction phase for installation of DCP for Contract 310, mistakes during site surveying led to miscalculations of the toe levels and caused the ordering of overlengthed precasted DCP. It resulted in a trimming of approximately 5 m of excessive lengths of many DCPs, resulting in a large amount of material (steel and concrete) wastage equivalent to about 4% reduction of the total energy.

The fact that the energy per metre of CMC being less than that of the tunnel was unexpected, as one may expect tunnel construction to require more energy with its complicated techniques and the building of a TBM. But in fact, the proportion of all energy related to the TBM is surprisingly small at 18% of total, with the use of cement prevailing as the determining factor. However, it is important to note that the TBM energy maybe dependent on the economy of scale where a tunnel of a smaller scale may have a much larger energy per metre.

## ***Case 3 – Alternative Hypothetical Embankment Design for Contract 310***

The total embodied energy of the alternative embankment design comes to 640 TJ as shown in Fig. 4.5 or 74 GJ/m as shown in Fig. 4.6a of the 7.3 km soil embankment required to replace the pile-slab structure evaluated. A 4.5 m high standard double

layered fibreglass reflective sound barrier was designed for this study. The calculation is dominated by the large volume of compacted fill required, the noise barrier design and the transportation associated with long haul distances to import the quarried materials, due to the shortage in SE England.

Figure 4.6 shows that the concrete and steel based pile-slab design proves to be a material (indirect) energy intensive project where the embankment is a transportation and installation (direct) energy heavy type of project, with indirect energy occupying about a third of the total. It can be seen from Fig. 4.6b that about 66% the energy is embedded in the materials. As the EEI of compacted fill has one of the largest range by percentage difference (0.05–1 MJ/kg, average of 0.15 MJ/kg), coupled with the large amount of the materials used, it gives the largest range of uncertainty (see Fig. 4.5).

Due to the large amount of soil imported for the embankment design, the transportation energy occupies 176 TJ (28%) of the total compared to less than 10% of total energy in the other two cases. This can be evidenced by comparing the total weight of materials moved: the almost  $1 \times 10^6$  t of materials for the embankment design is over twice that of the other two designs.

The mean EE values for the two 310 projects assumes half the aggregates and compacted fill are taken in through shipping and all are taken from either quarries from SE England or the port using trains, which is the most energy efficient method on land. If the transportation on road uses a 25t truck instead of the rails, the Contract 310 built design and the hypothetical embankment design results in an additional 53 and 227 TJ respectively (See Fig. 4.8). This makes the latter case a much more energy consuming design than the former. This signifies the importance of choosing the correct mean of transportation, particularly with the transportation intensive type of projects.

The installation energy is 44 TJ (7%). This percentage is similar to that of Contract 310 but much less than that of the tunnel case; suggesting that the building of embankment is a relatively simple construction process, like the

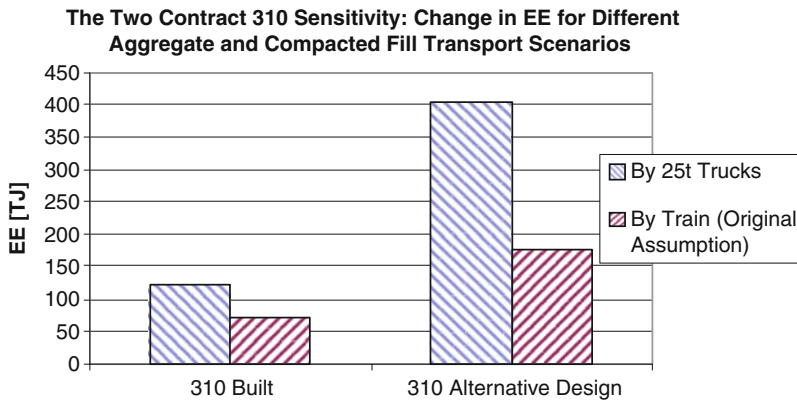


Fig. 4.8 Embodied energy for different transport scenarios

concrete pile-slab structures, compared to the more complex and energy intensive tunnel building.

Figure 4.5 shows the chosen pile-slab design consumes about 6% more energy overall than the hypothetical embankment design, at the order of 650 TJ. Although its mean value is less, the range of uncertainties for the hypothetical embankment design is much larger than that of the pile-slab; due to large range of compacted fill's EEI. Therefore, one can argue that the pile-slab has a much larger probability of being the more environmentally friendly option.

There are various types of uncertainties in this study; some are based on adopted assumptions or problem boundaries and others are due to the quality of data or parameters. Given the same scenarios, the uncertainties due to assumptions of transportations and installations are relatively insignificant at merely +10%. In contrast, the uncertainty due in the materials energy (i.e. uncertainty due to EEI) is very large: it leads to overestimation of +54, +71 and +143% of overall EE for the tunnel, pile-slab and the hypothetical design respectively. This is due to the large quantities of materials required for each case and their large ranges of EEI. This shows that the selection of EEI for any EE study is of utmost importance.

## 4.5 What Do These Values Mean?

It may be worthwhile to compare the numbers obtained in this study to the numbers reported for other types of structures and to examine the importance of the embodied energy or carbon calculation for decision making. Although various numbers quoted and computed in this section are very approximate figures, such comparison and examination would highlight the contribution that geotechnical engineers could make to reduce the global environmental impact.

The total embodied energies of the two cases are 950 and 680 TJ for Contract 220 and 310, respectively. A similar calculation can be conducted for CO<sub>2</sub> emission and the values are approximately 53,000 ton for Contract 220 and 49,000 ton for Contract 310. If we bravely extrapolate these values to the whole length of the CTRL (i.e. 108 km), the estimated embodied energy of the whole project would become approximately 10,000 TJ and the estimated CO<sub>2</sub> emission would be 616,000 ton. If the embodied energy of a typical residential house with a floor area of 100 m<sup>2</sup> is around 200 GJ (Sustainable Homes, 1999), the energy used to construct CTRL is equivalent to that of 50,000 houses. This is roughly equal to the number of new houses built in the UK every 6 months.

The energy used to travel 100 people every kilometre is 245 MJ for car and 22 MJ for train. The difference is therefore 223 MJ/100 people every kilometre. Approximately 10 million uses Eurostar every year to travel through the Channel tunnel between the UK and France. As a hypothetical scenario (but probably not realistic), if all these people use the new train line to the entrance of the Channel tunnel rather than drive there by car, the saving will be 2,400 TJ every year. Hence the energy payback is 4 years, which is much smaller than the design life of the

railway. Similar calculation can be made for different scenarios and other methods of transport.

A typical person in the UK consumes about 450 MJ/day (=125 kWh/day/person by MacKay (2008)) or 160 GJ/year for transport, heating, electrical things, etc. If CTRL operates for 100 years, the energy usage per person for the same duration becomes 16 TJ. Hence the CTRL construction energy is equivalent to the consuming energy of 625 people. The debate then becomes whether this number is large or not. For example, one (as an extreme) may argue that the energy produced from the limited natural resources was wasted to the construction and affected the lives of 625 people. If each person is worth about 2 million pounds in the UK insurance term, the equivalent monetary value will be 1.25 billion pounds.

The CO<sub>2</sub> emission from the CTRL construction was 616,000 ton. If we use the current carbon tax price of £10/tonne, then the amount of CO<sub>2</sub> emission becomes equal to £6.2 million. On the other hand, the total cost of the CTRL project was approximately £5 billion. Hence the additional cost to pay the carbon tax will be only 0.1% of the total cost of the project. This indicates that the carbon tax will probably not make a significant impact to change the details of the CTRL project (for example construction methods, route, etc). Even if the carbon tax becomes £100/tonne, which starts to make impact on domestic heating (MacKay, 2008), the total carbon tax would be £62 million, which still is small compared to the project cost. Perhaps the driver to reduce the embodied energy or carbon has to come from the political and the moral interests of the parties involved in the project.

## 4.6 Conclusions

The embodied energies of two built sections of the CTRL and an alternative design were evaluated in this study. The Contract 220's 7.15 m diameter twin bored tunnel section of 7.5 km has an embodied energy of 949 TJ, while 7.3 km of the Contract 310's consisting mainly of the pile-slab section consumed 678 TJ when a alternative embankment design would have consumed 640 TJ but with a larger uncertainty. Although there are differences in the embodied energy mix of the three cases, materials is the dominating energy consumer. Out of the three cases, there are two types of constructions: (1) Pile-slab structure where the materials are totally dominant at approximately 90% of the total energy, and (2) a more direct energy intensive construction where the sum of transportation and installation energy can be as much as 40% of the total, the tunnel and embankment are examples of this. Understanding the energy mix and uncertainties of a construction is the key to good project management. For example, e.g. optimisation in distances of compacted fill import and understanding the energy efficiencies of the processes involved are crucial factors for energy minimisation in the building of embankments. Another important point to note as is the maximisation of reuse of spoils within the site, as demonstrated in Contract 220, in contrast to the wasted lengths in piles experienced in Contract 310.

Based on the results, the keys to energy savings are (a) to optimise the usage of materials with high EEI value (b) to optimise the transportation network and logistics for processes using primarily low EEI materials and (c) to reuse as much materials on-site as possible to minimise the quantity of spoils or distance to disposal sites. Opportunities for energy/cost savings and wastages are equally ubiquitous: detailed surveys, the reuse of spoils, the location of landfills and the means of transport can all individually be a determining factor for the outcome. The evaluated embodied energy and embodied carbon values were compared to those of other types of structures and of other activities and carbon tax values. Such comparisons can be used to discuss among various interested parties (clients, contractors, consultants, policy makers, etc) to make the construction industry more energy efficient.

**Acknowledgments** The author would like to thank Chris Chau, Ronan Workman, and Wilson Kwang, who conducting the case studies as part of their PhD or Masters projects, Arup and EPSRC for their financial support and Nishimatsu Construction, Kawasaki Heavy Industries and RLE for providing their valuable data. The details of the case study described in this paper are given in Chau et al. (2011).

## References

- Chau C, Soga K, Nicholson D (2006) Comparison of embodied energy of four different retaining wall systems. In: Butcher AP, Powel JJM, Skinner HD (eds) Reuse of foundations for urban sites: proceedings of international conference. IHS BRE Press, Bracknell, UK, pp 277–285
- Chau C, Soga K, Nicholson D, O’Riordan N, Inui T (2008) Embodied energy as an environmental impact indicator for geotechnical infrastructures. In: Alshawabkeh AN, Reddy KR, Khire MV (eds) Proceedings of the GeoCongress. ASCE, USA, pp 867–874
- Chau C, Soga K, Nicholson D, O’Riordan N (2011) Embodied energy evaluation for sections of the CTRL. Proceedings of the ICE-Geotechnical Engineering (accepted for publication)
- Guggemos AA, Horvath A (2006) Decision-support tool for assessing the environmental effects of constructing commercial buildings. *J Archit Eng* 12:187–195
- Hammond GP, Jones CI (2006) Inventory of (embodied) carbon & energy (ice). Department of Mechanical Engineering, University of Bath, UK
- Highways Agency (2007) Design manual for roads and bridges; vol 11: Environmental assessment; Section 3: Environmental assessment techniques; Part 1: Air quality, London: The Stationery Office Ltd.
- Howard N, Edwards S, Anderson J (2000) BRE methodology for environmental profiles of construction materials, components and buildings. BRE and DETR, London
- Inui T, Chau C, Soga K, Nicholson D, O’Riordan N (2011) Embodied energy and gas emissions of retaining wall structures. *ASCE J Geotech Geoenviron J* (accepted for publication)
- Kiani M (2006) The whole life environmental impact of glass within glazed commercial building envelopes. Ph.D thesis, University of Brighton, Brighton
- MacKay DJC (2008) Sustainable energy – without hot air. UIT Cambridge Ltd., Cambridge, 380 pp
- Ministry of Land, Infrastructure and Transport, Japan (2008) Construction machinery models and specifications manual (in Japanese). ISBN : 978-4-7676-7307-3
- Sustainable Homes (1999) Embodied energy in residential property development, Hastoe Housing Association, 15 pp
- Suzuki M, Oka T (1998) Estimation of life cycle energy consumption and CO<sub>2</sub> emission of office buildings in Japan. *Energy Build* 28:33–41

# Chapter 5

## Geotechnics and Society

### Carbon, a New Focus for Delivering Sustainable Geotechnical Engineering

R. Scott Steedman

**Abstract** In the UK today, sustainability is seen as embracing a wide range of issues that engineers have to consider in projects, from biodiversity to employment. Sustainability risks becoming diluted to the point that it represents “business as usual”. The consequence of the Copenhagen summit of December 2009 for the engineering profession may be that we start to see carbon as a primary design determinant, not simply as one of a list of desirable environmental outcomes to be traded one against the other. As a proxy, carbon is now providing the focus for political action that sustainability could never achieve. In this context, arguments over climate change science and the extent of man’s contribution to global warming have become irrelevant. The much quoted 1987 Brundtland Commission definition of sustainability as “development which meets the needs of the present without compromising the ability of future generations to meet their own needs” is unhelpful in the sense that it sets no base standard against which the engineering profession can deliver buildings and infrastructure that will have an impact over many future generations. It is imperative politically that public confidence is maintained in any lifestyle changes that may be required over the decades ahead. A more useful definition of sustainability for policy makers and the engineering profession would reflect the importance first, of technological innovation and second, of setting a baseline for engineers to design against: “Sustainability is managing our use of resources, energy and human capital to ensure that future generations have the potential to enjoy a quality of life at least as good as our own”. For the geotechnical engineering community, the key issue for debate will be how the emerging low carbon economy will affect the design and delivery of low-carbon infrastructure, such as transportation projects, renewable energy or a new generation of nuclear power plants. The maintenance and upgrading of existing infrastructure, such as water and waste water systems, road and rail infrastructure or flood and landslide protection will also require fresh thinking to minimise use of materials, energy and labour. The challenge for geotechnical engineers is to recognise that after years of important but

---

R.S. Steedman (✉)  
Steedman & Associates Ltd., W8 7ST London, UK  
e-mail: contact@scottsteedman.com

low level commitment to sustainable engineering solutions, very soon we will be required to design, to tender, to construct and to operate our buildings and infrastructure not only within the usual constraints of time and money but also within the constraints of carbon accounting. For geotechnical engineers around the world this will require new models, new tools and new training, all of which need urgent research and rapid implementation.

## 5.1 Introduction

The Copenhagen Accord reached on 19 December 2009 with the support of China and the US may be the first real steps taken by the international community towards a new, global low carbon economy. The importance of this cannot be underestimated for the engineering profession. Informed clients have demanded more “sustainable” engineering solutions from our industry for some years, but sustainability as a concept has become diluted.

In the UK today, sustainability is seen as embracing a wide range of issues that engineers have to consider in projects, from biodiversity to employment. Sustainability as a concept now represents “business as usual”. Environmental Impact Assessments are carried out; boxes are ticked, yet we cannot point to any significant advance in geotechnical engineering over at least the last 20 years that has resulted from considerations of sustainability to reduce our use of materials, energy or labour. Such advances that have occurred have happened as a result of traditional business processes. Our capability to innovate in codes and standards or to introduce new construction products is painfully slow. Indeed the “innovation cycle” in civil and geotechnical engineering is probably of the order of 15–25 years. This will not achieve the step change that is required if the geotechnical profession is to play its part in reducing our footprint on the planet in time to meet the pressures of rising population and increased consumption worldwide.

## 5.2 A New Definition of Sustainability

The consequence of the Copenhagen summit of December 2009 for the engineering profession may be that we start to see carbon as a primary design determinant, not simply as one of a list of desirable environmental outcomes to be traded one against the other. As a proxy, carbon is now providing the focus for political action that sustainability could never achieve.

In this context, arguments over climate change science and the extent of man’s contribution to global warming have become irrelevant. For the engineering profession, the 1987 Brundtland Commission definition of sustainability could be usefully updated to focus on the trajectory ahead, perhaps along the lines: “Sustainability is managing our use of resources, energy and human capital to ensure that future generations have the potential to enjoy a quality of life at least as good as our own”. Innovation – achieving more for less – is the key to achieving a sustainable future.

### ***5.2.1 The European Construction Industry***

Before examining the role of the geotechnical profession, it is worth reviewing the scale and importance of the construction industry in Europe. European construction faces competition from developments in the US and in the Far East and must innovate to survive. The industry is a key element of the European economy.

FIEC, the European Construction Industry Federation's annual report covering the EU27 concludes that European construction in 2009 was around 9.9% of GDP or about EUR €1173 Bn pa, slightly down on the numbers for 2008. The market is divided in four major sectors: 29% rehabilitation and maintenance, 18% new house-building, 31% non-residential building and 22% civil engineering (FIEC, 2009). Construction is responsible for around 14.9 million jobs, 7.1% of all jobs, 29% of industrial employment. This means that construction is the largest employer in Europe.

Enterprises working in construction are thought to number around 3 million, the vast majority of which are SME (small and medium sized enterprises). An interesting study of European SMEs by EURAB (European Research Advisory Board) suggests that there are major differences between innovation leaders and followers (EURAB, 2004). The EURAB analysis found that less than 3% of the sector (by number) could be classed as "technology pioneers", with a high level of involvement in R&D (research and development). Less than 10% were deemed capable of developing new knowledge and technology and were classed as "leading technology users". A larger group, perhaps around 20% were considered to be capable of adopting new knowledge and technology but the large majority, around 70%, were classed as "basic" companies, driven entirely by following norms and guidance.

The implication for the construction sector is that different strategies are needed to achieve innovation in different sectors of the industry. For a small number of companies, it may be appropriate to focus on innovation tools and new technologies. For the majority of companies, however, it is essential to shorten the cycle of new norms, guidance, codes and standards.

The length of the innovation cycle is a crucial parameter in the capacity of the industry to adapt to new circumstances. In geotechnical engineering, the evidence suggests that the widespread take up of innovations takes perhaps 15–25 years from research to mainstream practice. Examples of major transformational technologies in geotechnical engineering which took many years to be adopted widely across industry include diaphragm walling (first pioneered in the early 1950s), NATM (introduced around 1964) and geosynthetics (introduced in the late 1970s). This is very different to the length of the innovation cycle in other engineering sectors, which can be as low as a few years. For example, each new generation of mobile telephony since the 1980s has brought orders of magnitude improvements in capability and entire new ranges of products by manufacturers – first in the transition from analogue to digital, and then from 2G to 3G and now 4G (fourth generation) systems. The length of the innovation cycle in construction is a major barrier to industry transformation in Europe.

In the UK SMEs also dominate the construction sector. Figures suggest that the number of companies active in construction in Britain with less than 10 employees is probably in excess of 70,000 (Office for National Statistics, UK). Overall, the industry employs around 2 million people in more than 250,000 companies and has an annual turnover of more than £100 Bn. Although the industry appears to be dominated by a few “famous names”, in practice professional engineers are spread across a very large number of companies operating in the sector. This fragmentation of the industry is a second factor that makes industry transformation particularly difficult to deliver.

For the geotechnical engineering community, this means that any initiative to introduce new methods of working, new products, codes or standards aimed at a low carbon model of sustainability must reflect the wide range of attitudes towards new knowledge and capability to take up new knowledge that is found across the industry. Different strategies will be needed for different parts of the community.

### **5.3 The Political Imperative**

In the UK, there are a wide range of political drivers that are now affecting the industry. Government has recently taken steps to try to improve the industry’s performance. The engineering profession, through the Royal Academy of Engineering and the Institution of Civil Engineers has been very active in responding to Government’s concerns and has proposed initiatives at a number of different levels.

In the UK the construction industry is perceived by government to be expensive, time consuming and of mixed quality. The sector is also often characterised as being mainly “old jobs” (dirty, difficult, dangerous) as opposed to the service sector or “new jobs” in high tech industries.

Energy security and better regulation are important political drivers, and climate change policy has led to new measures to address adaptation and mitigation and the retrofit of the existing building stock. The UK Government passed a Climate Change Act in November 2008, making the UK the first country in the world to have a legally binding long-term framework to cut carbon emissions.

Carbon budgets have now been imposed on government departments with aggressive targets to be achieved between now and 2020. Industry in the UK cannot achieve these targets by following a “business as usual” approach and instead will need to make a step change in performance.

In the run-up to Copenhagen and in the months since the conference, following one of the worst winters for decades in the northern hemisphere, there has been considerable public debate over the scientific basis for global warming and “climate change”.

The scientific arguments over climate change are now irrelevant. The construction sector (with a few notable exceptions) has underperformed for many years in the

UK. The stimulus provided by the Climate Change Act 2008 and the prioritisation of carbon over other parameters of sustainability can provide the focus for innovation and performance improvement that sustainability as a package could never achieve. On the contrary, sustainability in the UK has become “business as usual”, with long checklists of competing environmental, social and economic parameters adding cost and complexity to engineering projects without any obvious strategic direction. How can jobs be compared to biodiversity? Or health and safety be compared with waste? All of these are important measures of the success of civil engineering projects, but as a package they cannot provide clear direction to clients, owners and the supply chain.

## 5.4 The Impact of a Low Carbon Economy

For the geotechnical engineering community, the key issue for debate will be how the emerging low carbon economy will affect the design and delivery of low-carbon infrastructure, such as transportation projects, renewable energy or a new generation of nuclear power plants. The maintenance and upgrading of existing infrastructure, such as water and waste water systems, road and rail infrastructure or flood and landslide protection will also require fresh thinking to minimise use of materials, energy and labour.

The challenge for geotechnical engineers is to recognise that after years of important but low level commitment to sustainable engineering solutions, very soon we will be required to design, to tender, to construct and to operate our buildings and infrastructure not only within the usual constraints of time and money but also within the constraints of carbon accounting. For geotechnical engineers around the world this will require new models, new tools and new training, all of which need urgent research and rapid implementation.

Carbon accounting in the UK is already here. Government departments in the UK were working in 2009 to budgets calculated on a non-traded price of £51/tonne (around ¥7,500/tonne) based on the cost of mitigating emissions. This price was almost twice the previous shadow price, which was based on an assessment of damage caused by the impacts of climate change. In March 2010, eighteen UK Government Departments published their Carbon Reduction Delivery Plans, detailing how they intended to comply with the national carbon budgets introduced under the 2008 Climate Change Act. In June 2010, the new government in the UK announced that it would introduce legislation on a floor price for carbon in 2011 but it did not propose to repeal the 2008 Act, thus confirming the trajectory set by the previous government. Government is a major construction client and it is easy to see how the traditional approach to procurement based on time and money will be replaced by new cost-benefit analyses for investment in infrastructure and engineering based on time, money and carbon. This will have profound effects on the way in which design and through-life performance assessment is undertaken.

### 5.4.1 Industry Transformation for a Low Carbon Economy

The Secretary of State for the UK Government Department for Business, Innovation and Skills, Lord Mandelson, launched a study on the construction industry in November 2009, to be carried out by an “Innovation and Growth Team” (IGT) made up of industry leaders. The IGT was asked to report within a year on how to prepare the construction industry to be competitive in a low carbon economy. The IGT had four main subgroups looking at residential buildings, commercial buildings, major projects and infrastructure. Geotechnical engineering was particularly represented in the infrastructure group. The infrastructure chapter highlighted the importance not only of de-carbonising every individual infrastructure project during the design and construction phase but also of carefully considering what the purpose of the project really was in advance, before determining any specific conceptual solution (BIS, 2009).

UK policy has advanced very rapidly in this area. In June 2008, the UK Sustainable Construction Strategy referred to four key indices: biodiversity, water, waste and carbon as part of a wide set of targets addressing “the means” and “the ends” for the construction industry. These are summarised from the Strategy report in Table 5.1.

The Strategic Forum for Construction is a high level group in the UK that brings together the main representative bodies in the industry. The SFfC has set its own headline targets in six areas, including sustainability. The published targets for 2012 are set out in Table 5.2. These are more focussed on the construction process and

**Table 5.1** UK Sustainable Construction Strategy headline targets

Chapter	Overarching target (summary)
Procurement	Improved whole life value through best practice procurement and supply side integration
Design	Ensure construction is buildable, fit for purpose, resource efficient, sustainable, resilient, adaptable and attractive
Innovation	Enhance industry’s capacity to innovate and increase sustainability of both process and resultant assets
People	Increase training and reduce fatal and major injury accidents
Better regulation	Reduce the administrative burden
Climate change mitigation	Reduce UK GHG emissions by at least 80% by 2050 (and by at least 34% by 2020)
Climate change adaptation	Develop a robust approach to adaptation to climate change
Water	Reduce the per capita consumption of water in the home to an average of 130 l/person/day
Biodiversity	That the conservation and enhancement of biodiversity in and around construction sites is considered throughout all stages
Waste	Achieve a 50% reduction of construction, demolition and excavation waste to landfill by 2012 (from 2008)
Materials	That materials used in construction have the least feasible environmental and social impact, socially and economically

**Table 5.2** UK SFfC headline targets for 2012

Waste	A 50% reduction in construction, demolition and excavation waste to landfill by 2012 compared to 2008 levels
Carbon	A 15% reduction in carbon emissions from construction processes and associated transport by 2012 compared to 2008 levels
Product sourcing	25% of products used in construction projects to be from schemes recognised for responsible sourcing by 2012
Water	A 20% reduction in water usage in the manufacturing and construction phase compared to 2008 levels
Biodiversity	All construction projects in excess of £1 m to have biodiversity surveys taken and necessary actions instigated

more immediate than the government's Sustainable Construction Strategy targets in Table 5.1, but they reflect the same trajectory that the industry needs to follow. Carbon is given an explicit target for the first time, although it is associated only with construction processes, not the resultant assets or through-life emissions.

Following the 2008 Climate Change Act the UK government published the UK Low Carbon Transition Plan in July 2009, which was focussed on:

- Transforming the power sector and rebalancing energy infrastructure
- De-carbonising transport
- Creating energy efficient homes and communities
- Transforming workplaces and creating jobs in the green economy
- Transforming farming and managing land and waste sustainably

For geotechnical engineering, the priorities are clear. Energy infrastructure in particular will form a major part of the work to be achieved in the forthcoming years. The government's commitment to this programme has been illustrated by the slow but steady progress towards a new nuclear fleet and also by the release of vast new areas of seabed for offshore wind development. The successful bidders for the Round 3 wind zones were announced on 8 January 2010, increasing the scale of development of offshore wind around the UK by a further 25 GW to a total target installed capacity by 2020 of 32 GW. If this is achieved, then it would represent around 25% of the UK's electricity needs. Geotechnical engineering, in the form of offshore geotechnics, novel foundation solutions and construction technologies will play a major part in this extraordinary transformation of infrastructure policy.

The scale of the challenge for infrastructure in the UK was forcefully set out in a UK Government report published in 2010 by IUK, a public private partnership within HM Treasury tasked with investigating the factors influencing the cost of major infrastructure projects (IUK, 2010).

Carbon will become the currency for sustainability. Elevating carbon to a position where it has equal importance to time and money will require a whole range of new skills for engineers to learn. "Value engineering" will become "carbon value engineering", not only driving out excess cost, but excess carbon.

In this new structure, will the traditional image of sustainability as a basket of social, environmental and economic parameters become a lower priority?

### 5.4.2 Valuing Infrastructure in Sustainability Terms

Of the two natural hazards that threaten the city of London, flooding and windstorm, flooding is the better understood. Models of the flooding of London consider two cases, flooding from the sea and riverine flooding, down the Thames river. The city is protected from sea flooding by the Thames Barrier, constructed during the government of Margaret Thatcher and now being closed on a more and more frequent basis (Fig. 5.1). The barrier sits relatively far upstream, in the city, and there is a system of levees, flood walls and gates that protect the farmland and communities that live on the banks of the river along the estuary. All of these structures require constant maintenance. The computer models show that closure of the Thames Barrier to protect the city of London from a major sea surge will create a reflected wave that will overwhelm the lower defences along the estuary. Is this acceptable? The land behind the levees is not of the same value as the city of London, but it clearly is very important to the people who live there. How will such decisions be taken in future, if carbon is to be considered a priority as important as time and money?

Infrastructure projects typically have a very long time frame attached to them. This long time horizon has also conditioned public attitudes towards the delivery of infrastructure, which is often thought of as having an effectively infinite design life. One example of this might be the system of sewers designed by Joseph Bazalgette, Chief Engineer of the Metropolitan Board of Works for London in 1865.



**Fig. 5.1** The Thames Barrier open to shipping, with one of the ten rotating gates closed (*on left hand side*), photograph © Scott Steedman

Bazalgette's sewers transformed London from a disease-ridden slum into the great city we see today. The banks of the river were reclaimed, with large retaining walls constructed to form "the Victoria Embankment", which characterises the riverbank today on the north (and south) side. The sewers were constructed behind the retaining wall, along with a subway for services and the underground railway.

We still depend on Bazalgette's system of large interceptor sewers, which collect waste water flowing downhill towards the river and channel it along large diameter culverts flowing parallel to the Thames downriver to sewage treatment works on the north and south banks. In the event of heavy downpours of rain, the sewers were designed to overflow into the Thames, and this still happens a few times each year (Fig. 5.2).

Major infrastructure projects are unlike private building projects in that their scale and longevity require special consideration. Although in the UK the provision of infrastructure is in the hands of private utilities, these companies are tightly regulated and it is effectively under public control. The regulatory framework has a major influence on the selection and delivery of infrastructure projects. In the UK, a new "environmental" project has recently been approved by the Water Services Regulation Authority (known as Ofwat) to construct a diversion tunnel under the Thames some 32 km long. The tunnel is intended to intercept any storm overflow from Bazalgette's sewer system and carry it downriver to the sewerage treatment works on the eastern side of the city. Cost estimates vary, but the project is thought

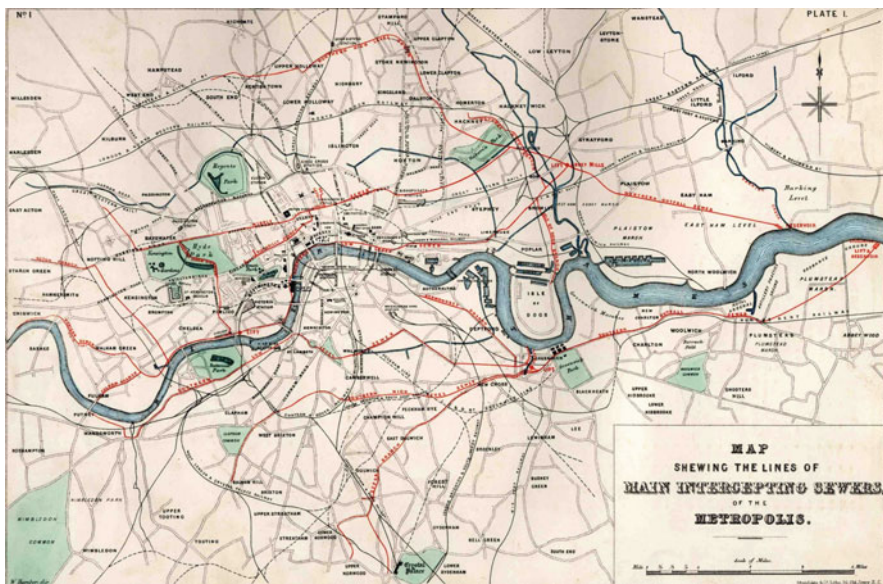


**Fig. 5.2** Map of London showing Bazalgette's proposals in 1865 for a sewer system in the city, courtesy of the Institution of Civil Engineers, London

to be costing around £2Bn, which will be passed on to the consumer. Justification for the project has been made solely on the basis of the improving the quality of the river and reducing the environmental impact of sewer overflows.

From an environmental perspective, then, the Thames Tideway tunnel project proposal is deemed a success. However, the tunnel is very deep, up to 80 m below ground and 32 km long. Having dropped from street level down to the tunnel, sewer overflows must be pumped back up to the surface again for treatment for the lifetime of the project. From a carbon perspective, common sense would say that the Thames Tideway tunnel project is a carbon disaster.

### 5.4.3 Assessing Sustainability on Infrastructure Projects

It is easy to see how sustainability has become overloaded with issues to the point that for civil engineering projects, sustainability simply means “good practice”, “business as usual”. The challenge for today’s engineers is to prioritise between these conflicting demands, when the concept of sustainability itself has become so dilute.

The UK’s main civil engineering environmental assessment scheme has been designed to champion sustainable infrastructure projects. CEEQUAL was developed by a group of experts led by the Institution of Civil Engineers and the scheme was launched in 2003. CEEQUAL followed the development of environmental assessment schemes aimed at the building sector (e.g. BREEAM in the UK, LEED in the USA, CASBEE in Japan). The list of topics to be considered under a CEEQUAL assessment totals 12 in number, with some categories covering several sub-topics. Table 5.3 summarises the scoring system.

CEEQUAL is a checklist based approach, which is intended to support the industry to address environmental quality and social issues on its projects. Award grades are given on the basis of scoring against the 12 sections with 25% representing a Pass, 40% Good, 60% Very Good and 75% Excellent. The CEEQUAL assessment rewards achievement beyond the minimum, so a Pass mark is an indication of a

**Table 5.3** CEEQUAL weighting factors for the 12 sections of the scheme

Project management	10.9%
Land use	7.9%
Landscape	7.4%
Ecology and biodiversity	8.8%
The historic environment	6.7%
Water resources and environment	8.5%
Energy and carbon	9.5%
Material use, including embodied energy	9.4%
Waste management	8.4%
Transport	8.1%
Effects on neighbours	7.0%
Community relations	7.4%

modest improvement over the basic requirement. At the top end of the scale, the structure of the assessment is such that a 100% score is effectively impossible to achieve as achievement in some sections inevitably compromises achievement in others.

A wide basket of targets can provide encouragement to lift the general level of performance by rewarding almost any aspect of “sustainability” on a project. Setting the industry on a path that will deliver against a specific target requires prioritisation.

The Institution of Civil Engineers recognised this issue in their recently published State of the Nation report on Low Carbon Infrastructure, in November 2009. The ICE concludes that. “Over time, low carbon infrastructure must cease to be a choice and become the norm.” The report continues, “The challenge for engineers in the low carbon age is to understand and minimise the carbon emissions associated with designing, constructing, operating and maintaining this network, while still meeting society’s needs.”

#### ***5.4.4 Creating a Low Carbon Construction Industry***

The UK is now embarked on creating a low carbon construction industry. By identifying carbon as the primary design determinant industry and the profession will be able to focus much more clearly on the steps that need to be taken to achieve real improvements in performance. By focussing on carbon, alongside cost and time, in construction projects the UK is seeking to create a high-performing industry that can quantify the risks and benefits of its outputs in a meaningful way. With carbon as the currency for sustainability, sustainability will become embedded within the traditional investment decision process.

New professional skills will be needed. “Carbon value engineering” is an obvious example. Value engineering is a common process on major projects, using experience in the supply chain to find cost savings in the design. In future, the same process will need to drive out carbon as well. New models will be needed to support the engineering decision making process, modelling the feasibility and through life performance of projects in terms of carbon as well as cost and programme.

These models will depend in part on the methods of carbon accounting that are adopted by national governments and international agreement. Issues such as the discount rate for carbon must be urgently resolved as this will have a significant effect on the long term planning for infrastructure provision and the choices available to geotechnical and civil engineers.

In traditional infrastructure procurement, assets were designed, constructed and operated almost independently of one another. For example, in a British street it has been typical that different infrastructure companies design, construct and maintain their networks completely independently of each other or the highway authority. Traffic is constantly disrupted. Resources and energy are clearly wasted. The approach is clearly “unsustainable”. A systems approach to the provision of infrastructure and built assets would require more coordinated planning and prioritising over alternative solutions.

The planning system in the UK has for a long time been seen as a major obstacle to the delivery of new infrastructure because of the long duration of the approvals process and the uncertainty over the final outcome, a strong disincentive for investors. In 2008, in a major shift in policy direction, a new agency known as the Infrastructure Planning Commission (IPC) was established by the last government to implement a series of “National Policy Statements” on different subjects, such as energy, transport, water and waste. The NPS are intended to streamline the planning process by securing Parliamentary approval of the overall need for key infrastructure projects in different regions, reducing the scope for objections (at least on the basis of need). However in May 2010 the new government announced that the IPC would be replaced in 2011 by a Major Infrastructure Unit closely aligned to the Planning Inspectorate, under the control of the Department for Communities and Local Government. The IUK’s National Infrastructure Plan was published in the autumn of 2010 by HM Treasury and includes a 50 year vision, attempting to set the pace and direction of infrastructure investment (HM Treasury, 2010). This will clearly have to be in the context of the government’s own carbon targets. Whether or not these initiatives succeed in accelerating the low carbon economy, it is clear that the UK government is heavily committed and industry must follow.

## 5.5 Characteristics of Infrastructure in a Low Carbon Economy

The characteristics of infrastructure in the future are likely to be different from the past. If geotechnical engineering and civil engineering is to deliver real sustainability using carbon as the primary determinant, then it will be necessary to revisit our traditional model of infrastructure, the Victorian model that has constrained so much recent thinking.

Perhaps infrastructure in the future needs to be more flexible, adaptable, with a shorter life to accommodate new and emerging technologies, to have low embodied energy and low operating and disposal costs. Above all, future infrastructure needs to generate an “income stream” in terms of carbon benefit (i.e. carbon reduction). This could be through carbon reduction in the project being designed, or carbon savings achieved through the interaction of the operation of that project on other infrastructure. To be efficient in resources and energy, to be *sustainable*, engineers will need to engineer their infrastructure projects within a much wider context than before. The adoption of carbon as a proxy for sustainability makes this possible in a way that a basket of parameters cannot. Common sense would say that the Thames Tideway Tunnel was not sustainable, despite the fact that it ticks many of the boxes.

It is time therefore, for geotechnical engineers to revisit their understanding of sustainability. On the present basis, any engineered solution can be made to fit the criteria (in Table 5.2, for example) provided that reasonable care is taken in the design and delivery. The opportunity that now faces the industry, arising on the back of the climate change debate, is to argue for a new, more consistent approach towards delivering sustainability in future.

New regulatory drivers will be needed, based on a more sophisticated understanding. More integrated working will be essential, working with other engineering disciplines and with non-construction professionals to develop and implement models for assessing and designing future solutions. New tools and performance measures will be needed that will reward engineering approaches that are clearly “common sense” in terms of sustainability. The innovation cycle must be shortened considerably, so that new materials, products and technologies can be introduced within a much shorter timeframe. This will mean a fresh look at codes and standards and their use as part of risk management.

## 5.6 Conclusions

Carbon will become the proxy for sustainability and “green” construction and engineers will need to consider carbon alongside cost and time in the selection of engineering solutions.

The prioritisation of carbon, which has become possible only because of the climate change debate, is an extraordinary opportunity for the construction industry to achieve a transformation in performance, because it has focussed political will in an unprecedented manner. This opportunity for change is completely independent of the scientific arguments over man’s contribution to global warming, which are now irrelevant.

Ticking boxes will not deliver a sustainable built environment in the sense that society requires. Engineers need to design sustainability into their solutions at the outset, using carbon as a proxy of equal weight to cost and time, considering all phases of the life cycle. Geotechnical engineers must urgently develop their models and thinking to deliver the industry transformation that is required and to remain competitive in a new low carbon economy.

## References and Further Reading

- Bazalgette JW (1865) On the main drainage of London, and the interception of the sewage from the River Thames. Minutes of the proceedings of the institution of civil engineers, London, vol 24, Issue 1865, January, pp 280–314
- BREEAM. [www.breeam.org](http://www.breeam.org)
- CASBEE. [www.ibec.or.jp/CASBEE/english/overviewE.htm](http://www.ibec.or.jp/CASBEE/english/overviewE.htm)
- CEEQUAL. [www.ceequal.co.uk](http://www.ceequal.co.uk)
- Department for Business, Innovation & Skills, Strategy for sustainable construction. [www.berr.gov.uk/whatwedo/sectors/construction/sustainability/page13691.html](http://www.berr.gov.uk/whatwedo/sectors/construction/sustainability/page13691.html), 2008
- Department for Business, Innovation & Skills, Low Carbon Construction IGT, Final Report, [www.bis.gov.uk/constructionigt](http://www.bis.gov.uk/constructionigt), 17 September 2009
- Department for Communities and Local Government, Infrastructure Planning Commission announcement. [www.communities.gov.uk/news/corporate/1626220](http://www.communities.gov.uk/news/corporate/1626220)
- Department of Energy & Climate Change, The UK low carbon transition plan. [www.decc.gov.uk/en/content/cms/publications/lc\\_trans\\_plan/lc\\_trans\\_plan.aspx](http://www.decc.gov.uk/en/content/cms/publications/lc_trans_plan/lc_trans_plan.aspx), 2009
- Department of Energy & Climate Change, Departmental Carbon Budgets. [www.decc.gov.uk/en/content/cms/what\\_we\\_do/lc\\_uk/carbon\\_budgets/departments/departments.aspx](http://www.decc.gov.uk/en/content/cms/what_we_do/lc_uk/carbon_budgets/departments/departments.aspx)

EU Research Advisory Body, EURAB report on SMEs and ERA, 04.028-final, June 2004  
European Construction Industry Federation (FIEC). [www.fiec.org](http://www.fiec.org)  
HM Treasury, Infrastructure UK public-private partnerships. [www.hm-treasury.gov.uk/ppp\\_infrastructureuk.htm](http://www.hm-treasury.gov.uk/ppp_infrastructureuk.htm)  
HM Treasury, Infrastructure UK, National Infrastructure Plan 2010, [www.hm-treasury.gov.uk/d/nationalinfrastructureplan251010.pdf](http://www.hm-treasury.gov.uk/d/nationalinfrastructureplan251010.pdf), October 2010  
Institution of Civil Engineers, London, The State of the Nation, Low carbon infrastructure. [www.ice.org.uk/downloads//sotn\\_lci.pdf](http://www.ice.org.uk/downloads//sotn_lci.pdf), Nov 2009  
LEED. [www.usgbc.org/DisplayPage.aspx?CategoryID=19](http://www.usgbc.org/DisplayPage.aspx?CategoryID=19)  
Office for National Statistics, Construction statistics annual report 2009. [www.statistics.gov.uk/downloads/theme\\_commerce/CSA-2009/Openingpage.pdf](http://www.statistics.gov.uk/downloads/theme_commerce/CSA-2009/Openingpage.pdf)  
Strategic Forum for Construction (SFfC), London. [www.strategicforum.org.uk](http://www.strategicforum.org.uk)

## Chapter 6

# World Heritage in Asia

### Geotechnical Overview of Sustainable Conservation and Development for the World Heritage Area of Angkor, Cambodia

Yoshinori Iwasaki

**Abstract** Two case studies are described in terms of sustainable conservation of cultural heritage as well as social development in the World Heritage Site of Angkor, Cambodia. These problems are very unique in a sense that the phenomena were found quite different from what geotechnical engineers had been used to expect in daily practice. A tower of masonry structure that JSA (Japanese Government Team for Safeguarding Angkor) selected for structural conservation was inclined about 5 degrees. Since the deformation of the step stones showed the same inclination, tilting of the foundation was considered as major mechanism for the inclination of the Tower. After trenching of the soil mound, the compacted soil layer was not inclined but horizontal. This was quite different what we had expected. What was the mechanism to cause the inclination? Further study revealed that the slip-down of the side step stones along the foundation platform was the true mechanism. JICA (Japan International Cooperation Agency) made a study of water resource from pumping underground water. They have monitored seasonal fluctuation of shallow water level at more than 50 surface wells and tried to simulate the seasonal changes caused by horizontal flow from higher mountain to lower lake zones. Finally, JICA had installed a facility to pump water more than 8,000 ton/day. After the pumping started, a monitoring well at 3 km from pumping zone showed 1 m of drawdown of water level that was predicted as little effect by the simulation. Since the plain in Angkor has very gentle slope of the order of 0.001, horizontal flow of underground water is very slow and negligible. The seasonal changes of the water level of 4–5 m was caused not by horizontal flow but infiltration of rain water and evaporation water from the deep layers that was not included in the model JICA used.

---

Y. Iwasaki (✉)  
Cyber University, Fukuoka, Japan; Geo Research Institute, Osaka 550-0012, Japan  
e-mail: yoshi-iw@geor.or.jp

## 6.1 Introduction

When the turmoil in Cambodia has ended, Japanese Government had an inter-governmental conference on Safeguarding Angkor in October, 1993, Tokyo (UNESCO, 1997).

The Japanese Government Team for Safeguarding Angkor (JSA) was formed in 1994 and the author had joined as geotechnical member. We have been engaged in studying geotechnical problems in Angkor, Cambodia since then. JICA (Japanese International Cooperation Agency) worked since 1996 to perform a feasibility study of possible water resources in the Angkor area for citizens in Siem Reap city. Based upon the study, a pumping station was constructed at the south of the West Barai and started its operation in 2006.

## 6.2 Geotechnical Setting of Angkor Region (JSA Report (1995–2001))

Angkor locates at a western north part in Cambodia in the Angkor plain north of Tonle Sap Lake as shown in Fig. 6.1. The Angkor plain extends between Kulen Mt. and Tonle Sap Lake as shown in 6.2.

The change of the ground height at the lake to the foot of the mountain is about 50 m with a distance of 50 km. The slope of the Angkor plain is very gentle

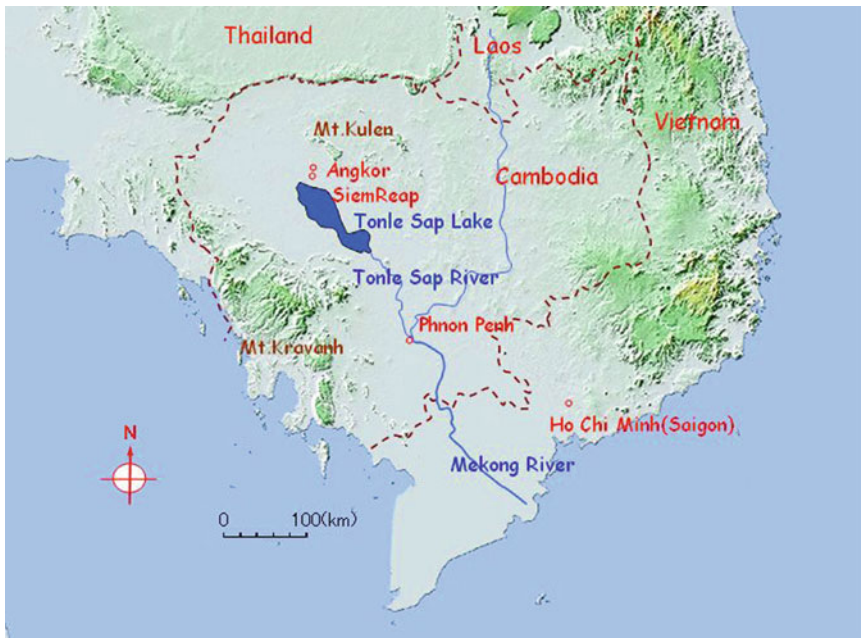


Fig. 6.1 Map of Cambodia

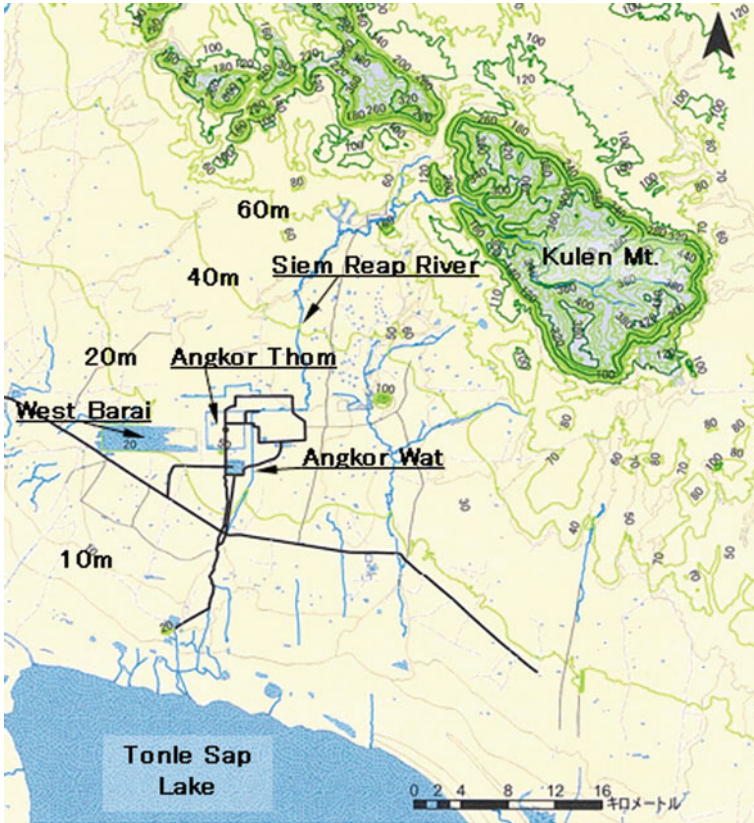


Fig. 6.2 Cambodia and Angkor

of 1:1000, in which Siem Reap River, originating from the Mt. Kulen runs southwards to the lake. The eastern Kulen shows a special topology of bowl type shape and is a water reservoir during rainy season. The Siem Reap River flows continuously even in the end of dry season after no rainy of 6 months.

Geology of Mt. Kulen composes from sandstones that had been used for construction material for masonry structures in Angkor.

JSA performed several deep drillings of 100 m to reach the bedrock geology. The geological layers found by the boring study are sediments of Quaternary, Tertiary, and base rock. Base rock is igneous rock of andesite. The results at the center in Angkor region are shown in Fig. 6.3. The base rock in the Angkor region consists from igneous rock to sandstone in Mesozoic era.

Figure 6.4 shows one of the boring logs at the north of Bayon temple. The upper 40 m is Quaternary deposits of silty fine sand with several clayey rich layers. In general SPT (Standard Penetration Test) N-value increases with depth except at the top surface. N-value at the top surface is 20 and decreases to 10 at the depth of 5 m. The boring was carried out in March 1995 of dry season. The cone penetration test

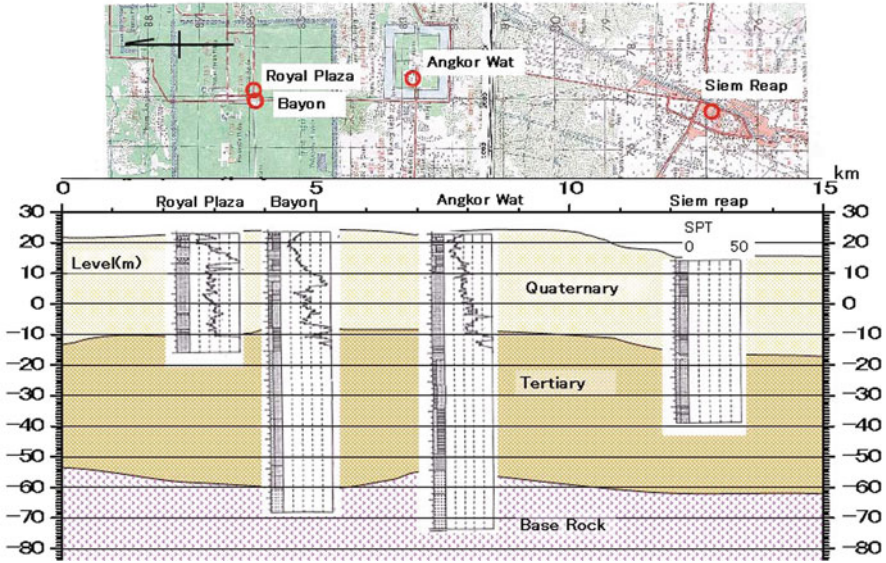


Fig. 6.3 Geological structure in Angkor region

that was performed in rainy season at the same site revealed that the cone resistance decreased to zero at the surface and increased with depth down to about 5 m. The top surface of 5 m may be affected by the seasonal change of water level.

The pore pressure sensors were installed at two depths as shown in Fig. 6.5. Pore water increases during rainy season from May to October and decreases in dry season from November to April. The fluctuation of the water level was 4–5 m.

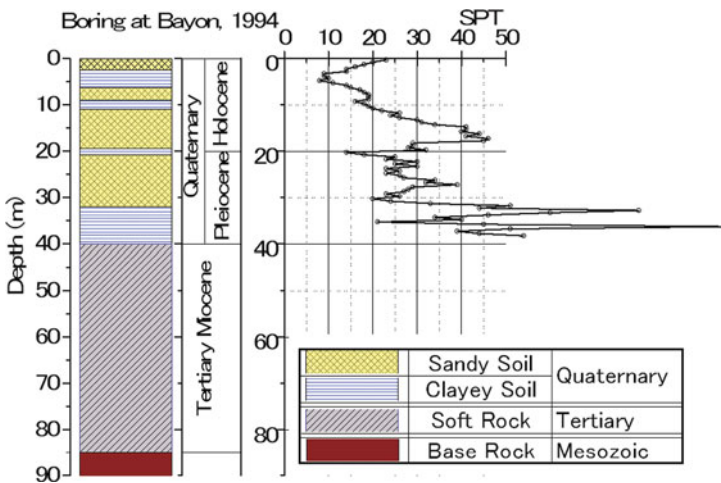


Fig. 6.4 Geological boring at Bayon, Angkor Thom

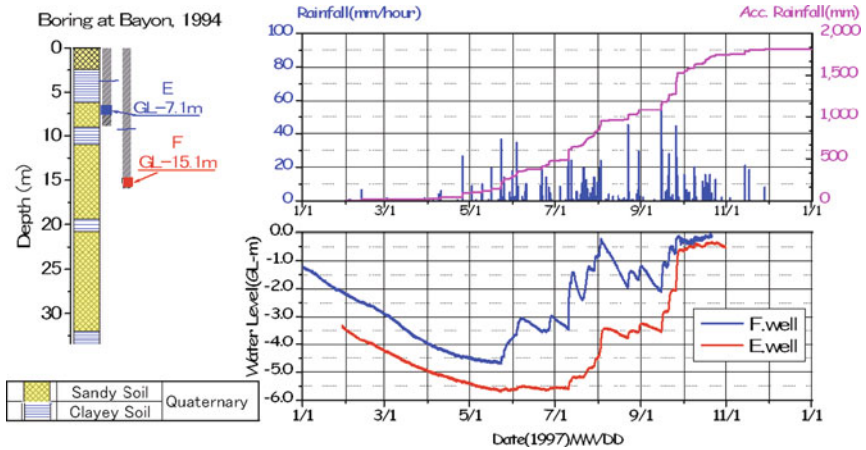


Fig. 6.5 Rainfall and seasonal change of pore water pressure at Bayon site (JSA Report)

### 6.3 Tower of Prasat Suor Prat (JSA Report (2005))

Prasat Suor Prat (Tower of Rope Dancer) is a group of 12 independent towers in the Royal Plaza, Angkor Thom as shown in Photo 6.1 (Report on the Conservation and Restoration Work of the Prasat Sour Prat Tower, 2005).

One of the 12 towers named as N1 that is inclined about 5 degrees northwards was selected by JSA for safeguarding work as shown in Photo 6.2. The tower consists from a main tower with a front room called antechamber. The main tower is three story masonry structures with laterite bricks with 10 m in width at foundation and about 20 m in height. The inside of the tower is hollow structure with four open windows at every wall.



Photo 6.1 Tower of Prasat Sour Prat

**Photo 6.2** N1 tower Prasat Sour Prat selected as one of structures for reconstitution by JSA



Figure 6.6 shows vertical section and plan view of the N1 tower nearby the north pond. The differential settlement of the foundation was measured about 40 cm at the north-west corner lower than that of the south-east corner. Figure 6.6 also shows contour lines of equi-settlement relative to the south-east corner of the foundation.

The open window of the west wall is deformed as shown in Photo 6.3. The widths of the bottom of the window are wider than those of the top for all four walls and the measured results are shown in Table 6.1. The laterite blocks of the side face of the foundation are found widened. The characteristics of the deformation of the foundation are settlement and horizontal spreading. What kinds of deformation could result in the measured characteristics of settlement and horizontal spreading?

### ***6.3.1 Expected Mechanisms of Spreading with Inclination***

Possible modes of deformation are shown in Fig. 6.7. They are as follows,

- A. Uni-axial compression with lateral expansion with differential settlement,
- B. Base failure with bi-lateral failure, or
- C. Base failure with unilateral sliding.

Case A may be under rather confined plastic state with differential compression, Case B and C are under yielded compression with sliding state. Since the horizontal expansion at the foundation is 6–8%, the axial compression strain may have reached more than 10%, the deformation are very likely under failure and B or C was considered more appropriate than A.

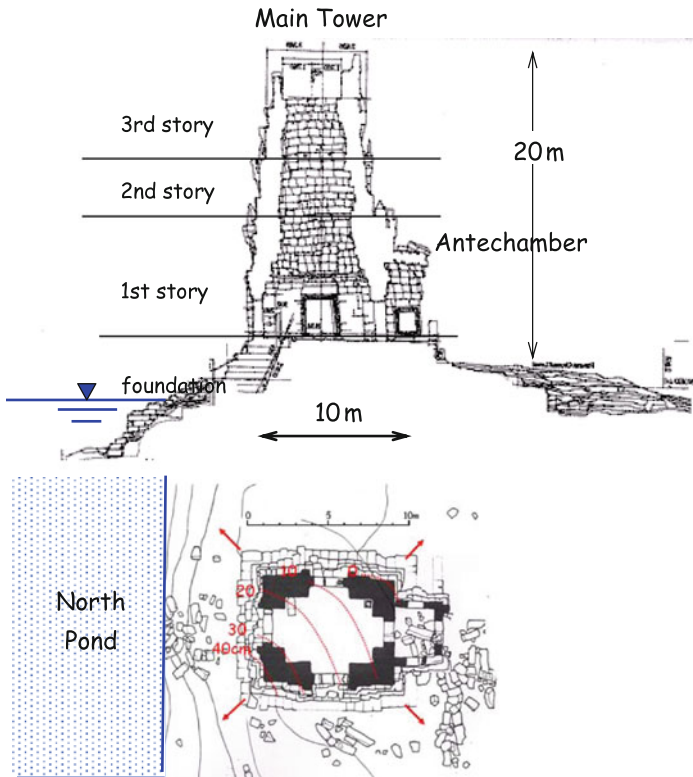


Fig. 6.6 Vertical section and plan of N1 tower

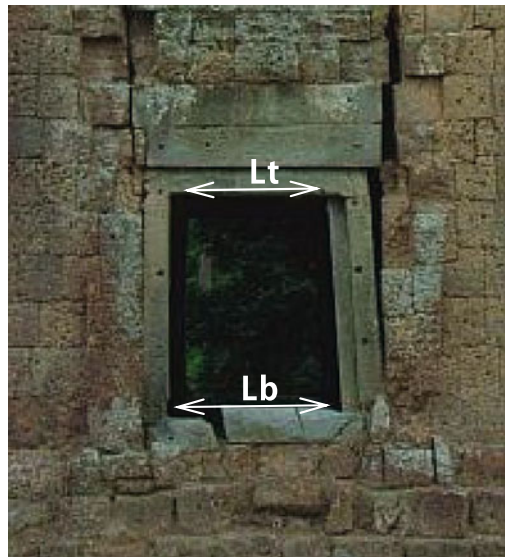
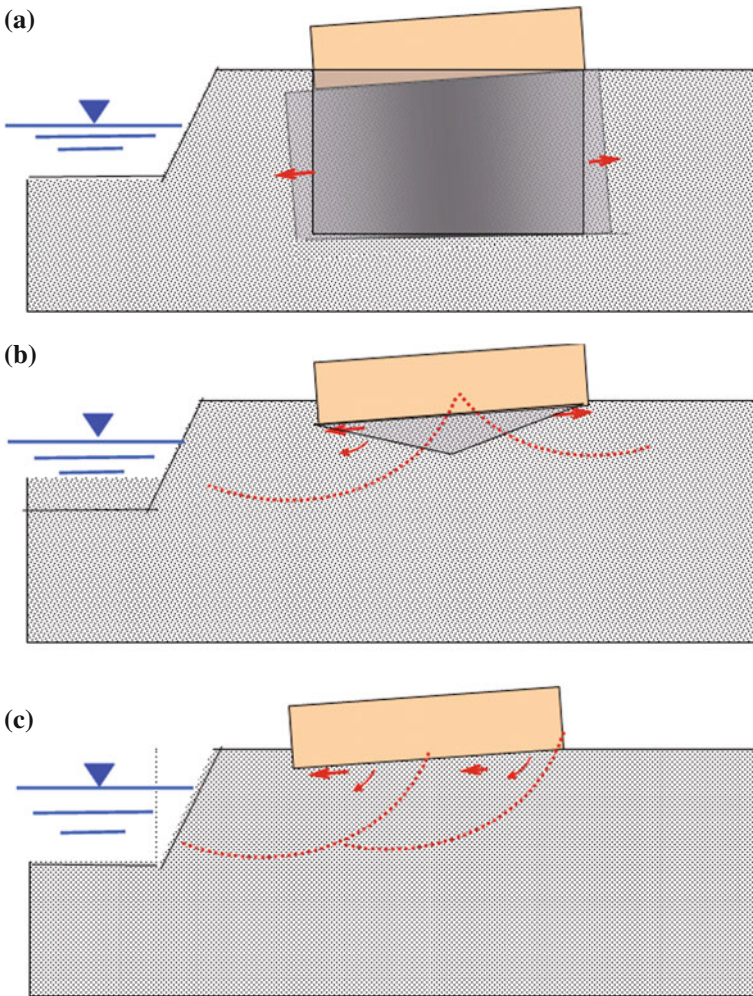


Photo 6.3 Open window, west side

**Table 6.1** Width of open window at top and bottom

Wall position	Width of the opening		Difference	
	Top Lt (cm)	Bottom Lb (cm)	$\Delta L$ Lb-Lt (cm)	Expansion (%)
East	170.3	182.0	12	7.1
West	171.3	185.0	14	8.2
North	168.0	178.0	10	6.0
South	124.0	131.7	7.7	6.2



**Fig. 6.7** Possible three geotechnical models for the inclined foundation. (a) Uni-axial compression with lateral expansion with differential settlement; (b) base failure with bi-lateral failure; (c) base failure with unilateral sliding

### 6.3.2 *Trenching of the Foundation*

Dismantling of N1 Tower of Prasat Sour Prat was carried out before reconstruction of the Tower for safeguarding the structure. After dismantling laterite blocks of the upper structure, the soil mound was further excavated down to reach natural ground layer.

Archaeological team of JSA excavated several sections as shown in Photo 6.4. Sketch of the NS-section along the center line is shown in Fig. 6.8. To our surprise, each layers of the compacted soil mound were found horizontal. If the scenario of the deformation was as shown in Fig. 6.7, in any cases, the soil layer must have been inclined to northwards. The excavated horizontal layers were out of our scope before dismantling. However, soon later, we found interesting facts and could get out of the pitfall.

### 6.3.3 *Streak Lines on the Excavated Trench Surface* (*Iwasaki et al. (2009)*)

Photo 6.5 shows a typical trenched section that revealed many streaks in whitish color. The widths of the lines of the streaks are about 5 mm and somewhat weaker than the surrounding soil surface. These streak patterns of the area are shown in Fig. 6.8. The part shown as Fig. 6.9 was photographed and was analyzed.

The distribution of the angles of the streaks from the vertical line were analyzed. Typical results are shown in right part in Fig. 6.9. It turned out that two angles of +30 and -30 degrees from the vertical plane are predominant in the pattern.

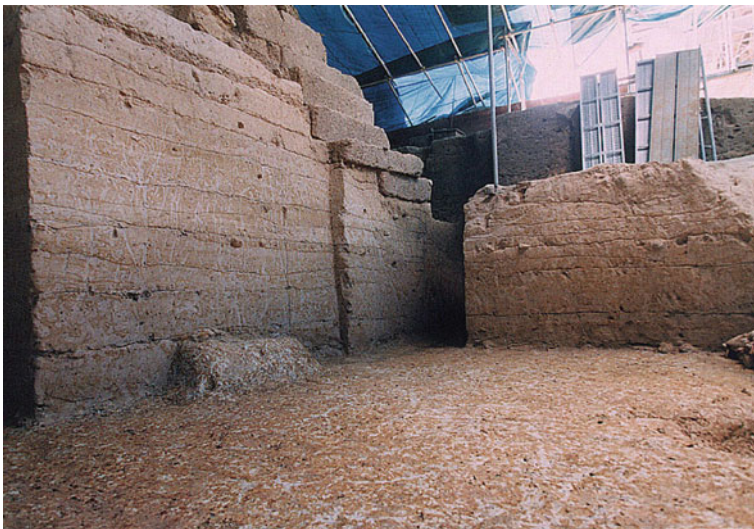


**Photo 6.4** Trench of soil mound

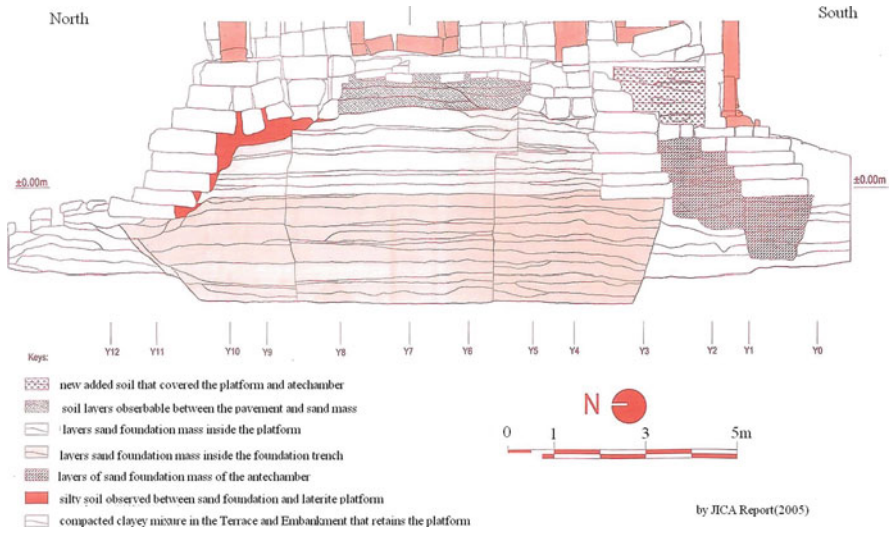


Fig. 6.8 Trenched N-S section

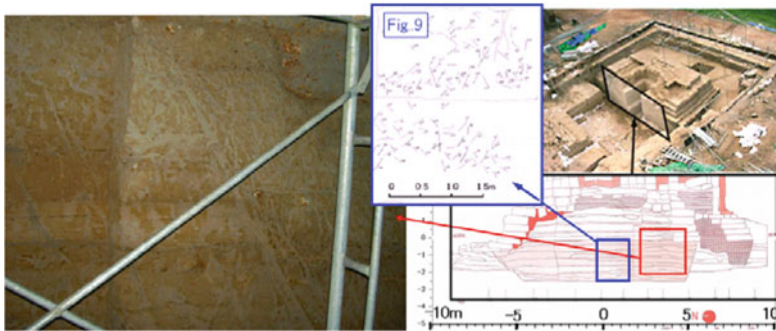


Photo 6.5 Streak pattern found on the trench section

$$\theta = 45 \pm \phi/2 \tag{1}$$

The laboratory triaxial test for unsaturated sample showed that the internal friction showed is  $\phi = 30$  degree, which result in  $\theta = 30$  and  $60$  degrees.

The coincidence between the estimated angle of shear failure line from the laboratory test and field observation, the streak lines is very likely the shear failure line that have occurred in the soil mound under the vertical load of the upper masonry structures.

### 6.3.4 FEM Simulation of the Stress in the Soil Mound

FEM simulation was carried out to check the stress state in the soil mound of the platform foundation (Iwasaki et al., 2009).

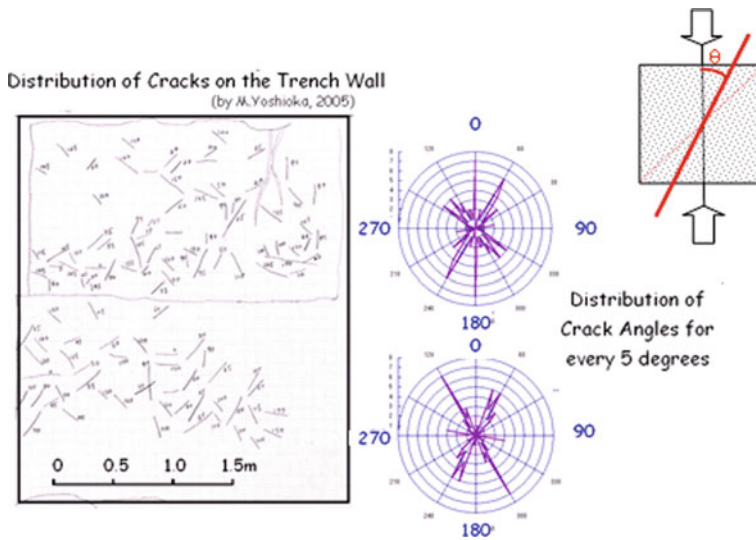


**Fig. 6.9** Streaks on the trenched face and the distribution of the angle from the vertical line under the Mohr-Coulomb criteria, the angle between the direction of failure surface and principal stress line is expressed by the following Eq. (1) with  $\phi$  as the angle of internal friction of the material. The area is divided into *upper* and *lower parts* and two charts correspond respectively

The FEM analysis was performed assuming the Mohr-Coulomb criteria for yielding with parameters as listed in Table 6.2. The FEM model is only for natural soil ground, man made mound of platform, and step stones as shown in Fig. 6.10. Vertical force is assumed from the upper structures at the top of the stone surfaces on the top of the platform. The results were obtained for two cases of loads of 100 and 400 kPa upon the foundation mound from the upper structures. Figure 6.11 shows distribution of plastic points in the soil mound induced by these steps. The 400 kPa is the expected load from the upper structure. The result shows that the shear yielding took place at the initial stage of the loading and the yielding points are spread widely in the mound section.

The yielding points become to include the upper region of the mound when the load is increased from 100 to 400 kPa. Simulation results, though preliminary, show the reasonable stress states compared to the yielded condition that is estimated by streak lines.

**Table 6.2** Material parameter for Prasat Sour Prat

	E: Young's modulus (kPa)	Poisson's ratio	c (kPa)	$\phi$	$\gamma$ (kN/m <sup>3</sup> )
Compacted fill	25,000	0.3	25	30	18
Natural ground	10,000	0.3	20	30	18
Laterite/sand stone	1,000,000	0.2		30	

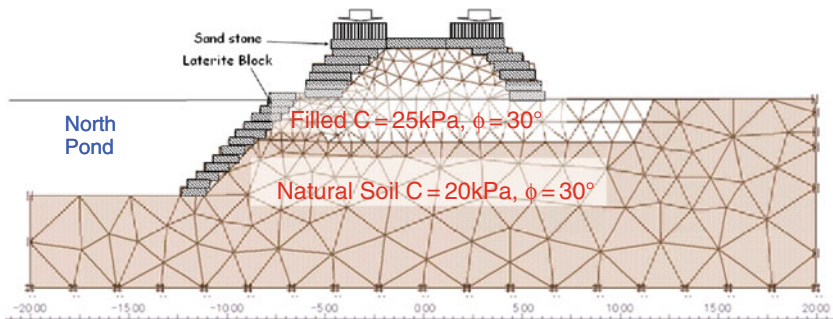


Fig. 6.10 FEM mesh for N1 foundation

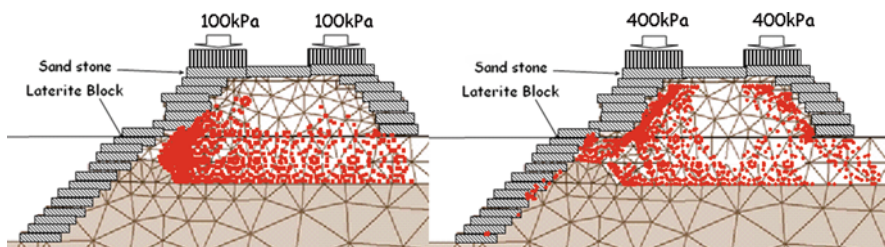


Fig. 6.11 Distribution of yielded points caused by loading from upper structures

### 6.3.5 Slip Down of Step Stones Surrounding Foundation Mound

In contrast with the horizontal layer of the compacted mound, the laterite blocks of the step stones that had been installed to cover side slope of the mound were found slipped down along the northern side slope of the mound as shown in Fig. 6.12.

It is also found that the northern mound beneath the bottom of the side stone block is lower than the continuous layer of the left part. This deformation is considered as to have been caused by foundation failure that resulted in the slip down of the side blocks of laterite.

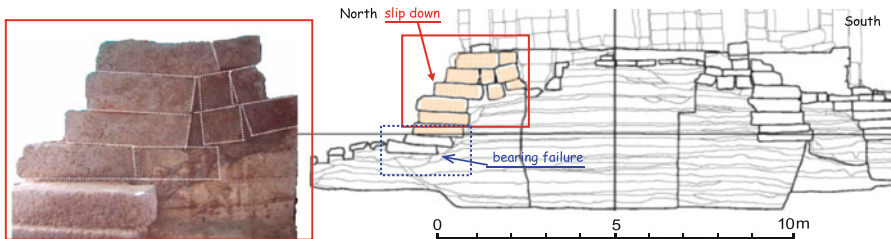


Fig. 6.12 Deformed and slipped down step stone along the northern slope of the mound

### ***6.3.6 Mechanism of the Spreading and Inclination of the Foundation***

It was revealed that the several presumed mechanisms to explain lateral spreading and inclination of the foundation were wrong. The real situation was the slip down of the side step block along the northern slope of the foundation.

The geotechnical mechanism for lateral spreading was large horizontal expansion associated with vertical compression in the yielded state.

The mechanism for the inclination was not caused by differential settlement of the ground but the slip down of the side stone along the foundation slope. We had fallen in a pitfall of geotechnical engineering. Without the excavation, we never get out the hole and arrived at the correct mechanism.

## **6.4 Water Resource from Underground Water in Angkor**

Japanese International Cooperation Agency (JICA) began Feasibility Study on possible water resources for water supply to Siem Reap area from 1996 for several years. One of the studied sources was underground water in the Angkor plain. To estimate geohydraulic model of the area, JICA team carried out borings and monitoring seasonal changes of water level in existing shallow wells in the area.

Subsurface structure based upon geological boring is shown in Fig. 6.13. The top surface of about 30–40 m is sandy layer of Quaternary formation followed by weathered tuff formation of tertiary sediment. Permeability of Quaternary formation is much larger than that of tuff formation and is considered as major formation that the underground water flows in the region.

### ***6.4.1 Modeling Hydraulic Condition of Angkor Plain***

Monitoring the seasonal change of the underground water in Angkor plain was carried out from February 1998 at more than 50 points by JICA including shallow wells as shown in Fig. 6.14 (JICA Report, 2000). In Fig. 6.15, typical monitoring points along N-S line (upper part in the Figure) and the seasonal change of water levels are shown as well as the monthly rainfall (the lower right part). The variation of the highest and the lowest water level during the monitored year along the line are also shown in the lower left part Fig. 6.15.

At every monitored wells, water level increases during rainy season and decreases in dry season. JICA had performed water balance simulation within a boundary shown in Fig. 6.17 by MODFLOW96 to obtain hydraulic parameters including of permeability of the ground.

The water balance was simulated by considering several factors of rainfall, irrigation, surface runoff, surface evaporation from shallow ground, and infiltration as shown in Fig. 6.16.

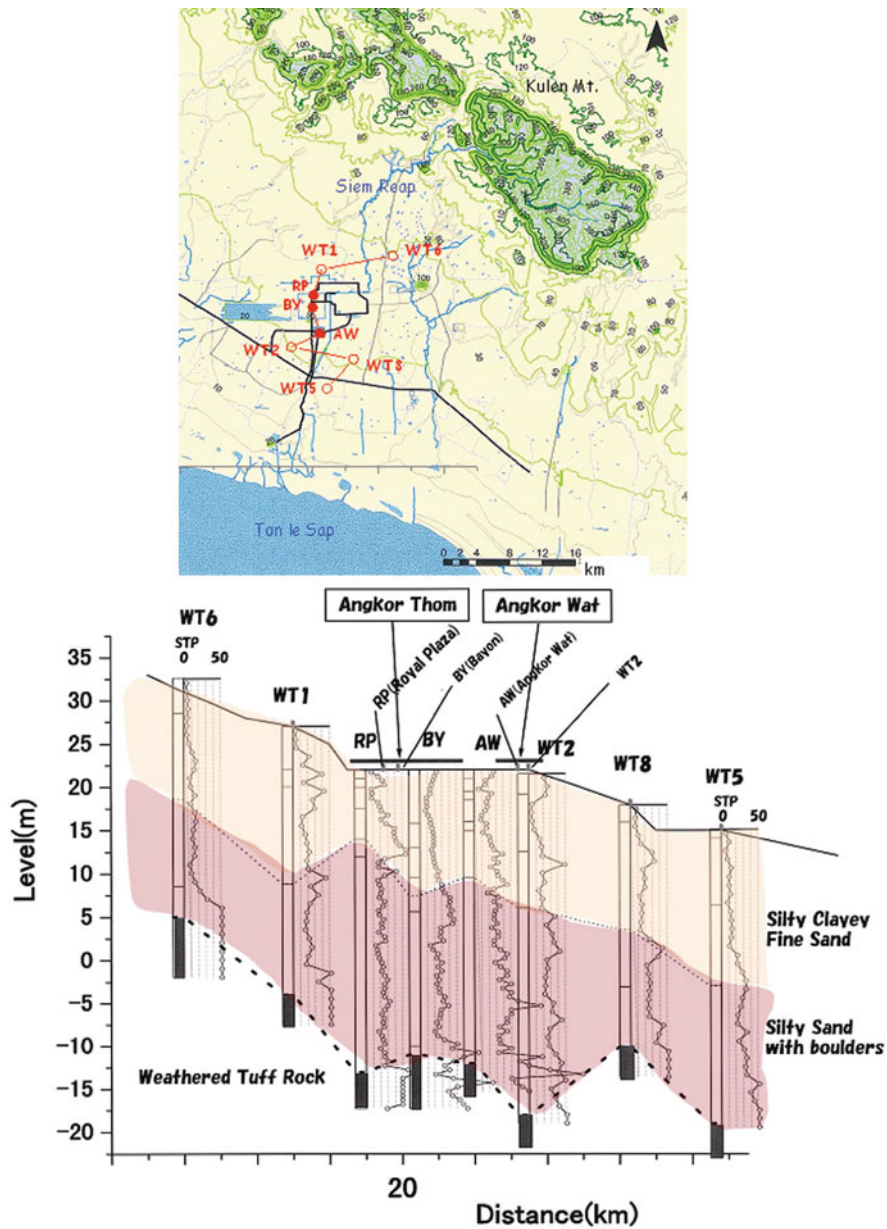


Fig. 6.13 Surface geotechnical structure in Angkor plain

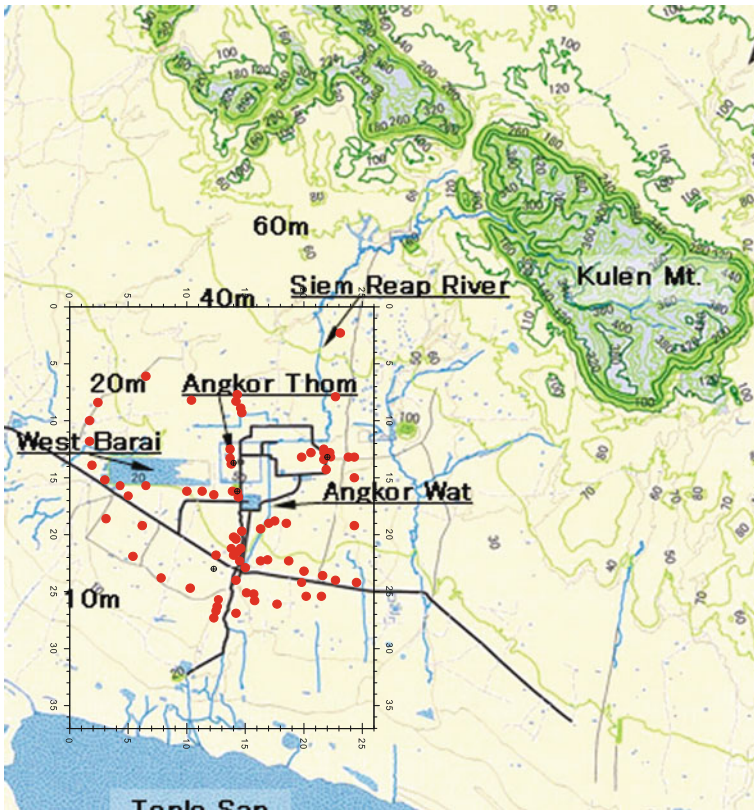
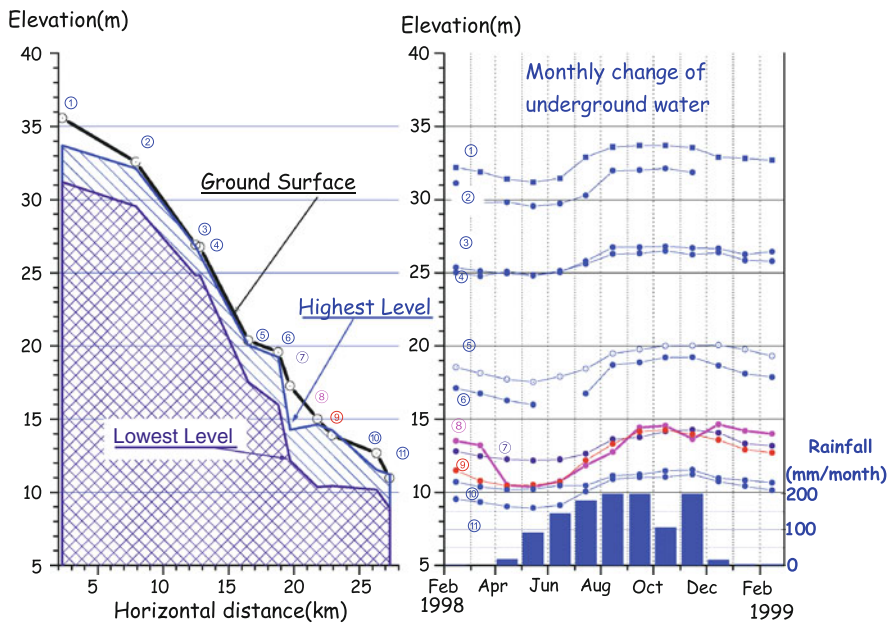


Fig. 6.14 Distribution of monitoring points in Angkor plain by JICA

The estimated horizontal flows shown in Fig. 6.17 by Takahashi et al. (2002) is the basic concept of water movement in the ground in Angkor by the experts of JICA project. The water balance calculation based upon monitored results was intended to simulate the horizontal flow from Mt. Kulen to Ton le Sap and to obtain hydraulic parameters of FEM model in the area for pumping water from the ground.

### 6.4.2 Prediction of Pumping Effects and Construction of Pumping Wells

Based upon the obtained permeability of the ground, group wells were assumed to pump underground water to predict the effect to the underground water in the area.



**Fig. 6.15** The highest and lowest water surface, seasonal change of water level as well as rainfall, positions of the wells along NS direction from Mt. Kulen to Ton le Sap Lake

**Fig. 6.16** Water balance analysis (Takahashi et al., 2002)

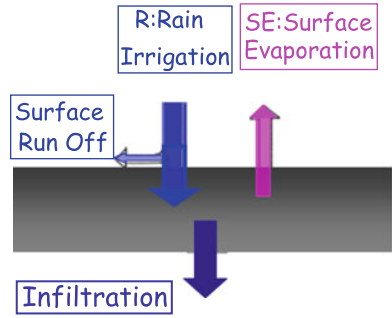
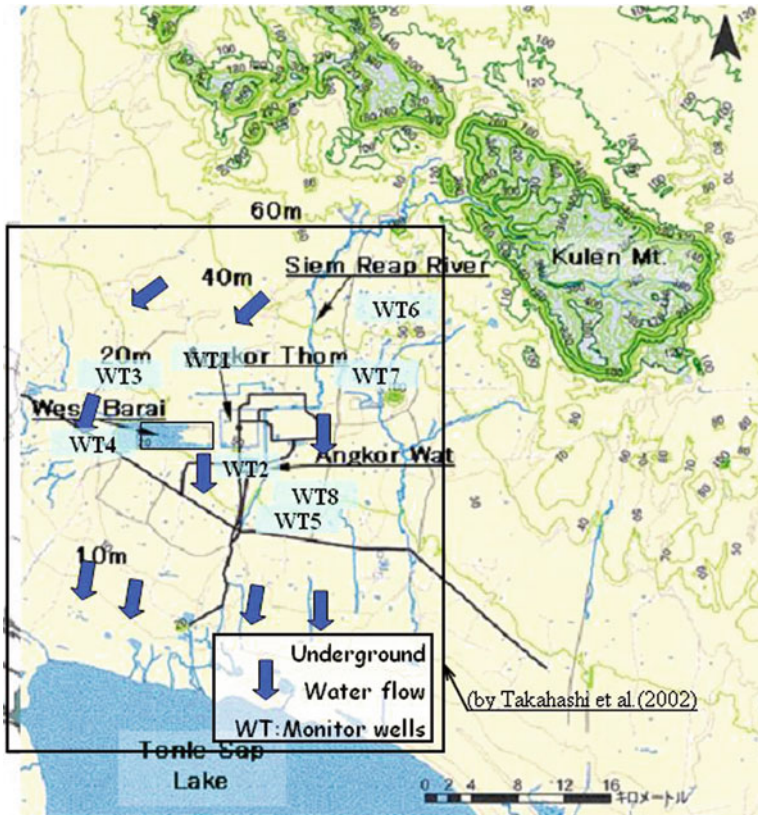
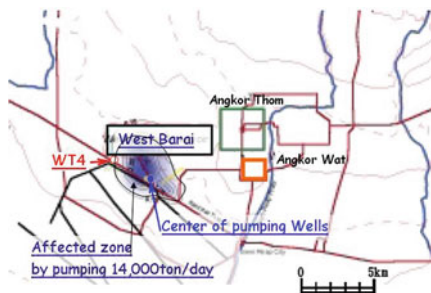


Figure 6.18 shows the center of the group wells and affected area by pumping water 14,000 m<sup>3</sup>/day. In 2003, JICA had continued to carry out to the detailed design of water pumping facility and completed the construction of the facility in 2006.



**Fig. 6.17** Flow of ground water for simulation (Takahashi et al., 2002)

**Fig. 6.18** Simulation of pumping with affected zone (Takahashi et al., 2002)



### 6.4.3 Completion of Pumping Facility and Water Level of Monitored (JICA, 2007) vs. Predicted (Takahashi et al., 2002)

The operation of the pumping station started in 2006. When the UNESCO, Phnom Penh Office, organized “Water Colloquium in Angkor” in 2007, JICA reported monitoring water levels at several points (JICA, 2007). Among monitoring results, an interesting point was well of WT-4 that locates about 3 km from the pumping area. Figure 6.19 shows a comparison between the predicted and observed changes of water level at the monitoring point of WT4. WT4 locates at the boundary of the affected region by prediction by Takahashi et al. (2002). The prediction was based by pumping 14,000 m<sup>3</sup>/day and the predicted water level at WT4 shows little effect by the pumping and keeps almost the same seasonal change as it was. On the contrary, the observed water level at WT4 shows sudden decrease in 2006 about 1.0 m under the pumping operation of 8,000 m<sup>3</sup>/day, which is about 60% of the

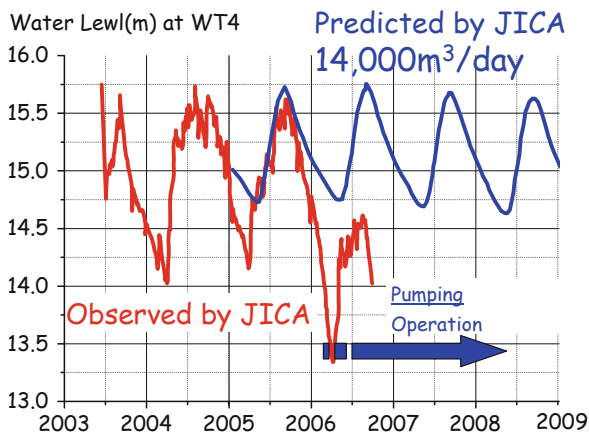


**Fig. 6.19** Observed and simulated at WT4

**Photo 6.6** Constructed water tank by JICA



pumping water used for the prediction. There is some difference of pumping positions between the predicted and the real situation, the effects of the pumping water becomes obvious and must be reevaluated.

#### ***6.4.4 Simulation of Angkor Plain by JICA Project***

As well as JICA, JSA has also monitored water at a few points with different depths within the Quaternary deposit. The measurements of different depths have revealed the special characteristics in geohydraulics of Angkor plain.

JICA might have taken different approach, if they had realized the important fact data that annual JSA report had supplied.

There are two possible reasons for these difficulties. One is the horizontal flow of underground water in Angkor plain. Another is vertical flow of the underground water, especially under dry season.

#### ***6.4.5 Vertical Flow***

JSA had installed pore pressure measurement at Bayon and general trend of seasonal change is shown in Fig. 6.5. There are two measuring depths that respond differently to the rainfall.

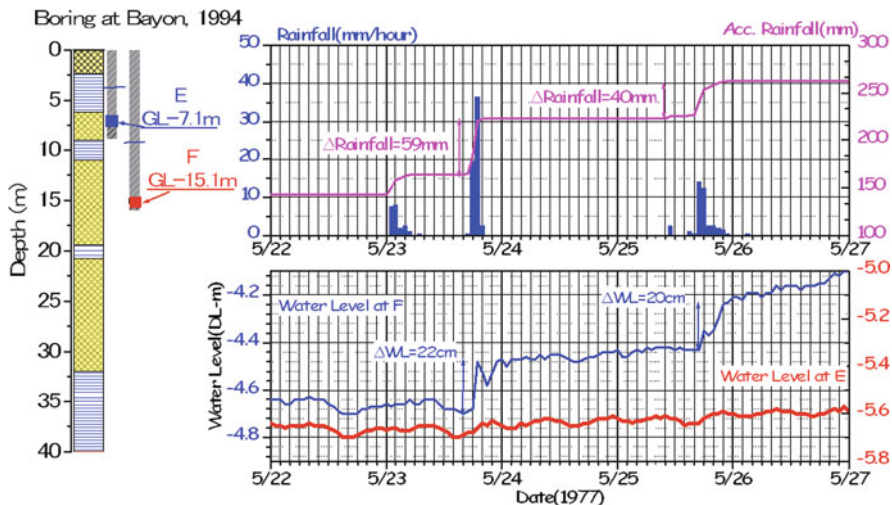


Fig. 6.20 Increase of water level for monitoring well at E and F depth

The water level at shallower point F decreases as the rain falls. Figure 6.20 shows these relationships from May 22 to 27 more clearly. In May 23 and 25, rainfall of 59 and 40 mm are recognized to result in 22 and 20 cm within a few hours after the rainfall. At the deeper depth E, the water level is not the same as the shallow depth but lower value. The lower water level at the deeper depth means that water is flowing from upper surface to deeper layer.

Figure 6.21 shows decrease of water level in dry season. The more detailed changes of water table in dry season are shown in Fig. 6.22. It is shown that the water level decreases during daytime from sunrise to sunset and increases in nighttime with a tendency of constant decrease every day. This decrease corresponds to evaporation from the deep water rather than from the shallow surface.

JICA did not recognize the effect of the evaporation upon the deep water level. The simulation by JICA report considered the evaporation effect only from shallow surface and should have included the effect of deep evaporation that could be only evaluated by field measurement.

### 6.4.6 Horizontal Flow

When we stand at the Angkor site, we see the mountain in the north and the Ton le Sap lake in the south, we think the effect of the horizontal flow may affect significantly upon the seasonal variation of the underground water. However, the basic equation that controls the flow velocity is the permeability and the gradient of the ground surface.

$$v = k \times i \tag{2}$$

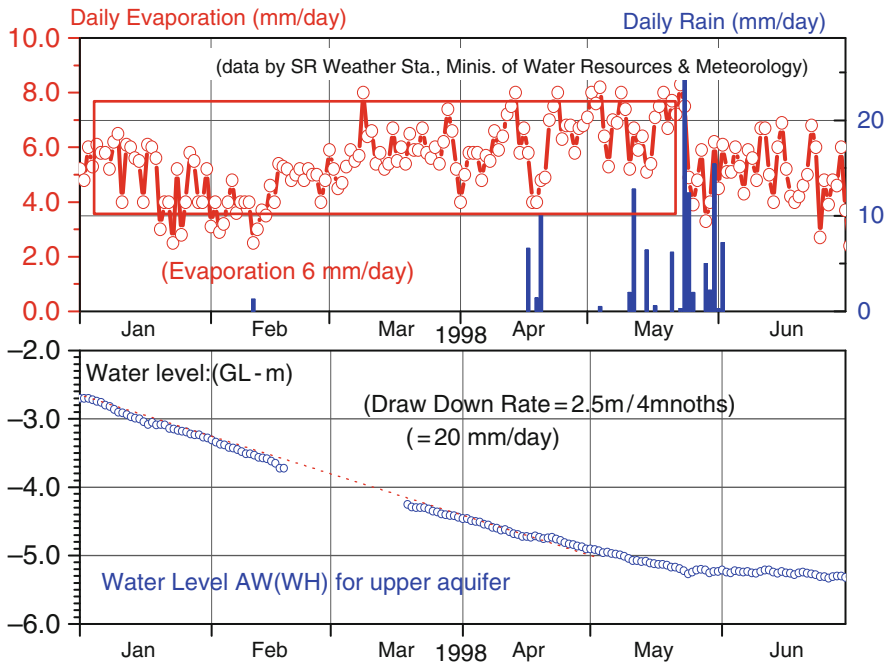


Fig. 6.21 Evaporation vs. drawdown of water level

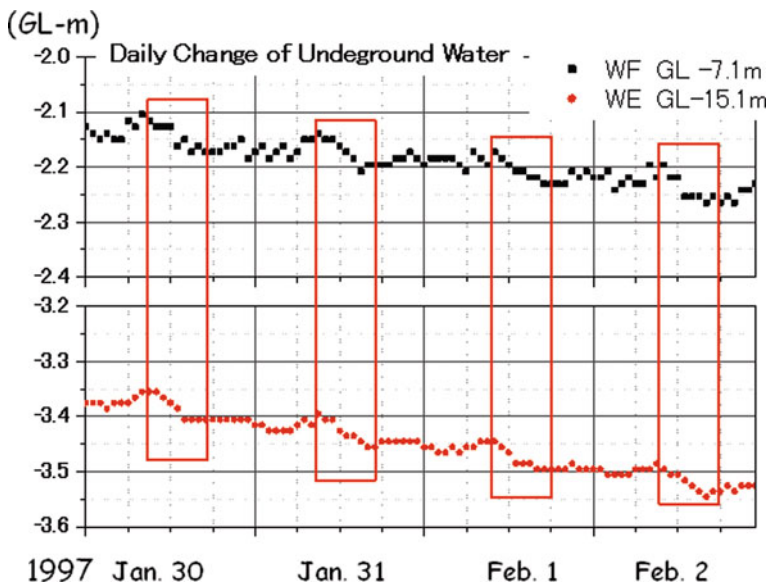
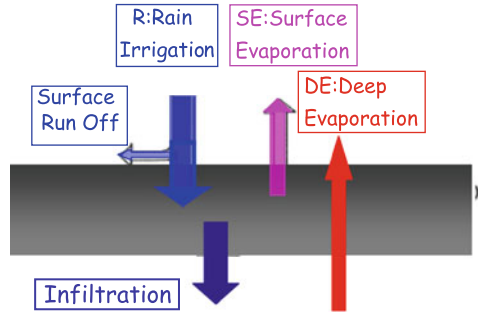
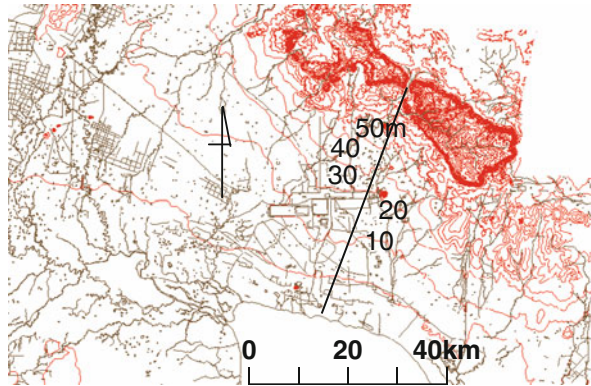


Fig. 6.22 Daily change of water level

**Fig. 6.23** Correct flow chart of water balance



**Fig. 6.24** Slow level change of Angkor plain



where,

- $v$ : velocity of underground water
- $k$ : permeability
- $i$ : inclination of the ground

The inclination of the Angkor plain is in the order of 0.001 based upon the height change of about 50 m with horizontal distance of 50 km as shown in Fig. 6.24. The possible and measured permeability of the silty sandy soil or sand is in the order of  $k = 10^{-3} - 10^{-2}$  cm/s.

The estimated apparent velocity of the underground water in Angkor plain is shown in Table 6.3 for the silty sand and sandy ground layers and only 0.3 – 3.0 m/year.

As shown in the simple calculation, the horizontal apparent water flow is less than several meters per year and gives little effect upon the seasonal change of the under ground water level except some special conditions.

**Table 6.3** Soil type and horizontal velocity

Soil type	Permeability (k (cm/s))	Inclination (i)	Apparent velocity (v (m/year))
Silty sand	0.001	0.001	0.31
Sand	0.01	0.001	3.1

### 6.4.7 Underground Water Condition in Siem Reap

As shown in Fig. 6.15 of continuous NS-lines of the highest and the lowest water level, it was found that peculiar local drawdown in the city of Siem Reap area was recognized. The monitored wells are distributed as shown in Fig. 6.25 and the highest and the lowest water level are plotted against the distance from the center of the Siem Reap city in Figs. 6.26 and 6.27.

It is clearly found that the level of the underground surface shows the lowest at the center at the Siem Reap city and gradually increases with the distance from the center. The bell shape of the surface of the ground water is kept in rainy as well as dry season.

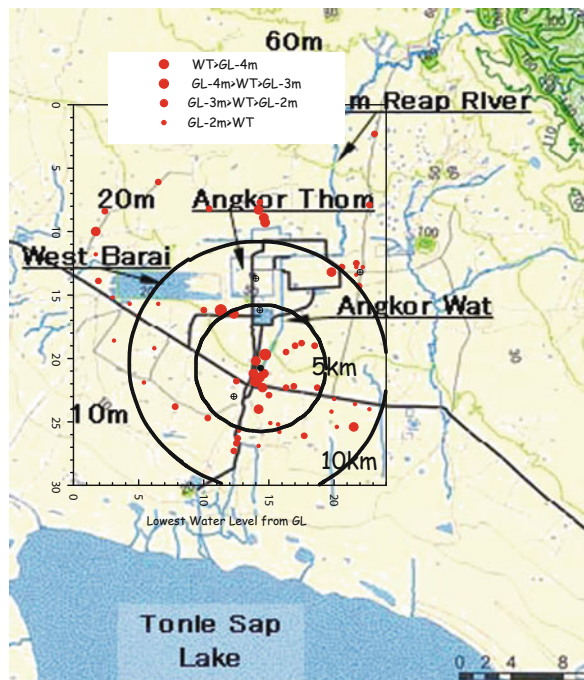


**Fig. 6.25** Distribution of well points around Siem Reap city with equi-distance circle

**Fig. 6.26** Distribution of the highest underground water around the Siem Reap city

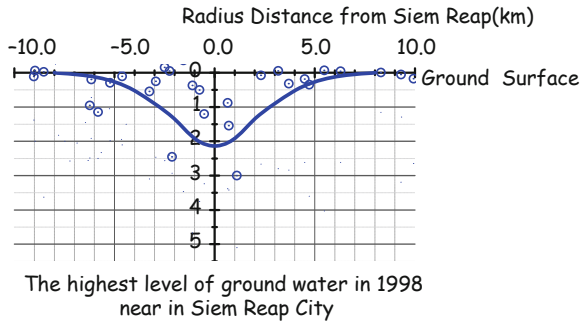
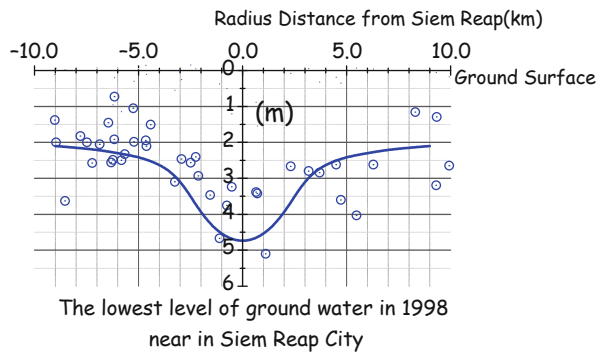


**Fig. 6.27** Distribution of the highest and the lowest underground water around the Siem Reap city



The draw down of the underground water level in Siem Reap city have been caused by too much extraction of the underground water compared to the natural capacity of recoverable water resource in the city.

## 6.5 Conclusions

The chapter shows two case histories in which the geotechnical engineers observe the unique characteristics of Angkor area that had affected upon the study of safe-guarding heritage and a project of regional sustainable development in Angkor region.

The first case of the inclination of N1 Tower of the Prasat Sour Prut was really out of the conventional concept of geotechnical engineering. The true mechanism had become apparent in the process of exposure of the trench section of the soil mound.

The second case of JICA project shows that the pitfall comes from the unique geo-hydraulic characteristics in Angkor region. JICA team did not realize the pitfall and unfortunately completed pumping facilities based upon wrong assumption. It is not clear if there is any relationship between the pitfall and the difference between predicted and observed level of water. However, they need to reevaluate the situation

based upon monitoring in the area and provide any action of feedback, if necessary, based upon the concept of observational procedure.

In geotechnical engineering, speculation, or assumed theoretical ideas are very important to grasp the physical phenomena and to understand the problems. However, the latter case shows a good example that even well experienced engineers working so many years might well fall into a very deep pitfall from where they could not find any exist to come out. As usual in geotechnical engineering, the traditional solution of observational method is the best way out.

## References

- Iwasaki Y, Nakagawa K, Fukuda M, Akazawa Y, Shimoda I, Yoshioka M (2009) Stress states of the Manmade Foundation Mound of the N1 Tower, Prasat Sour Prat, Angkor, Cambodia. Proceedings of the annual convention of Japanese Geotechnical Society, Yokohama, pp 111–112, August (in Japanese)
- JICA Report (2000) Nippon Koei Co. Ltd. and Nihon Suido Consultants Co. Ltd, The study on water supply system for Siem Reap region in Cambodia. JICA Report to Ministry of Industry, Mines, and Energy, The Royal Government of Cambodia, June
- JICA (2007) JICA study report on the observation facility and land subsidence in Siem Reap areas, handout. Water Colloquium on Siem Reap, UNESCO Phnom Penh Office, 27 Nov
- JSA Report (1995, 1996, 1997, 1998, 1999, 2000, 2001). Annual report on the technical Survey of Angkor monument, 1995–2001
- JSA Report (2005) Report on the Conservation and Restoration Work of the Prasat Sour Prat Tower (2005) Royal Plaza of Angkor Thom, Kingdom of Cambodia, JSA, Sep 2005
- Takahashi S, Suzumura T, Takahashi M (2002) Perennial groundwater yield planning for the Siem Reap region, Cambodia. KOEI Forum, vol 10, pp 51–57, Nippon Koei Co. Ltd. (in Japanese)
- UNESCO (1997) Safeguarding and development of Angkor. UNESCO Tokyo Office

# Chapter 7

## Coastal Protection

### Recent Development in the Construction of Coastal Protection Structures

Jian Chu and Shuwang Yan

**Abstract** In recent years, global warming has caused the sea level to rise. The river or coastal related disasters such as tsunami, cyclone and flood have also become higher in frequency and stronger in intensity. As one of the counter measures, some of the existing coastal protection structures need to be rehabilitated and new, stronger or taller coastal structures have to be built. How to construct coastal protection structures in a quicker and yet cost-effective way becomes a challenge to geotechnical engineers. The coastal protection structures can be classified into different categories according to the materials used. In this chapter, several new construction methods for coastal protection structures will be presented. These include the use of geo-tubes, geo-bags, geo-mattresses, geo-containers, precast concrete segments, suction caissons and assembly structures. The applications of some of these new techniques in the construction of coastal protection structures are illustrated using case histories.

#### 7.1 Introduction

There has been an increasing trend in both frequency and intensity of river and coastal related disasters in recent years. There are also concerns of the effect of seawater rising due to global warming. As a result, the construction of dikes or coastal protection structures or the rehabilitation of existing dikes or coastal protection structures has become an important part of disaster mitigation strategies. It is a challenge to geotechnical engineers to develop cost-effective methods or techniques for river or coastal protective structures that can be constructed speedily, conveniently, including techniques suitable for disaster mitigation. As dikes or other types

---

J. Chu (✉)

School of Civil and Environmental Engineering, Nanyang Technological University, Singapore, Singapore 639798

e-mail: cjchu@ntu.edu.sg

of coastal protection structures normally extend longitudinally over a long distance, a small improvement in the design could result in a significant amount of saving. Therefore, it is beneficial to review the existing design and construction methods so that some more cost-effective methods or new approaches can be established. In this chapter, several types of existing dike or coastal protection structures are reviewed. Four innovative dike construction methods for flood control, coastal protection or coastal disaster rehabilitation works are introduced. These include the use of clay filled geomats for dike construction, the use of prefabricated semi-circular caissons for offshore breakwater, the use of suction caisson for dike construction, and the use of assembly structures. Some case histories are also presented to illustrate the applications of some of these methods.

## 7.2 Types of Coastal Protection Structures

Several different types of river or coastal protection structures are summarized in Table 7.1 according to the materials used. For a complete discussion, see Chu et al. (2009). The first three are conventional types of which three typical examples from New Orleans are shown in Fig. 7.1. It can be seen in Fig. 7.1 that often more than one type of structures are adopted for dike construction. For example, compacted earth dikes can be used together with sheetpile walls as shown in Fig. 7.1b and geotextiles can be used to reduce the settlement and enhance the stability of a dike. It is important to note that the “T” wall design in Fig. 7.1b did not always perform well in the flooding following Hurricane Katrina in 2005 due to cracks forming on the flood side of the wall. These conventional forms of dike construction are not

**Table 7.1** Classification of coastal structures according to materials used (after Chu et al., 2009)

Type	Construction method
Earth-fill dike or levee	<ol style="list-style-type: none"> <li>1. Using compacted soils</li> <li>2. Using cement mix soils or bagged soil</li> <li>3. Using dumped rocks</li> </ol>
Masonry and concrete	<ol style="list-style-type: none"> <li>1. Using cast-in-place or precast concrete walls</li> <li>2. Using precast concrete panels</li> <li>3. Using roller compacted concrete</li> </ol>
Steel sheetpiles or bored piles	<ol style="list-style-type: none"> <li>1. Driven steel sheetpile wall</li> <li>2. Contiguous bored pile or prefabricated sprung piles</li> </ol>
Geotextile or geosynthetic materials	<ol style="list-style-type: none"> <li>1. Geo-tube filled with concrete mortar, sand or clay</li> <li>2. Rubber dam</li> <li>3. Geo-bag or geo-container</li> <li>4. Geo-mattress</li> </ol>
Prefabricated concrete segment	<ol style="list-style-type: none"> <li>1. Concrete caissons</li> <li>2. Semi-circular concrete caissons</li> <li>3. Steel or concrete suction piles or caissons</li> <li>4. Tongtu assembly method</li> </ol>
Mix types	Dike construction involving the use two or more of the above methods

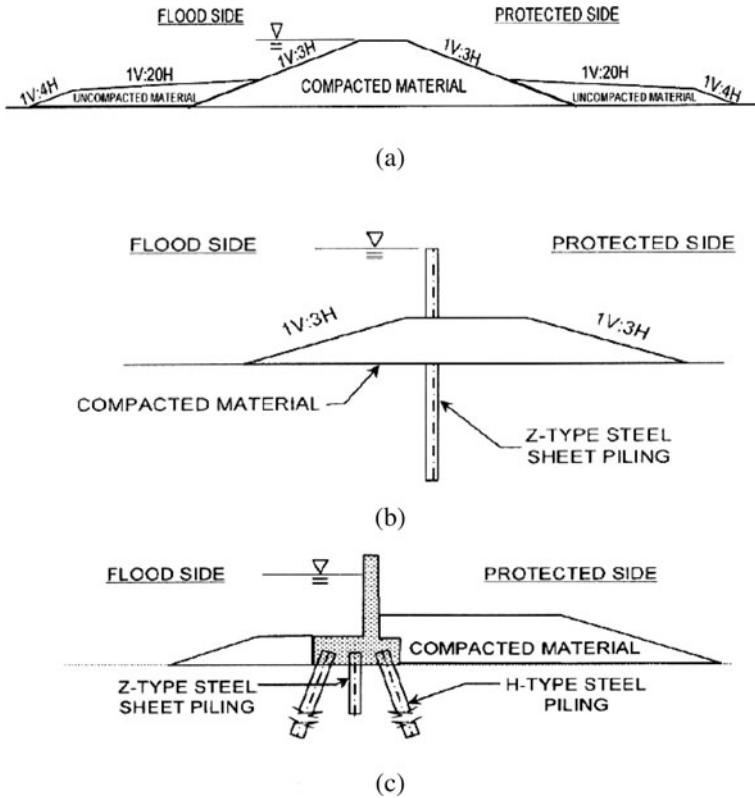


**Fig. 7.1** Flood protection structures used in the New Orleans area. (a) Dike made of compacted soil; (b) dike made of steel-sheetpiles; dike made of precast concrete wall (after Mosher and Duncan, 2007)

discussed further in this chapter, which will focus instead on the three novel types of structure in Table 7.1, use of geo-tubes and geo-bags, caissons and mixed types.

### 7.3 Geotextile Mat Method

The traditional method of constructing shoreline structures is to use rock or precast concrete units. In recent years, several methods have been developed to use geotextile materials for the construction of coastal structures such as breakwaters and dikes. One of them is to use geotextiles acting as formwork for cement mortar units cast in situ, see Fig. 7.2 (Silvester and Hsu, 1993). The mortar mix needs be only of sufficient compressive strength to support the weight above, plus the moment from the side force of the waves. Since the flexible membrane is required to hold the mixture in place until it sets, any subsequent deterioration due to UV rays or

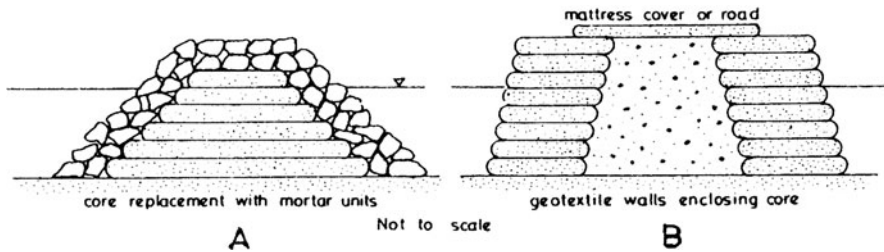


**Fig. 7.2** Use of geotextiles: (a) to replace core material and (b) to provide a space for core fill (after Silvester and Hsu, 1993)

other conditions is of little concern. Thus, the method tends to be cheaper than the conventional methods.

Water or air inflated rubber bags have also been used to provide a flexible and sometimes temporary barrier (Zhang et al., 2002; Chu et al., 2009). One example is shown in Fig. 7.3 for adjusting the water level in a river for flood control or irrigation purposes in China. Rubber dams have also been used for relatively large scale projects in recent years. One of the largest so far is the rubber dam used for the Ramspol storm surge barrier in Netherlands. To protect West Overijssel, a province in The Netherlands, against flooding due to high water at the Jsselmeer and Ketelmeer, a storm surge barrier as shown schematically in Fig. 7.4 has been constructed. Three identical inflatable rubber dams were used. The dimensions of each rubber dam are 75 m long, 13 m wide and a design height of 8.35 m. A unique feature of this project is that a combination of air and water was used as the inflation medium. This minimised the dimensions of the rubber body and also allowed the



**Fig. 7.3** A rubber dam crossing a river

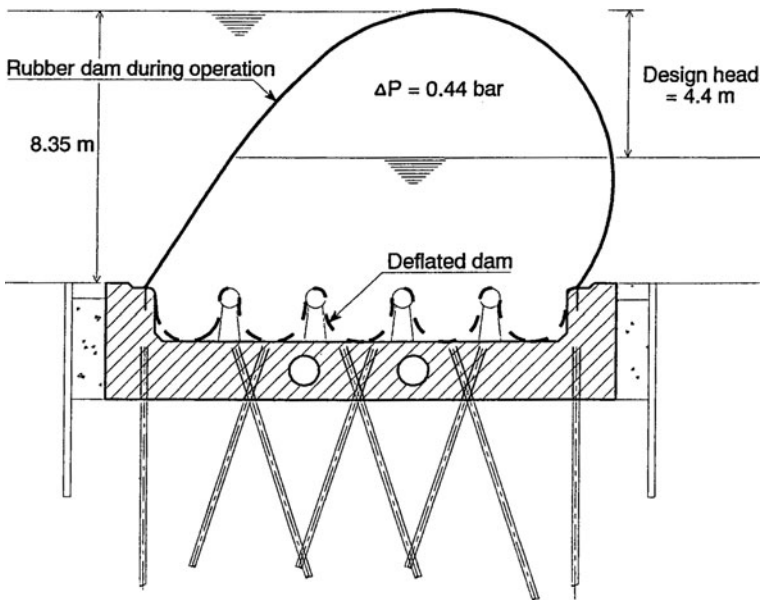


**Fig. 7.4** Rubber dam used for the Ramspol storm surge barrier in Netherlands (after Rövekamp, 1999)

height of the dam to be adjusted quickly. More information on this project can be found in (Rövekamp, 1999).

Similar methods, but using sand or soil slurry as the fill material have also been used for dike construction (Kazimierowicz, 1994; Miki et al., 1996; Leshchinsky et al., 1996). Sand or sandy soil is the most ideal fill material for this purpose. For near shore or offshore project, a suction dredger can be used to pump sand from the seabed or a sand pit directly into the geotextile tubes. In case sand is not readily available, silty clay or soft clay may also be used. In this case, the clayey fill would have to be in a slurry state in order to be pumped and flow in the tube. The slurry then has to be dewatered in the geotextile bags or tubes to reduce the water content and allow excess pore pressures to dissipate. Then the selection of the geotextile used for the bags or tubes becomes important. The geotextile has to be chosen to meet both the strength and filter design criteria. Some analytical methods have been developed to estimate the required tensile strength for the geotextile (Kazimierowicz, 1994; Miki et al., 1996). The apparent opening size (AOS) of the geotextile needs to be selected to allow the pore pressure to dissipate freely and yet retain the soil particles in the bags.

The technique of using clay slurry fill geomats (geotextile mats) for dike construction was developed in Tianjin, China, and used for one land reclamation project along the coast of Tianjin (Chu and Yan, 2007; Yan and Chu, 2010). The cross-section of the dike is illustrated in Fig. 7.5 and a picture showing the alignment of the bags is shown in Fig. 7.6. It can be seen that large flat geotextile bags in the form

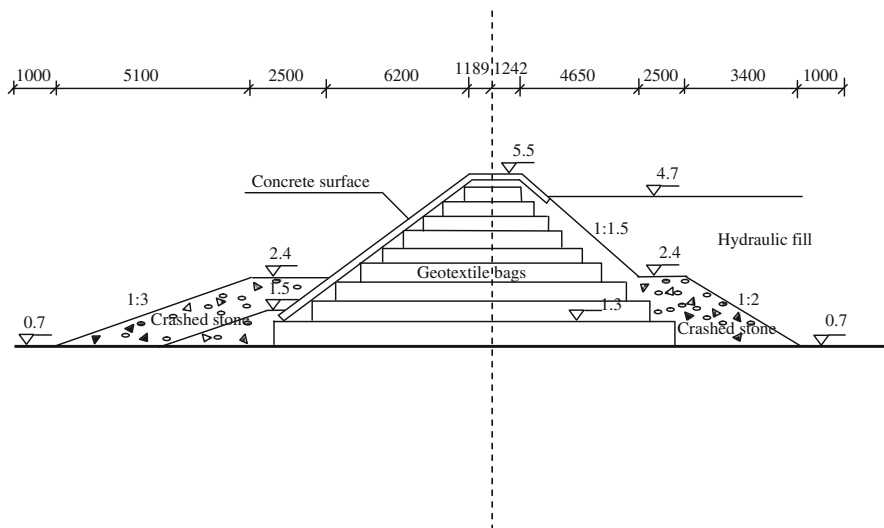


Fig. 7.5 Schematic illustration of the dike made of clay slurry filled geotextile bags

of geomats, instead of tubes, were adopted in this example. As shown in Fig. 7.5, the designed height of the dike was 4.8 m with base and top elevations at 0.7 and 5.5 m respectively. The top width of the dike was 2.43 m. The water levels were at 4.7 m elevation during high tide and at nearly 0.7 m elevation during low tide. The outer and inner slopes of the dike were chosen to be 2L:1H and 1.5L:1H, respectively.



Fig. 7.6 A picture showing the formation of a dike using clay slurry filled geotextile bags

For the bottom bag, the dimension used was 30 m in circumference. Clay slurry was dredged from the seabed of a selected area and pumped directly into the bags through an injection hole. The height of the bag after consolidation was around 0.5 m. Nine layers of geomats were used.

The dike built with the large size geomats was then protected by casting a 25 mm thick grouted geotextile mattress on top of the surface after the settlement of dike stabilized. The grouted geotextile mattress was formed by pumping lean concrete into a mould made of geotextile. A picture showing the dike covered by the cast-in-place concrete mattress is given in Fig. 7.7. Berms were used to enhance the stability of the dike and to protect the toes of the slopes. The berms were made of crushed stones of 50–80 kg. The slopes of the berms were 2L:1H for the inner side and 3L:1H for the outer side, see Fig. 7.5. A woven polypropylene geotextile with a mass density of 131 g/m<sup>3</sup> was used for the bags. It had a tensile strength of 28 kN/m in the longitudinal and 26 kN/m in the transverse direction respectively. The AOS (O<sub>95</sub>) of the geotextile was 0.145 mm. The bags are sewn together using sewing machines on site. The soil used to fill the bags was classified as SC-CL according to the Unified Soil Classification System (USCS). The liquid limit and plastic limit of the soil were 20.4 and 11.5% respectively and the plasticity index was 8.9%. A more detailed description of this method can be found in Yan and Chu (2010).

There are a number of advantages for using mats for dike construction. Firstly, as the lateral dimension is very large comparing to its height, geomat does not have



**Fig. 7.7** A concrete cover made of grouted geotextile mattress

lateral stability problems. Secondly, construction can also be speedier as pumping can be carried out at a number of points. Thirdly, the dike made of geomats can accommodate relatively large differential settlement. This may result in savings in the foundation treatment. Despite of the various advantages, there is a lack of design or analysis method for dikes constructed using this method. To overcome this problem, some analytical methods are being developed (Guo, 2009). Finite element methods have also been used (Guo, 2009).

## 7.4 Prefabricated Caisson Method

The geobag or geomat method may only be feasible when dikes are to be constructed in relative shallow or quiet water. When the depth of water is too great or waves are rough, gravity retaining structures using prefabricated reinforced concrete segments or caissons may be a better option. The use of caisson or concrete segments is not new. However, the most cost-effective design methods are still to be established. These concrete segments or caissons have to be tall enough to match the water depth and heavy enough to provide stability against the waves. However, when the concrete segments or caissons are too heavy, they cause settlement or bearing capacity problems. This is particularly the case when the foundation soil is soft. Weak foundation soil can be improved. However, it is difficult and costly to treat soil offshore and over a large area or distance. Therefore, the construction of large size gravity structures on soft soil offshore remains a challenge.

In one of the coastal protection projects along the Yangtze Estuary, some dikes for navigation purposes needed to be constructed. The method of using prefabricated reinforced concrete caissons was adopted. The dike was to be constructed 40 km away from the coast where the water depth ranged from 5.0 to 8.5 m. The design wave height was 3.32–5.90 m with a return period of 25 years. The total length of the dike was about 17 km.

The design of the dike is schematically shown in Fig. 7.8 (Yan et al., 2009). The caisson used was a prefabricated reinforced concrete hollow segment. It was semicircular in cross-section, as shown in Fig. 7.8, with a radius of 5.7 m. The advantage of using a semicircular cross-section is that the direction of the resultant wave force on the semicircular shaped structure will always pass through the center of the circle, which will greatly improve the loading condition of the structure. The hollow caisson would be filled with sand after installation through a 600 mm diameter hole on top of the caisson. In order to prevent the foundation soil from scouring, a geotextile sheet was used to cover the seabed. A cushion which acted as the foundation bed was placed on top of the geotextile. The cushion was 1–2 m high. It was made of crushed stones of 1 ~ 100 kg for the centre and 200 ~ 400 kg for the edge. After the caisson was placed, berms were placed on two sides of the caisson. The berms were made of 400 ~ 600 kg crushed stones. An artistic illustration of the dike is shown in Fig. 7.9.

The soil profile below the dike consisted of a 1.5–3.5 m thick silt sand followed by 2–4 m thick clay mud and a roughly 30 m thick soft clay underlying the mud.

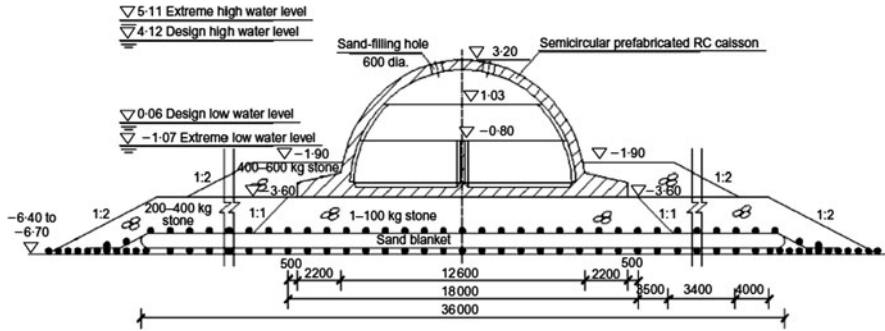


**Fig. 7.8** Cross-section of the dike (after Yan et al., 2009)

To ensure the stability of the breakwater against future storms, a soil improvement scheme was adopted to improve the soft soil layers below the caissons. The seabed was 5–8.5 m below the mean sea level. Several soil improvement methods were considered. The chosen method was to use prefabricated vertical drains (PVDs) to accelerate the consolidation process of soft clay as this was considered to be the most economical option. The method was also relatively easy to implement. The PVD used had a core made of transparent polypropylene plastic and a filter made of long-fiber hot-bonded non-woven filter fabric. PVDs were installed offshore from a specially designed PVD installation barge, as illustrated by a photo in Fig. 7.10.

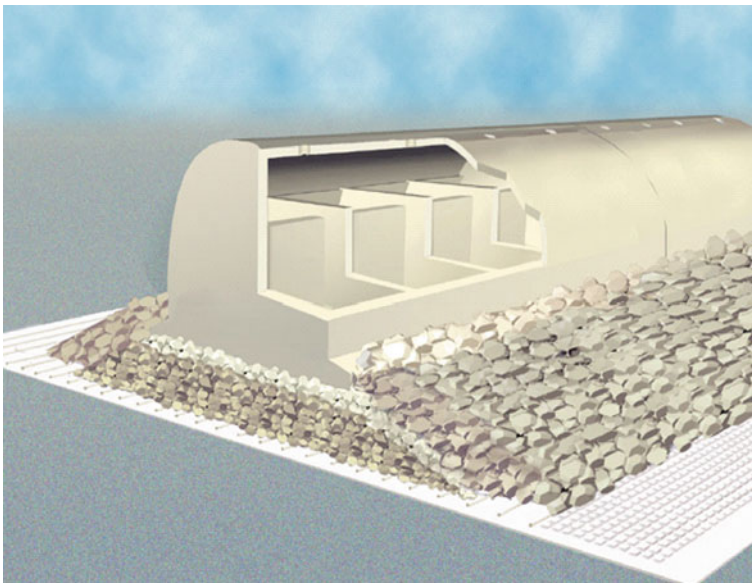


**Fig. 7.9** Illustration of the prefabricated caisson supported on a rubble mound with scour protection cover



**Fig. 7.10** Offshore PVD installation barge (after Yan et al., 2009)

There were 12 drain installation rigs on each barge with preset spacing of 1 m on a square grid. The position of each drain was located using GPS. Each barge could install 1,185 drains/day on the average.

An analysis of the stress distribution in the foundation from the design width of the dike (Fig. 7.8) indicated that the influence of the surcharge was mainly within the top 7 m below the seabed. Therefore, it was only necessary to install PVDs to a depth of 10 m. The weight of the rubble mound was considered sufficient surcharge with the weight of the 3 m thick crushed stone cushion giving an effective vertical stress of 30 kPa. The designed loading duration was 90 days.

The procedure for improving the soft soil before the placement of the rubble mound and the caissons was as follows: (1) PVDs were installed from the PVD installation barge at a spacing of 1.0 m on a square grid to a depth of 10 m below the seabed; (2) a layer of geotextile with sand filled geotextile tubes was installed on the seabed; the tubes were formed by filling sand into 300 mm diameter geotextile tubes from a barge on site before the geotextile and sand tube composite was placed, as shown in Fig. 7.11; the tubes were spaced every 500 mm apart under the toe and 1,000 mm apart below the centre of the rubble mound; (3) a 700 mm thick sand cushion was placed over the lower geotextile layer with sand tubes before the second layer of geotextile with sand filled geotextile tubes was laid on top; (4) crushed stones were then laid from a barge on to the second layer of geotextile with sand tubes which also acted as a surcharge to consolidate the soil below; (5) the caisson segments were only placed after an average degree of consolidation of 80% was achieved, which took about 90 days after the placement of the rubble mound; (6) a 40 m wide geotextile and precast concrete block composite was then used to cover



**Fig. 7.11** Placement of geotextile with sand filled geotextile tubes (after Yan et al., 2009)

the seabed outside the toe of the rubble mound where it faced the open sea for the prevention of scour. The geotextile and concrete block composite and its installation process are shown in Fig. 7.12. The concrete blocks were  $400 \times 400$  mm on a square and 160 mm thick. They were attached to the geotextile sheet to form a composite.



**Fig. 7.12** Installation of the geotextile and concrete block composite (after Yan et al., 2009)

In addition to soil improvement, anti-sliding rubber pads were also used to cover the base of the caisson to enhance its ability to resist lateral sliding. The rubber pads were embedded into the base of the caisson during the casting stage. The dimension of each rubber pad was  $1,994 \times 1,000 \times 30$  mm. Pins of 20 mm in diameter and 100 mm long were also precast into the base of the caisson to enhance the anchoring effect. The spacing of the pins was 400 mm in square grid.

## 7.5 Suction Caisson Method

One of the disadvantages of the prefabricated concrete caisson method described above is the need to treat the soft seabed soil and to construct the rubble mound which can be time consuming and expensive. For these reasons, the gravity caisson method may not be considered suitable for disaster mitigation purposes. Another method for breakwaters or seawalls construction is the use of cylindrical steel or concrete suction piles or caissons. This method is particularly suitable to the construction of breakwaters on soft seabed or in deep water. A suction caisson is like an open ended cylindrical pile with the top sealed. The suction caissons can be sunk into the seabed using suction applied into the inner chamber of the pile until sufficient bearing capacity is obtained. In this way, the soft foundation soil does not have to be improved. This method is particularly suitable for disaster rehabilitation or restoration of failed seawalls requiring a rapid construction solution. The concrete caissons can be fabricated using standard modulus. They can be towed into position and installed from a barge. The installation can then be done quickly as no soil treatment is required.

This method has been used in China in a breakwater project recently. Four 12 m in diameter prefabricated reinforced concrete cylinders were connected together using four concrete walls to form one unit as shown in Fig. 7.13a. The top opening

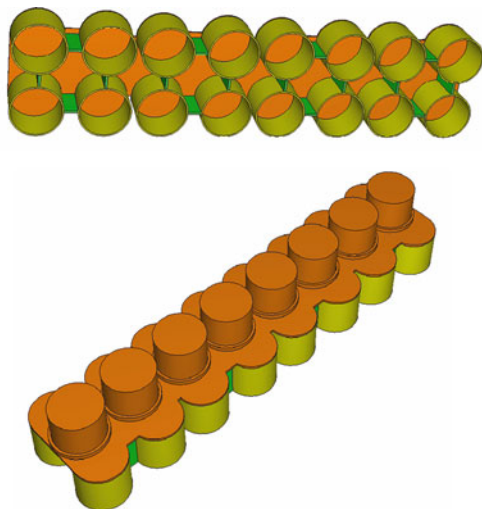


**Fig. 7.13** Layout of the suction caissons: (a) view of the bottom of the suction caissons; (b) view of the top of the concrete suction caissons showing the top cylinders used as part of the breakwater



**Fig. 7.14** Installation of concrete suction caissons

of the four cylinders was sealed by a precast concrete plate as shown in Fig. 7.13a. The unit formed by the four cylinders was towed to the required position and sunk onto the seabed by ballasting. Suction was then applied simultaneously to the inner chambers of the four cylinders which were sealed at the bottom by the seabed clay. Under the suction and the hydrostatic pressure, the four cylinders were dragged down to penetrate into the seabed soil. The suction was removed after the penetration depth of the cylinder was sufficient. The amount of penetration required were calculated in accordance with the bearing capacity that had to be provided by the shaft friction. After the four cylinder units were installed, another row of prefabricated concrete cylinders of the same diameter was installed on top of the bottom units as shown in Fig. 7.13b. The operations for the installation of the lower four cylinder unit and the upper cylinders are shown presented in Figs. 7.14 and 7.15 respectively.

## 7.6 Tongtu Assembly Method

Another innovative method, the so-called Tongtu assembly method, has been developed by Tongtu Technology Ltd, China (<http://www.tongtutech.com/>). This method can be used for the construction of sea dikes, breakwaters or man-made island on soft or weak seabed. In this method, precast concrete beams and columns are used together with stones to form a seawall as shown in Fig. 7.16, see <http://www.tongtutech.com/> or Chu et al. (2009) for more detail. As all the elements are prefabricated and no specialized machineries are required, this method is also suitable for disaster mitigation and rehabilitation works.



**Fig. 7.15** Installation of upper cylinders to form breakwater

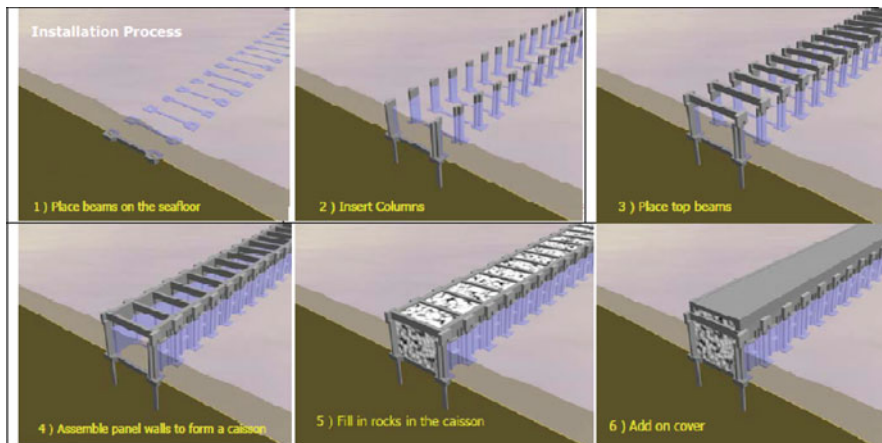


**Fig. 7.16** Construction procedures for the Tongtu Assembly Methods (Courtesy of TongTu Technology, Ltd. Co.)

## 7.7 Conclusions

Several innovative dike construction methods have been introduced in this chapter. Some case studies are also presented. It should be pointed out that certain methods may only be suitable for specific site conditions. The cost effectiveness of each

method also depends on the cost and availability of the materials and construction machines as well as the construction processes. The advantages and limitations of each method are summarised as follows:

1. The geotextile mattress or geomat method is suitable for the construction of a breakwater or dikes in relatively shallow water. It has the advantage of providing good lateral stability and ease of construction. The case study presented shows that clay slurry can also be used as fill material for the mats. However, design and analysis methods for the use of clay slurry as filling for the geomat have not been fully established yet and more studies and field verifications are required. The dike constructed using this method is normally covered by a thin layer of grouted geotextile mattress after the settlement of dike stabilized.
2. The prefabricated concrete caisson method is suitable for the construction of seawalls or sea dikes in relatively rough water conditions. When the seabed soil is soft, ground improvement will be necessary before constructing the dike even though a thick cushion made of crushed rocks is used. In the case study presented, prefabricated vertical drains installed from an offshore drain installation barge were used with the rubble mount as surcharge. To enhance the lateral stability, rubber mats with pins should also be used for the base of the caisson. Two new seabed scour protection methods were also adopted in this case study.
3. The suction caisson method is a relatively new, but promising technique. It is particularly suitable to the installation of seawalls in relatively deep water and soft seabed. With the use of suction caissons, treatment of soft seabed soil is no longer required. However, more field experience needs to be established. More theoretical studies are also required to guide the design and construction.
4. The Tongtu Assembly Method allows quick installation of breakwaters or other types of coastal structures without the use of heavy construction plant. However, it may only be suitable to relative soft seabed conditions and is also limited to relatively shallow water.

**Acknowledgments** The writers would like to thank Tongtu Technologies, China, for their permission of using the figures shown in Fig. 7.16.

## References

- Chu J, Varaksin S, Klotz U, Menge P (2009) Construction processes, State-of-the-art report. Proceedings of 17th international conference on soil mechanics and geotechnical engineering, Alexandria, Egypt, 5–9 Oct, pp 3006–3135
- Chu J, Yan SW (2007) Ground improvement in disaster mitigation and rehabilitation works. Invited special lecture. Proceedings of the 16th Southeast Asian geotechnical conference, 8–11 May, Kuala Lumpur, pp 163–170
- Guo W (2009) Dike construction using geotubes. First year progress report, Nanyang Technological University, Singapore
- Kazmierowicz K (1994) Simple analysis of deformation of sand-sausages. Proceedings of the 5th international conference on geotextiles, geomembranes and related products, Singapore, 5–9 Sept, vol 2, pp 775–778

- Leshchinsky D, Leshchinsky O, Ling HI, Gilbert A (1996) Geosynthetic tubes for confining pressurized slurry: some design aspects. *J Geotech Eng ASCE*, 122(8):682–690
- Miki H, Yamada T, Takahashi I, Shinsha H, Kushima M (1996) Application of geotextile tube dehydrated soil to form embankments. Proceedings of the 2nd international conference on environmental geotechnics, Osaka, 5–8 Nov, pp 385–390
- Mosher RL, Duncan JM (2007) Levee failure mechanisms. *Geo-Strata*, ASCE, 8(1):20–238
- Rövekamp NH (1999) Storm surge barrier Ramspol. *Baustatik-Baupraxis* 7, CRC Press (Available from <http://www.dmc.nl/publications/infra/storm-surge-barrier-ramspol/item161>)
- Silvester R, Hsu JRC (1993) Coastal stabilization – innovative concepts, Prentice-Hall Inc., Englewood Cliffs, NJ
- Yan SW, Chu J (2010) Construction of an offshore dike using slurry filled geotextile mats. *Geotext Geomembranes* 28:422–432
- Yan SW, Chu J, Fan QJ, Yan Y (2009) Construction of offshore breakwater on soft clay using prefabricated caissons. *Geotechnical engineering*, Proceedings of the ICE, London, vol 162, GE1, pp 3–12
- Zhang XQ, Tam PWM, Zhang W (2002) Construction, operation, and maintenance of rubber dam. *Can J Civil Eng* 29:409–420

## Chapter 8

# Combined Hazards

### Seismic Hazard Maps of Indonesia and Geotechnical and Tsunami Hazard Assessment for Banda Aceh

Masyhur Irsyam, H. Hendriyawan, M. Asrurifak, Hamzah Latif, Nazili Razali, and Anita Firmanti

**Abstract** This chapter presents research works carried out in developing the latest spectral hazard maps proposed as input for revision of Indonesian Earthquake Resistant Building Code, the SNI 03-1726-2002. Improvement in seismic hazard analysis and careful inclusion of recent seismic records were augmented. Seismic sources were modeled by background, fault, and subduction zones considering truncated exponential model, pure characteristic model or both. Several well-known attenuation functions were selected including the Next Generation Attenuation (NGA). Maps of Peak Ground Acceleration (PGA) and Spectral Response Acceleration (SRA) for 0.2 s (short periods) and 1.0-s period for 2% probability of exceedance in 50 years were developed using PSHA. Additional geotechnical and tsunami hazard assessment researchs for Banda Aceh city, the capital of Aceh Province were also submitted. The results of site response analysis and liquefaction study at several points were utilized to generate contours of acceleration, amplification factor, design response spectra, and potential of liquefaction for Banda Aceh. The tsunami hazard study was conducted using mathematical simulation and modeling leading to estimate the potential tsunami that may occur in the future which covers tsunami inundation, run-up, and developing tsunami zonation map. The output of geotechnical and tsunami hazard assessment was then overlaid on top of the land use city planning in a Geographical Information Systems (GIS) database and used as criteria for tsunami warning system, an input in developing land use management for Banda Aceh, and enriching the basic regulation for new infrastructures and local building codes.

---

M. Irsyam (✉)  
Faculty of Civil and Environmental Engineering, Institut Teknologi Bandung,  
Bandung 40132, Indonesia  
e-mail: masyhur.irsyam@yahoo.co.id

## 8.1 Background Research

Indonesia has been well known as one of the most seismically active countries in the world. It is surrounded by three major active tectonic plates of the earth: Eurasian, Indo-Australian, and Philippine plates. Therefore, the construction design in Indonesia should consider these seismic activities. The most effective way to reduce disasters caused by earthquakes is to estimate the seismic hazard and to implement this information on a seismic code for use in building design and construction so that the structures possess adequate earthquake resistant capacity (Hu, 1996; Irsyam et al., 2008).

The need to revise current Indonesian Seismic Hazard Map expressed as PGA contained in our latest Indonesian Earthquake Resistant Building Code SNI 03-1726-2002 (Fig. 8.1) was driven among others by the desire to better reflect potential larger earthquake disasters faced by the nation predictably in the future (Irsyam et al., 2008). Two major expected revisions are the earthquake hazard map, to reflect the latest advancement in Probabilistic Seismic Hazard Analysis (PSHA) technology accounting for potential larger disasters predicted in the near future, and changing the provision from UBC-97 concept to the latest ASCE 7-05 and IBC-2009 provisions. It is targetted that the renewal of Indonesian Earthquake Resistant Building Code, the SNI 03-1726-2002, will be finished by mid of 2010.

Several great earthquake occurrences in Indonesia in the last 6 years inquire revision of seismic hazard parameters. Some of the great earthquakes are the 2004 Aceh Earthquake ( $M_w$  9.0–9.3) which was followed by tsunami, the 2005 Nias Earthquake ( $M_w$  8.7), the 2009 Tasik Earthquake ( $M_w$  7.3), and the latest 2009 Padang Earthquake ( $M_w$  7.6). The Aceh earthquake and the following tsunami

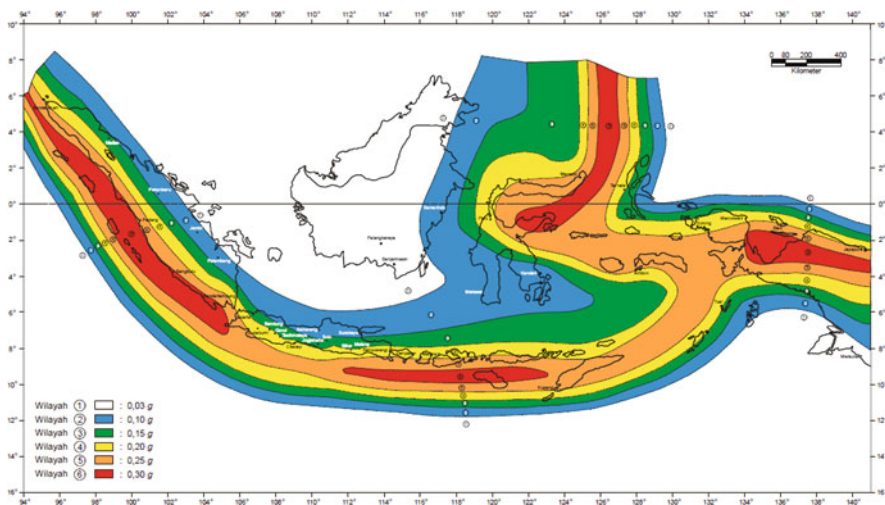


**Fig. 8.1** Indonesia seismic hazard map (SNI 03-1726-2002)

destroyed countless engineered and non-engineered buildings, infrastructure, and utilities. Therefore, geotechnical and tsunami hazard assessment researchs for Banda Aceh city in particular were also required to better reflect Indonesia overall potential disaster.

This chapter presents the latest research works for developing seismic hazard maps of Indonesia. The maps are based on spectral acceleration rather than PGA, two maps of SRA are selected: for short period (0.2 s) and for long-period (1.0 s). The purpose of this research is to provide input for revision of the current seismic hazard map. The research also covers geotechnical microzonation study for Banda Aceh city for estimating the effects of local soil conditions to the surface ground motion and to the potential of liquefaction. Furthermore, tsunami hazard study is also performed to obtain tsunami inundation and run-up for Banda Aceh city.

### 8.2 Tectonic Setting of Indonesia

Indonesia is located in a tectonically very active area at the point of convergence of three major plates and nine smaller plates as developed by Bird (2003). The Eurasian, Pacific and Australian-Indian plates, along with some smaller plates (i.e. Philippine Sea plate), are all actively moving toward each other in the Southeast Asia region (Fig. 8.2) creating a complex network of plate boundaries.

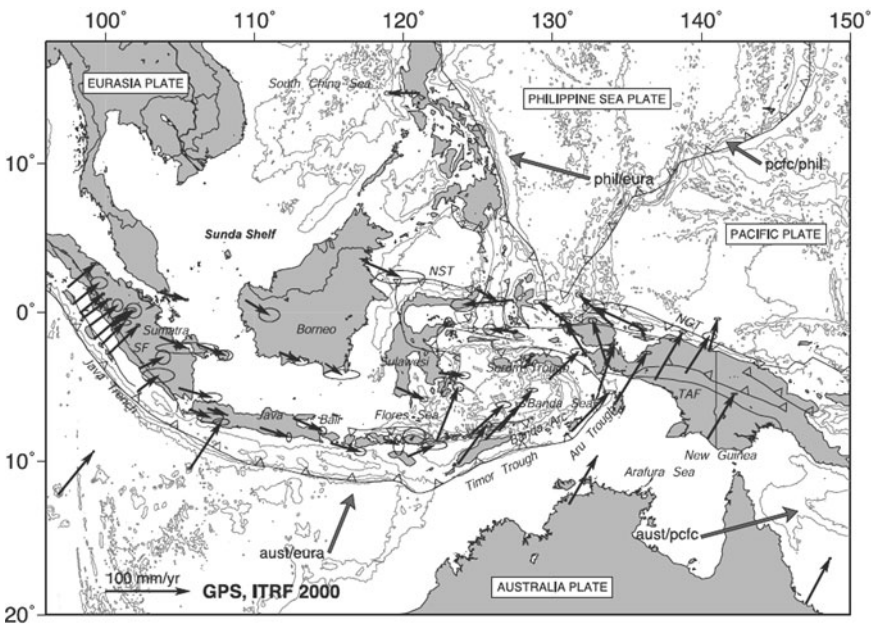


Fig. 8.2 Topographic and tectonic map of the Indonesian archipelago and surrounding region (Bock et al., 2003)

Western Indonesia tectonically consists of the Sunda Shelf which includes the islands of Sumatra, Java, Bali, Borneo, and the southwestern part of Sulawesi (Hamilton, 1979). The active tectonics of western Indonesia is dominated by convergence of the Australia plate with Sumatra and Java. Along Sumatra the direction of convergence is highly oblique to the trench strike, and is partitioned into nearly arc-perpendicular thrusting at the trench and arc-parallel, right lateral slip at the Sumatran fault (Bock et al., 2003).

For eastern Indonesia, the crustal composition south of Java and Bali and in the south Banda Sea are oceanic, and the Arafura sea and Timor trough are underlain by continental crust. This, along with the geological evidence of exposed overthrust sheets of the Banda allochthon on the island of Timor, indicates collision of a continent with an island arc along the outer Banda arc, and suggests underthrusting of continental crust under Timor. Two plates subduct beneath the Banda Sea, one from the south at the Timor and Aru troughs, and the other from the north at the Seram trough, and the two slabs are separated at the Tarera-Aiduna fault, which acts as a transform (Bock et al., 2003).

Further East, the continental part of the Australian plate collides with the Banda arc, resulting in widespread deformation throughout the Banda island-arc. Further complicating the tectonics of East Indonesia, Australian continent also collides with the Pacific oceanic plate, resulting in uplift and extensive faulting on the island of New Guinea. Australia-Pacific convergence is highly oblique and appears to be partitioned into components perpendicular and parallel to the margin. The perpendicular component is taken up by crustal shortening in the Highlands thrust belt and very likely, subduction along the New Guinea and Manokwari trenches. The margin-parallel component results in left-lateral shear zones along North New Guinea. The existence of subduction zones have created zones of earthquakes that contribute to the event earthquakes occurred in the Indonesian Region (Milsom et al., 1992).

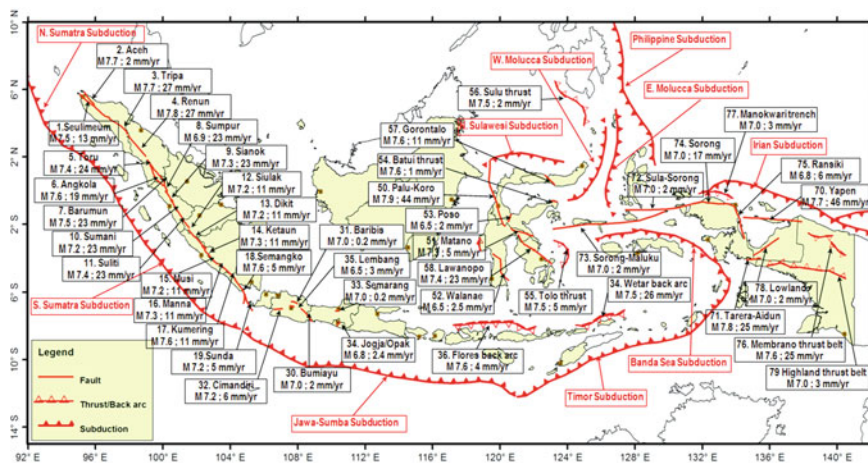


Fig. 8.3 Major tectonic features of Indonesia and their parameters

There are some potential active fault distributions around Indonesia islands (Fig. 8.3). The Sumatran fault zone (SFZ) is a 1,900-km-long structure that accommodates right lateral shear associated with the oblique convergence along the plate margin and widely accepted as highly segmented fault. Seismicity of Java is significantly low compared to that along the SFZ (Lasitha et al., 2006). The strike-slip events may account for the presence of the Cimanderi, Lembang, Bumiayu, Semarang or Opak (Jogja) fault. The island of Sulawesi in eastern Indonesia has more active faults as Palu-Koro, Matano, Walanae, Poso, Batui thrust, Tolo thrust, Sulu thrust, Gorontalo and Lawanopo (Socquet et al., 2006). In the island of Papua, faults that have been identified include Yapen, Tarera-Aiduna, Sorong, Ransiki, Membrano thrust-belt, Manokwari trench, Lowland and Highland thrust-belt.

## 8.3 Development of Seismic Hazard Maps of Indonesia

### 8.3.1 Earthquake Catalog

Historical earthquake events from 1900 to 2008 are compiled from many sources such as:

- a. Earthquake listings held by National Earthquake Information Service U.S. Geological Survey (NEIS-USGS) of the United State, which is a compilation of several catalogs from sources such as: The Bureau Central International de Séismologie (BCIS), the International Seismological Summaries (ISSN), the International Seismological Center (ISC), the Preliminary Determination of Epicenters (PDE), and The Advanced National Seismic System (ANSS) catalog.
- b. Indonesia earthquake listing prepared by the Bureau of Meteorology and Geophysics (BMG), Jakarta, Indonesia.
- c. Centennial Catalog which is compiled from Newcomb and McCann (1987) where several large event in Indonesia have been relocated and Pacheco and Sykes (1992) where the earthquakes were corrected for heterogeneity's caused presumably by changes in instrumentation, reporting and/or detection capabilities.

### 8.3.2 Seismic Source Model

The seismic source model for input to PSHA was defined using earthquake catalogs, tectonic boundaries, and fault information. The sources model was divided into subduction source, fault source, and background seismicity. This division followed previous studies by Irsyam et al. (2009a, b). However, updating of seismic source parameters used in the previous studies have been performed based upon the most recent work in Indonesia. The updated parameters are already included in Fig. 8.3.

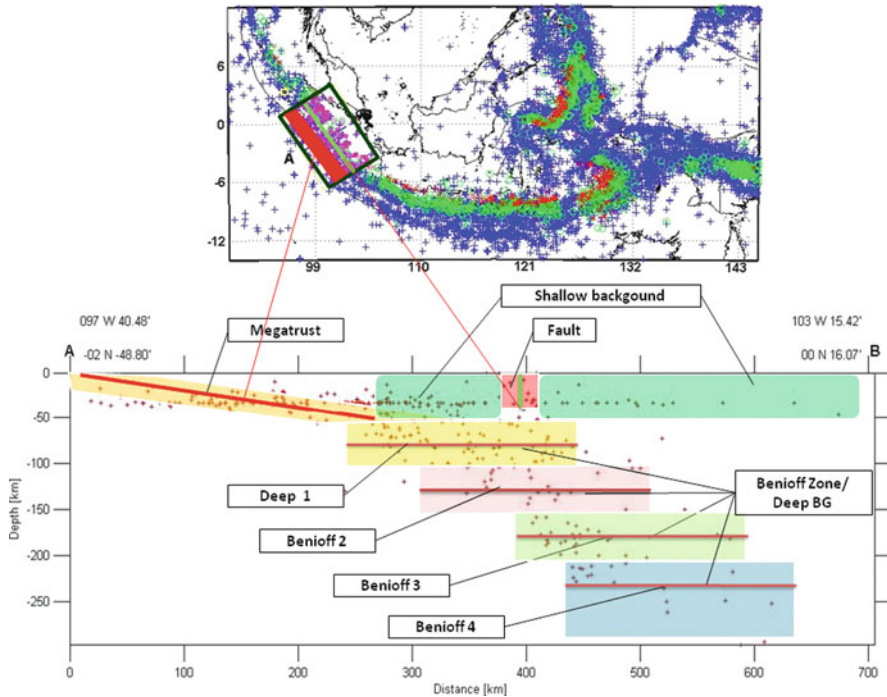


**Fig. 8.4** Classification of main shocks based on type of seismic sources

Subduction mechanism occurred when an oceanic plate is being subducted under an island arc or continent. Thrust fault mechanism may occur along the interface, while normal faulting may occur toward and along the outer-arc and in the trench. The subduction events source models were limited to Megathrust zones (Fig. 8.4). For earthquake events that occurred in the Benioff zones below the Megathrust were accounted in deep background sources.

Fault source represents individual fault for which data is sufficient to determine maximum earthquake magnitudes distributions and slip rate estimates. The major tectonic feature and sense of faulting, slip-rate, dip, width and maximum magnitude used in this work were estimated based on published data. At present, continuous updating of seismic source parameters is still conducted by the Indonesia Team for Revision of Seismic Hazards Map.

Background seismicity is used to account for region which lacks seismogenic data but has seismic activities report from small to moderate earthquakes. Background source zones were modeled using gridded seismicity based on spatially smoothed earthquake rates (Frankel, 1995). This model consists of five depth intervals, i.e. shallow earthquakes (0–50 km), intermediate earthquakes (50–100 and 100–150 km), and deep earthquakes (150–200 and 200–300 km).

### 8.3.3 Attenuation Relations

Selection of attenuation relations were conducted based on earthquake mechanism, which is generally categorized into background, fault and subduction source zones. This selection followed previous studies by Irsyam et al. (2009a, b). Attenuation from Geomatrix subduction (Youngs et al., 1997), Atkinson-Boore BC rock and global Source (Atkinson and Boore, 2003) and Zhao et al., with variable  $V_{s-30}$  (Zhao et al., 2006) were chosen for Megathrust zone (subduction interface). Attenuation from Boore-Atkinson NGA (Boore and Atkinson, 2008), Campbell-Bozorgnia NGA (Campbell and Bozorgnia, 2008) and Chiou-Young NGA (Chiou and Youngs, 2008) were selected for faults and background sources. Attenuation from Atkinson-Boore intraslab (Atkinson and Boore, 2003), Geomatrix slab seismicity rock (Youngs et al., 1997) and Atkinson-Boore intraslab seismicity world data BC-rock condition (Atkinson and Boore, 1995) were used for Benioff (deep background sources).

### 8.3.4 Seismic Hazard Maps of Indonesia

Hazard maps of PGA at bedrock with 10 and 2% probability of exceedance in 50 years (500 years and 2,500 years return period of earthquake) are presented in Figs. 8.5 and 8.6 and hazard maps of spectral acceleration at 0.2, and 1.0 s for 2% probability of exceedance in 50 years are shown in Figs. 8.7 and 8.8.

Near the location of faults and subduction, results of this study are significantly higher than that of the SNI 03-1726-2002 for the same return period of earthquake (10% probability of exceedance in 50 years).

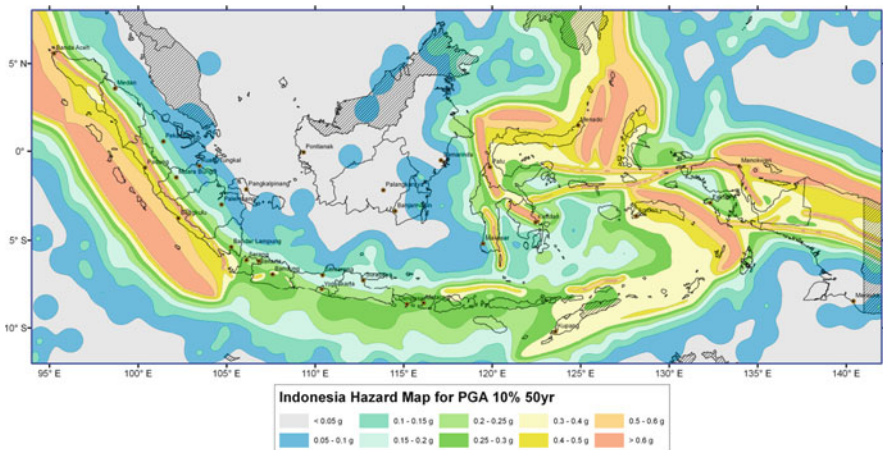


**Fig. 8.5** Map of Peak Ground Acceleration (PGA) of Indonesia for 10% probability of exceedance in 50 years

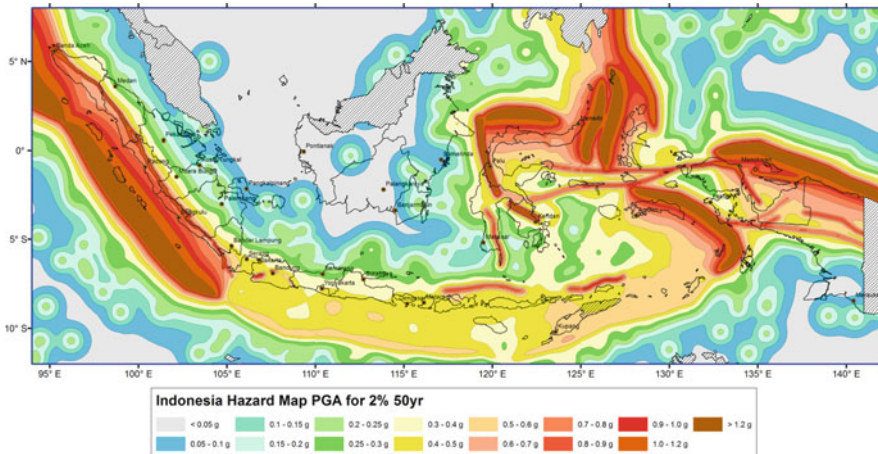


Fig. 8.6 Map of Peak Ground Acceleration (PGA) of Indonesia for 2% probability of exceedance in 50 years

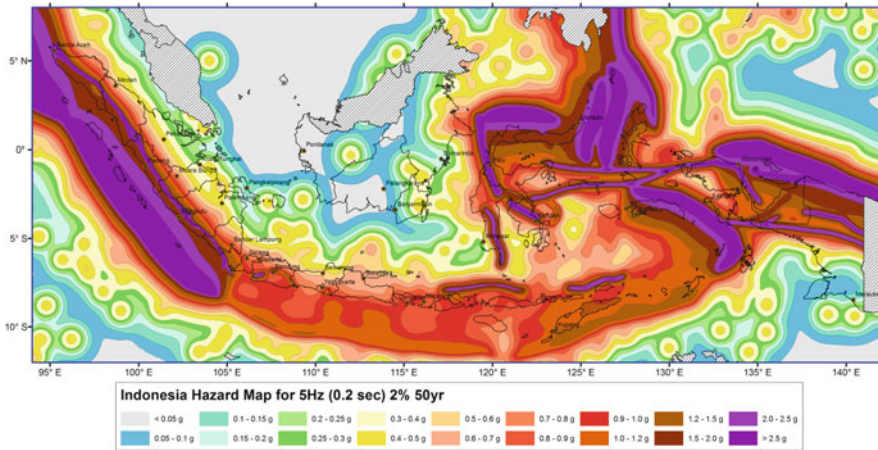
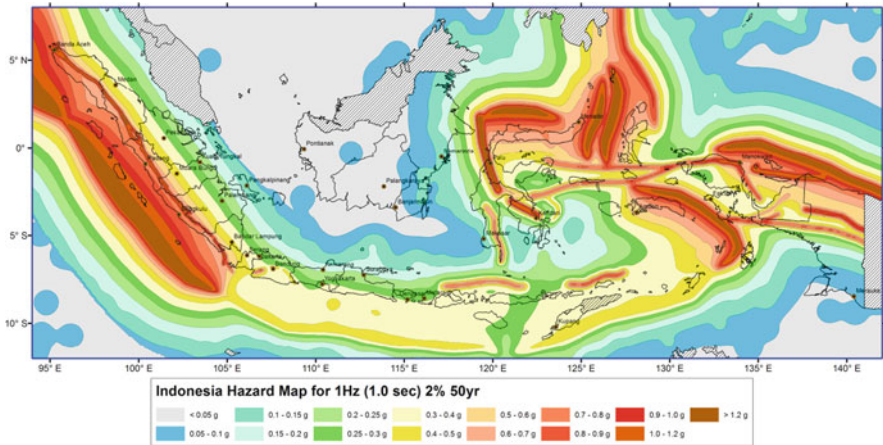


Fig. 8.7 Map of 0.2 s spectral acceleration of Indonesia for 2% probability of exceedance in 50 years



**Fig. 8.8** Map of 1.0 s spectral acceleration of Indonesia for 2% probability of exceedance in 50 years

### 8.4 Geotechnical Microzonation Study for Banda Aceh

This chapter also presents the results of seismic microzonation study of Banda Aceh to be utilized for reconstruction after the 2004 earthquake, enhancing land use management, and improving the accuracy of currently available and proposed new seismic resistant infrastructure and building codes. The map were obtained by performing ground response analysis utilizing one-dimensional (1-D) shear wave propagation method considering the nonlinearity of soil behavior and by evaluation the liquefaction resistance of soil deposits.

The ground response analysis was performed using NERA software (Bardet and Tobita, 2001) developed from SHAKE (Schnabel et al., 1972) and EERA (Bardet et al., 2000) and based on material model developed by Iwan (1967) and Mróz (1967). The nonlinearity of the shear modulus and damping was accounted for by employing equivalent linear soil properties using an iterative procedure to obtain values for modulus and damping compatible with the effective strains in each layer.

Shear wave propagation analysis was performed for 30 data of soil borings including 10 seismic downhole (SDH) test to obtain peak acceleration, amplification factor, and response spectra at the ground surface. Shear wave velocity ( $V_s$ ) profiles were developed based on interpretation of Bored Log and SDH (Fig. 8.9), around site location down to 30 m below ground surface. Wave propagation analysis from bedrock to ground surface showed that peak acceleration on the ground surface ranging from 0.50 to 0.58 g and from 0.42 to 0.68 g for soil type  $S_C$  (*very dense soil*) and  $S_D$  (*stiff soil*), respectively, for 10% probability of exceedance in 50 years. The results were then plotted to develop peak acceleration contour maps for Banda Aceh as shown in Fig. 8.10.

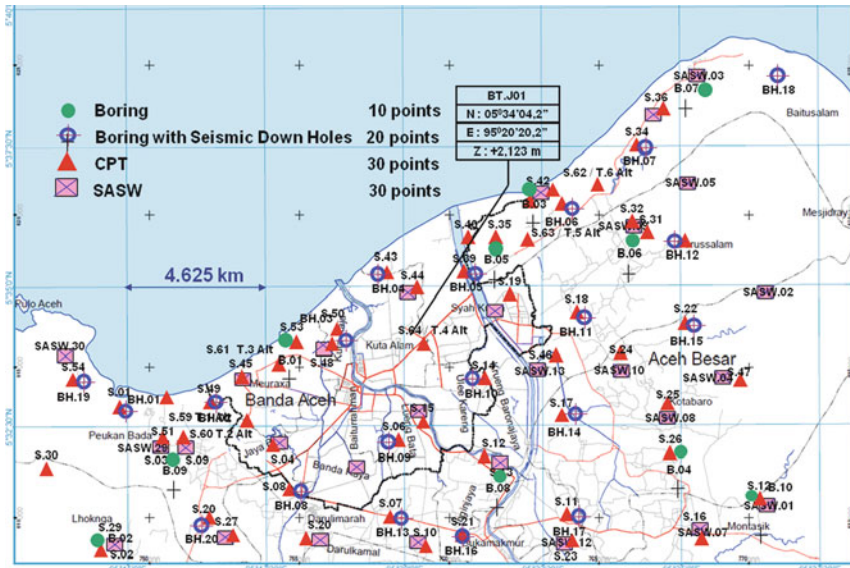


Fig. 8.9 Field investigations for microzonation study of Banda Aceh (Gitamandalaksana, 2009)

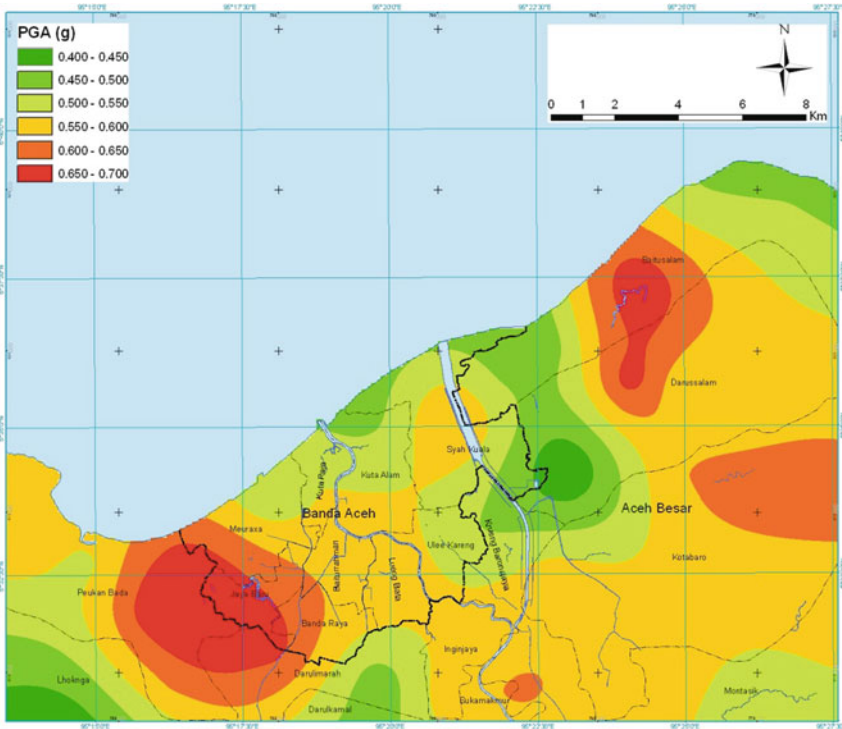


Fig. 8.10 Microzonation map of peak surface acceleration of Banda Aceh for 10% probability of exceedance in 50 years (Gitamandalaksana, 2009)

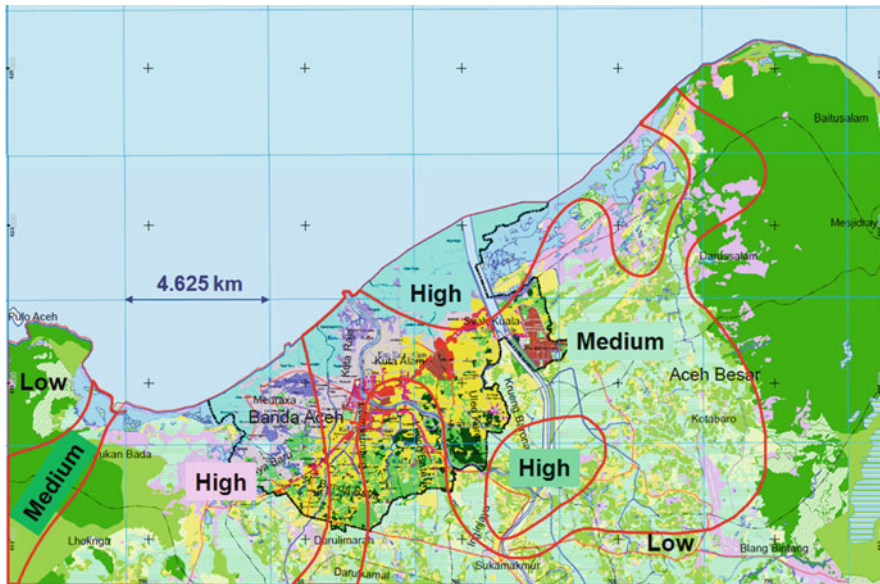


Fig. 8.11 Microzonation map of liquefaction potential of Banda Aceh (Gitamandalaksana, 2009)

Evaluation of the liquefaction resistance of soil deposits was also conducted in this study. It was carried out using simplified empirical procedure proposed by Seed and Idriss (1971), Seed et al. (1985) and was modified by NCEER (1997). The corrected SPT resistance of insitu soil stratum was compared with earthquake-induced cyclic shear stress. Proposed Iwasaki method (Iwasaki et al., 1982) was then adopted to estimate the severity of liquefaction degree at a given site based on the value of liquefaction potential index  $PL$ . Based on  $PL$ , Iwasaki et al. (1982) classified the liquefaction potential into five zones, i.e. catastrophic, very severe, severe, minor, and liquefaction unlikely. In this study, the classification of the liquefaction potential was simplified by combining catastrophic, very severe, and severe zones as high, minor as medium, and liquefaction unlikely as low, hence, local government can understand easily. The results of liqefaction study is presented in Fig. 8.11. Based on analysis, Banda Aceh can be divided into three zones, i.e. high, medium, and low liquefaction susceptibility.

## 8.5 Tsunami Hazard Assessment for Banda Aceh

Historically, subduction earthquakes and associated tsunamis have occurred repeatedly in Indonesia as reported by Ismail (1989) and by Puspito (2002) as shown in Fig. 8.12. On December 26, 2004 a devastating megathrust earthquake occurred on the interface area of Indian plate that subducts beneath the overriding Burma

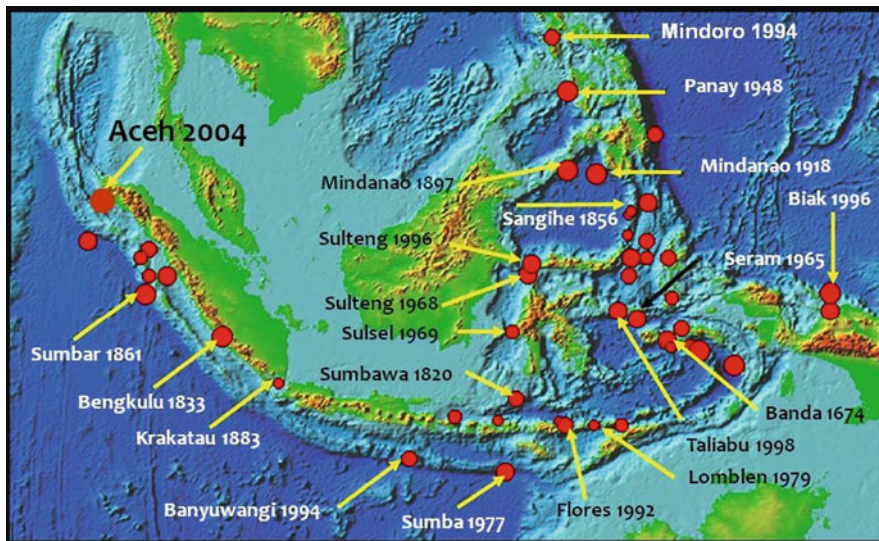


Fig. 8.12 Historical tsunami events in Indonesia (after Puspito, 2002)

plate with magnitude ( $M_w$ ) of 9.1–9.3 and rupture length of 1,600 km near Banda Aceh, Sumatra. The rupture propagated to the north along Andaman and Nicobar Islands (Lay et al., 2005). The earthquake generated huge tsunami and attacked coastal area along the South and South East Asia and reached the Eastern part of Africa that caused 283,000 deaths (Figs. 8.13, 8.14 and 8.15).



Fig. 8.13 Tsunami height and effect generated by the 2004 Aceh earthquake (International Tsunami Survey Team-2005 and [http://www.disasterscharter.org/disasters/CALLID\\_079a\\_e.html](http://www.disasterscharter.org/disasters/CALLID_079a_e.html))



**Fig. 8.14** Vast destruction at Lhoknga due to the 2004 Aceh earthquake



**Fig. 8.15** Tsunami damage to houses and buildings during the 2004 Aceh earthquake, Lam Paseh

Tsunami hazard criteria become essential as a basis for rehabilitation, reconstruction, and longterm development, as well as for developing tsunami warning system. Therefore, tsunami hazard assessment for Banda Aceh city was conducted. The 2004 Aceh tsunami source was designed based on the slip distribution given by Subarya et al. (2006), as shown on Fig. 8.16. The fault of Aceh-Andaman earthquake

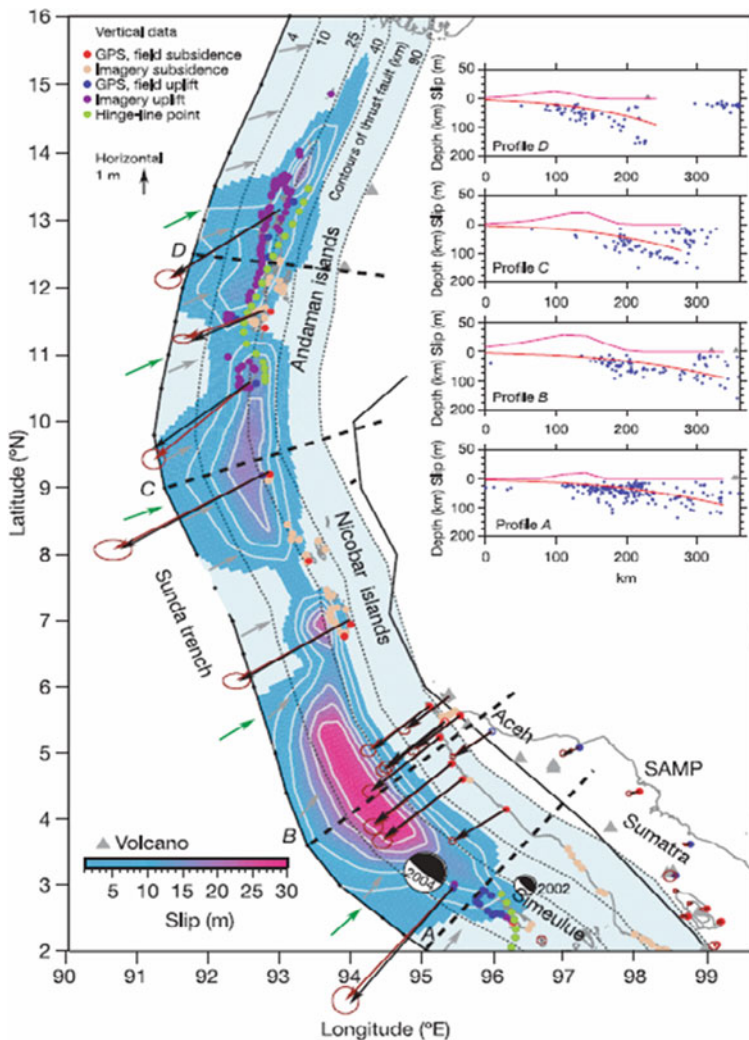


Fig. 8.16 Fault slip distribution determined from the geodetic data (Subarya et al., 2006)

was divided into 7 sub-faults as shown in Fig. 8.17, the velocity rupture propagation of the earthquake from Sumatra to Andaman averagely was taken 1.7 km/s (Latief et al., 2006).

Calculation of tsunami inundation of Banda Aceh city was conducted by using several nested domains. The nested domains were used to calculate tsunami run-up and inundation area using more detailed bathymetric and topography data. To obtain more accurate results, 5 nested domains were utilized, from domain-A up to domain-E, as presented in Fig. 8.18.

There were 4 scenarios selected to simulate inundation model of Banda Aceh city. The first one was backcalculation of the 2004 Aceh tsunami with Moment

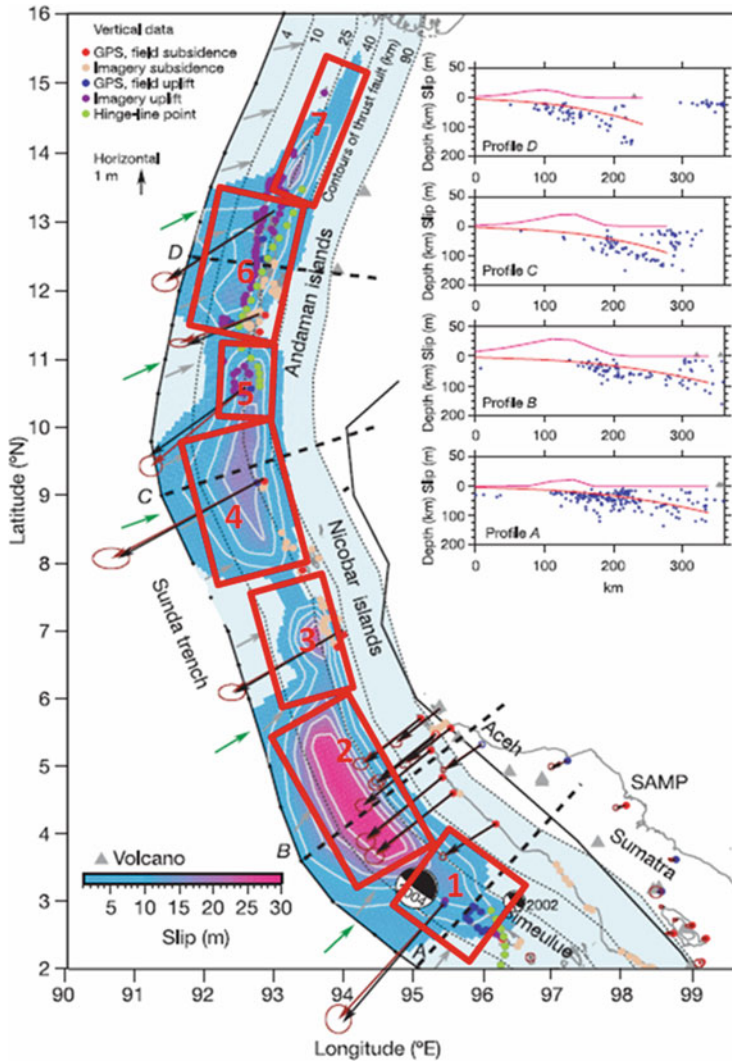
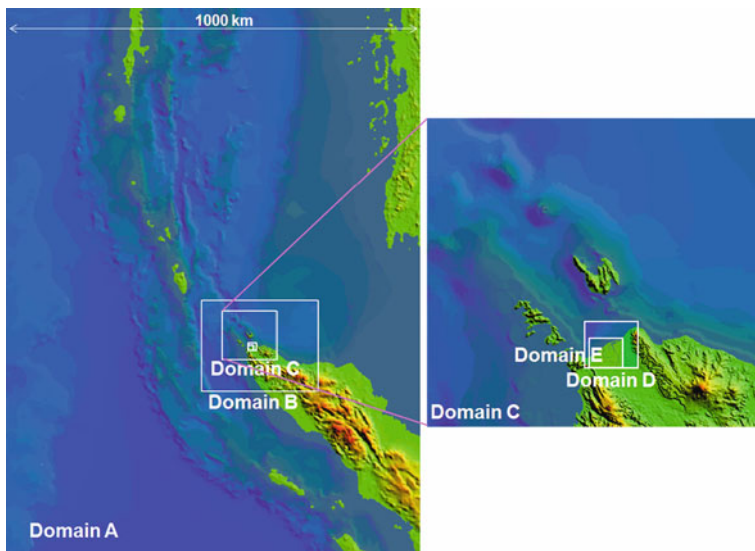


Fig. 8.17 Sub-fault positions depicted by red rectangular (Gitamandalaksana, 2009)

Magnitude ( $M_w$ ) of 9.2 used to calibrate input parameters. The other 3 cases were used to account for different magnitudes of earthquake;  $M_w = 8.5$ ,  $M_w = 8.0$ , and  $M_w = 7.5$ .

Calculation of tsunami inundation was conducted by using TUNAMI-Code (Goto and Ogawa, 1992; Imamura, 1995). The output of tsunami hazard assessment (Fig. 8.19) was then overlaid on top of the land use city planning in a Geographical Information Systems (GIS) database as shown in Fig. 8.20.



**Fig. 8.18** Grid size of nested domains

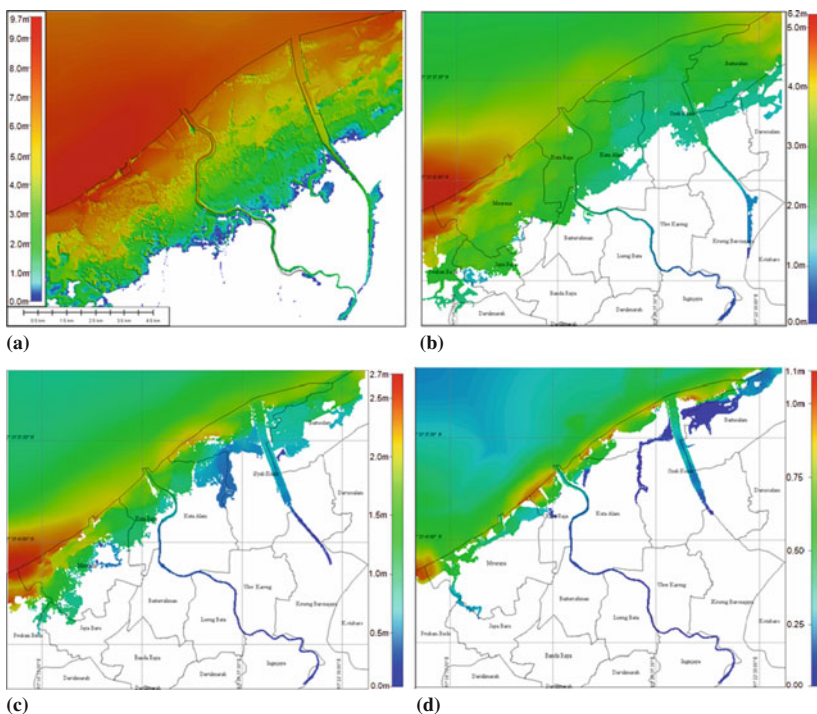


**Fig. 8.19** Tsunami inundation. (a) Inundation area for the 2004 Aceh tsunami,  $M_w = 9.2$ ; (b) inundation area for  $M_w = 8.5$ ; (c) inundation area for  $M_w = 8.0$ ; (d) inundation area for  $M_w = 7.5$

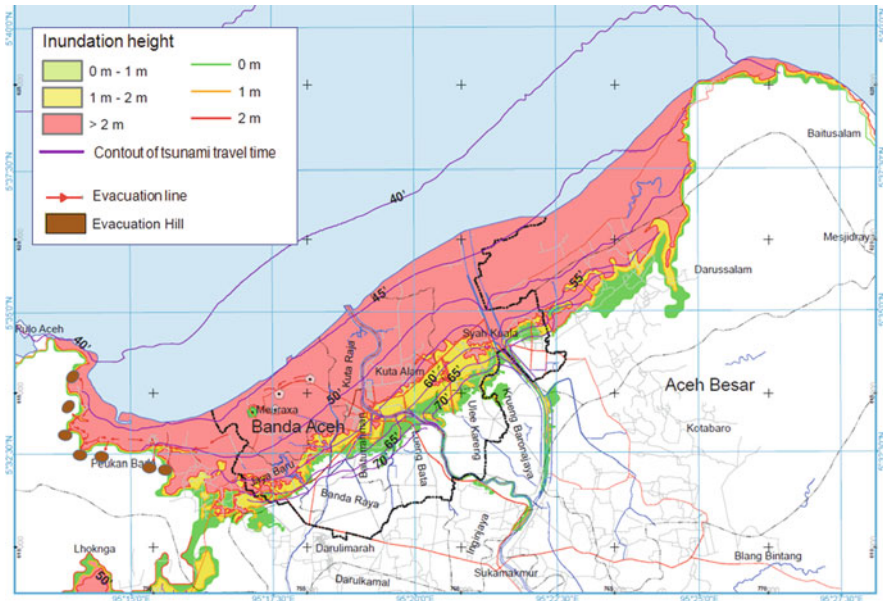


Fig. 8.20 Tsunami inundation map of Banda Aceh city (Gitamandalaksana, 2009)

### 8.6 Conclusions

A probabilistic hazard model for estimation of seismic hazard in Indonesia has been developed based upon updated available seismotectonic data, implementing new fault models, and incorporating new ground-motion prediction equations (NGA). Spectral hazard maps for 10 and 2% probability of exceedance in 50 years have been produced. Near the location of faults and subductions, results of this study are significantly higher than that of the SNI 03-1726-2002 for the same return period of earthquake. It indicates that the actual seismic hazard in Indonesia is higher than it was expected before.

Geotechnical and tsunami hazard assessment for Banda Aceh have been conducted. The results of seismic microzonation study and tsunami hazard assessment for Banda Aceh city are used as a criteria for development of tsunami warning system, an input in developing land use management, and enriching the basic regulation for new infrastructures and local building codes.

Considering the potential of big earthquakes followed by tsunami that can occur in Indonesia in the near future, it suggests that microzonation of geotechnical and tsunami hazard study is urgently required for big cities in Indonesia, particularly with high population.

## References

- Atkinson G, Boore D (1995) New ground motion relations for Eastern North America. *Bull Seismol Soc Am* 85:17–30
- Atkinson GM, Boore DM (2003) Empirical ground-motion relations for subduction zone earthquakes and their application to Cascadia and other regions. *Bull Seismol Soc Am* 93(4): 1703–1729
- Bardet JP, Ichii K, Lin CH (2000) *EERA-A* computer program for equivalent linear earthquake site response analyses of layered soil deposits. Department of Civil Engineering, University of Southern California
- Bardet JP, Tobita T (2001) *NERA-A* computer program for nonlinear earthquake site response analyses of layered soil deposits. Department of Civil Engineering, University of Southern California
- Bird P (2003) An updated digital model of plate boundaries. *Geochem Geophys Geosyst* 4(3):1027
- Bock Y, Prawirodirdjo L, Genrich JF, Stevens CW, McCaffrey R, Subarya C, Puntodewo SSO, Calais E (2003) Crustal motion in Indonesia from global positioning system measurements. *J Geophys Res* 108(B8):2367. doi:10.1029/2001JB000324
- Boore DM, Atkinson GM (2008) Ground-motion prediction equations for the average horizontal component of PGA, PGV, and 5%-damped PSA at spectral periods between 0.01 s and 10.0 s. *Earthquake Spectra* 24(1):99–138
- Campbell KW, Bozorgnia Y (2008) Ground motion model for the geometric mean horizontal component of PGA, PGV, PGD and 5%-damped linear elastic response spectra for periods ranging from 0.01 to 10 s. *Earthquake Spectra* 24(1):139–171
- Chiu B, Youngs R (2008) A NGA model for the average horizontal component of peak ground motion and response spectra. *Earthquake Spectra* 24(1):173–215
- Frankel A (1995) Mapping seismic hazard in the Central and Eastern United States. *Seismol Res Lett* 66(4):8–21
- Gitamandalaksana Consultant (2009) Final report: identification of seismic source's zone and tsunami hazard probability as considerations in development policy of Banda Aceh city, Nanggroe Aceh Darussalam Province (Package-1), Banda Aceh
- Goto C, Ogawa Y (1992) Numerical method of tsunami simulation with the leap-frog scheme. Disaster Control Research Center, Faculty of Engineering, Tohoku University
- Hamilton W (1979) Tectonics of the Indonesian region, U.S. Geological Survey Prof. Paper 1078
- Hu YX (1996) Earthquake engineering. E & FNSpon, London
- Imamura F (1995) Tsunami numerical simulation with the staggered leap-frog scheme (numerical code of TUNAMI-N1 and N2). Disaster Control Research Center, Tohoku University, 33 pp
- Irsyam M, Asrurifak M, Budiono B, Triyoso W, Merati M, Sengara IW, Firmanti A (2009a) Development of spectral hazard map for Indonesia using probabilistic method by considering difference values of  $M_{\max}$  for shallow background sources. Proceedings of the 1st international conference on sustainable infrastructure and built environment in developing countries, Bandung, Indonesia
- Irsyam M, Asrurifak M, Hendriyawan, Budiono M, Triyoso W, Firmanti A (2009b) Development of spectral hazard maps for proposed revision of Indonesia Seismic Building Code. *Geomech Geoen – An Int J* 5(1):35–47. doi:10.1080/17486020903452725
- Irsyam M, Dangkoa DT, Hendriyawan, Hoedajanto D, Hutapea BM, Kertapati E, Boen T, Petersen MD (2008) Proposed seismic hazard maps of Sumatra and Java islands and microzonation study of Jakarta City, Indonesia. *J Earth Syst Sci* 117:S2, November
- Ismail S (1989) Tsunami in Indonesia. Technical report, Meteorological and Geophysical Agency, Indonesia (in Indonesian)
- Iwan WD (1967) On a class of models for the yielding behavior of continuous and composite systems. *J Appl Mech, ASME* 34:612–617
- Iwasaki T, Arakawa T, Tokida K (1982) Simplified procedures for assessing soil liquefaction during earthquakes. Soil dynamics and earthquake engineering conference, Southampton, pp 925–939

- Lasitha S, Radhakrishna M, Sanu TD (2006) Seismically active deformation in the Sumatra–Java trench-arc region: geodynamic implications. *Current Sci* 90(5):690–696
- Lay T, Kanamori H, Amon CJ, Nettles M, Ward SN, Aster RC, Beck SL, Bilek SL, Brudzinski MR, Butler R, DeShon HR, Eksrom G, Satake K, Sipkin S (2005) The great Sumatra-Andaman earthquake of 26 December 2004. *Science* 308:1127–1133
- Milsom J, Masson D, Nichols G, Sikumbang N, Dwiyanto B, Parson L, Kallagher H (1992) The Manokwari trough and the western end of the New Guinea trench. *Tectonics* 11:145–153
- Mról Z (1967) On the description of anisotropic workhardening. *J Mech Phys Solids* 15:163–175
- NCEER (1997) Seismic factor for use in evaluating liquefaction resistance. In: Youd TL, Idriss IM (eds) Proceedings of the NCEER workshop on evaluation of liquefaction resistance of soils, Technical Report No. NCEER-97-0022, 31 Dec, pp. 191–200
- Newcomb KR, McCann WR (1987) Seismic history and seismotectonics of the Sunda Arc. *J Geophys Res* 92:421–439
- Pacheco JF, Sykes LR (1992) Seismic moment catalog of large shallow earthquakes, 1900 to 1989. *Bull Seismol Soc Am* 82:1306–1349
- Puspito N (2002) *Harian Kompas*, edisi 2 Nov
- Schnabel PB, Lysmer J, Seed HB (1972) SHAKE: a computer program for earthquake response analysis of horizontally layered sites. Report No. EERC 72-12, University of California, Berkeley, Dec
- Seed HB, Idriss IM (1971) Simplified procedure for evaluating soil liquefaction potential. *J Soil Mech Found Div, ASCE* 97(SM9), Proceeding Paper 8371, Sept, pp 1249–1273
- Seed HB, Tokimatsu K, Harder LF, Chung RM (1985) Influence of SPT procedures in soil liquefaction resistance evaluations. *J Geotech Eng, ASCE* 111(12):1425–1445
- Socquet A, Vigny C, Chamot-Rooke N, Simons W, Rangin C, Ambrosius B (2006) India and Sunda plates motion and deformation along their boundary in Myanmar determined by GPS. *J Geophys Res* 111 (B05406):1–11. doi:10.1029/2005JB003877
- Subarya C, Chlieh M, Prawirodirdjo L, Avouac J-P, Bock Y, Sieh K, Meltzner AJ, Natawidjaja DH, McCaffrey R (2006) Plate boundary deformation associated with the great Aceh-Andaman earthquake. *Nature* 440:46–51
- Youngs RR, Chiou SJ, Silva WJ, Humphrey JR (1997) Strong ground motion attenuation relationships for subduction zone earthquakes. *Seismol Res Lett* 68:58–73
- Zhao JX, Zhang J, Asano A, Ohno Y, Oouchi T, Takahashi T, Ogawa H, Irikura K, Thio H, Somerville P (2006) Attenuation relations of strong motion in Japan using site classification based on predominant period. *Bull Seismol Soc Am* 96:898

## Chapter 9

# Urban Microzonation

## Seismic Microzonation and Earthquake Scenarios for Urban Sustainability

Atila Ansal, Gökçe Tönük, and Ash Kurtuluş

**Abstract** Seismic microzonation and earthquake loss estimation scenarios are needed for city planning, disaster preparedness, risk reduction and hazard mitigation decisions, and urban rehabilitation actions in earthquake prone areas. Loss estimation due to earthquakes in an urban environment is a very complex process that requires detailed building inventories, realistic estimation of earthquake characteristics on the ground surface and comprehensive assessment of building vulnerabilities. The earthquake hazard is spatially distributed in relation to earthquake sources that need to be assessed based on the regional seismotectonic scale and local site conditions. Mapping the variation in earthquake hazard at an urban scale makes it possible to select relatively less affected zones for the allocation of appropriate land use. Urban development patterns can be oriented toward these relatively less affected zones to minimize possible earthquake damages. The three principal factors controlling earthquake loss are earthquake source characteristics, site response and structural features. The seismic microzonation maps would indicate the distribution of site response with respect to ground shaking intensity, liquefaction and landslide susceptibility; thus providing an input for urban planning and earthquake mitigation priorities at an urban scale. It is also possible to estimate building damage and causalities based on microzonation maps used as an input to earthquake damage scenarios. These estimates may be very approximate and may not always be on the conservative side based on the accuracy of the input data and methods of analyses. However, they can also be more realistic and more accurate when more comprehensive data and more sophisticated analysis methods are implemented. Thus one of the important issues is the estimation of the needed accuracy and corresponding level of complexity in the analytical studies. The results obtained using different levels of seismic hazard and site characterisation data will be summarised very briefly to

---

A. Ansal (✉)

Kandilli Observatory and Earthquake Research Institute, Boğaziçi University,  
Istanbul 34684, Turkey  
e-mail: ansal@boun.edu.tr

demonstrate the importance of the comprehensive site characterisation as well as the procedures used to estimate site effects for different levels of seismic hazard based on case studies conducted in Istanbul.

## 9.1 Introduction

In assessing the ground shaking intensity for microzonation at an urban scale, the purpose is to inform the urban planners as well as the city officials about the variation of the shaking level and thus the variation of the expected building damage for long term urban and land use planning. At this level, the absolute values of the estimated earthquake characteristics may not be very meaningful since it would not be very straight forward for a non earthquake engineer to estimate the building damage levels based on these numerical values. Therefore it was considered that it may be more meaningful to approach the problems from a simple perspective by defining three zones with high, intermediate and low shaking intensity based on the relative ground shaking intensity estimated by probabilistic seismic hazard and site response analysis.

An attempt will be made to demonstrate that there are different factors that need to be considered during microzonation with respect to ground shaking intensity. Firstly, the approach adopted to represent ground shaking intensity can vary based on the parameters selected for this purpose. The basic intention for microzonation with respect to ground shaking intensity is to identify the areas which may experience higher level of ground shaking and consequently higher level of damage and casualties. Thus, the key issue is to adopt a microzonation parameter that may be correlated with building damage. However, it is very difficult, almost impossible to find a single earthquake characteristic to model the observed damage in the previous earthquakes. One main reason for this dilemma is the diversity and differences in each building concerning the structural design as well as the construction process and material differences.

Different earthquake parameters have been adopted by different research groups as microzonation parameters or as parameters representing the ground shaking intensity such as peak ground acceleration (Grasso and Maugeri, 2009), peak ground velocity (Singh et al., 2007), peak ground displacement (Parvez et al., 2003), spectral accelerations and amplification ratios (Papadimitriou et al., 2008), Arias Intensity (Alvarez et al., 2005), normalized peak strain (Todorovska and Trifunac, 1996), response spectra ratio (Alvarez et al., 2004), and spectral intensity (Pergalania et al., 1999).

In the present study, all available data from site characterisation such as equivalent shear wave velocity as well as the results of site response analyses conducted for all available soil profiles need to be evaluated to achieve realistic and consistent results. In the adopted microzonation methodology, the first microzonation parameter is defined based on the empirical amplification relationships proposed by Borchardt (1994) that enable the estimation of site-specific peak spectral

accelerations with respect to equivalent shear wave velocities measured or estimated for the top 30 m of soil profiles and expected level of ground shaking at the bedrock level. The second microzonation parameter is defined as the average spectral accelerations between 0.1 and 1 s based on 1D site response analyses that yields acceleration time histories on the ground surface to estimate peak ground acceleration as well as elastic acceleration response spectrum (Ansal et al., 2007b). The results obtained were mapped by superposition using GIS techniques by applying soft transition boundaries to show the variation of the mapped parameters.

In earthquake damage scenarios, the earthquake characteristics on the ground surface are calculated in accordance with the required input parameters needed to estimate damage levels based on the adopted vulnerability functions (Ansal et al., 2006b, 2007a). The parameters used to assess the vulnerability of buildings vary in complexity depending on the reliability and accuracy of the available structural data in the building inventory.

## 9.2 Earthquake Hazard Assessment

There are generally two approaches for the estimation of earthquake hazard at an urban scale. The first one is the probabilistic seismic hazard analysis, considering all possible earthquake source characteristics that may take place in the vicinity of the investigated region and the results are generally presented in terms of uniform hazard spectrum on reference ground conditions (Erdik et al., 2004, 2005). The second approach is the deterministic earthquake hazard assessment conducted based on the available tectonic information and the de-aggregation analysis conducted following the probabilistic hazard to estimate the possible earthquake source that may contribute most to the estimated earthquake hazard for the investigated city or the region (Ansal et al., 2009a).

Considering the uncertainties associated with earthquake source, it is more relevant to adopt probabilistic approach in estimating the earthquake hazard than deterministic assessment. In addition, the performance based earthquake resistant design requires the definition of ground motion associated with different average return periods for each performance objective that can only be estimated based on the probabilistic assessment of the earthquake hazard.

The estimation of the probabilistic hazard requires significant efforts concerning the locations and characteristics of existing geological sources of possible earthquakes along with determinations of how frequently earthquakes occur in each of these sources, and how large the maximum earthquakes might be for each source. This group of models is defined as the “regional seismotectonic model”. An example of such a model developed by Erdik et al. (2005) for Istanbul Bakırköy Municipality is given schematically in Fig. 9.1. The first step is the development of the regional seismotectonic model that will allow at the second step the estimation of the earthquake characteristics on the reference ground conditions.

The most common modern method of describing the severity of earthquake hazard is in terms of acceleration response spectra. The earthquake hazard maps are

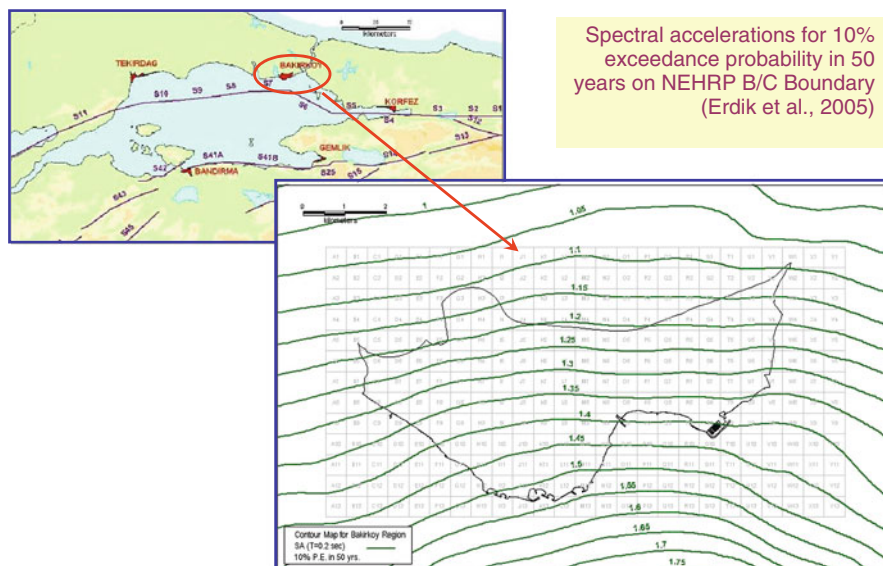


**Fig. 9.1** Earthquake hazard assessment for Bakırköy by Erdik et al. (2005) based on the regional seismotectonic model

generated for return periods of 2475, 475 and 72 years corresponding to 2, 10 and 50% exceedance probabilities in 50 years respectively. As an example, a study conducted by Erdik et al. (2005) for the town of Bakırköy in Istanbul for 10% exceedance in 50 years based on regional seismotectonic model is given in Fig. 9.1.

Geotechnical research in earthquake hazard has established that the soil thickness and physical properties significantly affect the amplitude and period of the earthquake shaking felt on the ground surface. Therefore, while the microzonation maps are produced on a uniform surface over a large region (such as a “soft rock” site class), the microzonation maps must be modified to account for the affect of the local soil column in order to be applicable to local site conditions. This process is defined as “site-response”.

Site response can be carried out based on empirical amplification factors or utilizing numerical schemes based on 1D wave propagation or 1D/2D finite element or finite difference analysis. Each alternative requires different degrees of complexity concerning the thicknesses and types and dynamic properties of the soil layers located in the soil profile.

### 9.3 Site Characterisation

In order to assess the effects of site conditions, the simplest approach is to utilize the surface geology maps. However, as demonstrated by many researchers, geological units or formations most likely may not have uniform engineering properties

with depth as well as in lateral directions. It would be oversimplification, if only geological units and formations are used to evaluate the site effects.

A more comprehensive approach would be based on soil borings conducted to observe the layer thicknesses as well as to determine engineering characteristics of soil layers based on laboratory and in-situ penetration and seismic wave velocity measurements (Ansal et al., 2004a). Most of the recent microzonation studies have been conducted based on detailed site explorations, such as the Istanbul Microzonation Project (Oyo, 2007).

The important soil properties used in empirical as well as in numerical site response analysis are the variation of shear wave velocity along the soil profile and the depth of the engineering bedrock or in other words reference site conditions that may be defined as the soil or rock layer with shear wave velocity  $\geq 750$  m/s. In the simplified assessments based on weighted average shear wave velocity for the top 30 m, the soil types were not considered. However, in case of 1D site response analysis, soil types are the essential ingredients in the selection of the modulus reduction and damping relationships with respect to shear strain level. It was shown over and over again by large number of researchers based on laboratory and field tests that different soils basically sands, silts and clays would show different response patterns depending on many inherent properties such as grain size distribution, fines content, and plasticity index or based on external factors such as confining pressure and over-consolidation ratio, ground water level and saturation. Thus the use of average shear wave velocity, even though it is a very straight forward engineering application, may lead to erroneous results since the oversimplifications are very significant.

A very detailed site investigation study was recently conducted for the European side of Istanbul for microzonation purpose. Large numbers of soil borings along with large numbers of geophysical tests were performed to determine the site conditions. In the present study, site conditions in the town of Zeytinburnu were determined based on this extensive data set. Zeytinburnu is composed of 209 cells with mesh size of 250 m  $\times$  250 m. The engineering bedrock is located around 200 m in the south toward the Marmara Sea while the depth of engineering bedrock is around 70 m in the northern sections. The average shear wave velocity varies in a limited range between 205 and 477 m/s which indicates again the shortcoming of the use of average shear wave velocity for the top 30 m in the areas like Zeytinburnu where the thickness of the soil layers plays a dominant role in site response analysis. Three typical soil profiles with depths extending between 85, 110, and 160 m are shown in Fig. 9.2.

## 9.4 Site Response

In accordance with the methodology adopted for the earthquake hazard analysis, hazard compatible (in terms of expected earthquake magnitude, epicentre distance and fault type) recorded acceleration time histories are used to conduct site response analyses to determine earthquake characteristics on the ground surface. It was

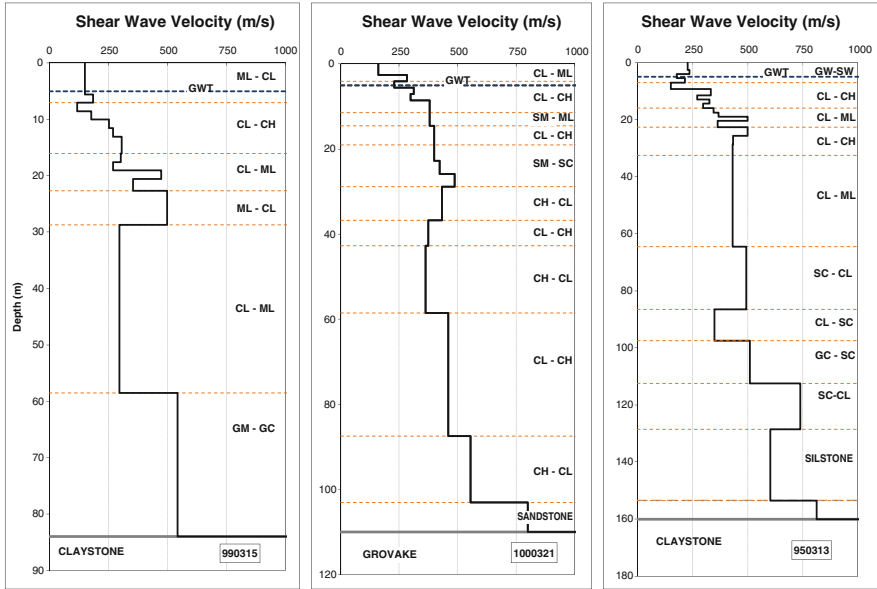
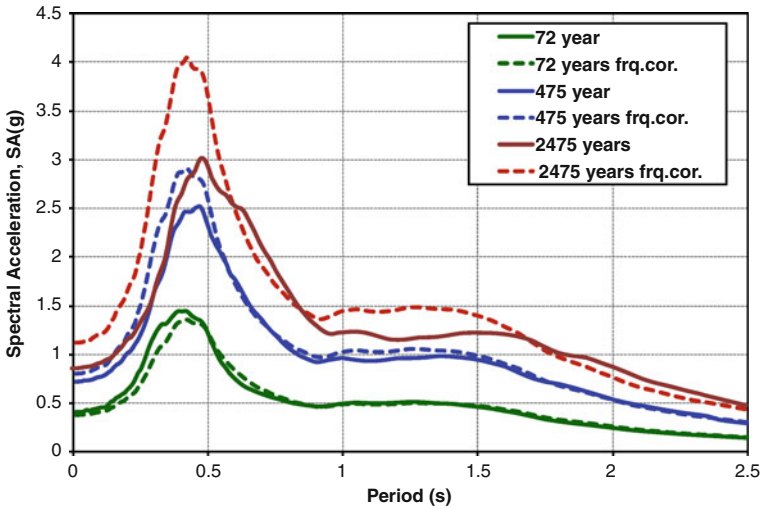


Fig. 9.2 Typical soil profiles for three depth ranges in Zeytinburnu town

observed by Ansal and Tönük (2007b) that if limited number of acceleration time histories (e.g. 3 records as specified in some earthquake codes) are used even with scaling to the same PGA, the results in terms of PGA and ground shaking intensity can be different for different sets of input acceleration time histories. Therefore, it was decided to conduct site response analyses using large number of input acceleration time histories to eliminate the differences that are observed between different sets (Ansal and Tönük, 2007a) and also to take into account the variability due to the earthquake characteristics on the ground surface for design and vulnerability assessment. This approach also enables a probabilistic interpretation of earthquake characteristics on the ground surface in compatible with the probabilistic hazard analysis (Ansal and Tönük, 2009).

Site specific earthquake characteristics on the ground surface are calculated using modified version (Ansal et al., 2010) of Shake91 by Idriss and Sun (1992) one dimensional, equivalent linear site response code. One of the issues in one dimensional, equivalent linear site response analyses is the variation of damping with depth for deep soil profiles. For deep soil profiles, the damping needs to be adjusted to account for the reduction with increasing depth in the site response analysis.

Generally, equivalent linear analysis has a tendency to give larger peak acceleration and shear stress under large earthquakes, and lower amplification in high frequency range. The reason of the latter phenomena is due to the evaluation of damping ratio from the effective strain that happens to be too large for small amplitude (high cycle) vibrations. This effect becomes dominant under the small to medium earthquakes, resulting in smaller accelerations (Yoshida et al., 2002).



**Fig. 9.3** The effect of hazard level and frequency correction on acceleration response spectra for the deep soil profile given in Fig. 9.2c in Zeytinburnu town

Shake91 site response code is modified to account for the frequency dependent characteristics of the modelled ground motions adopting methodology suggested by Sugito et al. (1994). Sugito et al. (1994) improved lower amplification in high frequency range of the equivalent linear analysis by defining frequency dependent characteristics of the effective strain in each frequency component.

As shown in Fig. 9.3 for the case of deep soil profile given in Fig. 9.2c, the effect of the frequency correction becomes more pronounced with the increase in hazard level or with the increase in the intensity of the ground shaking. A similar effect was also observed in the site response analysis conducted for relatively shallower soil profile as shown in Fig. 9.4, where the level of spectral accelerations are slightly lower in comparison to deeper soil profile.

### 9.5 Microzonation with Respect to Ground Motion

In assessing the ground shaking intensity, the purpose is to estimate relative effects of local site conditions on earthquake characteristics on the soil surface. All available data from site characterisation such as equivalent shear wave velocity ( $V_{s30}$ ) and the results of site response analyses should be evaluated to achieve a realistic solution. The empirical amplification relationships proposed by Borchardt (1994) enables the estimation of site-specific peak spectral accelerations based on equivalent (average) shear wave velocities ( $V_{s30}$ ) for the top 30 m of soil profile. Site response analyses yields acceleration time histories to estimate peak ground acceleration as well as elastic acceleration response spectrum on the ground surface.

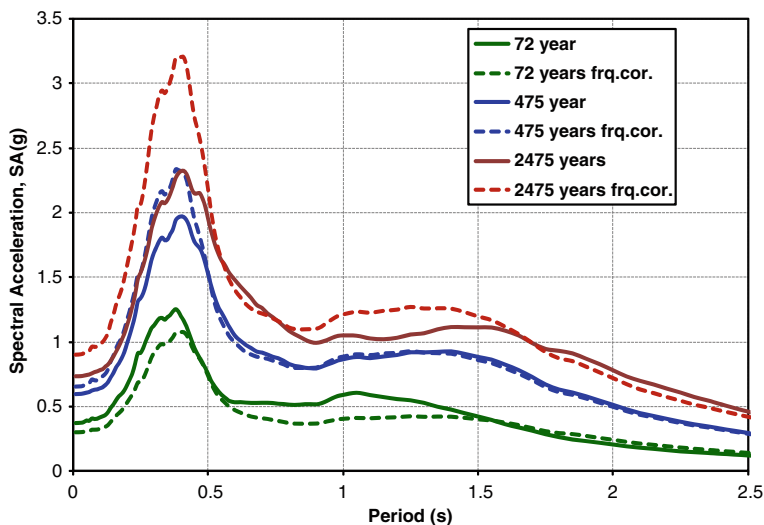


**Fig. 9.4** The effect of hazard level and frequency correction on acceleration response spectra for the midrange soil profile given in Fig. 9.2a in Zeytinburnu town

Soft transition boundaries are preferred to show the variation of the mapped parameter. More defined clear boundaries are not used due to the accuracy of the study. This allows some flexibility to the urban planners and avoids misinterpretation by the end users that may consider the clear boundaries as accurate estimations for the different zones.

The proposed methodology for microzonation is based on the division of the investigated urban area into three zones (as A, B, and C) with respect to frequency distribution of the selected ground shaking parameter corresponding to 33 and 67% percentiles (Ansal et al., 2004b, 2005, 2009b) as shown in Fig. 9.5. The site characterizations and all the analyses performed are based on various approximations and assumptions. Therefore, the absolute numerical values for the selected ground motion parameters will not be very accurate and their relative values are more important for urban planning.

The ground shaking intensity microzonation map that should reflect the estimated relative shaking intensity levels is based on the combination of two parameters: the cumulative average spectral acceleration between  $T = 0.1$  s and  $T = 1$  s periods of the average acceleration spectral spectrum of all site response analyses conducted for each cell is adopted as the first microzonation parameter and peak spectral accelerations at short period range calculated from Borchardt (1994) using  $V_{s30}$  is adopted as the second microzonation parameter as demonstrated schematically in Fig. 9.6.

The main reason for adopting superposition of two parameters for representing the ground shaking intensity was to combine the advantages of the empirical procedure which was based on observed data with the advantages of a numerical scheme

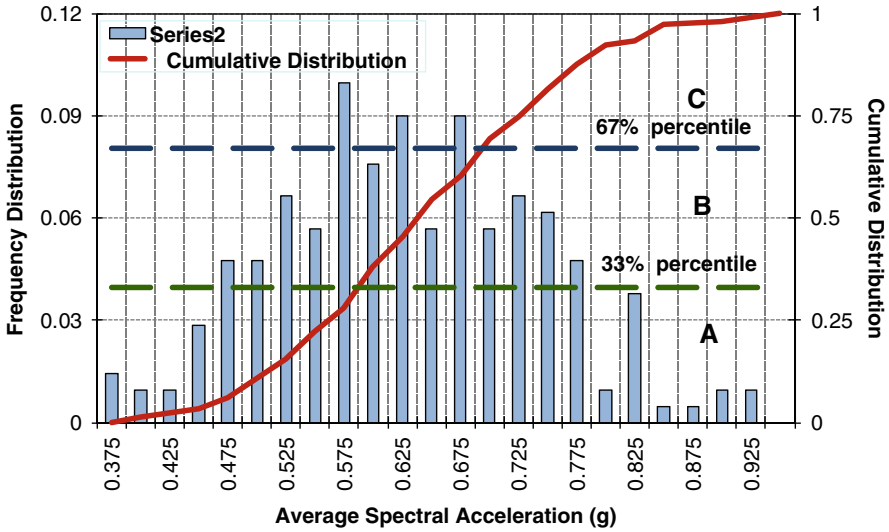


Fig. 9.5 Relative microzonation approach adopted with respect to the statistical distribution

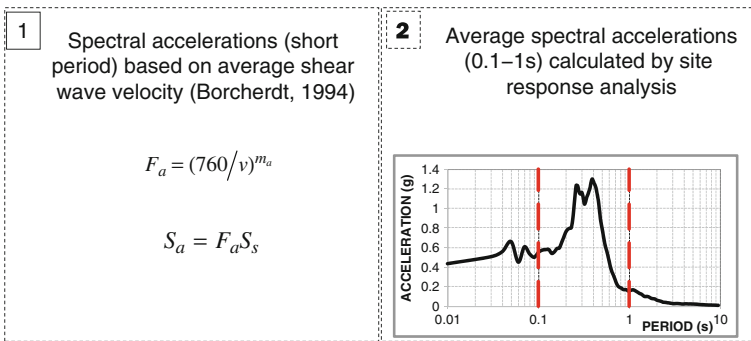


Fig. 9.6 Relative microzonation approach adopted with respect to the statistical distribution

which can account for different factors affecting the site response even though based on some simplifying assumptions. It was assumed that more reliable results can be obtained by combining an empirical and a numerical analysis.

In the present Zeytinburnu microzonation study, all available acceleration time histories compatible with the earthquake hazard analysis in terms of probable magnitude range ( $M_w = 7.0-7.4$ ) and distance range (20–30 km) with strike slip fault mechanism that were recorded on sites with NEHRP (BSSC, 2001) site classification of B/C boundary were selected as input outcrop motion and were downloaded from PEER website (PEER, 2009).

The results of the earthquake hazard analysis corresponding to 72, 475, and 2475 year return periods calculated in terms of peak ground (PGA) and spectral accelerations (SA) at  $T = 0.2$  s and  $T=1$  s periods for each cell by Erdik et al. (2005) were used for conducting site response analysis for microzonation of Zeytinburnu town.

The input acceleration time histories are scaled with respect to the peak ground accelerations determined from regional seismic hazard study for 72, 475, and 2475 year return periods in accordance with Ansal et al. (2006a). For the Zeytinburnu case study, 24 scaled acceleration time histories were used as input motion for site response analyses by Shake91 (Idriss and Sun, 1992) and the average of the acceleration response spectra on the ground surface were determined to obtain the necessary parameters for microzonation.

The microzonation map with respect to ground shaking intensity is based on the superposition of microzonation maps with respect to average spectral accelerations obtained from site response analyses and short period spectral accelerations calculated according to Borchardt (1994) in accordance with the microzonation methodology adopted in Turkey (Ansal et al., 2004b, 2005). The adopted approach is independent of the absolute values of the ground shaking intensity. Hence, the superposed map is composed of three relative zones ( $A_{GS}$ ,  $B_{GS}$ ,  $C_{GS}$ ) where  $A_{GS}$  shows the areas with lower ground shaking and  $C_{GS}$  shows the areas with higher ground shaking intensity as shown in Fig. 9.7.

A parametric study was conducted to evaluate the effects of earthquake hazard level as well as the effects of the modification applied to the site response analysis code to account for the frequency dependence of the solution algorithm. Site response analysis for 209 soil profiles using 24 PGA scaled real acceleration time histories were performed for three hazard levels corresponding to 72, 475, and 2475 years return periods.

As can be observed in Fig. 9.7, the hazard level or the level of earthquake input appears to have relatively significant effect on the microzonation map for the ground shaking intensity even though the microzonation procedure is based on relative classification of the calculated average spectral accelerations and peak spectral accelerations.

The effect of the hazard level observed in Fig. 9.7 indicates the influence of the possible nonlinear response calculated for higher input acceleration levels with the increase in the return periods. However, one should remember that these results are calculated using a numerical scheme using a computer code based on equivalent linear analysis. Even though the reliability of the computer code has been verified to a certain extent, the results are still numerical results. Considering that the main purpose in microzonation with respect to ground shaking intensity is to estimate the areas with higher ground shaking susceptibility with respect to some predefined earthquake parameters, it would be logical to conduct microzonation with respect to other earthquake characteristics such as peak ground acceleration or peak ground velocity to observe if the microzonation maps would be different.

Before proceeding to other microzonation parameters, as shown in Figs. 9.3 and 9.4, the effects of frequency correction on microzonation maps were evaluated for

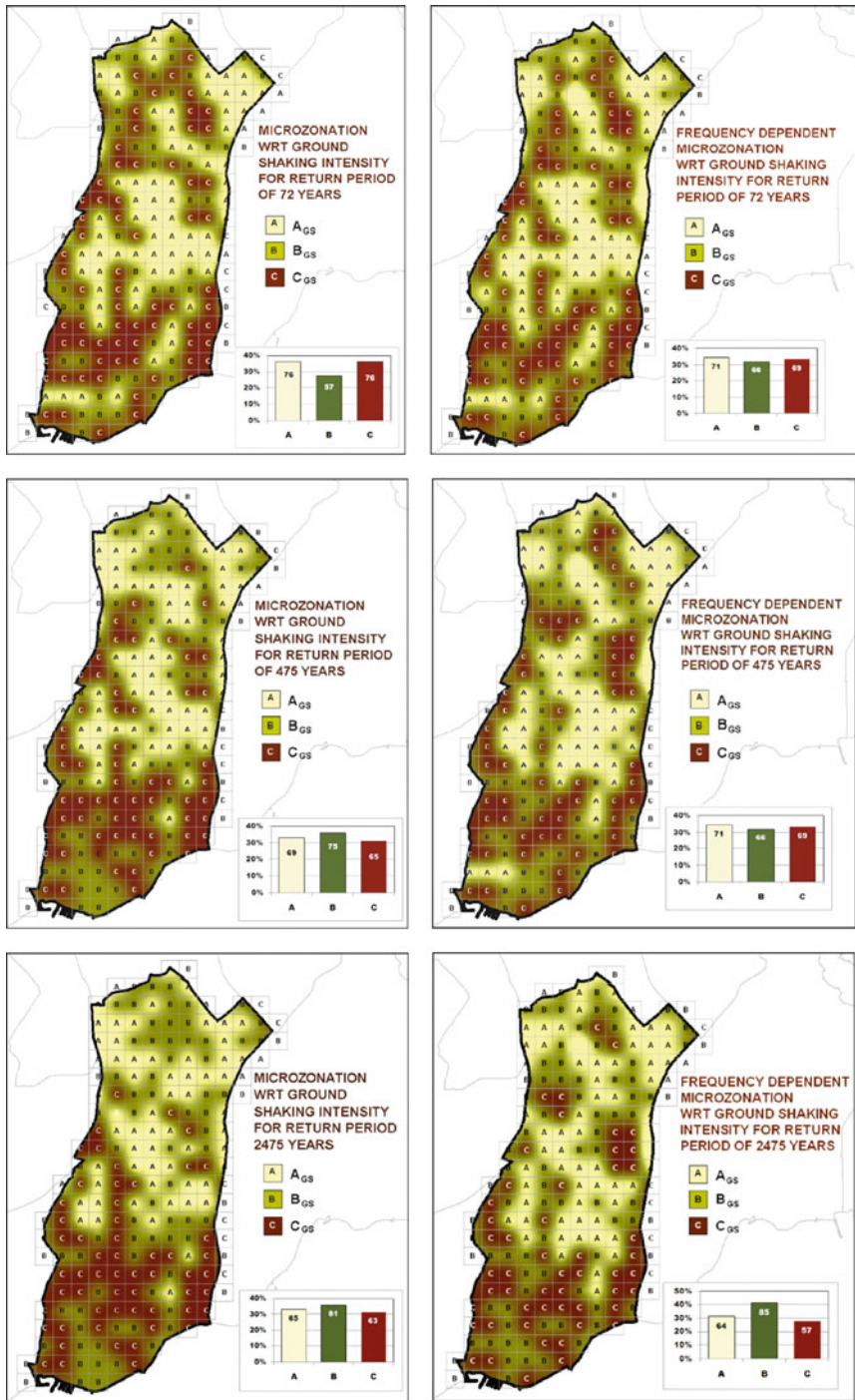


Fig. 9.7 The effect of hazard level and the influence of the frequency correction in site response analysis in microzonation with respect ground shaking intensity

the three input hazard levels as shown in Fig. 9.7 in comparison with the microzonation maps calculated without the frequency correction. As can be observed, both input hazard level and frequency correction affects the microzonation maps with respect to ground shaking intensity even though the differences are not very significant. The calculated number of cells in Zone C which indicates highest level of relative ground shaking intensity is decreasing with increasing hazard level from 75 to 63 for the case of frequency independent analysis, as in the case of frequency dependent analysis the number of cells in Zone C is decreasing from 71 to 57 indicating fewer number of cells susceptible with highest intensity of ground shaking.

Even though PGA is not considered as a good indicator for damage distribution, one other option is to adopt peak ground acceleration, PGA calculated by site response analysis as a microzonation parameter. As shown in Fig. 9.8, when relative mapping is applied, the hazard level appears to have no effect on the ground shaking intensity microzonation maps with respect to PGA. And likewise the effect of frequency correction is very insignificant. Regarding microzonation methodology, this is a very positive aspect of PGA microzonation since it eliminates the effects of the input earthquake level as well as the additional efforts for implementing the frequency correction.

Microzonation maps were also prepared with respect to peak ground velocity calculated on the ground surface based on site response analysis. As shown in Fig. 9.9, microzonation is dependent on the hazard level. In the case of PGV since the ratio of the difference between 33 and 67% percentile levels are less than 20%, it was considered that this narrow difference does not justify to adopt microzonation based on three zones. Instead, the total area is divided into two zones based on the 50% percentile (median) as shown in Fig. 9.9.

It is also interesting to observe that the microzonation maps produced based on PGV are very different to those produced based on PGA as given in Fig. 9.8. Firstly the range of calculated PGVs is much narrower than the range of PGAs. And in addition, the cells that are susceptible to higher levels of PGV do not coincide much with the cells of higher levels of PGA.

However, the main issue is the difference between the microzonation maps with respect to ground shaking intensity as given in Fig. 9.7 and PGA microzonation maps given in Fig. 9.8. This introduces a dilemma between the two approaches. One way to resolve this dilemma is to evaluate the ground shaking intensity microzonation map with respect to other earthquake parameters such as peak spectral accelerations, PGV, or parameters such as Arias Intensity.

However, as shown in Fig. 9.10, there are similarities and differences in the ground shaking microzonation produced with respect to different parameters. This indicates that ground shaking intensity microzonation maps are function of the parameter or parameters selected as the microzonation parameter. Therefore microzonation parameter need to be selected based on the main purpose or the main function of these microzonation maps.

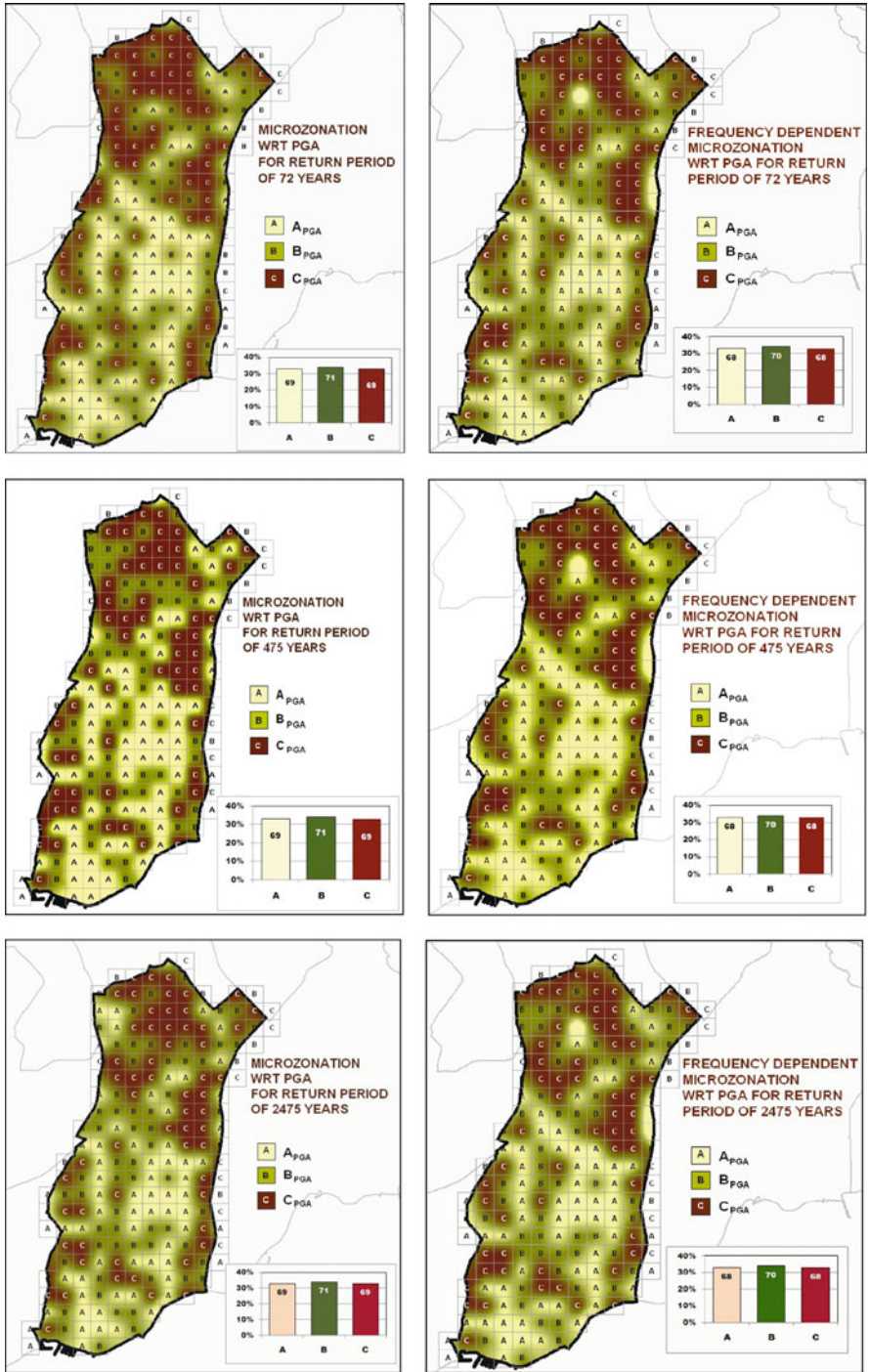


Fig. 9.8 The effect of hazard level and the influence of the frequency correction in site response analysis in microzonation with respect to ground shaking intensity based on PGA

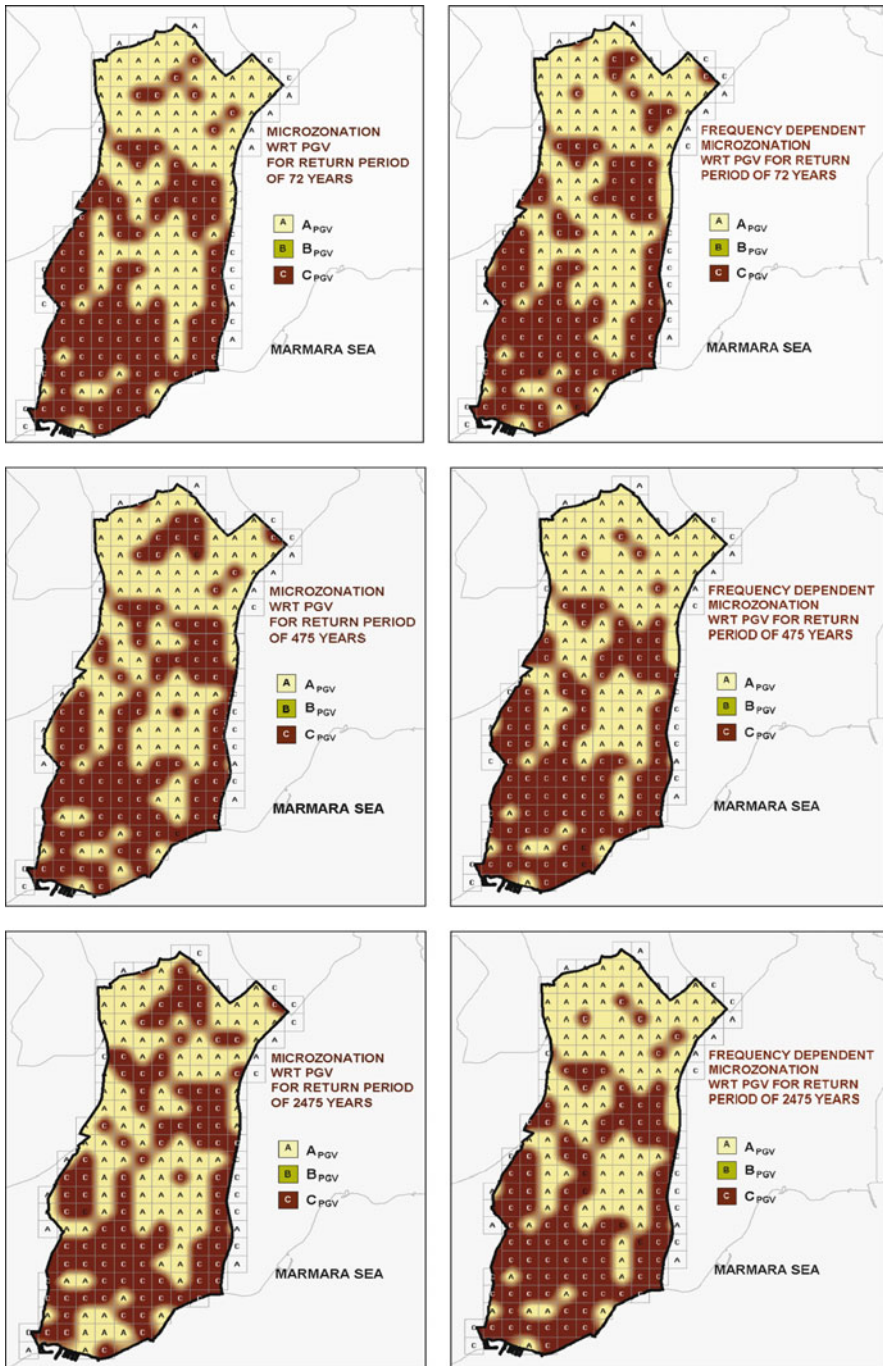
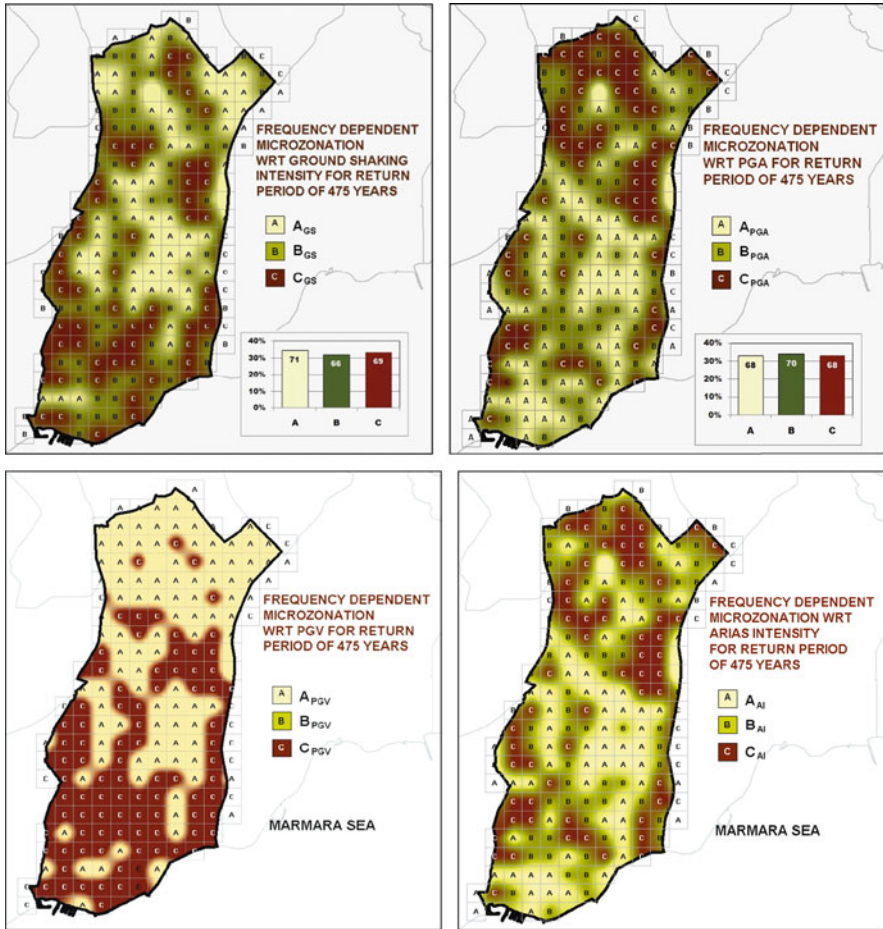


Fig. 9.9 The effect of hazard level and the influence of the frequency correction in site response analysis in microzonation with respect to ground shaking intensity based on PGV



**Fig. 9.10** The effect of the microzonation parameter in microzonation with respect to ground shaking intensity

### 9.6 Conclusions

Microzonation with respect to ground shaking intensity was based on two parameters: (1) average spectral accelerations calculated between 0.1 and 1 s periods using the average acceleration spectrum calculated from the results of 24 site response analysis conducted for each boring, (2) the peak spectral accelerations calculated from Borchardt (1994) using equivalent shear wave velocities. The microzonation with respect to ground shaking intensity is produced with respect to three regions where zone A<sub>GS</sub> shows the areas with very low ground shaking intensity, zone B<sub>GS</sub> shows the areas with low to medium ground shaking intensity, and zone C<sub>GS</sub> shows the areas with high ground shaking intensity.

Based on the microzonation studies conducted during the recent years, two conclusions may be drawn: (1) the detailed site investigation and related detailed site characterisation is very important and essential when performing site response analyses to have reliable and more accurate information on ground shaking characteristics for microzonation, and (2) the methodology followed and the type and number of acceleration time histories used for site response analysis to generate microzonation maps can have significant effect on the final microzonation.

The last issue is the selection of microzonation parameter. It was shown that microzonation with respect to different parameters such as PGA and PGV can give significantly different microzonation maps. Therefore, the selection of the microzonation parameter needs to be compatible with the main purpose of the microzonation project.

**Acknowledgments** The Authors would like to acknowledge the support and contributions of all their colleagues in the Earthquake Engineering Department of Kandilli Observatory and Earthquake Research Institute with special thanks to Prof. Mustafa Erdik, Dr. Mine Demircioğlu, and Dr. Karin Şeşetyan.

## References

- Alvarez L, Garcia J, Vaccari F, Panza GF, Gonzalez B, Reyes C (2004) Ground motion zoning of Santiago de Cuba: an approach by SH waves modelling. *Pure Appl Geophys* 161: 1041–1059
- Alvarez L, Garcia J, Vaccari F, Panza GF, Pico R (2005) Seismic microzoning from synthetic ground motion parameters: case study, Santiago de Cuba. *Soil Dyn Earthquake Eng* 25(5):383–401
- Ansal A, Akinci A, Cultrera G, Erdik M, Pessina V, Tönük G, Ameri G (2009a) Loss estimation in Istanbul based on deterministic earthquake scenarios of the Marmara Sea region (Turkey). *Soil Dyn Earthquake Eng* 29(4):699–709
- Ansal A, Durukal E, Tönük G (2006a) Selection and scaling of real acceleration time histories for site response analyses. *Proceedings of the ISSMGE ETC12 Workshop, Athens, Greece*
- Ansal A, Erdik M, Studer J, Springman S, Laue J, Buchheister J, Giardini D, Faeh D, Koksall D (2004b) Seismic microzonation for earthquake risk mitigation in Turkey. *Proceedings of the 13th world conference of earthquake engineering, Vancouver, Canada, CD Paper No. 1428*
- Ansal A, Kurtuluş A, Tönük G (2007a) Earthquake damage scenario software for urban areas. In: Papadrakakis M, Charnpis DC, Lagaros ND, Tsompanakis Y (eds) *Keynote lecture, Computational methods in structural dynamics and earthquake engineering, Rethymno, Crete, Greece*
- Ansal A, Laue J, Buchheister J, Erdik M, Springman S, Studer J, Koksall D (2004a) Site characterization and site amplification for a seismic microzonation study in Turkey. *Proceedings of the 11th international conference on soil dynamics and earthquake engineering and 3rd earthquake geotechnical engineering, San Francisco, CA*
- Ansal A, Özaydın K, Erdik M, Yıldırım Y, Kılıç H, Adatepe S, Özener PT, Tonaroglu M, Sesetyan K, Demircioğlu M (2005) Seismic microzonation for urban planning and vulnerability assessment. *Proceedings of the international symposium of earthquake engineering (ISEE2005), Awaji Island, Kobe*
- Ansal A, Tönük G (2007a) Ground motion parameters for loss estimation. *Keynote lecture, Proceedings of the 4th international conference on urban earthquake engineering, Tokyo Institute of Technology, Tokyo, Japan, 7–14*

- Ansal A, Tönük G (2007b) Source and Site Effects For Microzonation, Earthquake Geotechnical Engineering, Geotechnical geological and earthquake engineering, Ed. K. Ptilakis, Chapter 4. Springer, pp 73–92
- Ansal A, Tönük G (2009) Site specific earthquake characteristics for performance based design. Keynote lecture, Proceedings of the international conference on earthquake engineering, Seismology and engineering seismology volume, Banja Luka, Republic of Srpska, Bosna Herzegovina, pp 59–63
- Ansal A, Tönük G, Bayraklı Y (2007b) Microzonation with respect to ground shaking intensity based on 1D site response analysis. Proceedings of the XIV European conference on soil mechanics and geotechnical engineering, Madrid
- Ansal A, Tönük G, Demircioğlu M, Bayraklı Y, Sesetyan K, Erdik M (2006b) Ground motion parameters for vulnerability assessment. Proceedings of the 1st European conference on earthquake engineering and seismology, Geneva, Switzerland, Paper No 1790
- Ansal A, Tönük G, Kurtuluş A, Erdik M, Parolai S (2010) Modeling the observed site response from Istanbul strong motion network. State of art and practice lecture, Proceedings of the 5th international conference on recent advances in geotechnical earthquake engineering and soil dynamics, San Diego, CA, SOAP10
- Ansal A, Tönük G, Kurtuluş A (2009b) Microzonation for urban planning. Earthquakes and tsunamis – Civil engineering disaster mitigation activities – Implementing millennium development goals. Geotechnical geological and earthquake engineering, vol 11, Springer, pp 133–155
- Borcherdt RD (1994) Estimates of site dependent response spectra for design (methodology and justification). *Earthquake Spectra* 10(4):617–654
- BSSC-Building Seismic Safety Council (2001) NEHRP (National Earthquake Hazards Reduction Program) Recommended provisions for seismic regulations for new buildings and other structures, 2000 edn, Part 1: Provisions (FEMA 368), Chapter 4, Washington, DC
- Erdik M, Demircioğlu M, Sesetyan K, Durukal E (2005) Assessment of earthquake hazard for Bakirköy, Gemlik, Bandırma, Tekirdağ and Körfez. WB MEER Project – A3 component, Microzonation and hazard vulnerability studies for disaster mitigation in pilot municipalities, Bogazici University, Kandilli Observatory and Earthquake Engineering Research Institute
- Erdik M, Demircioğlu M, Sesetyan K, Durukal E, Siyahi B (2004) Earthquake hazard in Marmara region. *Soil Dyn Earthquake Eng* 24:605–631
- Grasso S, Maugeri M (2009) The seismic microzonation of the city of Catania (Italy) for the maximum expected scenario earthquake of January 11, 1693. *Soil Dyn Earthquake Eng* 29:953–962
- Idriss IM, Sun JI (1992) Shake91, A computer program for conducting equivalent linear seismic response analysis of horizontally layered soil deposits modified based on the original SHAKE program published in December 1972 by Schnabel, Lysmer and Seed, University of California OYO Inc., Japan (2007) Production of microzonation report and maps on European Side (South). Final Report to Istanbul Metropolitan Municipality
- Papadimitriou GA, Andreas AA, Bouckovalas GD, Marinos PG (2008) Methodology for automated GIS-aided seismic microzonation studies. *Comp Geotech* 35:505–523
- Parvez IA, Vaccari F, Panza GF (2003) A deterministic seismic hazard map of India and adjacent areas. *Geophys J Int* 155:489–508
- PEER (2009) Strong motion data bank. <http://peer.berkeley.edu>
- Pergalania F, Romeob R, Luzia L, Petrinia V, Pugliesec A, Sano T (1999) Seismic microzoning of the area struck by Umbria–Marche (Central Italy) Ms 5.9 earthquake of 26 September 1997. *Soil Dyn Earthquake Eng* 18:279–296
- Singh SK, Pimprikar SD, Bansal BK, Pacheco JF, Dattatrayam RS, Suresh G (2007) An analysis of the Mw 4.7 Jabalpur, India, earthquake of 16 October 2000: toward ground-motion estimation in the region from future events. *Bull Seismol Soc Am* 97(5):1475–1485

- Sugito M, Aida N, Masuda T (1994) Frequency dependent equilinearized technique for seismic response analysis of multi-layered ground. *J Geotech Eng, Proceedings of the JSCE* 493:49–58 (in Japanese)
- Todorovska MI, Trifunac MD (1996) Hazard mapping of normalized peak strain in soils during earthquakes: microzonation of a metropolitan area. *Soil Dyn Earthquake Eng* 15(5):321–329
- Yoshida N, Kobayashia S, Suetomia I, Miura K (2002) Equivalent linear method considering frequency dependent characteristics of stiffness and damping. *Soil Dyn Earthquake Eng* 22(3):205–222

# Chapter 10

## Slope Failure

### Effects of Heavy Rainfalls on Slope Behavior: The October 1, 2009 Disaster of Messina (Italy)

Michele Maugeri and Ernesto Motta

**Abstract** On October, 1 2009 a heavy rainfall hit the limited area on the N-E part of Sicily (Italy) near the town of Messina. At the station of St. Stefano di Briga a rainfall of 223 mm occurred in 7 h with a peak of 10.6 mm in 5 min. During the event many landslides such as sliding, debris flows and mud flows occurred in the 14 villages, causing 37 victims, mainly in the villages of Giampilieri and Scaletta Zanclea. Big damage occurred to the buildings, as well to roads and railways. The event caused about 1,652 homeless and the total cost for the recovery was estimated in about 800 M U.S. dollars. The microzoning of residual risk allows about 50% homeless to come back in the houses located in areas at very low risk. The assessment of the slope instability could be done by empirical correlation or analytical and numerical analyses. Some criteria for the stabilization works for risk mitigation are discussed. As the damaged area is prone to seismic risk (it was shaken by the 1908 Messina and Reggio Calabria earthquake), the analysis of slope instability and the evaluation of the behavior of the stabilization works must take into account the multidisciplinary risk analysis due to heavy rainfall and earthquakes.

## 10.1 Introduction

On October 1, 2009 a heavy rainfall hit the limited area on the N-E part of Sicily (Italy) near the town of Messina (Fig. 10.1). During the event many landslides such as slidings, debris flows and mud flows occurred in the 14 villages of Briga Superiore, Briga Marina, Pezzolo, Altolia, Molino, Giampilieri Superiore, Giampilieri Marina, Scaletta Zanclea, Scaletta Superiore, Guidomandri Superiore, Guidomandri Marina, Itala, Mannello, Borgo (Fig. 10.2).

---

M. Maugeri (✉)

Department of Civil and Environmental Engineering, University of Catania, 95125 Catania, Italy  
e-mail: mmaugeri@dica.unict.it

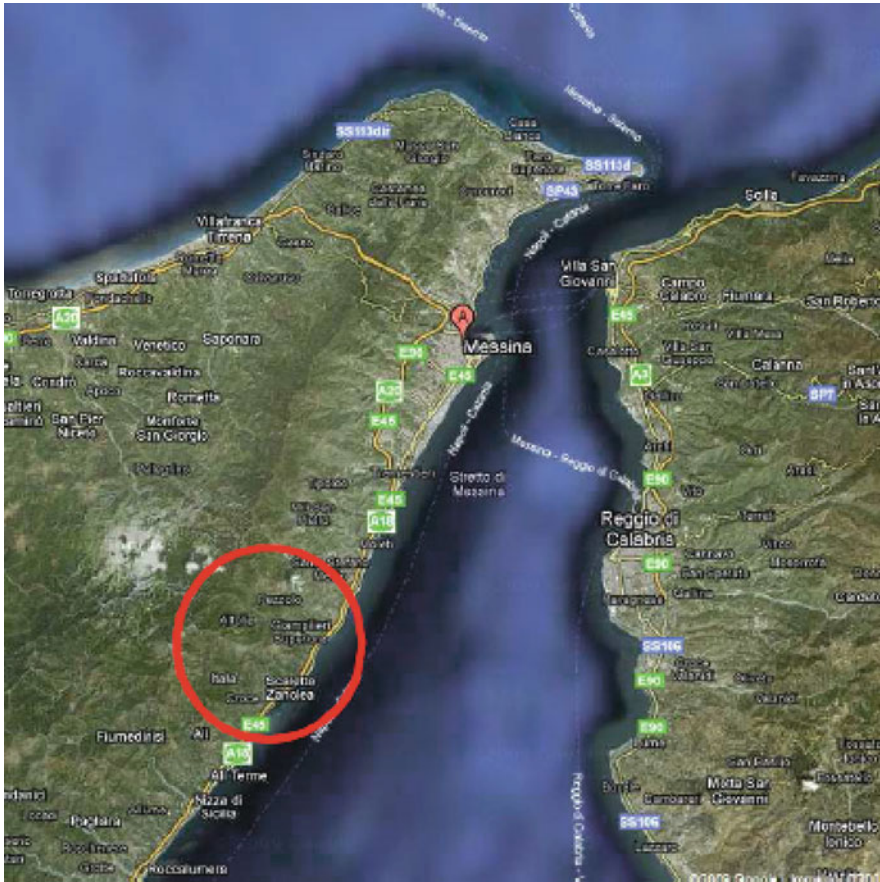


**Fig. 10.1** The damaged area by the rainfall of the October 1, 2009 is located South-West of the Strait of Messina (Italy)

Some landslides due to the heavy rainfall damaged in particular the village of Giampileri Superiore, that is built very close to a sloping hill. A landslide occurred in the Puntale stream and caused the collapse of some buildings and about 27 victims, living in the collapsed buildings. The sliding rapidly evolved in a fast debris flow propagating throughout the narrow and sloping roads, invading many buildings downstream. Similar landslides occurred in the close Sopra Urno stream rapidly evolving in a fast debris flow propagating, fortunately without any victims.

At Scaletta Zanclea the major damage was caused by the debris flow propagating along the Racinazzi stream, causing 6 victims. Some of them were probably brought up to the sea and never found.

Because of economical, social and cultural reasons the medieval villages cannot be abandoned and so the Authority decided to provide remedial works to allow the people to live safe in the village.

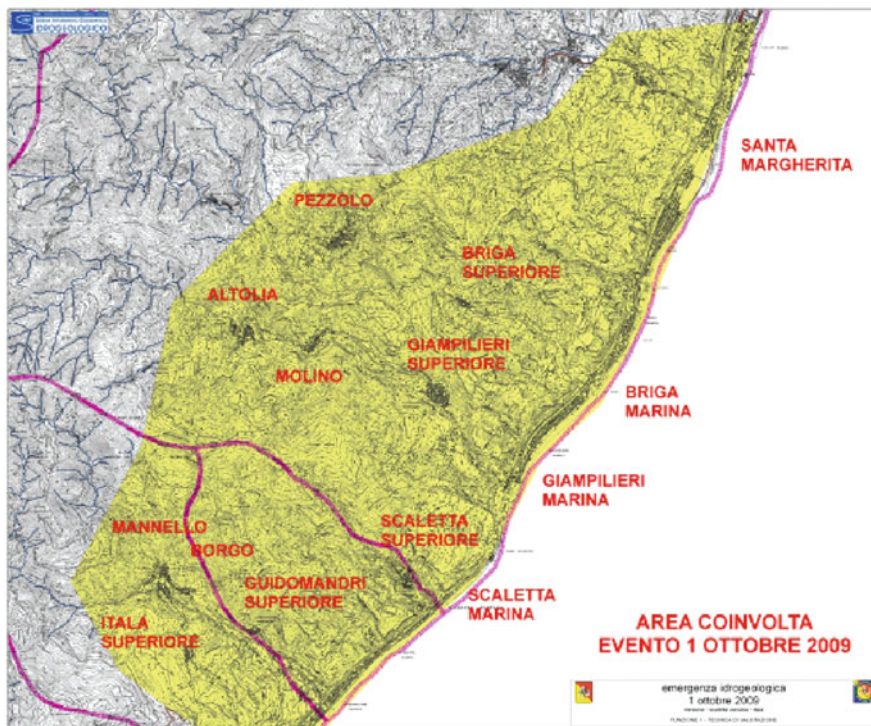
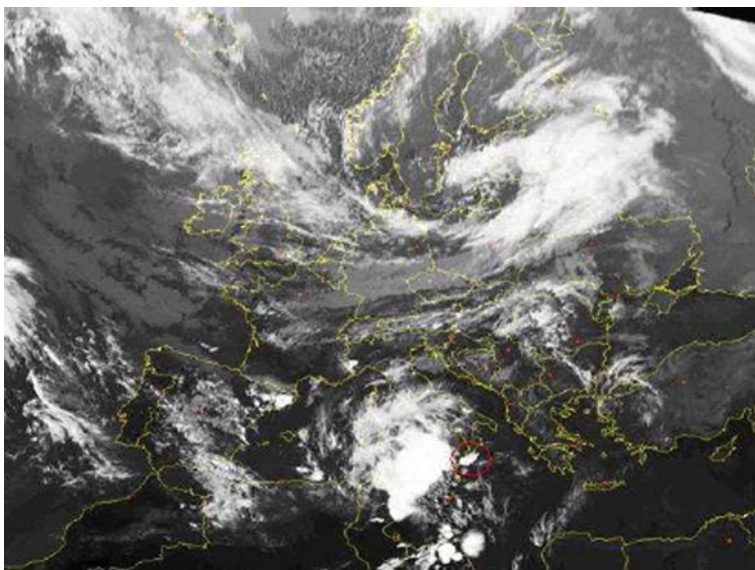


Fig. 10.2 Damaged villages by the rainfall of the October 1, 2010

## 10.2 The Rainfall Event

A great atmospheric disturbance occurred on October 1, 2009 in the Mediterranean sea in front of Taormina (Sicily), as shown in Fig. 10.3. The heavy rainfall hit the limited area on the N-E part of Sicily (Italy) near the town of Messina. The rainfall event reached a peak between 7:00 and 8:00 pm (Fig. 10.4) Fig. 10.5 shows the rainfall accumulation according to Fiumedinisi station. At the rain gauge station of St. Stefano di Briga a rainfall of 223 mm occurred in 7 h, with a peak of 10.6 mm in 5 min. Because the rain gauge stations of Santo Stefano di Briga and Fiumedinisi are located outside the damaged area, is very difficult to evaluate the rainfall intensity causing the disaster. Also is very difficult the evaluation of the critical duration of the rainfall, causing landslides. An estimation of critical duration was made considering the durations of 1 day up to 5 days. By the way, the return period of the rainfall at St. Stefano di Briga and Fiumedinisi rain gauge stations was estimated of about 100 years in the case of critical rainfall duration of 2 h and 210 years in the case of the critical duration of 6 h.

This event follows a rainfall event of similar intensity occurred on September 23–24, 2007. The event hit the same area of the 2009 event, causing landslides and debris flows with little damage and no victims at the Chiesa street at Giampilieri



**Fig. 10.3** The great atmospheric disturbance occurred on October 1, 2009 in the Mediterranean sea in front of Taormina (Sicily)

Superiore village. The flood evaluation on the Giampileri stream, with a catchment of 9.8 km was evaluated about 275 m/s, while the flood in the Racinazzi stream (at Scaletta Zanclea), with a catchment of 1.6 km was evaluated of about 80 m/s.

The flood was of about 28 m/s/km in the case of Giampileri catchment while it was of about 50 m/s/km, in the case of Racinazzi catchment. The flood per km is higher for the Racinazzi catchment comparing with the Giampileri catchment because the Racinazzi catchment is much smaller than the Giampileri catchment. It can be argued that for smaller streams such as the Loco stream (catchment 0.141 km), the Sopra Urno stream (catchment 0.086 km) and the Puntale stream (catchment 0.033 km), crossing the Giampileri village, the flood per km could be much higher. For these very small streams, the rainfall estimation by radar is not possible. Only a net of rain gauge is able to evaluate the real rainfall. But unfortunately the area was not monitored in the past. However, after the event a rain gauge net is going to be installed.

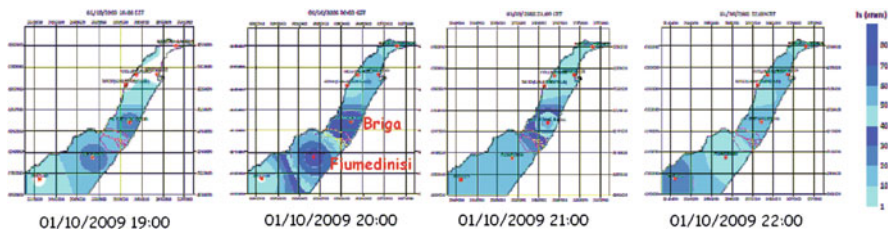


**Fig. 10.4** Rainfall on the damaged area from 7:00 to 10:00 pm; peak reached at 7:00 to 8:00 pm (after Aronica, 2009)

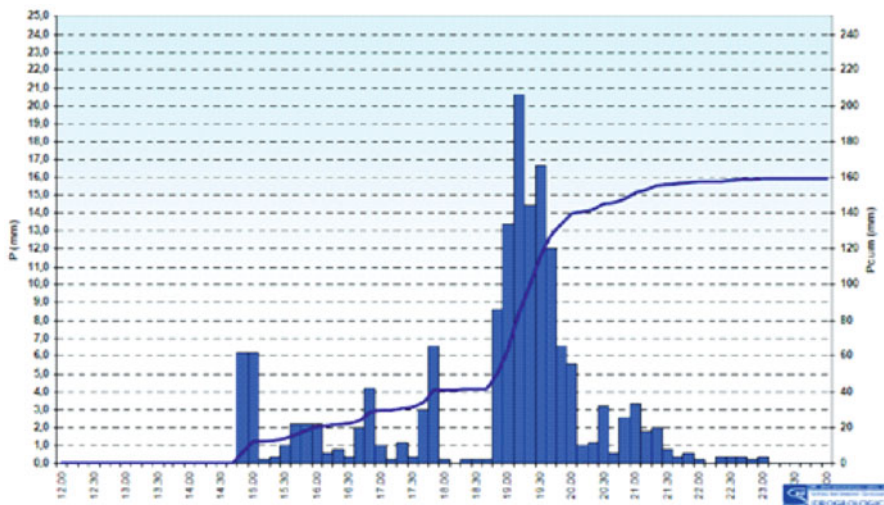


Fig. 10.5 Rainfall accumulation: Fiumedinisi station

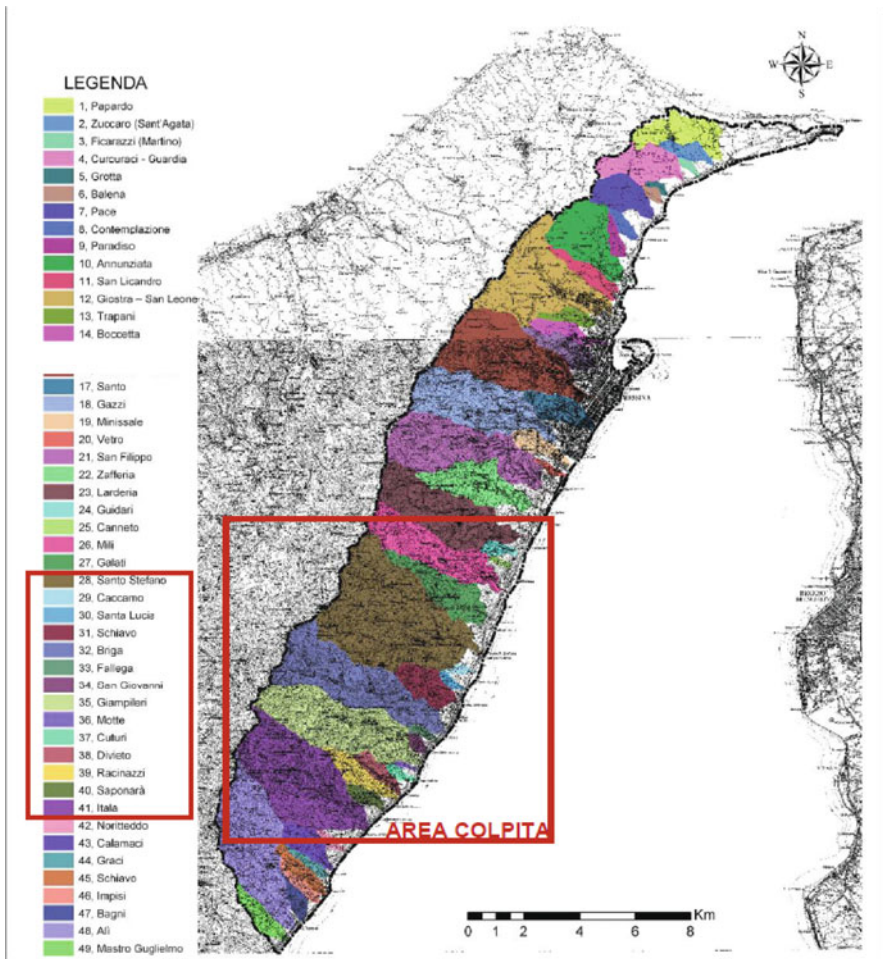
The hills around the damaged villages are very sloping with slopes around 30–40 degrees but locally they can reach even 60 degrees. From a geological point of view the area is characterized by metamorphic rocks belonging to the variscic metamorphic complex with an age between the paleozoic and the Carbonifer Permian. Figure 10.6 shows the geology, the catchments and the length of the rivers. The hills are covered with cohesionless soils with a thickness of about 2 m. The area is also characterized by a fault system with vertical dipping and Northeast-SouthWest direction.

This causes that the soils of the Aspromonte tectonic unit (PNA) overlap the phillades Mendaci tectonic unit. In the south area of Giampilieri village we can observe paleozoic Phillades and Metarenites with a scaly weaving because of the intense tectonic action and because of their own weaving. This intense fracturation action is the cause of coverings of debris soil of different thickness.

Up to now no laboratory tests have been carried on to investigate the geotechnical properties of the covering soils anyway these soils are mainly constituted by sands and gravels with some percentage of silt. The friction angle of these cohesionless materials is strongly influenced by the fine soil fraction. The friction angle can reach even 35 degrees but its value could be much less if a high percentage of silty soil is present.

### 10.3 Landslides and Damage

The October 1 rainfall event triggered about 550 landslides in the lower part of the catchments. Some landslides hit the buildings located at the toe of the landslides, causing the majority of victims. Some landslides evolved as debris flows, flowing



Rivers	Length (km)	Surface hydrographic basin (km <sup>2</sup> )	Municipal territories of the basin
Galati	5,7	3,5	Messina
Santo Stefano	8,4	16,4	Messina
Caccamo	1,2	0,3	Messina
Santa Lucia	1,3	0,3	Messina
Schiavo	3,2	2,2	Messina
Briga	9,0	9,6	Messina
Fallega	1,3	0,3	Messina
San Giovanni	1,0	0,3	Messina
Giampileri	8,5	9,2	Messina
Motte	1,1	0,2	Messina
Cuturi	1,3	0,4	Messina - Scaletta Zanclea
Divieto	2,6	1,0	Messina - Scaletta Zanclea
Racinazzi	3,4	1,6	Scaletta Zanclea
Saponarà	1,9	0,7	Scaletta Zanclea
Itala	7,5	11,3	Itala - Scaletta Zanclea

Fig. 10.6 Geology between the Fiumedinisi river and Capo Peloro with the main characteristics of the catchment area and river length



**Fig. 10.7** Debris flow originated by the Saponarà, Racinazzi and Divieto streams at Scaletta

into the village streets, reaching the streams crossing the villages. In many cases the debris flows flowing inside the streams reached the sea.

As an example, in Fig. 10.7 is shown the debris flow flowing through the Saponarà stream, the Racinazzi stream and the Divieto stream at Scaletta Zanclea. In particular Fig. 10.8 shows the damage caused by the debris flow flowing through the Racinazzi stream. Several houses were destroyed or severely damaged (Fig. 10.9), and 6 victims occurred, 5 of them never found.

As an example of landslides, triggered by heavy rainfall, in Fig. 10.10 are reported the landslides which hit the Itala, Mannello and Borgo medieval villages.

In particular the landslide caused the collapse of some houses at the Mannello village and at the medieval village of Borgo (Fig. 10.11).

## 10.4 Microzonation of Damaged Areas

The microzoning of residual risk was performed to allow homeless to come back in the houses located in areas at very low risk, as well as to evaluate the residual risk in the remaining area. The microzoning was carried out for all the damaged villages. As an example, only the case of the microzoning of Giampilieri, where the most people died, is discussed.



**Fig. 10.8** Damaged caused at Scaletta Zanclea by the debris flow flowing along the “Racinazzi” stream

Giampileri Superiore is a beautiful village to be preserved (Fig. 10.12). It is located along the Giampileri stream. The village is prone to the Loco stream, Sopra Urno stream and Puntale stream (Fig. 10.13). Along these streams some landslides occur, hitting some houses prone to the slope, evolving as debris flow, flowing through the village streets and reaching the Giampileri stream.

In Fig. 10.14 is reported a general view of the landslide occurred at the Puntale stream, which hit some buildings very near to the slope, causing 27 deaths. The



**Fig. 10.9** Scaletta Zanclea Village: a building damaged by the debris flow flowing in the Racinazzi stream

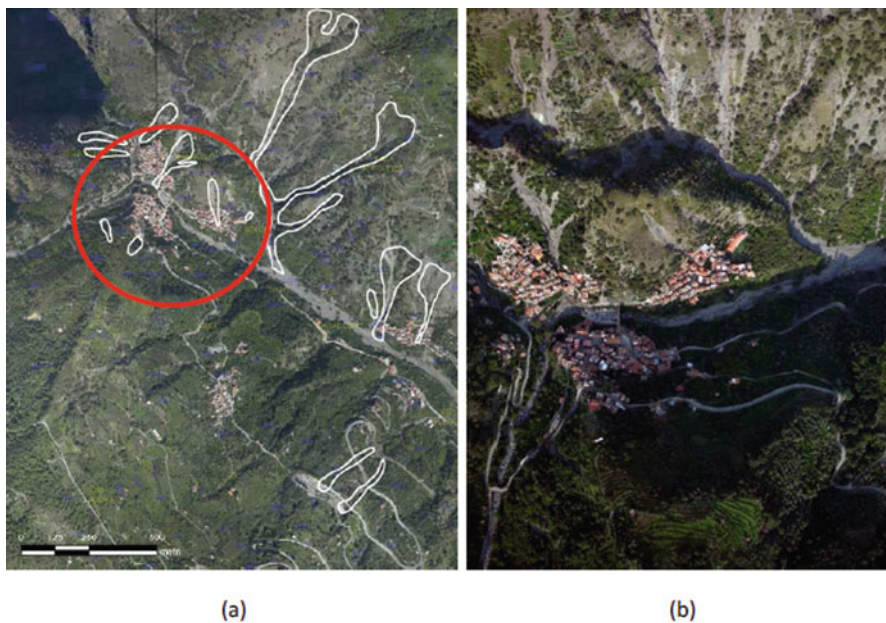


**Fig. 10.10** Landslides at the villages Itala, Borgo and Mannello, flowing in the Itala stream. (a) General view; (b) detail of the *circled area*

landslide evolved as debris flow along the Vallone street, reaching the Giampileri stream. The houses collapsed due to the landslides are shown in Fig. 10.15. The material cumulated along the Vallone street is reported In Fig. 10.16. It was removed carefully to find the deaths.



**Fig. 10.11** Collapsed and severely damaged houses at the Borgo village



**Fig. 10.12** A view of the Giampileri Superiore village, damaged by the event

The Sopra Urno stream released a small debris flow during the September 23–24, 2007 event. To mitigate the debris flow hazard, some gabions were realized (Fig. 10.17), but the October 1, 2009 event caused the collapse of these gabions by toe erosion. So the mitigation works were not effective to

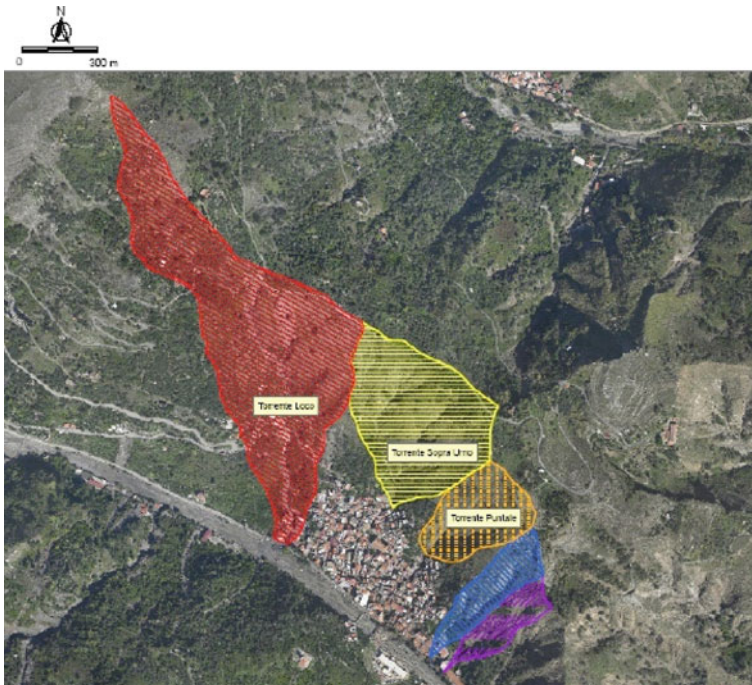


**Fig. 10.13** The catchment of the Loco stream ( $0.141 \text{ km}^2$ ), Sopra Urno stream



**Fig. 10.14** The Puntale stream landslide hitting the house located at the Vallone Street

protect the Chiesa street, along which the debris flowed up to Giampilieri stream (Fig. 10.18).

The Loco stream released also a debris flowing between some houses up to the Giampilieri stream (Fig. 10.19), without causing any dead. The decision to be made is to leave the existing path of the stream between the houses or to divert its path outside the existing buildings.

Some others landslides occurred at Giampilieri and all of them were classified and marked with an identification number. As an example, the landslide numbered G4, which hit the elementary school, is shown in Fig. 10.20.

On the basis of data acquisition during and after the event, a microzonation of the residual risk was done and reported in Fig. 10.21. The area is subdivided in 4



**Fig. 10.15** Damaged houses due to the landslide occurred at Puntale stream. The debris flow reached the third floor of the house in front of the stream



**Fig. 10.16** The debris cumulated in the Vallone street

zones with different risk levels, marked with different colors. The areas that were not significantly reached by the debris flow, marked green, are areas with a negligible residual risk and population is allowed to return to their houses. Areas reached by debris, marked yellow, are areas with low risk and buildings can be used with some caution; protection plan by the civil defense is required. Areas damaged by debris,



**Fig. 10.17** The damage occurred to gabions along the Sopra Urno stream



**Fig. 10.18** The debris cumulated in the Chiesa street in the day after the event

marked pink, are areas with medium risk and the buildings cannot be used unless the mitigation works will be done. Areas, marked red, where buildings collapsed by the debris flow or to be demolished to restore the flowing part for the streams, are areas at very high risk level and cannot be used unless mitigation and slope stabilization works will be executed.



**Fig. 10.19** The debris flowing between the houses at the Loco stream

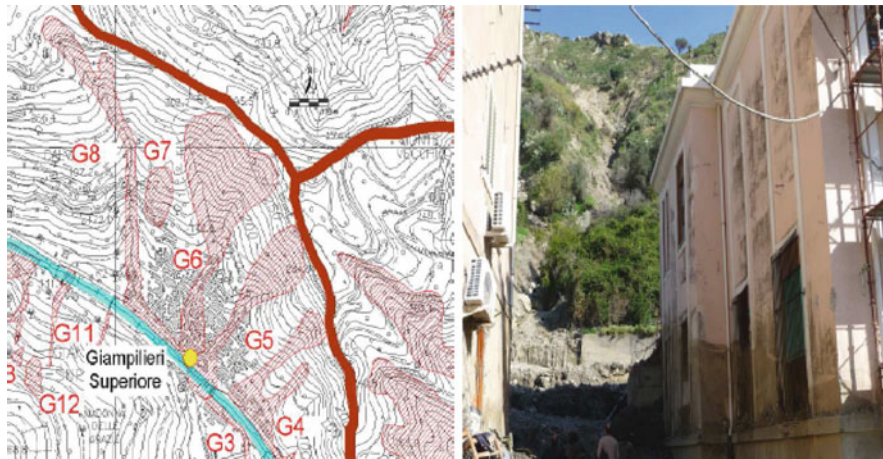


**Fig. 10.20** Plan of the numbered landslides at Giampileri and a view of the landslide No. G4, located in the proximity of the elementary school

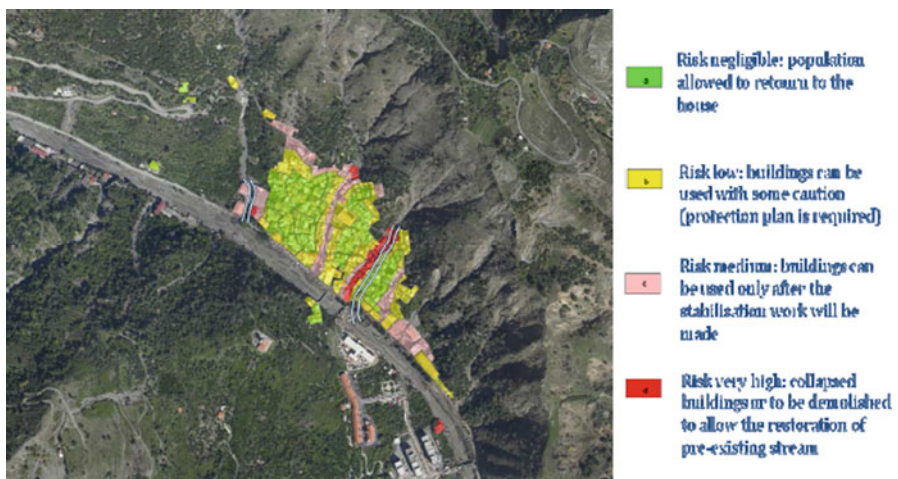


**Fig. 10.21** Microzonation of residual risk level at Giampileri Superiore village

Downstream to Puntale stream, a larger path must be restored. This can be done by demolishing the houses at the right side of via Vallone (marked red in the Fig. 10.21) or by demolishing the houses behind the via Vallone (path marked by blue lines). Furthermore also the slopes along the Puntale stream must be stabilized.

The Sopra Urno stream slopes must be also stabilized to protect Chiesa Street (pink areas in the middle of the village). Several debris flow barriers must be located along the Sopra Urno stream.

Along the Loco stream some debris flow barriers must be executed to mitigate the effects of debris flowing between the houses (pink area on the left side of the village). One existing house must be demolished to restore the path towards the Giampileri stream. To avoid the Loco stream bed will be used also as a street (as it was before the event), a new street must be open on the left side of the pink area to reach the houses marked pink.

The landslides which hit the elementary school (Fig. 10.20) must be also stabilized, as well as the landslide which hit some houses located in the pink area on the north-west part of the village (marked pink).

### 10.5 Assessment of Slope Instability

The assessment of the slope instability could be made by empirical correlation or analytical and numerical analyses. The most used empirical correlation is the rainfall intensity versus the occurrence of landslides. Several types of such correlation are reported in the scientific literature. Among these an empirical correlation of rainfall intensity versus occurrence of landslides is used in Hong Kong (ATC, 1997). On the basis of historical landslides caused by heavy rainfalls in Hong Kong (Premchitt et al., 1994; GEO, 1991–1996), a method based on 1-h and 24-h rainfalls was established. An application of this method for three different rainfall events is reported in Fig. 10.22. The method worked very well for 1-h critical rainfall over 70 mm and 24 h critical rainfall of 170 mm. When the critical rainfall was exceeded, the alarm

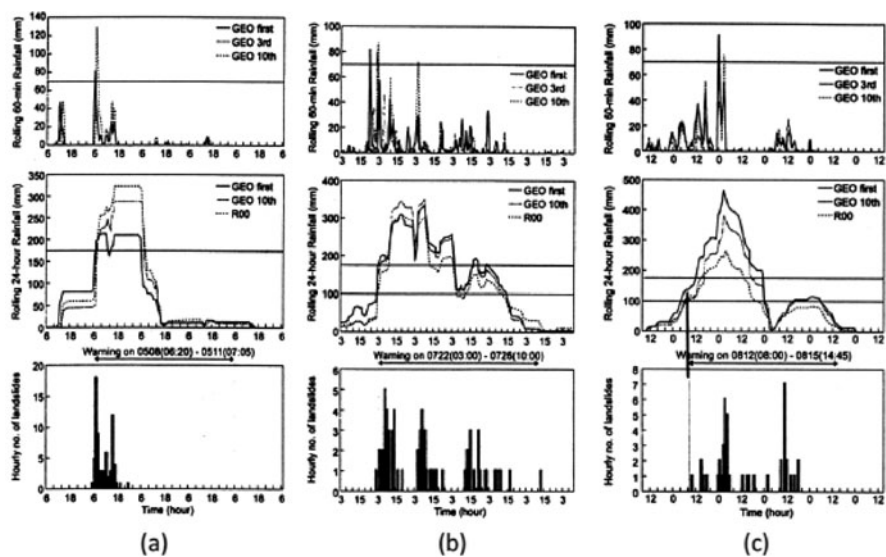


Fig. 10.22 Correlation between heavy rainfall and landslides in Hong Kong: (a) the event of 8–11 May, 1992; (b) the event of 22–26 July 1994; (c) the event of 12–15 August 1995

Date of event	Maximum rainfall (mm)					Landslide consequence				
	Royal Observatory			Other location		Number of landslides			Casualties	
	24 hr	1 hr	Antecedent 4 day	24 hr	1 hr	GEO	Newspaper	FSD	Killed	Injured
18/6/72	275	99	403	300	98	NA	dozens	14	147	103
25/8/76	416	52	96	500	82	NA	314	23	26	31
29/5/82	394	44	1	430	111	551	498	15	22	26
16/8/82	362	68	0	370	95	138	62	6	5	4
21/5/89	388	37	28	552	51	340	100	3	2	3
8/5/92	324	110	65	385	110	350	40	9	3	5
22/7/94	310	70	36	362	101	184	200	14	5	4
13/8/95	326	44	57	468	82	113	98	11	3	6

**Note: GEO = Geotechnical Engineering Office; FSD = Fire Services Department**

**Fig. 10.23** Effectiveness of the method based on the 24-h rainfall in Hong Kong; the number of casualties was very considerably reduced (ATC, 1997)

started and people were evacuated. Of course sometimes after the people evacuation, the landslides did not occur, but anyway people always follow strictly the alert because of cultural education, starting from primary school. This method is very well working in Hong Kong and mainly after the establishment of the Geotechnical Engineering Office, the risk of landslides was very significantly reduced (see Fig. 10.23).

The correlation between rainfall intensity versus occurrence of landslides, like that used in Hong Kong, needs a long series of historical data to be validated and cannot be used in a different environment, like the Messina damaged area, where such kind of historical data do not exist. Instead of using this kind of “black box” correlation, some others empirical correlation following more strictly physical phenomena can be used, such as: (i) rainfall intensity versus piezometric levels; (ii) piezometric levels versus slope movements; (iii) slope movements versus occurrence of landslides.

These kinds of empirical correlations, which are based on the monitoring of landslides movements, were used for the prediction of landslides (Fig. 10.24) occurred along the National Route 33 between the cities of Matsuyama and Kochi (Seki et al., 1980).

On the basis of rainfall intensity and slope movements measured by inclinometers and extensometers, the occurrence of the landslides was predicted on July 20 with an error of 30 mm (Fig. 10.25). On August 25, it was predicted that the second landslide will be occurred on August 27. On August 27 at 10 a.m. a further more accurate prediction was made, that is the landslide will be occurred at 12:30 of the same day. At 12:00 the traffic was halted; the landslide occurred at 12:50 with an error of 20 min.

The analysis and the prediction of a debris flow is mostly difficult. Analytical solutions, numerical analyses and physical models can be used. Analytical solutions are very complex approaches due also to boundary conditions. Among these,

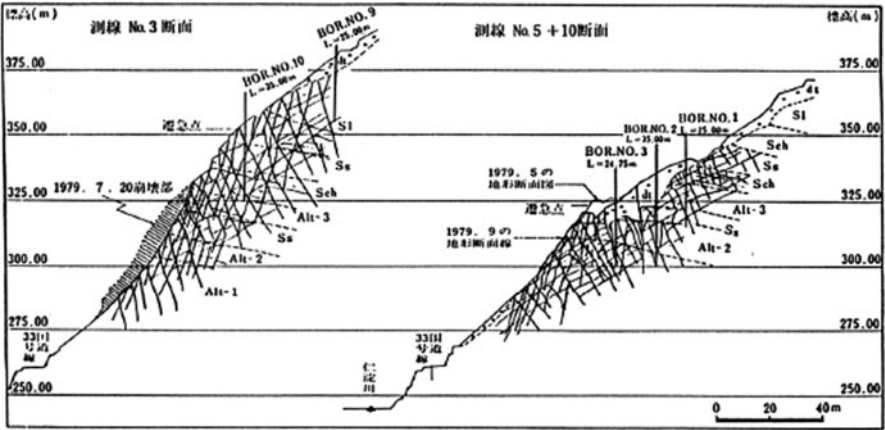


Fig. 10.24 Landslides No. 3 and No. 5 occurred along the National Route 33 (after Seki et al., 1980)

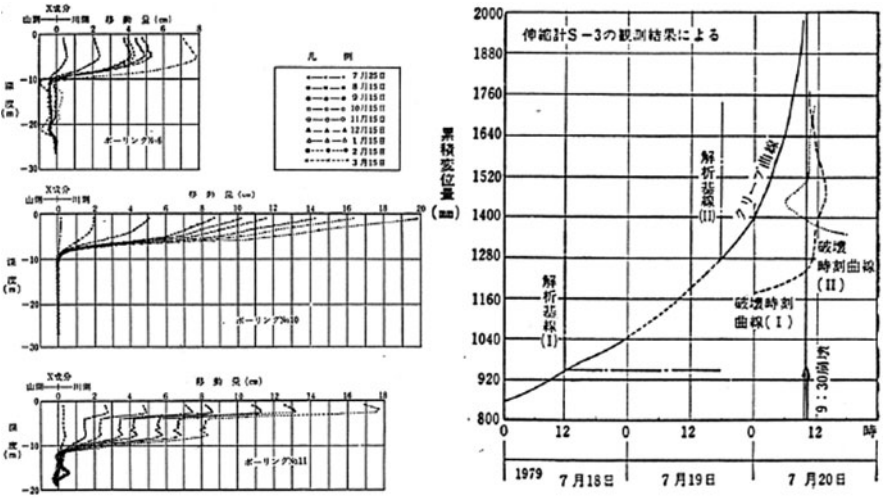
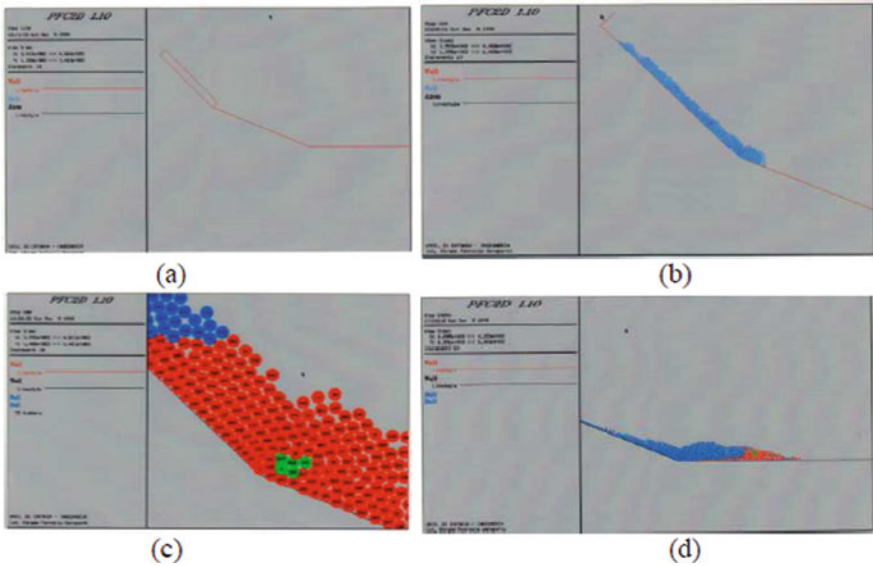


Fig. 10.25 Landslides No. 3 occurred along the National Route 33: (a) slope movement by boreholes inclinometers; (b) forecasting of the landslide (after Seki et al., 1980)

the well know approximate solution by Takahashi (1978) is often used. Among numerical methods (F.E.M., F.D.M. and D.E.M.), can be used.

An application of the Particle Flow Code (PFC2d) simulated the results shown in Fig. 10.26, including the triggering of the debris flow (a), the debris flow at the change of slope (b), the monitored green colored particles (c) and the arrest of the debris flow at the level land (d). The monitored green particles are identified by an ID number. Figure 10.27 shows the fluctuation velocity of the monitored particle ID = 9. The velocity is fluctuated in both directions x and y (Fig. 10.24a) because of



**Fig. 10.26** Numerical modeling by particle flow code. (a) triggering of the debris flow; (b) the debris flow at the change of slope; (c) the monitored green colored particles; (d) the arrest of the debris flow at the level land

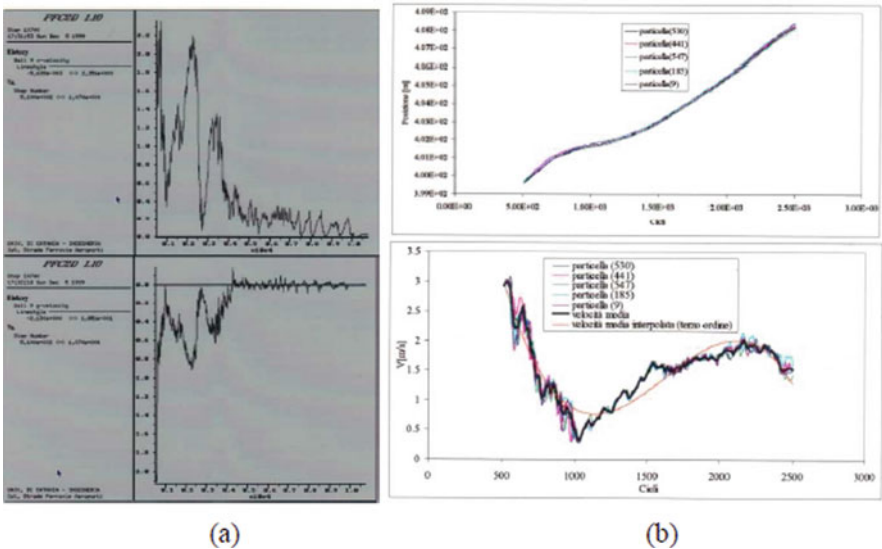


**Fig. 10.27** Velocity and position of monitored *green colored particles*. (a) Fluctuating x and y velocity of particle ID = 9; (b) position of the five monitored particles ID=530, 441, 547, 185, 9 (upper); velocity of the monitored particles, average and smoothed (down)

collisions with other particles. In the upper part of Fig. 10.27b is shown the positions and in the lower part the velocities of five monitored particles (ID = 9, 185, 441, 530, 547); in the lower part of Fig. 10.27b is also reported the average smoothed particle velocity.

The validation of the code was made by the comparisons with some case histories. As an example for the case of the debris flow at *Rio delle Fosse* (Bardonecchia, Italy), occurred on July 1994. The debris flow originated at 1,700 m above sea level, propagated for about 1,600 and arrested at the level land at a quote of 1,470 m above the sea level. The debris run for about 50 m at the level land while the computed run was of 23 m.

Physical models are generally affected by scale factors. However they are very useful for the understanding of the behavior of the phenomenon. A physical model of a debris flow was performed by Deangeli (1987) with an apparatus with two different slope inclinations and with a horizontal arresting channel. The debris flow was triggered by an artificial rain apparatus after the saturation of the soil. The test was monitored and the travelled space in the arresting channel was measured.

## 10.6 Stabilization Criteria for Risk Mitigation at Giampilieri

The landslides caused the collapse of many houses and the interruption of many roads. As an example a landslide hit the road to access to Giampilieri Superiore village as shown in Fig. 10.28. In the past these slopes were already affected by small landslide phenomena so some stabilization works were already existing. These stabilization works were not effective (Fig. 10.29a), so the new stabilization works (Fig. 10.29b), started just 3 days after the landslide event, to allow the opening of the road. Details of the new stabilization works are reported in Fig. 10.30.



**Fig. 10.28** The landslide hitting the road to access to Giampilieri Superiore village



**Fig. 10.29** Stabilization of the slope reported in Fig. 10.26: (a) old stabilization works; (b) new stabilization works

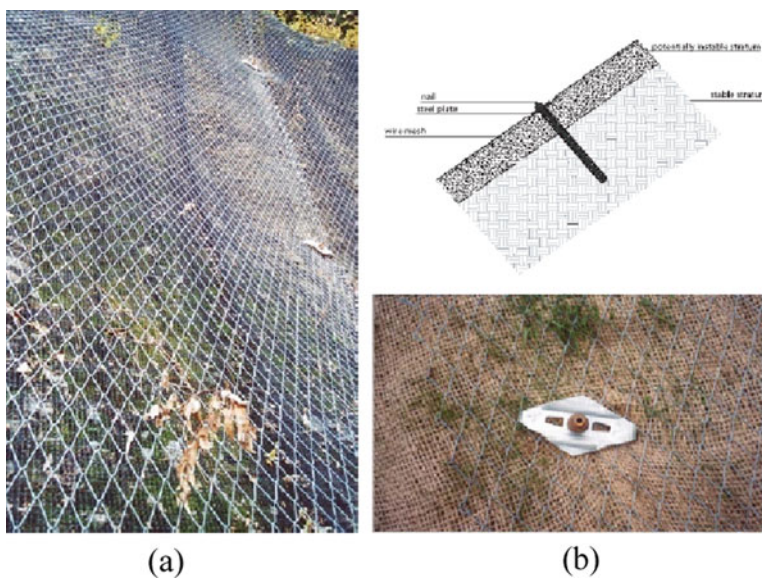


**Fig. 10.30** New stabilization works: (a) iron net used along the slope; (b) details of the anchorage system

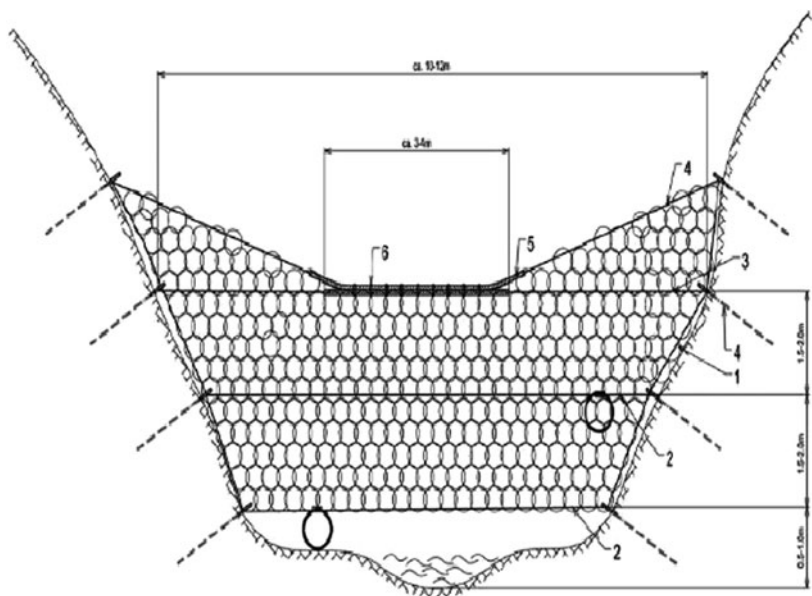


**Fig. 10.31** Sketch of an iron ring-net debris flow barrier

Where the slopes triggering debris flows are far away from the buildings, as in the case of Sopra Urno Stream and Loco Stream, it will be possible to use debris barriers to mitigate the effect of the flow and to reduce the mass flow captured by the debris tanks designed to this aim. In Fig. 10.31 is reported a sketch of an iron ring-net debris flow barrier anchored to both the sides of the stream. Behind the net, strong enough to withstand the debris flow energy, a ring-net with smaller opening can be associate with the function of reducing the grain size passing through.

It must be stressed that all slope stabilization systems, debris flow and landslides barriers, geosynthetic earth reinforced slopes and walls, must be properly designed with the aim to ensure adequate factors of safety against along the slopes. Also all the structure elements such as iron nets, slope anchorages etc must be designed on the basis of the force that they have to resist. Monitoring systems should be also installed to verify the correspondence between design and behavior of the executed works. Site and laboratory investigations are required for the assessment of geotechnical modeling. Quality controls of the materials are also required.

## 10.7 Conclusions

Conclusions are summarized as follows:

The evaluation of the October 1, 2009 disaster is an multidisciplinary topic involving Engineering Geology, Hydraulics and Geotechnics;

The evaluation of critical rainfalls (hazard) for triggering landslides by empirical correlations (black box) need to be developed along historical data, but they have a local validity and cannot be generalised to different environments;

Empirical correlations between critical rainfall, piezometric levels rising up, slope movement and landslides are more reliable because they follow more closely the physical phenomena but need an accurate slope monitoring;

Only a few deaths were caused by debris flow in the Racinazzi stream (Scaletta Zanclea) along national motorway near to the sea, while the majority of deaths were caused by landslides hitting house, build very close to slope become unstable because of very heavy rainfall;

The evaluation of slope vulnerability need accurate analytical, physical and numerical analysis; at the same time the stabilization design for the mitigation of slope vulnerability need accurate site investigations and an appropriate geotechnical modelling;

The stabilization work must mitigate the slope vulnerability on the base of the appropriate stability analysis to quantify the performance achieved; very often, stabilization work made without any type of calculation are ineffective;

As the damaged the area is prone to seismic hazard (see Messina and Reggio Calabria 1908 Earthquake) the work done is only a part of the total work to be done. A multi-risk analysis including landslide hazard due to heavy rainfall and landslide hazard due to seismic action is required.

## References

- Aronica GT (2009) Gli eventi del 1 ottobre 2009 – Analisi idrologica. Workshop, Messina, 4 Dec
- Asian Technical Committee on Geotechnology for Natural Hazard (1997) Manual for zonation on areas susceptible to rain-induced slope failure. Japanese Geotechnical Society
- Deangeli C (1987) Metodologie di studio delle colate rapide: modelli fisici, matematici e numerici. Phd thesis, Politecnico di Torino, Italy
- GEO (1991–1996) GEO report series on Hong Kong rainfall and landslides, produced annually for the years 1984 to 1995. Geotechnical Engineering Office, Hong Kong
- Premchitt J, Brand EW, Chen PYM (1994) Rain-induced landslides in Hong Kong, 1972–1992. *Asia Engineer, the Journal of the Hong Kong Institution of Engineers* 22(6):43–51
- Seki N, Hori S, Narita M (1980) Forecasting of slope failures in Rock Mass in the Yanadani Area. *Oyo Technical Report*, No. 2
- Takahashi T (1978) Mechanical characteristics of debris flow. *J Hydraul Div, ASCE* 104: 1153–1169

# Chapter 11

## Geo-Hazards

### Performance of Highway Bridges Under Extreme Natural Hazards: A Case Study of Bridge Damages During 2009 Typhoon Morakot

Wei F. Lee, Kenji Ishihara, and C.H. Chen

**Abstract** On August 8th, 2009, Typhoon Morakot invaded Taiwan and had caused serious damages to south of the island. A major portion of highway bridges located in the affected region were suffered from various natural hazards, such as slope failures, debris flows, floods, and scours. Despite the depressing fatalities and infrastructure damages, Typhoon Morakot did offer a great opportunity to observe behaviors of bridge foundations under different types of hazards. The presented study is in an effort to characterize the performance of bridge foundations under extreme natural hazards so as to investigate possible causes of the failures. In this chapter, basic information and analysis of Morakot are introduced first. Secondly, typical types of bridge failures are summarized and genuine causes of failures are discussed as well. Last, research progress of an intelligent safety monitoring system for bridge foundation is illustrated to further characterize performance of bridge foundation under scouring and flooding conditions. The proposed system is developed in an effort to access the vibration and deformation characteristics of bridge structures under various natural hazards. The system is concluded to be capable of providing valuable information of bridge stability during critical events; as well as to have better durability, functionality and efficiency than the conventional scour monitoring systems.

#### 11.1 Introduction

In the past decade, Taiwan had suffered several severe extreme natural hazards, including 1999 Chi–Chi earthquake, 2001 Typhoon Toraji, 2004 Mindulle Typhoon, and most recent Typhoon Morakot. Among all infrastructures, bridges have found to be the most important yet also most vulnerable during these natural hazards

---

W.F. Lee (✉)

Facilities and Assets Management Center for Infrastructures, National Taiwan University of Science and Technology, Taipei, Taiwan  
e-mail: weilee@mail.ntust.edu.tw



**Fig. 11.1** A bridge was damaged by fault rupture during Chi-Chi earthquake (provided by Professor Chen, Cheng-Hsin)



**Fig. 11.2** A bridge was damaged by progressive scour during 2009 Typhoon Sinlock

(Figs. 11.1 and 11.2). On August 8th, 2009, Typhoon Morakot invaded Taiwan and had caused serious damages to south of the island. It had brought record high precipitation in both accumulation and intensity aspects to Kao-Ping river watershed. A major portion of highway bridges located in the affected region were suffered from various natural hazards, such as slope failures, debris flows, floods, and scours. Despite the depressing fatalities and infrastructure damages, Typhoon Morakot did offer a great opportunity to observe behaviors of bridge foundations under different types of hazards.

In order to characterize the failures of highway bridges, the authors had collected 52 cases of highway bridge failures located in Kao-Ping River watershed. Performance of bridge foundations under different hazards, including landslides, debris flows, floods, and scours, is carefully investigated and analyzed. Genuine

causes of such bridge failures are also discussed in details. In addition to the study on bridge failures, research progress of an intelligent safety monitoring system for bridge foundation is also illustrated in this chapter to further characterize performance of bridge foundation under scouring and flooding conditions. Instrumentation contents of the developed system include accelerometers, inclinometers, water level sensors, and flow velocity sensors. The proposed system is developed in an effort to access the vibration and deformation characteristics of bridge structures under various natural hazards. During Typhoon Morakot, the developed system was operated as a demonstration project on a 2.7 km long highway bridge, Shi-Tzou Bridge. Instrumentation data obtained during the event had proved that to be capable of providing valuable information of bridge stability; as well as to have better durability, functionality and efficiency than the conventional scour monitoring systems. Progress of this study is hoped to be helpful for future hazard mitigation and design of bridge foundation. Moreover, future researches for performance analysis of bridge foundations under extreme natural hazards, and risk analysis for multi-hazards are also brought up for instructive discussion.

## 11.2 Typhoon Morakot

Typhoon Morakot was formed in south pacific and turned into mid-size typhoon while approaching Taiwan. Figure 11.3 shows the path of Morakot. As shown in the figure, Morakot strolled through northern Taiwan during the period from August 7th to 9th of 2009. Although center of Morakot went by northern Taiwan, enormous precipitation was brought into south-western Taiwan because of Morakot's counter-clockwise stream and turbulent clouds. Figure 11.4 presents the radar and

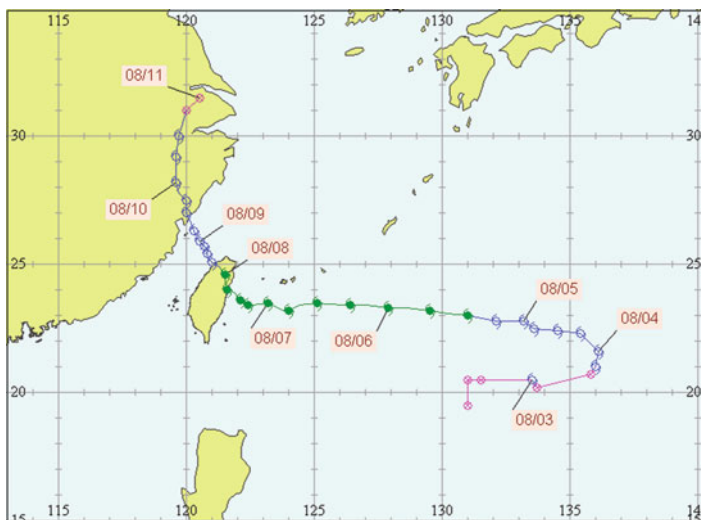


Fig. 11.3 Path of Typhoon Morakot (Central Weather Bureau, Taiwan, 2010)

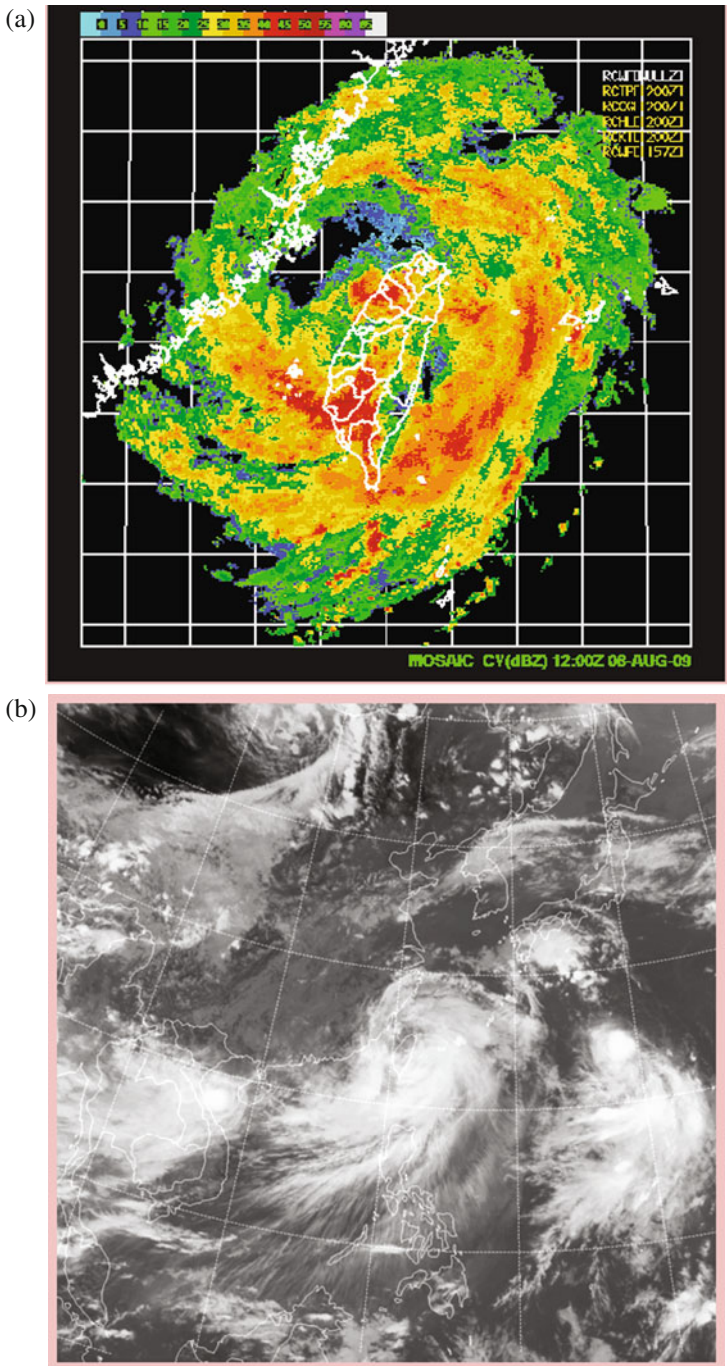
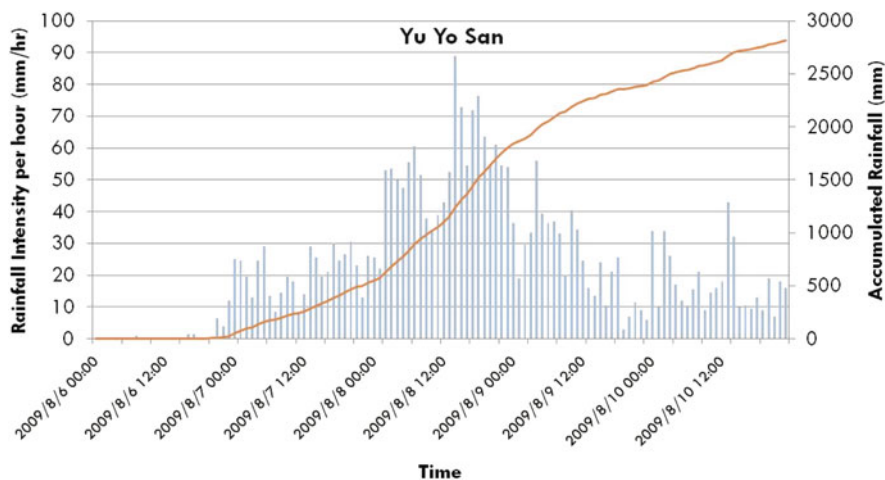


Fig. 11.4 Radar and satellite images of Typhoon Morakot (Central Weather Bureau, Taiwan, 2010)



**Fig. 11.5** Typical rainfall data recorded during Typhoon Morakot

satellite images of Morakot on August 7th of 2009. The strong stream and rain clouds were clearly seen on top of the southwest of the island where most damages were observed. As shown in Fig. 11.4a, the red part indicates the heaviest precipitation area, and it agrees well with the entire Ko-Ping River catchment region.

Figure 11.5 shows the recorded precipitation data of Yu-Yo San rain gage station during Typhoon Morakot. It locates in the Ko-Ping River catchment. As indicated in the data, on August 8th, rainfall intensities were larger than 50 mm/h for more than 18 hours. The accumulated rainfall from August 6th to 9th reached above 2,600 mm. Figures 11.6 and 11.7 present the statistical contours of accumulated rainfall and maximum rainfall intensity during Morakot's invasion. Accumulated rainfall exceeded 2,500 mm over a larger area in southern Taiwan; while the maximum rainfall intensity went beyond 70 mm/h and reached 100 mm/h for the most affected area down south. The observed enormous rainfall and rigorous rainfall intensity over southwestern Taiwan were believed to be the major factors resulted in the sever fatalities and infrastructure damages.

## 11.3 Damages of Highway Bridges During Typhoon Morakot

### 11.3.1 Investigation and Data Collection

In an effort to study the performance of highway bridges under such an extreme hazard event, the authors had collected damage data and environmental information of total 52 highway bridges those failed during Typhoon Morakot. Figure 11.8 shows locations of the investigated bridge sites. Major portion of the damaged highway bridges situated along Nan-Ji-Sian River and Lao-Non River, two major branches

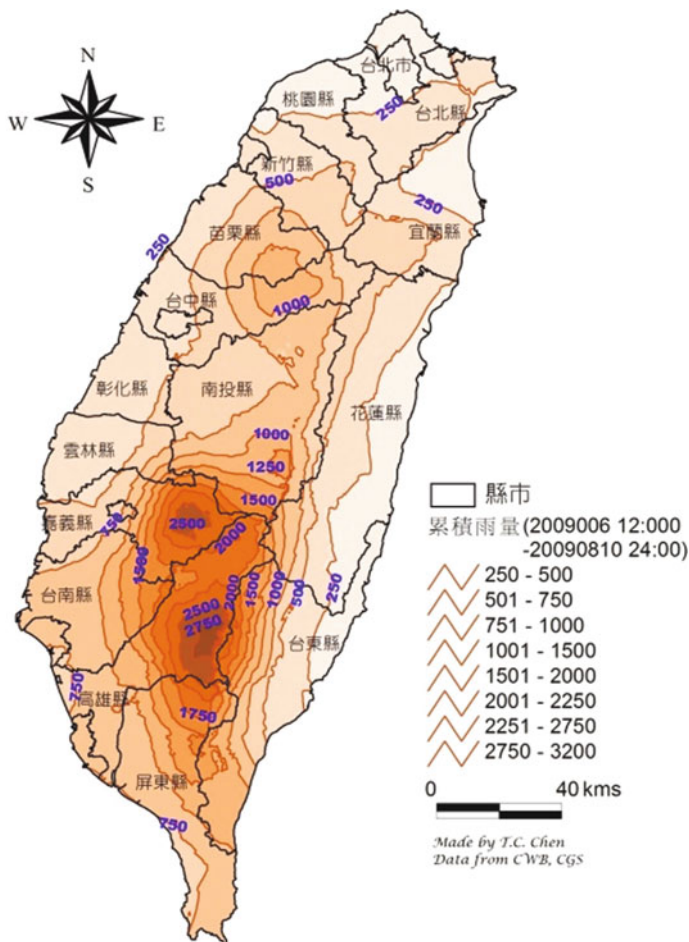


Fig. 11.6 Accumulated precipitation of Typhoon Morakot (courtesy by Professor T.C. Chen)

of Ko-Ping River. Both Nan-Ji-Sian River and Lao-Non River went from southern ridge the highest mountain, Jade Mountain in Taiwan. This area did suffer from Chi-Chi earthquake by serious ground shaking, yet no major typhoon event had ever attacked it directly before Typhoon Morakot.

Valuable data was collected through various efforts and so as to possible investigate the failure causes. First of all, fundamental data such as bridge data include as-built structural information, drawings, maintenance records and retrofit records were collected. Periodical photos, especially before and after hazard images, which is very helpful for identify failure causes were also gathered. Secondary, digitalized information, such as bridge locations, roadway maps, and maintenance unit locations, was reproduced in a unified geological information system (GIS) template. Moreover, digitalized environmental and geological information are very important

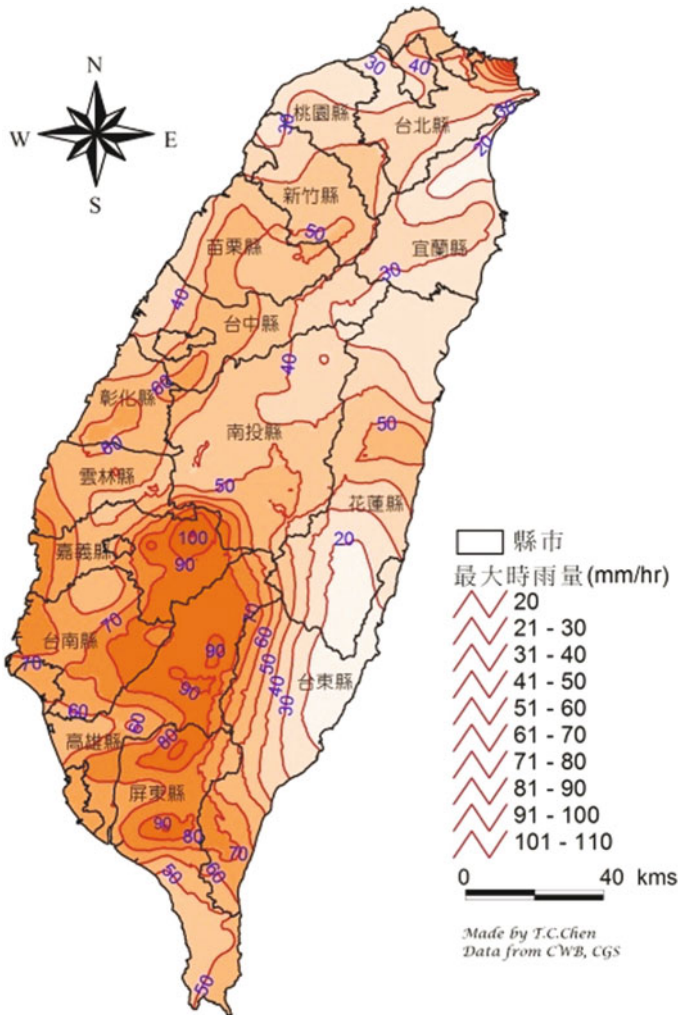


Fig. 11.7 Maximum rainfall intensity of Typhoon Morakot (courtesy by Professor T.C. Chen)

for evaluating risk potential. Basic information includes elevation contour maps, river system maps, catchment zoning data, and geological structure maps. Picture GIS information, such as satellite imaged and aerial photos, is mostly essential. Figure 11.9 shows the before and after photo images of one of the studied bridge. Clearly from the photos, the bridge experienced both debris flows and landslides during the typhoon. Debris flows had caused the under scouring to the bridge foundation and resulted in strong lateral forces breaking the piers into pieces. Landslides occurred on both sides of the valley crashed the approach ways and abutments of the bridge. To further study the failure causes, the digitalized information collected



**Fig. 11.8** Locations of the damaged highway bridges during Typhoon Morakot in 2009

could be easily mapped or analyzed spatially by taking the advantages of powerful GIS functions. Figure 11.10 shows the typical mapping results of elevation contour, river maps, and roadway information. Environmental information such as slope, flow inlets, size of watershed, as well as interaction between bridge alignment and stream ways of the studied bridge could be easily summarized via this mapping analysis. Figure 11.11 gives an example of the before event aerial image comparing to the post event one of the same area as shown in Fig. 11.10. By comparing



**Fig. 11.9** Before and after photo images of a bridge destroyed by Typhoon Morakot

the images, slope failures located within the studied watershed area could be easily identified. This information would be very useful for estimating possible amount of debris that could flow out. The aerial images mapping with contours could also be very helpful for observing the environment changes of rivers and valleys.

### ***11.3.2 Failures of Highway Bridges During Typhoon Morakot***

Data described above of all 52 highway bridges those seriously injured during Morakot is collected and analyzed (Lee et al., 2009), additional score table analyses on scour, debris flow, and landslide risk potentials were conducted using composed

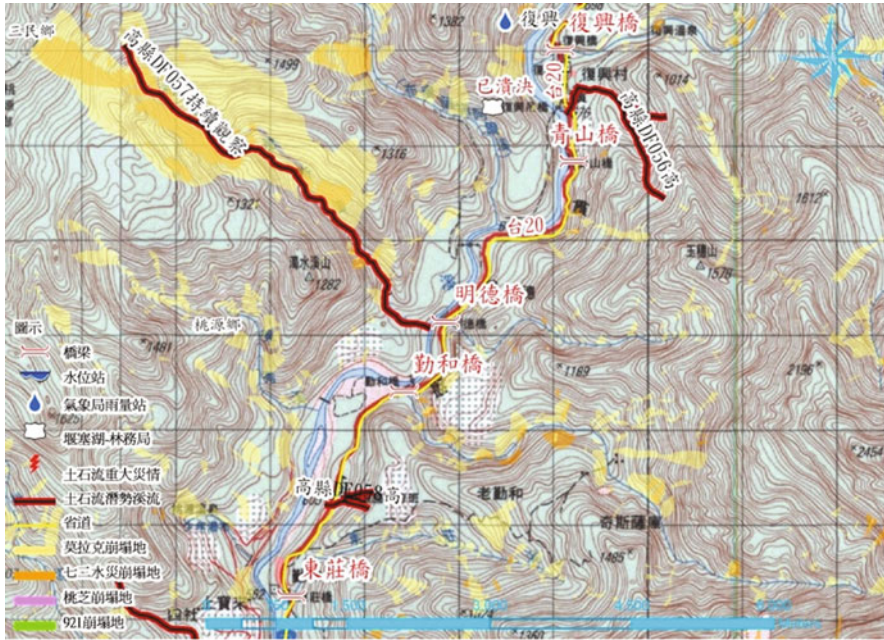


Fig. 11.10 Typical mapping result of elevation contour, river maps, and roadway information

data and Morakot’s weather information such as rainfall intensity and accumulated precipitation. Results of the proposed data mining and risk potential analyses provide us conclusive access to failure types and causes of the highway bridges. In conclusion, failure types and related causes are as follow:

- Type I: Slope Failures

Bridge structures such as abutments, foundations, and even approach ways were hit by enormous soil mass produced by nearby landslides (Fig. 11.12).

- Type II: Debris Flows

Bridges located at the outlets of the watersheds where serious debris flows occurred. Debris either piled up the channels or directly hit the bridges (Fig. 11.13).

- Type III: Over Scale Floods

The over-scale floods that caused by the record high heavy rainfall overflow the bridges and pushed the superstructures and substructures of bridges (Fig. 11.14).

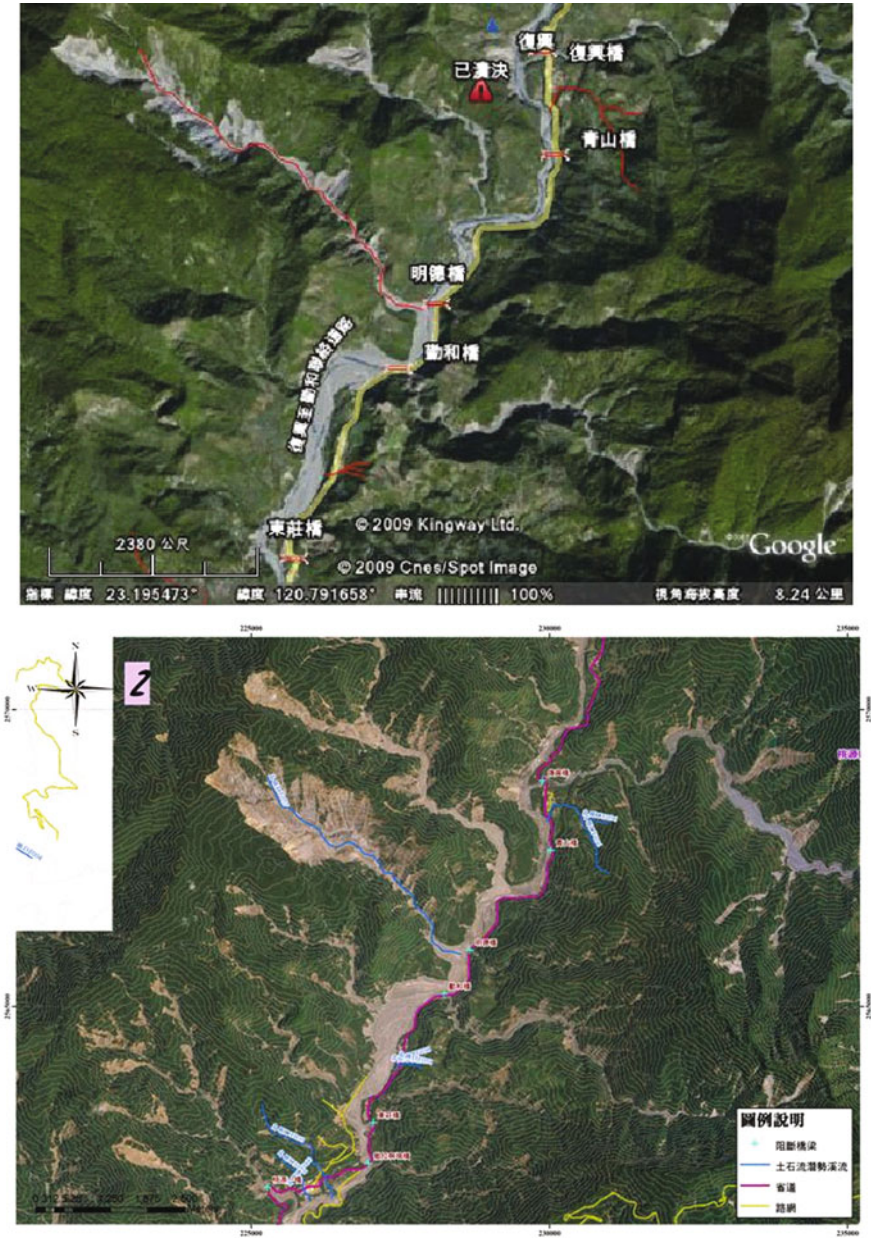


Fig. 11.11 Example of the before event image comparing to the post event image



**Fig. 11.12** A bridge was damaged by slope failure during Typhoon Morakot



**Fig. 11.13** A bridge was failed by debris flow during Typhoon Morakot

- Type IV: Improper Bridge Locations

Bridges located at the curved sides of the river channels. Large volume floods damaged the bridge foundations or related structures such as embankments or abutments. This type of failure could also be the results of sudden flow line changes or immense surges caused by debris or landslides mass blocking the river channels (Fig. 11.15).



**Fig. 11.14** A bridge was failed by over-scale flood during Typhoon Morakot



**Fig. 11.15** A bridge embankment and abutment were eroded away during Typhoon Morakot

- Type V: Flood Erosion

Large volume flood eroded the embankments, abutments, and approaches. Retaining structures failed by topping sliding, or backfill loss (Fig. 11.16).

- Type VI: Scour

Serious scours accompanied by floods damaged the bridge foundations (Fig. 11.17).



**Fig. 11.16** A bridge was failed by deep erosion of river flood during Typhoon Morakot



**Fig. 11.17** A bridge was failed by scour during Typhoon Morakot

### ***11.3.3 Lessons Learned and Mitigation Strategies Planned***

In reality, most damaged bridges had suffered the combination effects of at least two failure types. For upstream areas, most bridges were destroyed by debris and landslides. Locations of these affected bridges were at outlets of watershed areas or inlets of branches to main streams. For downstream areas, bridges were damaged by over-sized floods. It was a combination of heavy rainfall and massive debris pile up in the river channels. Observation and analysis throughout the damaged bridges also found that some important issues were overlooked in the past in risk analysis, failure scenarios of bridges, and design of bridges. Repeat of failures was

found for bridges failed by landslides or debris flows. Historical data of damages should be carefully evaluated when risk analyses of bridges were performed. In addition, analyzed area should be further extended from bridge location to upstream watersheds. Special attentions should be paid to bridge designs for alignment, span, clearance, erosion resistant of abutment, and adjacent slope stability. Failure scenarios of bridges such as debris collisions, oversized flow pressures caused by high flow density or immense floods should be taken into account in addition to regular bridge designs. As a consequence of Morakot's damage, highway engineers are facing challenges includes lack of experiences in mitigating vulnerable environment and risk analysis of multi-hazard potentials under such an extreme event. Mitigation strategies were organized in both short term and long term scales. For short term strategy, safety of the residents has become the first priority, especially for 2010 rainy season. Action plans for safety evacuating and precautions warning were over conservatively designed. Mostly, temporary structures were adapted to provide minimum functions of local transportation and emergency evacuation. For long term strategy, the coordinated work frame that includes regulation of river systems, planning of highway networks, and allocation of residential communities are underway. In addition to Morakot affected area, infrastructures in operations are subjected to intensive inspections and safety evaluations. Reinforcing and strengthening works on highway bridges located in high risk potential areas are carried out in an urgent manner. Moreover, safety monitoring and warning systems were equipped onto important bridges or those in danger.

## **11.4 Health Monitoring System for Bridges Under Scouring**

In addition to investigate failures of highway bridges under extreme weather condition such as Typhoon Morakot, the authors also conducted research on developing an intelligent safety monitoring system for bridge foundations under scouring and flooding conditions. Although scour has been recognized as the most critical cause for highway bridge failures in Taiwan, yet present monitoring systems for scour still remain in observing environmental factors such as water level and scour depth. Disadvantages of such instrumentations include less information of bridge structural stability as well as high vulnerability of instrumentation components under extreme flooding water or debris flows. Technologies for monitoring stability of bridges structures equipped with better durability are still under development until this study.

### ***11.4.1 Design of Intelligent Safety Monitoring System***

Purposes of the proposed intelligent safety monitoring system are to improve durability of the instrumentations, serviceability of the system, and monitoring coverage of bridge behaviors. The proposed system is a combination of accelerometers, inclinometers, flow velocity and water level sensors. Different from present

monitoring systems, the developed system could be applied to various hazards including scours, floods, debris flows, and even earthquake. The developed system aims to access the vibration and deformation characteristics of bridge structures. Features of frequency response spectrum, including dominant frequencies and amplitudes, are adapted as the performance indexes describing boundary conditions of the bridge structures as well as scales of external forces acting on bridges. Moreover, inclinations detected by dynamic inclinometers could be used to describe the deformation characteristics of the bridges. Advantages of the developed system include:

1. Because the system was designed to measure the vibration characteristics of the bridge, best location for installation is on top of the pier rather than adjacent to bridge foundations. The design system could be away from water and debris damages.
2. By measuring the vibration and deformation responses of the bridge, boundary condition such as scouring depth and scale of external forces could be analyzed directly. Moreover, the designed monitoring system is equipped with external sensors to monitor the water level and flow velocity as verification to the system.
3. The developed system is suggested to combine with structural modeling to further calibrate the measurements so as to conduct long term performance data mining of bridges.

Figure 11.18 depicts schematic drawing of the design of proposed system. As shown in the figure, the major instrumentation components including 3 accelerometers, 2

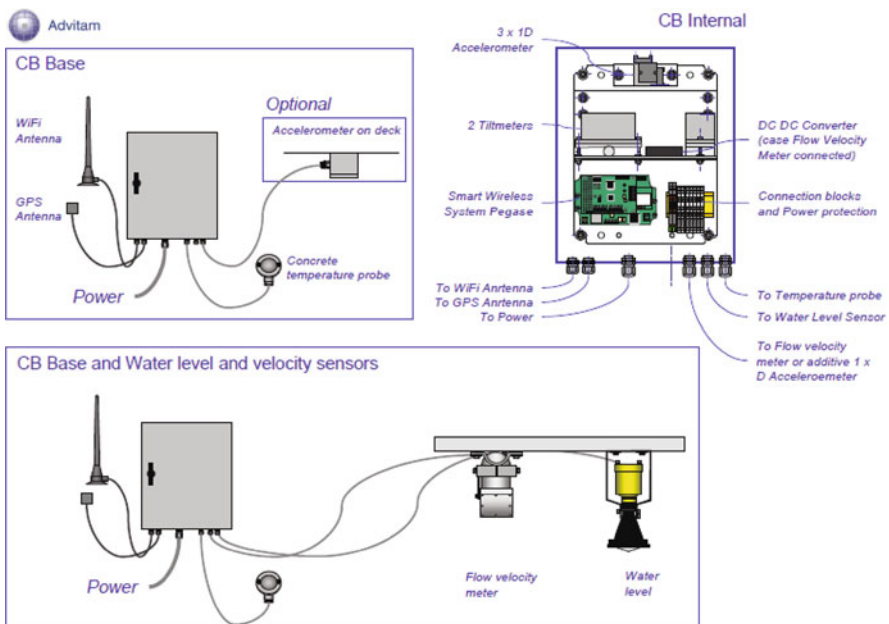
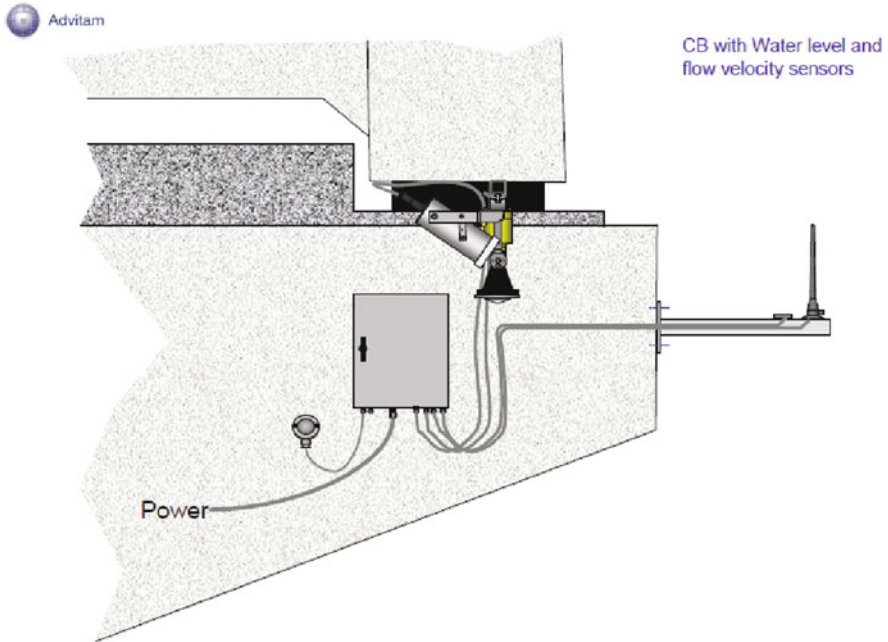


Fig. 11.18 Schematic drawing of the designed monitoring system (Lee et al., 2010)



**Fig. 11.19** Schematic drawing of the installation layout of the designed system (Lee et al., 2010)

inclinometers, a data logger, and transmitting devices are packed into a CB base box. The CB base could be installed onto the pier top as shown in Fig. 11.19. External components such as the temperature probe, the flow velocity meter, and the water level sensor would be installed outside the box and wired into the CB base as shown in Fig. 11.18. Also shown in Fig. 11.19, the optimized location for flow velocity meter and water level sensor is under the bridge deck.

#### ***11.4.2 Shi-Tzou Bridge Project***

As a demonstration research project, the proposed system was installed onto one of the major bridge, Shi-Tzou Bridge, crossing the largest river in Taiwan, Jou Suei River. Figure 11.20 depicts the location of Shi-Tzou Bridge and neighboring stream environment. Shi-Tzou Bridge is a 2.7 km long PC girder bridge with regular span length of 35 m. Foundations of Shi-Tzou Bridge were constructed by 28 m long pre-cast piles in group. They had suffered serious scour problem in the past (Fig. 11.21). Safety monitoring for progressive scouring has become priority issue.

The described research project was started with several vibration tests to obtain fundamental vibration characteristics, as well as to verify feasibility of the proposed method. The vibration tests were conducted in May, 2009. Figure 11.22

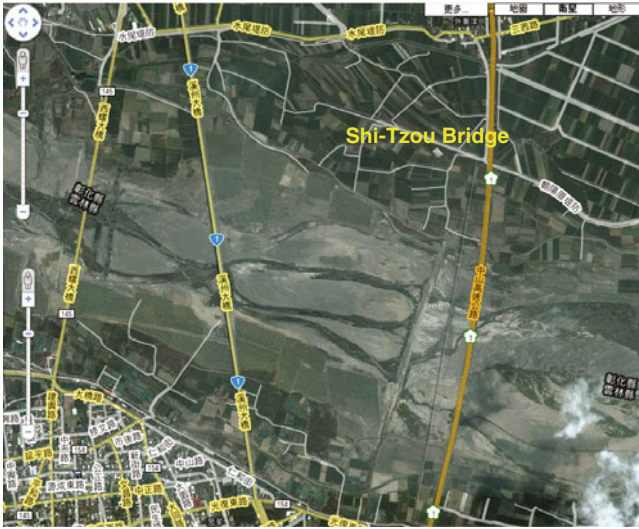


Fig. 11.20 Location and adjacent stream environment of Shi-Tzou Bridge



Fig. 11.21 Scour problems of Shi-Tzou Bridge

shows the result of vibration tests on piers experiencing different levels of scouring. As depicted in the figure, piers with less scour posse higher feature frequencies. Pier 36 which had server scour problem showed the lowest feature frequency. Correlation between pier lengths, i.e. scour depths, and feature frequencies were clearly identified in the figure.

After the vibration tests, the designed system was materialized and installed on to two piers, Pier 36 and Pier 42, for monitoring in June 2009 (Fig. 11.23). Pier

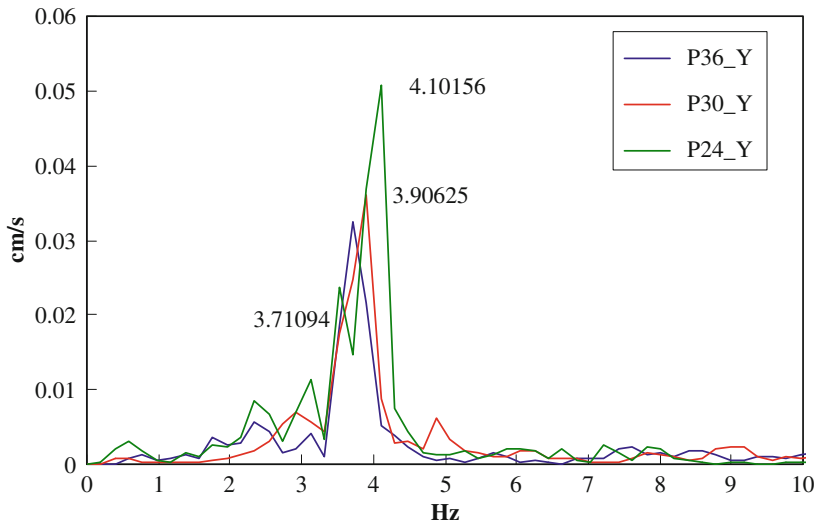


Fig. 11.22 Measured feature frequencies of Pier 24, Pier 30, and Pier 36 (vibration tests)



Fig. 11.23 Monitoring locations of Shi-Tzou bridge

36 was the pier suffered serious scouring problem. Pier 42 was the pier that situated in the main stream channel of the river, and it was retrofitted to have deeper and increasing numbers of pile foundation. Both piers were equipped with CB box and the water level sensor was installed on the deck connecting Pier 42 and Pier 43 (Fig. 11.24). During Typhoon Morakot, although Shi-Tzou Bridge was not located in the mostly affected area, it still experienced fairly high water levels and flow velocities (Fig. 11.25) and resulted in traffic closing on August 8th and 9th. Valuable bridge performance data was obtained by the system. Figure 11.26 shows the measured feature frequencies and water level according to time scale for both Piers 36 and 42. As depicted in the figure, the feature frequency had clearly dropped to lower frequency range when water level was high; and it recovered to high frequency range when water level went back down. Moreover, it was also observed in Fig. 11.26 that



**Fig. 11.24** Completed installation of the CB box, power supply system, and the water level sensor



**Fig. 11.25** Flood condition of Shi-Tzou bridge during Typhoon Morakot

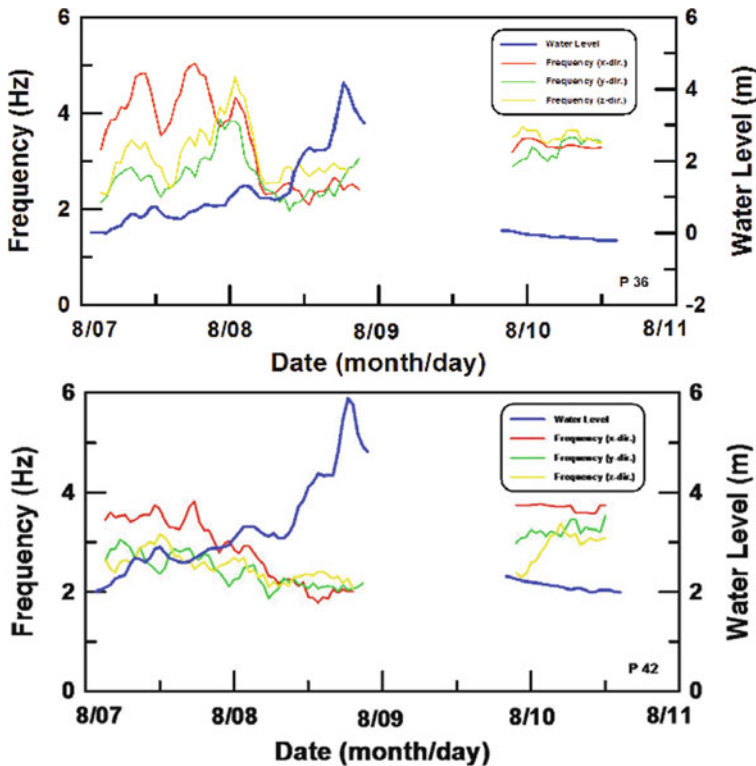


Fig. 11.26 Measured feature frequencies versus water levels

the feature frequency started to descend before clear water level rise was observed. This observation shows that scour of the monitored bridge foundations might have occurred before water level started to rise. Monitoring structure behavior appears to be more accurate and effective than monitoring the water level. Figure 11.27 shows measured amplitudes versus water levels according to time scale. The trend that scales of measured amplitudes increased with rise of water levels is clearly observed in the figure. When water level went down, measured amplitudes decreased as well. The observed correlation between measured water levels and vibration amplitudes verifies the feasibility of monitoring structural behavior and external loading conditions via the proposed system.

### 11.4.3 Summary

Comparing to traditional scour monitoring systems those only screen water level, or scouring depth, the proposed system could reveal structure performance and external loading condition directly. Moreover, for flow condition shown in Fig. 11.25,

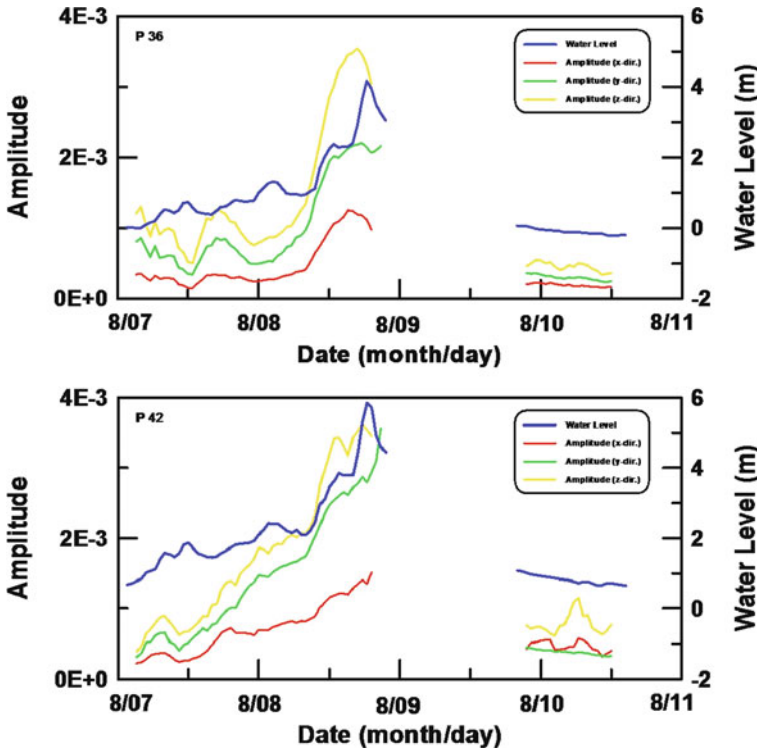


Fig. 11.27 Measured amplitudes versus water levels

traditional scouring depth monitoring systems could have high risk of damage. The developed system was able to record frequency, amplitude, rotation, and water level features of the Shi-Tzou bridge. Instrumentation data obtained during Typhoon Morakot had proved that the proposed monitoring system is capable of providing valuable information of bridge stability as well as better serviceability during critical flow conditions such as Typhoon Morakot.

### 11.5 Conclusions

The record high rainfall volume and intensity induced by Typhoon Morakot are concluded as the major cause to the serious damages of bridges. Effects of such an extreme natural hazard had raised people’s attention to recent global climate change. In addition to infrastructure stabilities, more attentions and considerations should be paid to improve present civilian warning systems, safety evacuation plans, and emergency rescue schemes. Moreover, engineers should build up better knowledge to access vulnerability of infrastructures under extreme natural hazards, to analyze multi-hazard risk, and to archive historical damage data. Immediate

research needs appear on systematic safety monitoring and warning systems, effective mitigation measures, risk analysis of oversize events, and efficient pre-warning systems. However, the indicated researches engage multi-discipline works of different aspects of civil engineering. Joint task forces must be structured in order to construct a safety response network. Documentation of damage and performance data of structures is essential to the proposed researches.

## References

- Lee WF, Chen CH, Yen CI (2010) High-Tech Scour Monitoring System for Highway Bridges- Si Bin Bridge Project midterm report, Highway Directorate General, Taiwan (in Chinese)
- Lee WF, Yen CI, Wang CW (2009) Causes of failures of 52 bridges, Report to Directorate General of Highways (in Chinese)

# Chapter 12

## Exploring Non-gravity Geotechnics

### Triaxial Compression Tests in Zero-Gravity Environment

Ikuo Towhata, Thi Lan Anh Trinh, and Suguru Yamada

**Abstract** The recent demand for performance-based seismic design of geotechnical structures requires knowledge about residual deformation of soils subjected to cyclic loading. This chapter concerns deformation characteristics of liquefied sand that may deform to a strain of 100% or more during and after strong ground shaking. To evaluate the liquefaction-induced ground deformation thus produced, it is essential to understand and validate the deformation characteristics of sand under very low effective stress. In this respect, a new type of triaxial shear test has been developed in which the effective stress is made extremely low by making the gravity effects very small. In other words, triaxial shear tests were conducted in a freefall capsule to achieve a state of null effective stress. It was shown that sand deforms in a viscous manner under constant load when effective stress has disappeared. The obtained coefficient of viscosity was then made use of to run deformation analyses on a geotechnical structures resting on liquefied sand.

#### 12.1 Introduction

Prediction of seismic performance of structures has been a chief issue in the recent years from the viewpoint of performance-based design. This design principle pays attention to the cost-performance issues and it is important therein to judge whether or not the induced seismic damage is acceptable. Since the resiliency of geotechnical structures depends highly on the residual deformation that remains after an earthquake, there is a strong need to develop a practical method for prediction of residual deformation. This is particularly the case in such structures as are subjected to subsoil liquefaction but whose minor deformation is acceptable. Some kinds of embankment and river levees may be examples of this kind (Fig. 12.1).

---

I. Towhata (✉)  
Department of Civil Engineering, University of Tokyo, Tokyo 113-8656, Japan  
e-mail: towhata@geot.t.u-tokyo.ac.jp



**Fig. 12.1** Liquefaction-induced subsidence of Yodo River Levee in Osaka after 1995 Kobe earthquake (Photo by Fudo Construction Company)

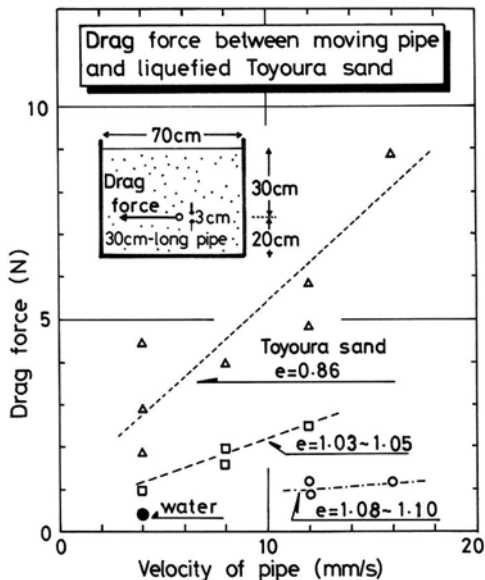
Liquefaction studies in 1960s and 1970s used to be focused on the mechanism of liquefaction, risk evaluation, and prevention. Thus, it was aimed to avoid the onset of liquefaction for the safety and reliability of structures. A new perspective was added in 1980s when seismic reliability of lifeline structures became an important issue. Since lifelines are extremely long and have to be installed on liquefaction-vulnerable soil conditions, without sufficient funding to install liquefaction-prevention measures, it has been supposed that consequence of subsoil liquefaction should be assessed in a practical manner and that a judgment should be made whether or not the estimated deformation is acceptable. A river levee is a kind of such lifeline structures together with embedded pipelines.

With these issues in mind, the present paper addresses the mechanical nature of liquefied sand and proposes a methodology by which liquefaction-induced ground deformation is assessed in a practical manner.

## 12.2 Discussion on Viscous Model of Liquefied Sand

The author carried out model tests on lateral pulling of a pipe in liquefied ground (Towhata et al., 1999a). Since the drag force needed for pulling a pipe increased with the velocity (Fig. 12.2), a viscous model of liquefied sand was proposed. However, there are discussions against this idea (Dungca et al., 2006; Dobry, 2007), saying that there is a pore water pressure difference between the front and the back sides of a pipe, the pressure difference increases as the velocity increases, and consequently the drag force, which is equal to the pore pressure difference, increases with the velocity. Thus, they claim that the rate dependent drag force does not come from the real nature of liquefied sand but is merely a product of seepage and pore pressure equalization.

**Fig. 12.2** Rate dependent variation of drag force needed for lateral pulling of pipe in liquefied ground



The authors first point out the problems in those opinions and are then going to present more recent test data. The problems can be written down as what follows:

1. Pore pressure discussions look realistic but actually do not say anything about quantitative issues.
2. The drag force is a product of total stress difference between the front and the back sides of an embedded pipe. Those discussions concern only with pore pressure and overlook the effective stress that is another important component of total stress.

The rate dependency of drag force is examined by referring to a large shaking table test in which a pile foundation was subjected to lateral flow of liquefied sand (Motamed et al., 2009). Figure 12.3 shows the soil container of 15 m in length in which a sheet-pile quay wall and liquefiable backfill ground were constructed together with a pile foundation. The diameter of the piles was 150 mm. Since this size of model is close to the prototype, the law of similitude is not a problem. After onset of liquefaction, the quay wall tilted and the backfill sand translated laterally, exerting lateral load on piles. Figure 12.4 illustrates the time histories of velocity (relative velocity between lateral soil flow and pile displacement) and lateral load exerted on one of the piles. There is clearly a good correlation between the load and the velocity, supporting the viscous idea. Figure 12.5 compares pore water pressures. Their difference is very small and, as Fig. 12.6 indicates, is much smaller than the lateral load (the earth pressure difference) exerted by the flow of liquefied ground. Thus, the viscous model of liquefied sand is not affected by the pore pressure difference.

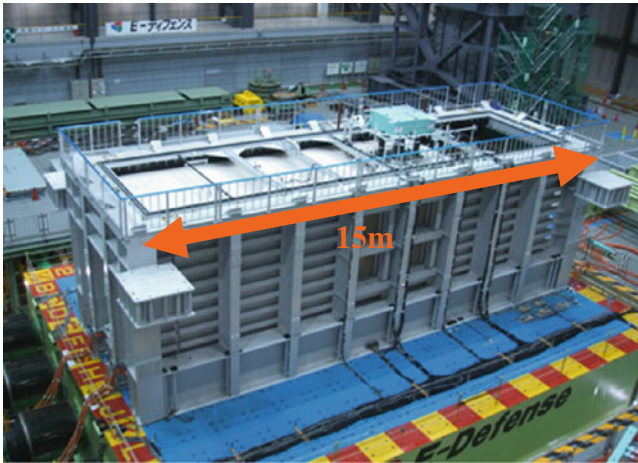


**Fig. 12.3** E-Defense large shaking model test on lateral flow of liquefied sand induced by failure of sheet-pile quay wall (Motamed et al., 2009)

**Fig. 12.4** Variation of lateral pressure on pile model and flow velocity of surrounding liquefied sand (E-Defense test; after Motamed et al., 2009)

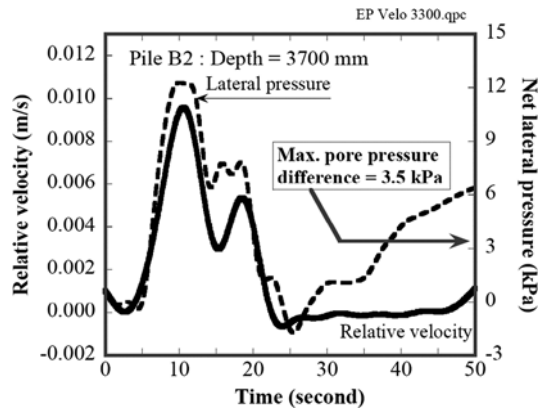


**Fig. 12.5** Time histories of excess pore water pressure in front of and behind a pile subjected to lateral flow of liquefied sand (E-Defense test; Motamed et al., 2009)

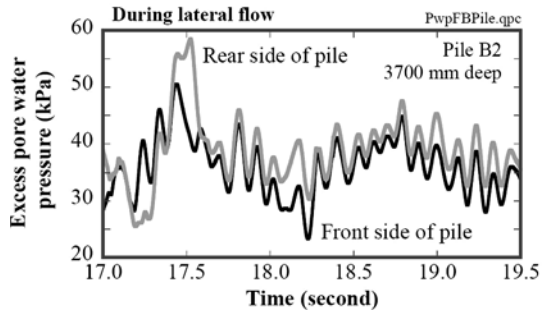
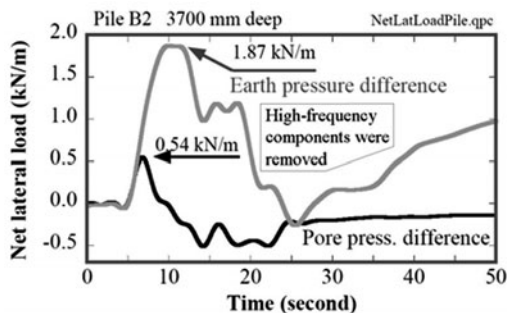


**Fig. 12.6** Comparison of net pore pressure difference and induced lateral load in pile subjected to lateral flow of liquefied subsoil (E-Defense test; after Motamed et al., 2009)



### 12.3 Problems in Experimental Study on Nature of Liquefied Sand

Interpretation of model test results is not the best method for accurate and quantitative determination of the stress–strain characteristics of liquefied sand because of the following reasons:

1. States of stress and strain are not uniform in a model ground. Therefore, it is not easy to determine the stress–strain relationships from model tests.
2. Although a fluid-dynamic theory was employed in interpretation of former model tests in Fig. 12.2, that theory is not fully reliable when the material property is neither linear nor uniform.
3. The nonlinearity and heterogeneity of material property are substantial in soil under low effective stress and heterogeneous stress–strain state.

Accordingly, it is preferred to run laboratory shear tests as an alternative method. However, tests on liquefied sand have encountered following problems.

1. A specimen of liquefied sand with null effective stress cannot maintain its shape due to its own weight.
2. Weight of sand grains increases the effective stress in the lower part of a specimen. This heterogeneous stress state becomes significant in a liquefied sand specimen in which the externally applied effective stress is negligible.
3. The heterogeneous state of effective stress within a specimen affects the stress–strain relationship and the interpretation of test results is made difficult.

After many attempts, it was finally decided to run triaxial shear tests in a micro-gravity environment in which the effect of the weight of sand grains becomes negligible.



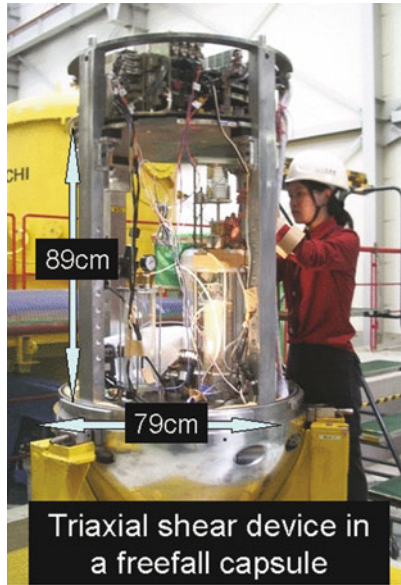


Fig. 12.8 Triaxial device in a freefall capsule

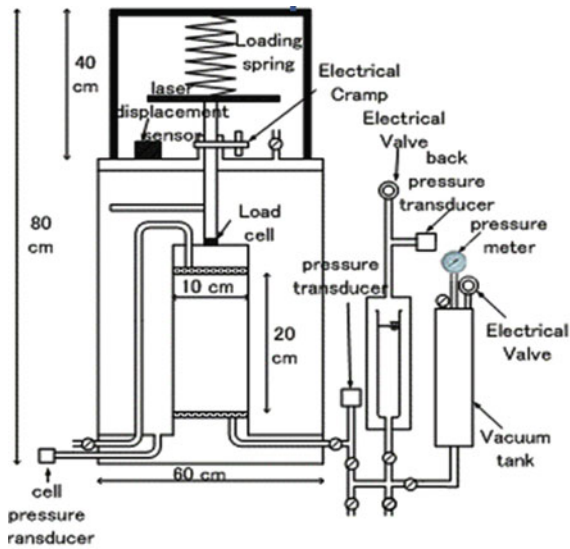


Fig. 12.9 Triaxial device for freefall tests

3. Electromagnetic mechanisms are controlled from the control room so that the confining pressure is released and the axial stress is loaded during the short time of freefall.

The time sequence of testing procedure was as what follows:

1. A Toyoura-sand specimen was prepared in a sample preparation room by using the air-pluviation technique in 1-G field with the target relative density of around 50%. The sample size was 200 mm in height and 100 mm in diameter. De-aired distilled water was circulated through the sample so that Skempton's  $B$  value might be greater than 0.95. Later, however, the use of water-saturated specimens was replaced by that of dry sand, as will be discussed later.
2. The specimen was isotropically consolidated under 100 kPa by applying air confining pressure as conducted in regular procedure of triaxial tests.
3. Spring mechanism for axial stress was compressed but locked so that no effect would occur prior to freefall.
4. The confining pressure was reduced to 20 kPa that is generated by negative pore pressure. Thus, the air confining pressure as mentioned in (1) was released to null. The triaxial device was placed in a capsule and transported to the top of the vertical shaft (Fig. 12.7).
5. Immediately after the beginning of freefall through a vacuumed shaft, the negative back pressure was released to generate the state of very low effective stress. The stress history thus conducted intends to reproduce what happens in real liquefaction where sand is initially consolidated by the overburden and the effective stress level then decreases to null due to excess pore water pressure during shaking.
6. Then, the locking of the spring was released quickly and the deviator shear stress was loaded. The induced creep deformation was measured and recorded. The viscosity coefficient was obtained by dividing the shear stress,  $(\sigma_a - \sigma_r)/2$ , by shear strain rate,  $d(\varepsilon_a - \varepsilon_r)/dt$ , where  $\varepsilon_a$  stands for the axial strain and  $\varepsilon_r$  the radial strain that is approximately given by  $-\varepsilon_a/2$ .

## 12.5 Test Results

The first freefall test was not successful. Since no significant deformation occurred, the axial load was increased by replacing the loading spring. Despite this, the second test was unsuccessful either. The reason for this was that the diameter of a pipe, connecting the specimen and the air in the freefall capsule, was too small. Usually this pipe supplies pore pressure or negative pressure during sample preparation, and its small diameter does not make a problem. However, during freefall, this pipe had to quickly dissipate any negative pore pressure that was produced by dilatant behavior of loose sand under low effective stress. This requirement was not satisfied by the small diameter. Note that even loose sand dilates upon shear and produces

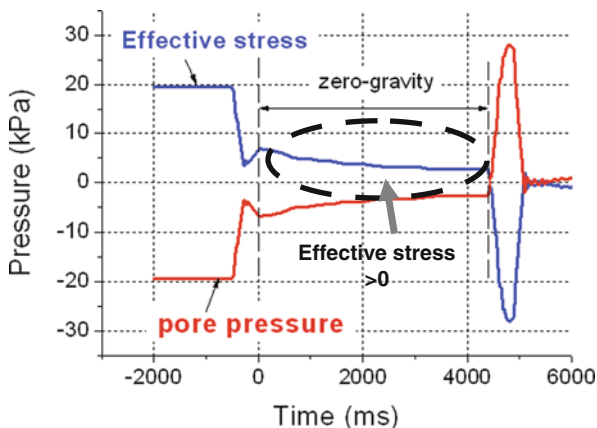


**Fig. 12.10** Change of pore pressure during unsuccessful freefall test on water-saturated specimen

positive effective stress under low confining pressure. This effective stress prevented further deformation of the sample (Fig. 12.10). Consequently, it was decided to use dry sandy specimen in place of a saturated one so that pore air can quickly migrate through the thin pipe and dissipate the unfavorable effective stress.

Two freefall tests on air-dry samples of Toyoura sand were successful, and, from the rate of deformation under constant axial load, the viscous property of sand under very low effective stress was determined. Figure 12.11 illustrates the shape of a tested specimen during creep deformation and after landing.

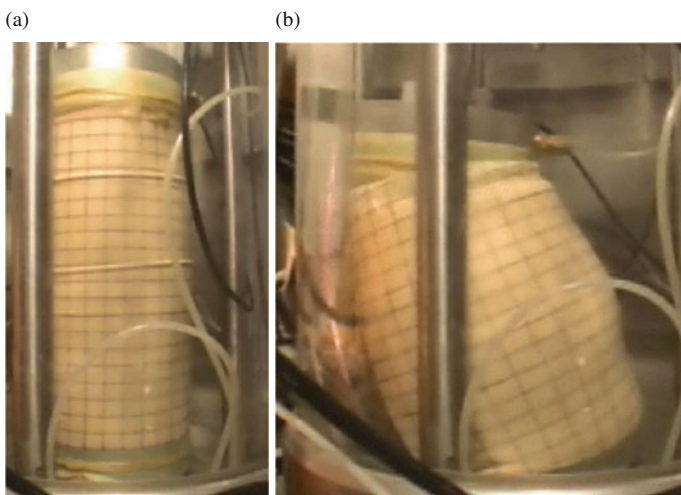


**Fig. 12.11** Appearance of specimen during and after freefall (Test 4). (a) During creep; (b) after landing and impact

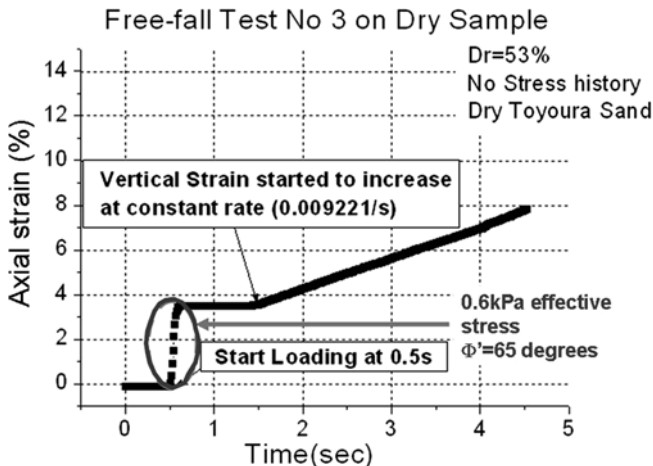


Fig. 12.12 Time history of axial strain of dry specimen during freefall test No. 3

Figure 12.12 exhibits the time history of axial strain. After the initial increment caused by loading of the specified axial load, the strain continued to increase at a constant rate under a constant level of load, suggesting creep or viscous nature of sand. Figure 12.13 demonstrates the stress-strain relationship. The stress was calculated by considering the changing area of the sample’s cross section. Thus, it decreased gradually after the peak stress. Furthermore, after assessing the radial stress by considering the stress caused by membrane tension, the effective mean principal stress,  $P' = (\sigma'_a + 2\sigma'_r)/3$ , was obtained to be 0.6 kPa in this test. If the peak stress is employed for calculation of the internal friction angle,  $\phi = 65$  degrees is obtained. This large value of friction angle may appear abnormal, but it is consistent with 70 degrees that was obtained from a zero gravity test conducted in NASA Space

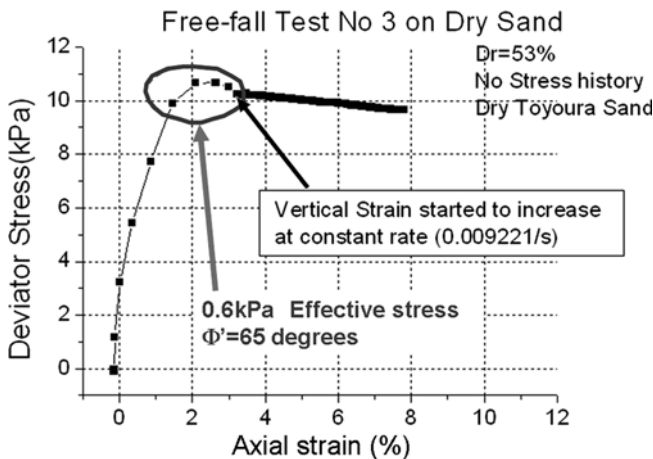


Fig. 12.13 Stress–strain behavior of dry sand during freefall test No. 3

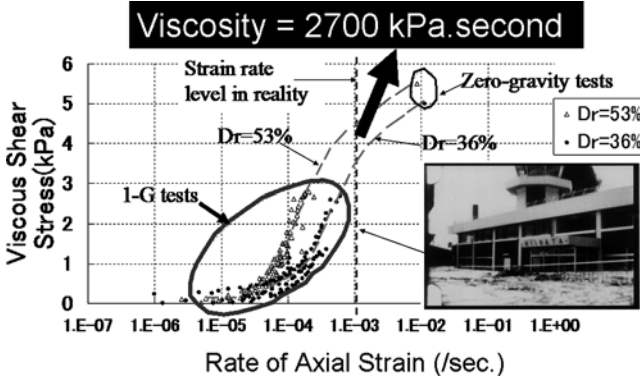


Fig. 12.14 Relationship between viscous shear stress and axial strain rate under low effective stress and normal gravity conditions

Shuttle (Sture et al., 1998). Finally, the viscosity coefficient of shear deformation of sand under low effective stress was obtained by the following formula:

$$\text{shear viscosity coefficient} = \frac{(\sigma_1 - \sigma_3)/2}{\frac{d}{dt} (\epsilon_a - \epsilon_r)} \approx \frac{(\sigma_1 - \sigma_3)/2}{\frac{d}{dt} (\epsilon_a \times 1.5)}$$

in which Poisson ratio = 0.5 is assumed and 400 kPa-s was obtained.

The number of successful freefall tests was only two and the generated rate of axial strain was 1%/s in both of them. Because the nature of sand is often nonlinear and strain-rate dependent, supplementary tests were carried out in a normal gravity environment. While the testing procedure was identical with freefall tests, the effective stress had to be maintained higher around 5 kPa for the stability of specimens.



Fig. 12.15 Boiled water around Niigata Airport (air photograph taken by Mr. Yuminamochi immediately after the quake)

Hence, the induced strain rate was much smaller. Moreover, the frictional (inviscid) component of stress was subtracted from the measured axial stress and the viscous stress component was calculated; for its detailed procedure, refer to Gallage et al. (2005).

Figure 12.14 illustrates the obtained viscous shear stress  $(\sigma_a - \sigma_r)/2$ , changing with the rate of axial strain. By using the rate of subsidence of Niigata Airport Building (Fig. 12.15) of 10 mm/s in 10-m-thick liquefied soil (Towhata and Horikoshi, 1997), the realistic rate of strain was determined to be 0.001/s (=0.1%/s). Accordingly, the realistic value of shear viscosity was determined in Fig. 12.14 at this strain rate and it is approximately 2,700 kPa·s.

### 12.6 Prediction on Liquefaction-Induced Subsidence of Embankment by Using Viscous Modelling

Subsidence of a river levee resting on liquefiable subsoil was calculated by using a viscous modeling of liquefaction-induced flow of ground (Towhata et al., 1999b; Towhata, 2009). The viscosity coefficient of 2,700 kPa·s as obtained above was put in the analysis. Figure 12.16 indicates the configuration of the river levee. Moreover, the effects of several measures to mitigate subsidence were examined by the same method. Those measures are an earth berm as a counter weight, a sheet pile wall to reduce lateral soil displacement, and their combination (Fig. 12.17).

The deformation after 20 s of strong shaking and soil flow is going to be presented in what follows. When no mitigation is installed, the subsidence and uplift in and around the levee are as shown in Fig. 12.18. The crest of the levee subsides

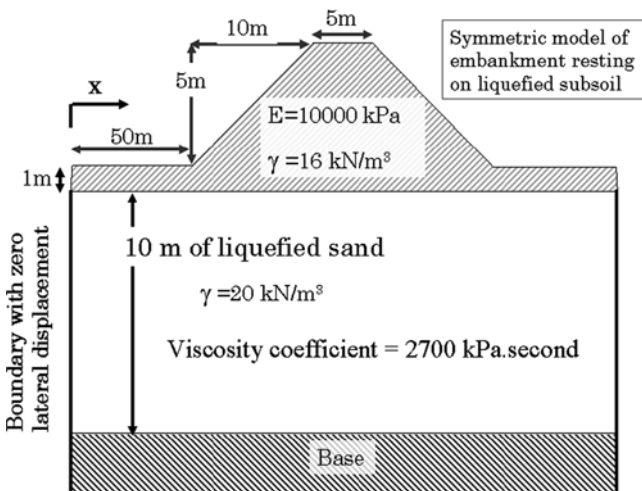
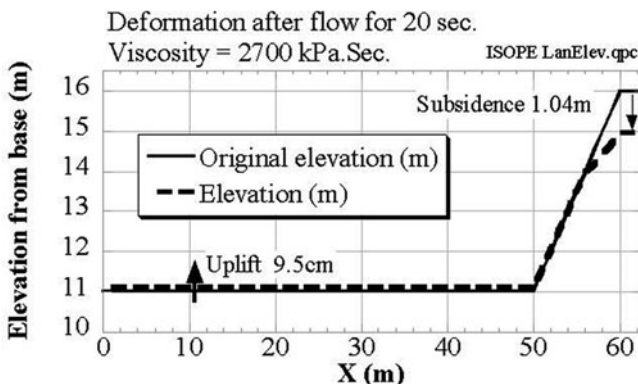
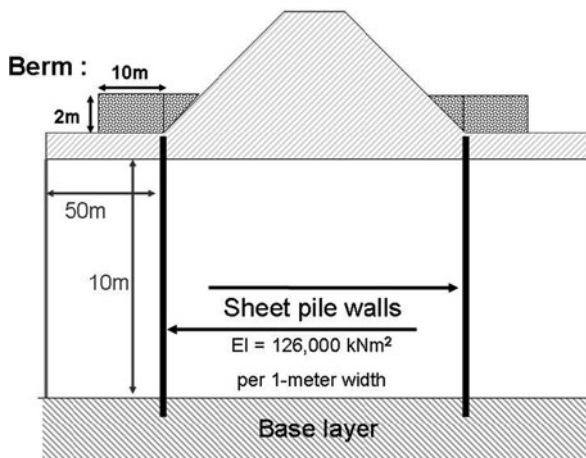


Fig. 12.16 Model of embankment subjected to liquefaction-induced subsidence and lateral spread

**Fig. 12.17** Mitigation of liquefaction-induced subsidence of embankment



**Fig. 12.18** Subsidence of levee after 20 s of soil flow

by 1.04 m. The subsidence of the body of the levee induces lateral flow of underlying liquefied sand, causing lateral displacement at the toe of the slope as shown in Fig. 12.19.

Then the analysis proceeded to the effects of mitigation measures in Fig. 12.17. The sheet pile walls were assumed to penetrate firmly into the base layer so that no translation and no rotation might occur. Thus, the bottom of the wall was treated as a fixed boundary in the analysis. The calculated results in Fig. 12.20 show that a berm of 10-m width is not very effective. In contrast, sheet pile walls can more efficiently reduce the crest subsidence and its combination with a berm is further effective.

Furthermore, it is often the case in practice that sheet pile walls under a river levee do not firmly penetrate into unliquefiable base layer, because the aim of their installation is not the mitigation of liquefaction-induced damage but reduction of the seepage flow of water during flooding. Hence, the effects of insufficient length of

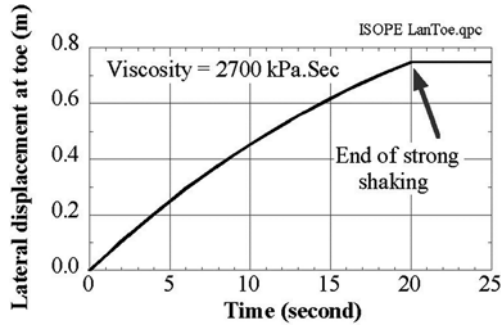


Fig. 12.19 Time history of lateral displacement at toe of slope

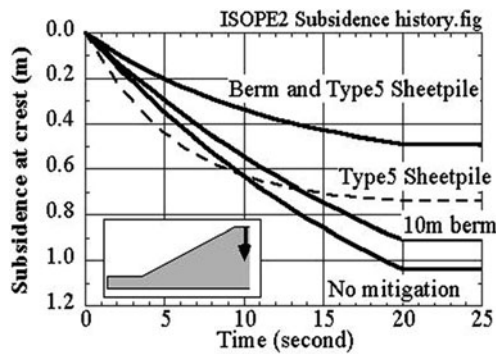


Fig. 12.20 Effects of two mitigation measures on subsidence of crest of embankment underlying liquefiable subsoil

sheet pile walls were analyzed by using the method by Towhata (2009). The bottom end of sheet pile walls was considered as a free end where shear force and bending moment are zero and free translation and rotation can occur. The results in Fig. 12.21 show that the intermediate length of 5 m is not effective, because the thickness of liquefied sand is 10 m. Two calculations with the same wall length of 10 m exhibit significantly different mitigation effects. This is because one calculation assumed free bottom boundary (null shear force and null bending moment at the bottom), while the other assumed a fixed boundary condition (null lateral displacement and null rotation). In other words, the first case assumes that the wall bottom is only in contact with the base, and the second case stands for a longer wall penetrating well into the stable base. It is found therein that even when the length is 10 m but is still insufficient to achieve any fixing effects, the mitigation effects is not significant. This figure demonstrates the remarkably improved effects of firm penetration into subsoil.

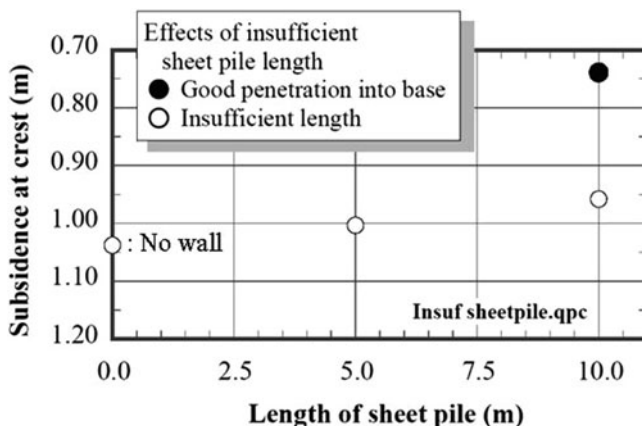


Fig. 12.21 Effects of insufficient length of sheet pile walls on magnitude of crest subsidence

## 12.7 Conclusions

The present study investigated the deformation characteristics of liquefied sand undergoing very low effective stress. Although early model tests suggested rate-dependent or viscous nature of liquefied sand, the non-uniformity of stress and strain in the model ground made it difficult to examine the stress and strain states. Accordingly, the authors carried out triaxial compression tests in which the extremely low effective stress was produced by free-falling tests where the gravity effects disappeared. Major conclusions drawn from this study are as what follows.

1. Liquefied sand behaves like viscous liquid.
2. The viscosity coefficient of sand exhibits significant nonlinearity in which the coefficient varies with the change of shear strain rate.
3. The strain rate and viscosity coefficient that are relevant for practical calculation were determined with referring to a case history during the 1964 Niigata earthquake.
4. The obtained viscosity coefficient was utilized in numerical analyses in which the liquefaction induced deformation of geotechnical structures was assessed and the effects of mitigation measures were assessed.

**Acknowledgments** The present study was supported by the financial grant by the Ministry of Education, Culture, Sports, Science and Technology. The free-fall tests were conducted with the assistance of Mr. M. Nokura at Micro-Gravity Laboratory of Japan, Toki, Japan. Performance tests of a developed free-fall triaxial device were helped by Prof. Tsue, Department of Aeronautics and Astronautics, University of Tokyo. Data obtained by the full-scale shaking table test at E-Defense was very valuable. These supports are deeply appreciated by the authors.

## References

- Dobry R (2007) Discussion. Proceedings of the 4th international conference on earthquake geotechnical engineering, Thessaloniki, Greece
- Dungca JR, Kuwano J, Takahashi A, Saruwatari T, Izawa J, Suzuki H, Tokimatsu K (2006) Shaking table tests on the lateral response of a pile buried in liquefied sand. *Soil Dyn Earthquake Eng* 26:287–295
- Gallage CPK, Towhata I, Nishimura S (2005) Laboratory investigation on rate-dependent properties of sand undergoing low confining effective stress. *Soil Found* 45(4):43–60
- Motamed R, Towhata I, Honda T, Yasuda S, Tabata K, Nakazawa H (2009) Behaviour of pile group behind a sheet pile quay wall subjected to liquefaction-induced large ground deformation observed in shaking test in E-defense project. *Soil Found* 49(3):459–475
- Sture S, Costes N, Batiste S, Lankton M, Alshibli K, Jeremic B, Swanson R, Frank M (1998) Mechanics of granular materials under low effective stresses. *J Aerospace Eng, ASCE* 11(3):67–72
- Towhata I (2009) User's manual for SOLIFLUK analysis for flow deformation of liquefied ground. Japan Institute of Construction Engineering, Tokyo (in Japanese)
- Towhata I, Horikoshi K (1997) Case history study on liquefaction-induced subsidence of Niigata Airport Building. Proceedings of the 32nd annual convention of Japan. *Geotech Soc* 1:973–974 (in Japanese)
- Towhata I, Orense RP, Toyota H (1999b) Mathematical principles in prediction of lateral ground displacement induced by seismic liquefaction. *Soil Found* 39(2):1–19
- Towhata I, Vargas-Monge W, Orense RP, Yao M (1999a) Shaking table tests on subgrade reaction of pipe embedded in sandy liquefied subsoil. *Soil Dyn Earthquake Eng* 18(5):347–361

# Chapter 13

## Soil Mechanics

### Constitutive Modelling for Soft Cohesive Soils

Hideki Ohta, Atsushi Iizuka, and Shintaro Ohno

**Abstract** Constitutive models developed in 1960s and 1970s by a group in Kyoto, with Shibata as the central figure, happen to have a theoretical framework mathematically similar to that of the Cam Clay models developed by the Cambridge Soil Mechanics Group in 1960s. The models developed in Kyoto were based on volume changes measured during constant stress ratio consolidation ( $q/p'$ -constant drained shear), and negative dilatancy (or contractancy) measured during  $p'$ -constant drained shear. The Cam Clay models were developed from assumptions of energy dissipation during shear. This chapter presents an interpretation of the physical meaning of dissipated energy and reveals the mathematical similarity between these two groups of constitutive models.

#### 13.1 Introduction

Two dissipated energy concepts were assumed in developing the Cambridge constitutive models. Cam Clay, proposed by Roscoe et al. (1963), is based on one. Modified Cam Clay, proposed by Burland (1965) and by Roscoe and Burland (1968), is based on another. These are compared in this chapter which is aimed at a critical evaluation of these two dissipated energy assumptions. Introduced then is the empirical equation proposed by Shibata (1963) based on his results obtained from  $p'$ -constant drained tests on normally consolidated clays. Shibata measured the negative dilatancy (or contractancy) characteristics of soils in a wide variety of states. Shibata's empirical equation happens to be essentially the same as the (Original) Cam Clay equation; this implies that the choice of dissipated energy function is equivalent to the choice of a function that represents  $p'$ -constant drained test results.

---

H. Ohta (✉)

Research and Development Initiative, Chuo University, Bunkyo, Tokyo 112-8551, Japan  
e-mail: ohta@tamacc.chuo-u.ac.jp

It is thus possible to develop a group of constitutive models by assuming appropriate functions representing the results of  $p'$ -constant drained tests on samples of any chosen clay. This chapter describes the relations between these groups of models and shows that all of the models, including (Original) Cam Clay and Modified Cam Clay, could be derived experimentally from the systematic description of the negative dilatancy (or contractancy) characteristics available from  $p'$ -constant drained tests. This means that the differences between the models can be seen as differences in the functions representing the  $p'$ -constant drained test results equally as well as from differences in assumed dissipated energy functions.

### 13.2 Dissipated Energy

Replacing the failure state concept defined by the combination of the  $c'$ -intercept and the  $\phi'$ -parameter, widely accepted in the classical soil mechanics, Roscoe et al. (1958) and Roscoe and Poorooshasb (1963) proposed the concept of critical state defined by

$$\eta = M \quad (1)$$

in which

$$\eta = \frac{q}{p'} \quad p' = \frac{1}{3} (\sigma'_a + 2\sigma'_r) \quad q = \sigma'_a - \sigma'_r \quad (2)$$

where  $\sigma'_a$  and  $\sigma'_r$  are axial and radial effective stresses in a triaxial test specimen.

The critical state defined by Eq. (1) in the effective stress space, is also defined in the  $p' - v$  space by

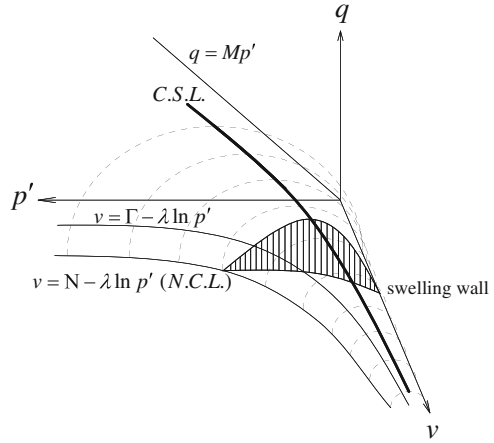
$$v = \Gamma - \lambda \ln p' \quad (3)$$

Specific volume,  $v$ , is defined as  $v = 1 + e$  where  $e$  is void ratio. The line given by Eq. (3) is parallel to the normal (isotropic) consolidation line represented by

$$v = N - \lambda \ln p' \quad (4)$$

in which  $\lambda$  is the compression index (0.4343Cc),  $\Gamma$  in Eq. (3) is the specific volume at the critical state under the unit pressure  $p' = 1$  and  $N$  in Eq. (4) is the specific volume in the normal (isotropic) consolidation under the unit pressure  $p' = 1$ . The critical state line in  $p' - q - v$  space is defined by Eqs. (1) and (3) and shown in Fig. 13.1. The intersection of the state boundary surface (elasto-plastic state) and swelling wall (elastic state) gives a curve that is the elastic limit. This elastic limit curve, when projected onto the stress space, becomes the yield locus (as suggested by Calladine (1963)).

**Fig. 13.1** Critical state line, state boundary surface and swelling wall in the  $p' - q - v$  space



Let us consider a situation where infinitesimal strains  $d\varepsilon_a$  and  $d\varepsilon_r$  are induced in a triaxial specimen by a set of small stress increases  $d\sigma'_a$  and  $d\sigma'_r$ . The total energy  $dE$  applied to a unit volume of soil is given, by definition, as

$$dE = \sigma'_a d\varepsilon_a + 2\sigma'_r d\varepsilon_r. \tag{5}$$

Equation (5) is rewritten as

$$dE = p' d\varepsilon_v + q d\varepsilon_s \tag{6}$$

by using effective mean principal stress  $p'$ , principal stress difference  $q$ , infinitesimal volumetric strain  $d\varepsilon_v$  and infinitesimal shear strain  $d\varepsilon_s$  in which

$$d\varepsilon_v = d\varepsilon_a + 2d\varepsilon_r \quad d\varepsilon_s = \frac{2}{3} (d\varepsilon_a - d\varepsilon_r). \tag{7}$$

The total energy  $dE$  per unit volume of soil consists of internal energy  $dU$  and energy dissipated by irreversible work during the plastic deformation  $dW$  as shown by

$$dE = dU + dW. \tag{8}$$

Dissipated energy  $dW$  is given, by definition, as

$$dW = \sigma'_a d\varepsilon_a^p + 2\sigma'_r d\varepsilon_r^p \tag{9}$$

in which superscript  $p$  represents a plastic component.

Equation (9) is rewritten as

$$dW = p' d\varepsilon_v^p + q d\varepsilon_s^p \tag{10}$$

in which

$$d\varepsilon_v^p = d\varepsilon_a^p + 2d\varepsilon_r^p \quad d\varepsilon_s^p = \frac{2}{3} (d\varepsilon_a^p - d\varepsilon_r^p). \quad (11)$$

Assuming that there is no increment of plastic volumetric strain after reaching the critical state, we get

$$d\varepsilon_v^p = 0 \text{ at critical state.} \quad (12)$$

Substituting Eqs. (1) and (12) into Eq. (10), Eq. (13) is obtained which was assumed by Roscoe et al. (1963) to be valid not only at the critical state but also during the whole process of shearing up to the critical state:

$$dW = Mp' d\varepsilon_s^p. \quad (13)$$

Substitution of Eq. (13) into Eq. (10) results in

$$\left( -\frac{d\varepsilon_v^p}{d\varepsilon_s^p} \right) = \frac{q}{p'} - M. \quad (14)$$

Combining the associated flow rule

$$d\varepsilon_v^p = \gamma \frac{\partial f}{\partial p'}, \quad d\varepsilon_s^p = \gamma \frac{\partial f}{\partial q} \quad (15)$$

with the consistency condition

$$df = \frac{\partial f}{\partial p'} dp' + \frac{\partial f}{\partial q} dq = 0 \quad (16)$$

in which  $\gamma$  is a proportionality constant and  $f$  is the yield surface in the effective stress space, we get

$$\frac{dq}{dp'} = -\frac{d\varepsilon_v^p}{d\varepsilon_s^p}. \quad (17)$$

Substituting Eq. (17) into Eq. (14), gives

$$\frac{dq}{dp'} = \frac{q}{p'} - M. \quad (18)$$

The definition given by Eq. (2) results in

$$q = \eta p' \quad (19)$$

which is differentiated with respect to  $p'$  as

$$\frac{dq}{dp'} = \eta + p' \frac{d\eta}{dp'}. \quad (20)$$

Substituting Eq. (20) into Eq. (18), we get

$$d\eta = -M \frac{dp'}{p'} \quad (21)$$

which is integrated with the initial condition that  $(p', \eta) = (p'_0, 0)$  as

$$M \ln \left( \frac{p'}{p'_0} \right) + \eta = 0 \quad (22)$$

defining the initial yield surface in the effective stress space as

$$f(p', \eta) = M \ln \left( \frac{p'}{p'_0} \right) + \eta = 0. \quad (23)$$

This is the derivation of the (Original) Cam Clay model proposed by Roscoe et al. (1963).

Since the dissipated energy,  $dW = Mp' d\varepsilon_s^p$  (Eq. 13), assumed by Roscoe et al. (1963) seems to have no contribution from the plastic volumetric strain during the whole process of shearing (at least from its appearance), Burland (1965) suggested the replacement of Eq. (13) with

$$dW = p' \sqrt{(d\varepsilon_v^p)^2 + (Md\varepsilon_s^p)^2} \quad (24)$$

which is reduced to Eq. (13) at the critical state (see Eq. 12) while apparently including the contribution of the plastic volumetric strain during the process of shearing up to the critical state. Substituting Eqs. (17) and (24) into Eq. (10), we get

$$\frac{2q}{p'} \frac{dq}{dp'} = \left( \frac{q}{p'} \right)^2 - M^2. \quad (25)$$

Now we define:

$$(q)^2 = \hat{\eta} (p')^2 \quad (26)$$

in which

$$\hat{\eta} = \eta^2. \quad (27)$$

Differentiation of Eq. (26) with respect to  $p'$  results in

$$\frac{2q}{p'} \frac{dq}{dp'} = 2\hat{\eta} + p' \frac{d\hat{\eta}}{dp'} \quad (28)$$

which is substituted into Eq. (25) leading to

$$\frac{d\hat{\eta}}{\hat{\eta} + M^2} = -\frac{dp'}{p'}. \quad (29)$$

On integration of Eq. (29) with the initial condition  $(p', \eta) = (p'_0, 0)$ , we get

$$\ln\left(\frac{p'}{p'_0}\right) + \ln\left(\frac{\hat{\eta} + M^2}{M^2}\right) = 0 \quad (30)$$

which is rewritten as

$$\ln\left(\frac{p'}{p'_0}\right) + \ln\left(\frac{\eta^2 + M^2}{M^2}\right) = 0 \quad (31)$$

by employing Eq. (27). Thus the initial yield surface of the Modified Cam Clay model proposed by Burland (1965) and Roscoe and Burland (1968) is given as

$$f(p', q) = \ln\left(\frac{p'}{p'_0}\right) + \ln\left(\frac{\eta^2 + M^2}{M^2}\right) = 0. \quad (32)$$

Thus Eq. (24),  $dW = p' \sqrt{(d\varepsilon_v^p)^2 + (Md\varepsilon_s^p)^2}$ , appears to be successful in justifying the criticism made by Burland (1965) that the dissipated energy assumed by Roscoe et al. (1963), Eq. (13)  $dW = Mp'd\varepsilon_s^p$ , has no contribution from the plastic volumetric strain. However, Ohta (1971) concluded that Eq. (13) actually includes the contribution of the plastic volumetric strain to the dissipated energy. His argument is as follows. Substituting Eq. (23) into the associated flow rule Eq. (15), we get

$$d\varepsilon_v^p = \gamma \frac{1}{p'} \left(M - \frac{q}{p'}\right) \quad (33)$$

$$d\varepsilon_s^p = \gamma \frac{1}{p'} \quad (34)$$

in which  $\gamma$  is obtained from Eq. (34) as

$$\gamma = p'd\varepsilon_s^p. \quad (35)$$

Substituting Eqs. (33) and (35) into the definition of dissipated energy given in Eq. (10), leads to

$$dW = Mp'd\varepsilon_s^p \quad (36)$$

which is exactly the same as the dissipated energy assumed by Roscoe et al. (1963). This implies that Eq. (24),  $dW = p' \sqrt{(d\varepsilon_v^p)^2 + (Md\varepsilon_s^p)^2}$ , assumed by Burland

(1965) takes the contribution of the plastic volumetric strain into account in both the first and second terms in the square root part of Eq. (24) and thus may double count the contribution of the plastic volumetric strain.

### 13.3 Contractancy Models

Shibata (1963) carried out a series of  $p'$ -constant drained tests on two undisturbed samples of Amagasaki Clay (liquid limit = 105.5%, plastic limit = 32.4%, plasticity index = 73.1, natural water content = 74%) after isotropically consolidating one specimen with the consolidation pressure of 268 kPa and the other specimen with the consolidation pressure of 441 kPa; both pressures being greater than the pre-consolidation pressure of the clay. Tests were done with increasing principal stress difference  $q = \sigma'_a - \sigma'_r$  keeping the effective mean principal stress  $p' = \frac{1}{3} (\sigma'_a + 2\sigma'_r)$  unchanged from the consolidation pressure. The principal stress difference was increased stepwise (5 steps for the specimen consolidated with the pressure of 268 kPa and 8 steps for the other specimen). About 2 weeks were needed in completing the pore water drainage at each step during which the change in specimen diameter was measured directly aiming at accurate area correction during the whole test process.

Shibata's work is summarized in Fig. 13.2 which shows not only his test results on Amagasaki Clay but also his interpretation of the data published by Henkel (1960) on Weald and London clays and that of Mizuno et al. (1962) on Fukuoka clay. The slopes of these straight lines in Fig. 13.2 give values for a coefficient that

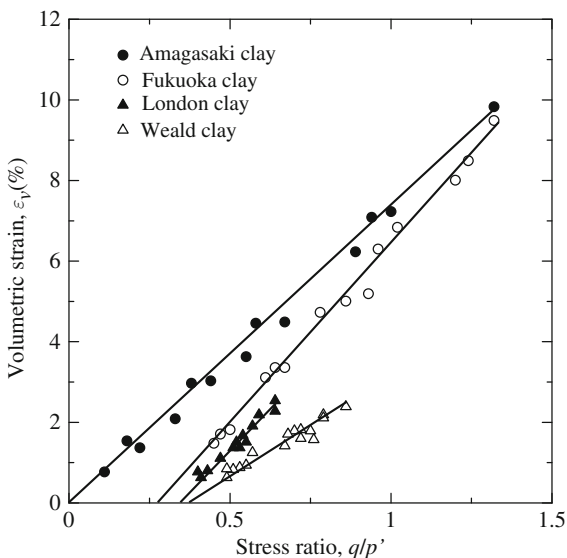


Fig. 13.2 Shibata's plot of (negative) dilatancy

may be called Shibata’s coefficient of (negative) dilatancy,  $D$ , or more concisely Shibata’s coefficient of contractancy, which is obtained from the following equation.

$$\frac{\Delta V_d}{V_1} = D \left\{ \frac{(\sigma_1 - \sigma_3) - \sigma_c}{\sigma'_m} \right\} \tag{37}$$

in which  $\Delta V_d$  is the volume decrease due to  $p'$ -constant drained shear,  $V_1 = V_0 - \Delta V_c$  is the volume after isotropic consolidation (i.e. original volume of the specimen – volume decrease due to isotropic consolidation),  $\sigma'_m$  is the effective mean principal stress and  $\sigma_c$  is the threshold principal stress difference from which the volume decrease due to  $p'$ -constant drained shear starts to occur. Shibata then gave an equation describing the volumetric strain caused by the general (axisymmetric) stress condition which includes that due both to (negative) dilatancy and isotropic consolidation as

$$\begin{aligned} \frac{\Delta V}{V_0} &= \frac{\Delta V_c}{V_0} + \frac{V_1}{V_0} \cdot \frac{\Delta V_d}{V_1} \\ &= C \cdot \log \frac{\sigma'_m}{\sigma'_0} + D \left( 1 - C \cdot \log \frac{\sigma'_m}{\sigma'_0} \right) \left\{ \frac{(\sigma_1 - \sigma_3) - \sigma_c}{\sigma'_m} \right\} \end{aligned} \tag{38}$$

where  $C$  is a constant corresponding to compression index  $C_c$ .

Equation (38) is essentially identical to the state boundary surface defined by Roscoe et al. (1963); although the form of Eq. (38) looks totally different to that of the Cam Clay surface. It is interesting to note that two totally independent works, which reached essentially the same conclusion, were published in the same year.

As conceptually shown by Shibata (1963), Eq. (38) gives the volumetric change of normally consolidated clays as consisting of two components: (i) consolidation caused by constant stress ratio ( $\eta = \frac{q}{p'}$ ) drained shear and (ii) negative dilatancy (contractancy) caused by  $p'$ -constant drained shear. The volume change due to consolidation is traditionally accepted as represented by

$$de = -\lambda d(\ln p') \text{ (in elasto-plastic state)} \tag{39}$$

and

$$de = -\kappa d(\ln p') \text{ (in elastic state)} \tag{40}$$

where  $\lambda$  and  $\kappa$  are the compression index ( $\lambda = 0.4343C_c$ ) and the swelling index ( $\kappa = 0.4343C_s$ ). The volume change due to contractancy is described by Ohta and Hata (1971) as

$$de = -(1 + e_0) D |d\eta| \text{ when } |\eta| \geq \eta_l \text{ (in elasto-plastic state)} \tag{41}$$

$$de = 0 \text{ when } |\eta| < \eta_l \text{ (in elasto-plastic state)} \tag{42}$$

in which  $D$  is Shibata's coefficient,  $\eta_l$  is the stress ratio from which contractancy starts to take place, and  $e_0$  is the void ratio at the completion of consolidation prior to the shearing process. No elastic component of volume change due to contractancy was assumed by Ohta and Hata (1971). By adding Eqs. (39), (40) and (41) or Eq. (42), the volume change in the elasto-plastic state, the overall volume change caused by both of consolidation and contractancy in the elasto-plastic state, is described as

$$de = -\lambda d(\ln p') - (1 + e_0) D |d\eta| \quad \text{when } |\eta| \geq \eta_l \quad (\text{in elasto-plastic state}) \quad (43)$$

$$de = -\lambda d(\ln p') \quad \text{when } |\eta| < \eta_l \quad (\text{in elasto-plastic state}). \quad (44)$$

Keeping in mind that the void ratio of clays under general stress states in a triaxial chamber is stress path independent (void ratio is a function only of the current effective stress state and independent of the past stress history during shear) as implied by the data given by Henkel (1960), we integrate Eqs. (43) and (44) with the initial condition  $(e, p', \eta) = (e_0, p'_0, 0)$  and obtain the void ratio as the function of the current effective stress state as

$$e - e_0 = -\lambda \ln \frac{p'}{p'_0} - (1 + e_0) D |\eta - \eta_l| \quad \text{when } |\eta| \geq \eta_l \quad (\text{in elasto-plastic state}) \quad (45)$$

$$e - e_0 = -\lambda \ln \frac{p'}{p'_0} \quad \text{when } |\eta| < \eta_l \quad (\text{in elasto-plastic state}). \quad (46)$$

In the same manner, the relationship between void ratio and current effective stress state in the elastic state is given as

$$e - e_0 = -\kappa \ln \frac{p'}{p'_0} \quad (\text{in elastic state}) \quad (47)$$

by integrating Eq. (40) with the initial condition  $(e, p') = (e_0, p'_0)$ . Equations (45) and (46) are rewritten as

$$\varepsilon_v = \frac{\lambda}{1 + e_0} \ln \frac{p'}{p'_0} + D |\eta - \eta_l| \quad \text{when } |\eta| \geq \eta_l \quad (\text{in elasto-plastic state}) \quad (48)$$

$$\varepsilon_v = \frac{\lambda}{1 + e_0} \ln \frac{p'}{p'_0} \quad \text{when } |\eta| < \eta_l \quad (\text{in elasto-plastic state}) \quad (49)$$

in which volumetric strain is defined as

$$\varepsilon_v = \frac{e_0 - e}{1 + e_0}. \quad (50)$$

In a similar way, Eq. (47) is rewritten as

$$\varepsilon_v^e = \frac{\kappa}{1 + e_0} \ln \frac{p'}{p'_0} \quad (\text{in elastic state}). \quad (51)$$

Subtracting the elastic component of volumetric strain given by Eq. (51) from the elasto-plastic volumetric strain given by Eqs. (48) and (49), we get plastic component of volumetric strain  $\varepsilon_v^p$  as

$$\varepsilon_v^p = \frac{\lambda - \kappa}{1 + e_0} \ln \frac{p'}{p'_0} + D |\eta - \eta_l| \quad \text{when } |\eta| \geq \eta_l \quad (52)$$

$$\varepsilon_v^p = \frac{\lambda - \kappa}{1 + e_0} \ln \frac{p'}{p'_0} \quad \text{when } |\eta| < \eta_l. \quad (53)$$

A pair of yield functions based on Eqs. (52) and (53), with the plastic component of volumetric strain  $\varepsilon_v^p$  as the hardening parameter, is defined as follows

$$f(p', q, \varepsilon_v^p) = MD \ln \frac{p'}{p'_0} + D |\eta - \eta_l| - \varepsilon_v^p = 0 \quad \text{when } |\eta| \geq \eta_l \quad (54)$$

$$f(p', q, \varepsilon_v^p) = MD \ln \frac{p'}{p'_0} - \varepsilon_v^p = 0 \quad \text{when } |\eta| < \eta_l \quad (55)$$

in which  $M$  is the stress ratio at the critical state defined by Roscoe et al. (1963) and related to Shibata's coefficient  $D$  as

$$M = \frac{\lambda - \kappa}{(1 + e_0) D}. \quad (56)$$

This is the outline of the constitutive model developed by Ohta and Hata (1971) as an extension of Eq. (38) proposed by Shibata (1963) based on his  $p'$ -constant drained tests on two undisturbed samples of Amagasaki Clay. It is obvious that Eq. (54) is reduced to a form identical with the (Original) Cam Clay model when  $\eta_l$  is zero, as is seen to be in the case with Shibata's experimental line for Amagasaki Clay which passes through the origin in Fig. 13.2. Ohta and Hata (1971) extended their model into a form applicable to anisotropically consolidated clays, and this was further extended by Sekiguchi and Ohta (1977) employing a new stress parameter  $\eta^*$  which is discussed later in this chapter. This Sekiguchi and Ohta model has been implemented in soil/water coupled finite element programmes. These include DACSAR (Deformation Analysis Considering Stress Anisotropy and Reorientation), coded by Iizuka and Ohta (1987), which has been widely used in the engineering practice in Japan. It should be noted that the Sekiguchi-Ohta model is also reduced to a form identical with the (Original) Cam Clay when applied to isotropically consolidated clays.

### 13.4 Exponential Contractancy Model and Logarithmic Contractancy Model

The key point of the theoretical framework of the above contractancy models is that in Fig. 13.2 the experimental data-points are linearly related. However, this does not preclude other non-linear functions, such as exponential and/or logarithmic curves, being used to represent the experimental data. Ohno et al. (2006) proposed two categories of contractancy model in which (Original) Cam Clay, Modified Cam Clay and Sekiguchi-Ohta models are included as special cases. Ohno et al. (2007) demonstrated the use of the models in engineering practice. They started modelling by assuming a general function  $H$  which can be replaced by any functions appropriate to fit experimental data-points such as those shown in Fig. 13.2 obtained from  $p'$ -constant drained triaxial tests as follows

$$e = e_0 - (e_0 - e_M) H \quad (57)$$

in which  $e_M$  is the void ratio at the critical state. The following relations are assumed

$$H = H(\eta) \quad (58)$$

$$0 \leq H \leq 1 \quad (59)$$

$$\begin{cases} H = 0 & \text{when } |\eta| = 0 \\ H = 1 & \text{when } |\eta| = M \end{cases} \quad (60)$$

It is well understood that there exist many parallel lines between the normal consolidation line and the critical state line plotted in the  $e$ - $\ln p'$  diagram.  $H$  is a function of stress ratio  $\eta (= q/p')$  and indicates the relative positioning of one of these lines corresponding to any chosen value of  $\eta$ . A line for a value of  $\eta$  is at a vertical distance (difference in void ratio) from the normal consolidation line. This distance physically means the void ratio change caused by  $p'$ -constant drained shear from normally consolidated state up to a particular stress ratio  $\eta$ .  $H$  gives a number between 0 and 1 indicating the relative distance of the line between the normal consolidation line and the critical state line. This is also mentioned by Asaoka et al. (2002). Void ratio change caused by contractancy ( $p'$ -constant drained shear) is given by differentiating Eq. (57) as

$$de = -(e_0 - e_M) dH. \quad (61)$$

Adding the void ratio change caused by consolidation, Eq. (39), and contractancy, Eq. (61), we get

$$de = -\lambda d(\ln p') - (e_0 - e_M) dH. \quad (62)$$

Since the void ratio of clays under a general stress state in a triaxial chamber is stress path independent as implied by the data given by Henkel (1960), we integrate Eq. (62) with the initial condition  $(e, p', \eta) = (e_0, p'_0, 0)$  in the same manner that we employed in obtaining Eq. (45) as

$$e - e_0 = -\lambda \ln \frac{p'}{p'_0} - (e_0 - e_M)H \quad (63)$$

Equation (63) is converted into

$$\varepsilon_v = \frac{\lambda}{1 + e_0} \ln \frac{p'}{p'_0} + \varepsilon_{vM}H \quad (64)$$

in which the volumetric strain  $\varepsilon_{vM}$  at the critical state is given by

$$\varepsilon_{vM} = \frac{e_0 - e_M}{1 + e_0}. \quad (65)$$

Subtracting the elastic component of volumetric strain Eq. (51) from the total strain Eq. (64), we get the plastic component of volumetric strain as

$$\varepsilon_v^p = \frac{\lambda - \kappa}{1 + e_0} \ln \frac{p'}{p'_0} + \varepsilon_{vM}H. \quad (66)$$

Then the yield function with  $\varepsilon_v^p$  as the hardening parameter is obtained as

$$f(p', q, \varepsilon_v^p) = \frac{\lambda - \kappa}{1 + e_0} \ln \frac{p'}{p'_0} + \varepsilon_{vM}H - \varepsilon_v^p = 0. \quad (67)$$

It is widely accepted that no further volumetric plastic strain occurs after the critical state is reached, as shown by

$$\dot{\varepsilon}_v^p = 0 \quad \text{when } |\eta| = M : \text{critical state}. \quad (68)$$

From the associated flow rule, the plastic component of the volumetric strain increment  $\dot{\varepsilon}_v^p$  is obtained as

$$\dot{\varepsilon}_v^p = \gamma \frac{\partial f}{\partial p'}. \quad (69)$$

Substituting Eq. (69) into Eq. (68), we get

$$\frac{\partial f}{\partial p'} = 0 \quad \text{when } |\eta| = M : \text{critical state} \quad (70)$$

because  $\gamma > 0$ . Partially differentiating Eq. (67) with respect to  $p'$ , we get

$$\frac{\partial f}{\partial p'} = \frac{\lambda - \kappa}{1 + e_0} \frac{1}{p'} + \varepsilon_{vM} \frac{\partial H}{\partial p'}. \quad (71)$$

Substituting Eq. (71) into Eq. (70), we get

$$\varepsilon_{vM} = - \left( \frac{\lambda - \kappa}{1 + e_0} \right) \Big/ \left( p' \frac{\partial H}{\partial p'} \right) \text{ when } |\eta| = M : \text{critical state}. \quad (72)$$

Thus the volumetric strain at the critical state  $\varepsilon_{vM}$  becomes available by specifying the functional form of H. Ohno et al. (2006) proposed a couple of categories of functional form of H as follows:

(1) Exponential form of H (Exponential Contractancy model) is

$$H = \left( \frac{|\eta|}{M} \right)^{n_E}. \quad (73)$$

The volumetric strain at the critical state  $\varepsilon_{vM}$  given by Eq. (72) is

$$\varepsilon_{vM} = \frac{\lambda - \kappa}{n_E (1 + e_0)}. \quad (74)$$

The yield function is obtained by substituting Eqs. (56), (73) and (74) into Eq. (67) as

$$f(p', q, \varepsilon_v^p) = MD \ln \frac{p'}{p'_0} + \frac{MD}{n_E} \left( \frac{|\eta|}{M} \right)^{n_E} - \varepsilon_v^p = 0. \quad (75)$$

(2) Logarithmic form of H (Logarithmic Contractancy model) is

$$H = \frac{1}{\ln 2} \ln \left( \frac{M^{n_L} + |\eta|^{n_L}}{M^{n_L}} \right). \quad (76)$$

The volumetric strain at the critical state  $\varepsilon_{vM}$  given by Eq. (72) is

$$\varepsilon_{vM} = \frac{2 \ln 2}{n_L} \frac{\lambda - \kappa}{1 + e_0}. \quad (77)$$

The yield function obtained by substituting Eqs. (56), (76) and (77) into Eq. (67) is

$$f(p', q, \varepsilon_v^p) = MD \ln \frac{p'}{p'_0} + \frac{2MD}{n_L} \ln \left( \frac{M^{n_L} + |\eta|^{n_L}}{M^{n_L}} \right) - \varepsilon_v^p = 0. \quad (78)$$

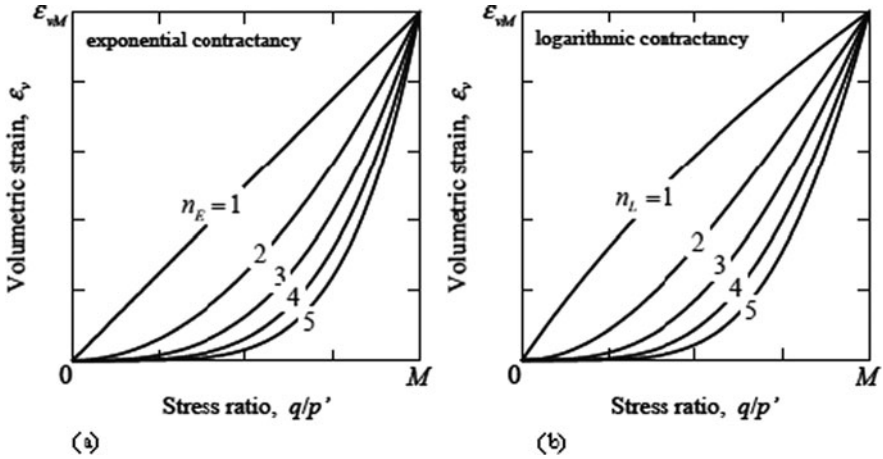


Fig. 13.3 Contractancy characteristics represented by (a) exponential and (b) logarithmic functions

The parameters  $n_E$ ,  $n_L$  are to be employed in fitting the results of  $p'$ -constant drained tests such as shown in Fig. 13.2. It should be noted that Eq. (75) is reduced to

$$f(p', q, \varepsilon_v^p) = MD \ln \frac{p'}{p_0} + D |\eta| - \varepsilon_v^p = 0 \tag{79}$$

when  $n_E = 1.0$ . And Eq. (78) is reduced to

$$f(p', q, \varepsilon_v^p) = MD \ln \frac{p'}{p_0} + MD \ln \left( \frac{M^2 + \eta^2}{M^2} \right) - \varepsilon_v^p = 0 \tag{80}$$

when  $n_L = 2.0$ . Equations (79) and (80) are identical with the (Original) Cam Clay and Modified Cam Clay equations. This means that (Original) Cam Clay is a member of the Exponential Contractancy family of models and Modified Cam Clay is a member of the Logarithmic Contractancy family of models. Thus the difference between the two Cam Clays exists only in the way of describing the contractancy characteristics of the clay.

The contractancy curves represented by Eqs. (73) and (76) are shown in Fig. 13.3a, b and are expected to work well in fitting experimental results. Let us see the performance of these equations by fitting the data in Fig. 13.2 given by Shibata (1963).

Shibata's four sets of experimental contractancy data, shown in Fig. 13.2, are represented by both Exponential Contractancy and Logarithmic Contractancy functions in Fig. 13.4a, b. The fitting parameters are listed in Table 13.1. The yield surfaces for the four sets of data obtained with the two contractancy functions are shown Fig. 13.5a, b.

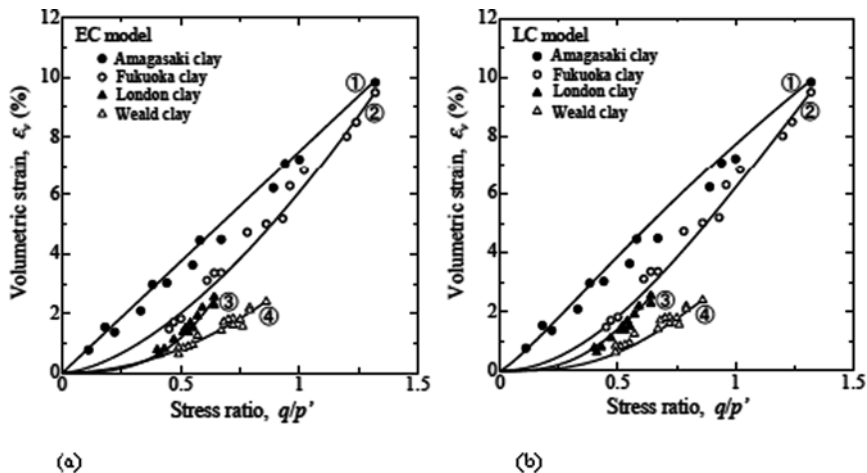


Fig. 13.4 Modelling of the experimental contractancy data-points (a exponential contractancy modeling; b logarithmic contractancy modeling) given by Shibata (1963)

Table 13.1 Parameters specified in modelling

	$M$	$n_E$	$n_L$
1. Amagasaki clay	1.32	1.0	1.2
2. Fukuoka clay	1.32	1.6	2.0
3. London clay	0.65	3.0	3.0
4. Weald clay	0.86	2.0	3.0

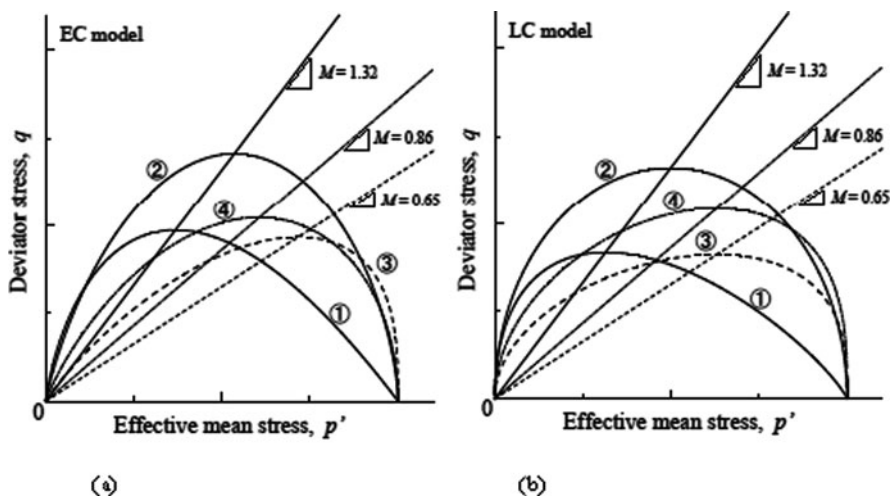


Fig. 13.5 Yield surfaces of 4 clays modelled by (a) EC and (b) LC models

### 13.5 Extended Sekiguchi-Ohta Models

As briefly mentioned above, Sekiguchi and Ohta (1977) extended the elasto-plastic model developed by Ohta and Hata (1971) by proposing a new stress parameter  $\eta^*$  which made it logically consistent to extend the model not only to anisotropically consolidated clays but also to clays subjected to general stress conditions. Hashiguchi and Chen (1998) and Asaoka et al. (2002) extended the Modified Cam Clay model to anisotropically consolidated clays when subjected to general stress conditions by employing the  $\eta^*$  parameter proposed by Sekiguchi and Ohta (1977). Let us now extend the EC and LC models in the same manner.

The stress parameter  $\eta^*$  is defined as

$$\eta^* = \sqrt{\frac{3}{2}} \|\boldsymbol{\eta} - \boldsymbol{\eta}_0\| \quad (81)$$

in which

$$\boldsymbol{\eta} = \frac{\mathbf{s}}{p'}, \quad \boldsymbol{\eta}_0 = \frac{\mathbf{s}_0}{p'_0} \quad (82)$$

$$\mathbf{s} = \boldsymbol{\sigma}' - p'\mathbf{1}, \quad \mathbf{s}_0 = \boldsymbol{\sigma}'_0 - p'_0\mathbf{1}, \quad p' = \frac{1}{3}\boldsymbol{\sigma}'\mathbf{1}, \quad p'_0 = \frac{1}{3}\boldsymbol{\sigma}'_0\mathbf{1} \quad (83)$$

where  $\boldsymbol{\sigma}'$  is the current effective stress tensor,  $\boldsymbol{\sigma}'_0$  is the effective stress tensor at the completion of anisotropic consolidation and  $\boldsymbol{\eta}_0$  indicates the degree of stress anisotropy at the completion of anisotropic consolidation.

#### 13.5.1 Extended Exponential Contractancy Model

Replacing  $|\eta|$  in Eq. (75) by  $\eta^*$ , we get the yield function of the Extended Exponential Contractancy model as

$$f(\boldsymbol{\sigma}', \varepsilon_v^p) = MD \ln \frac{p'}{p'_0} + \frac{MD}{n_E} \left( \frac{\eta^*}{M} \right)^{n_E} - \varepsilon_v^p = 0 \quad (84)$$

which is reduced to the (Original) Sekiguchi-Ohta model when  $n_E = 1.0$  as

$$f(\boldsymbol{\sigma}', \varepsilon_v^p) = MD \ln \left( \frac{p'}{p'_0} \right) + D\eta^* - \varepsilon_v^p = 0 \quad (85)$$

#### 13.5.2 Extended Logarithmic Contractancy Model

Replacing  $|\eta|$  in Eq. (78) by  $\eta^*$  in the same way we employed above, we get the yield function of the Extended Logarithmic Contractancy model as

$$f(\sigma', \varepsilon_v^p) = MD \ln \frac{p'}{p'_0} + \frac{2MD}{n_L} \ln \left( \frac{M^{n_L} + \eta^{*n_L}}{M^{n_L}} \right) - \varepsilon_v^p = 0 \tag{86}$$

which is reduced to Modified Cam Clay extended by Hashiguchi and Chen (1998) and Asaoka et al. (2002) when  $n_L = 2.0$  as

$$f(\sigma', \varepsilon_v^p) = MD \ln \frac{p'}{p'_0} + MD \ln \left( \frac{M^2 + \eta^{*2}}{M^2} \right) - \varepsilon_v^p = 0 \tag{87}$$

Equations (84) and (86) give two categories of the constitutive models derived employing the method proposed by Sekiguchi and Ohta (1977). These happen to include not only (Original) Cam Clay and Modified Cam Clay for isotropically consolidated clays, but also the models for anisotropically consolidated clays such as the Sekiguchi-Ohta model, and the models proposed by Hashiguchi and Chen (1998) and Asaoka et al. (2002). In this chapter, the authors give a collective name to the models given by Eqs. (84) and (86) as Extended Sekiguchi-Ohta models simply because the method of deriving these models was originally proposed and employed by Sekiguchi and Ohta (1977). It should be emphasized again that the difference between any of the models given either by Eq. (84) or by Eq. (86) is only in the functional form fitting the contractancy characteristics experimentally available from  $p'$ -constant drained shear. There exists no physically meaningful difference if we look at any of these models from the viewpoint of the contractancy modelling. We can choose any of the Extended Sekiguchi-Ohta models by selecting parameters  $n_E$  or  $n_L$  to get a model best fitting to the experimentally obtained mechanical behaviour of the clay encountered at the site under investigation.

Figure 13.6a, b show the yield surfaces of the Extended Sekiguchi-Ohta models for isotropically consolidated clays in the case that  $M = 1.0$ ,  $\eta_0 = 0.0$  in which

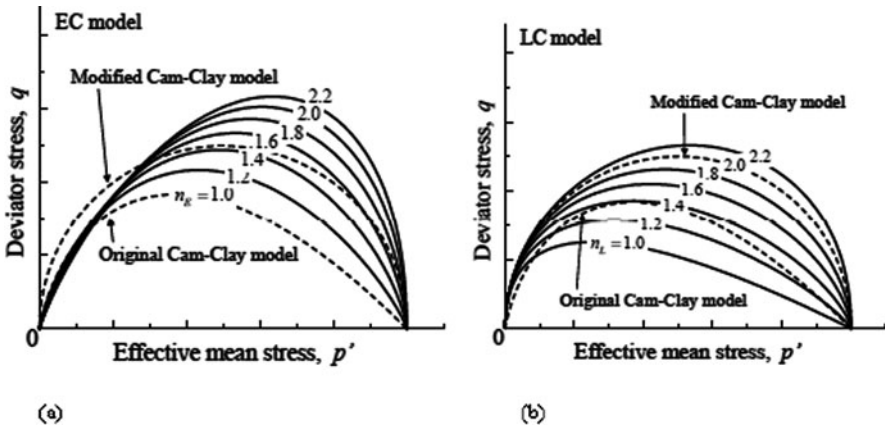
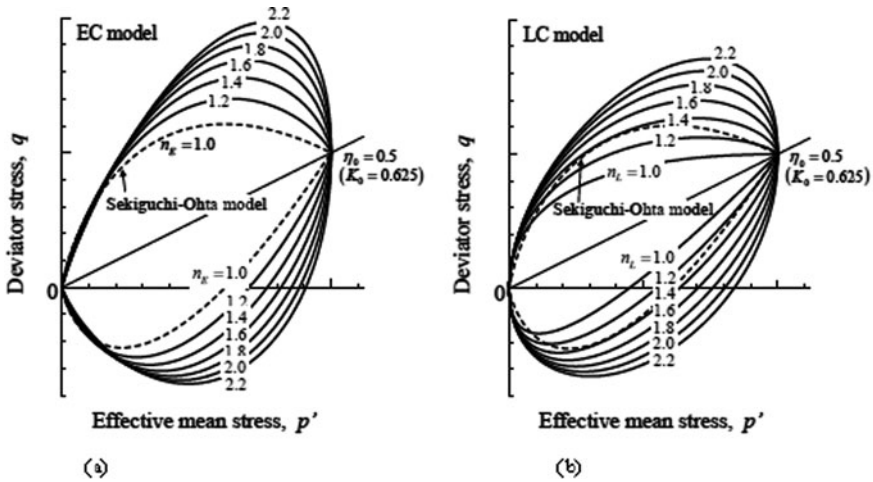


Fig. 13.6 Yield surfaces of the Extended Sekiguchi-Ohta models for isotropically consolidated clays (a) EC models ( $M = 1.0$ ,  $\eta_0 = 0.0$ ), (b) LC models ( $M = 1.0$ ,  $\eta_0 = 0.0$ ) (see Appendix for further details)



**Fig. 13.7** Yield surfaces of the Extended Sekiguchi-Ohta models for anisotropically consolidated clays (a) EC models ( $M = 1.0$ ,  $\eta_0 = 0.0$ ), (b) LC models ( $M = 1.0$ ,  $\eta_0 = 0.0$ ) (see Appendix for further details)

$$\eta_0 = \frac{q_0}{p'_0}, \quad q_0 = \sqrt{\frac{3}{2} \mathbf{s}_0 : \mathbf{s}_0}. \tag{88}$$

Dotted curves shown in Fig. 13.6 are the (Original) Cam Clay ( $n_E = 1.0$ ,  $\eta_0 = 0.0$ ) and the Modified Cam Clay ( $n_L = 2.0$ ,  $\eta_0 = 0.0$ ).

Figure 13.7a, b show the yield surfaces of the Extended Sekiguchi-Ohta models for anisotropically consolidated clays in the case that  $M = 1.0$ ,  $\eta_0 = 0.5$ .

### 13.6 Concluding Remarks

Looking at a group of constitutive models from two independent viewpoints arising from totally different thoughts, one philosophical and the other is physical, it was found that the concept of dissipated energy is deeply related to the mechanical response of clays subjected to  $p'$ -constant drained shear. This finding showed that many of the constitutive models developed by the Cambridge Group can be considered as belonging to the family of constitutive models developed by the Kyoto Group. In this chapter, the authors gave a name “Extended Sekiguchi-Ohta” models to this family because they were derived employing the method proposed by Sekiguchi and Ohta (1977) in developing their model, a model which has been widely used in engineering practice in Japan under the name of “Sekiguchi-Ohta”

model. On the other hand, the above finding did not give the authors any hint to search for the deep-rooted philosophical meaning of the energy concept. Energy must be dissipated during inelastic deformation accompanied by irreversible change in the structure of the soil skeleton, along with sound and heat etc resulting from frictional slippage and breakage of soil particles. This will be a subject for future work.

**Acknowledgments** The authors wish to express their gratitude to Prof. A. N. Schofield for having continuously discussed the subject of critical state constitutive modelling of soils for several decades and for having suggested that we call the models developed in Kyoto “Kamo Clay” as the Kamo river runs through the middle of Kyoto in the same way that the Cam runs through Cambridge. The present study was supported by the Grant-in-Aid for Scientific Research (C) No. 20560459, Ministry of Education, Culture, Sports, Science and Technology and the Japan Society for the Promotion of Science.

### Appendix

It should be noted that the yield surfaces for  $n_E=1.0$  and  $n_L=1.0$  shown in Figs. 13.6 and 13.7 have singular points as seen at the right ends of the yield surfaces. To avoid additional procedures needed in handling the singular points in numerical analysis, it may be a practical solution to assume  $n_E$  or  $n_L$  very close to 1.0 but not exactly 1.0. The yield surfaces around the singular points for those cases are shown in Figs. 13.8 and 13.9. Another difficulty arises from such solution since  $K_0$ -values theoretically derived from these yield surfaces are not in accordance with the input value of  $\eta_0$ .

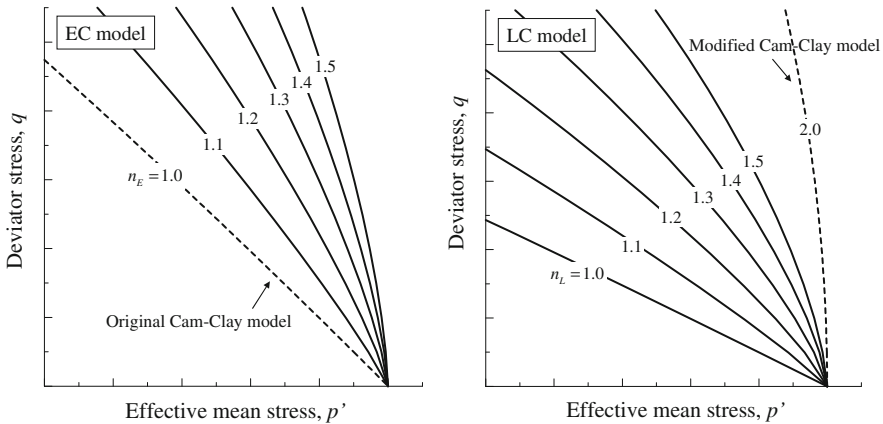


**Fig. 13.8** Yield surfaces around the singular points for  $n_E = 1.0$  and  $n_L = 1.0$  ( $M = 1.0$ ,  $\eta_0 = 0.0$ )

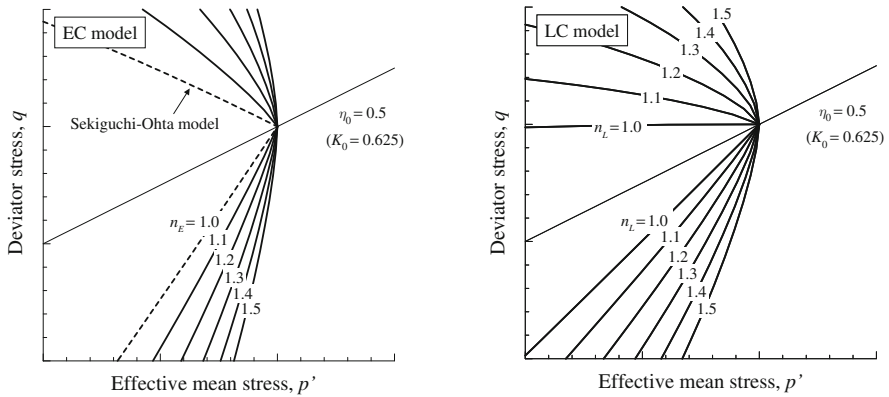


**Fig. 13.9** Yield surfaces around the singular points for  $n_E = 1.0$  and  $n_L = 1.0$  ( $M = 1.0$ ,  $\eta_0 = 0.5$ )

## References

- Asaoka A, Noda T, Yamada E, Kaneda K, Nakano M (2002) An elasto-plastic description of two distinct volume change mechanisms of soils. *Soils Found* 42(5):47–57
- Burland JB (1965) The yielding and dilation of clay (correspondence). *Géotechnique* 15:211–214
- Calladine CR (1963) The yielding of clay (correspondence). *Géotechnique* 13(3):250–255
- Hashiguchi K, Chen ZP (1998) Elastoplastic constitutive equation of soils with the subloading surface and rotational hardening. *Int J Numer Anal Meth Geomech* 22:197–277
- Henkel DJ (1960) The shear strength of saturated remoulded clays. *Proceedings of the research conference on shear strength of cohesive soils, ASCE, Boulder, CO*, pp 533–554
- Iizuka A, Ohta H (1987) A determination procedure of input parameters in elasto-viscoplastic finite element analysis. *Soil Found* 27(3):71–87
- Mizuno T, Tokumitsu Y, Kawakami H (1962) Behaviour of pore water pressure during triaxial tests. *Proceedings of the 17th annual meeting of civil engineers, vol III*, pp 25–26 (in Japanese)
- Ohno S, Iizuka A, Ohta H (2006) Two categories of new constitutive model derived from non-linear description of soil contractancy. *J Appl Mech, JSCE* 9:407–414 (in Japanese)
- Ohno S, Takeyama T, Pipatpongsa T, Iizuka A, Ohta H (2007) Analysis of embankment by non-linear contractancy description. *Proceedings of the 13th Asian regional conference on soil mechanics and geotechnical engineering, Kolkata, India*, pp 1097–1100
- Ohta H (1971) Panel discussion on stress-strain characteristics and time effects. *Proceedings of the 4th Asian regional conference on S.M.F.E., Bangkok*, 2:141–147
- Ohta H, Hata S (1971) A theoretical study of the stress-strain relations for clays. *Soil Found* 11(3):195–219
- Roscoe KH, Burland JB (1968) On the generalized stress-strain behavior of ‘wet’ clay. In: Heyman J, Leckie FA (eds) *Engineering plasticity*. Cambridge University Press, Cambridge, pp 535–609
- Roscoe KH, Poorooshasb HB (1963) A theoretical and experimental study of strains in triaxial compression tests on normally consolidated clays. *Géotechnique* 13(1):12–38
- Roscoe KH, Schofield AN, Thurairajah A (1963) Yielding of clays in states wetter than critical. *Géotechnique* 13(3):211–240
- Roscoe KH, Schofield AN, Wroth CP (1958) On the yielding of soils. *Géotechnique* 8(1):22–53
- Sekiguchi H, Ohta H (1977) Induced anisotropy and time dependency in clays, Constitutive equation of soils. *Proceedings of the specialty session 9, 9th international conference on soil mechanics and foundation engineering, Tokyo*, pp 306–315
- Shibata T (1963) On the volume changes of normally consolidated clays. *Disaster Prevention Research Institute Annuals, Kyoto University, vol 6*, pp 128–134 (in Japanese)

# Index

## A

Acceleration response spectra, 153  
Acceleration time histories, 156  
Adaptation, 11, 13, 19  
Adobe, xii  
Advanced modeling systems, 57  
Aerial images, 199  
Aesthetic, ix  
Agglomeration, 39  
Alternative fuels, x  
Angkor, 90  
Anisotropically consolidated clays, 240  
Aqueducts, 48  
Arias Intensity, 162  
Assembly method, 127  
Asset management, 53  
Attenuation relations, 137  
Australia plate, 134  
Average acceleration spectrum, 158

## B

Background seismicity, 135–136  
Basho, ix  
Bayon temple, 91  
Beauty of the world, vii  
Biological capacity, 3–4  
Bridge foundations, 211  
Bridge stability, 212  
Building blocks, xi  
Business interruption losses, 52  
Business as usual, 79

## C

Cam Clay, 231  
Carbon, 75  
Carbon benefit, 86  
Carbon emissions, 78, 85  
Carbon tax, 73  
Carbon value engineering, 81, 85

Case histories, 116

Casualties, 32  
CEEQUAL, 84  
Channel Tunnel Rail Link (CTRL), 60  
Climate Change Act, 78  
CO<sub>2</sub> emission, 60  
Coastal protection, 14, 17  
Coastal protection structures, 115  
Combined hazards, 15  
Combustion products, x  
Conditional probability of drift exceedance, 27  
Consequences of failure, 10  
Construction industry, 77  
Construction materials, 70  
Contractancy characteristics, 247  
Contractancy curves, 244  
Contractancy functions, 244  
Contractancy models, 237, 241, 247  
Copenhagen Accord, 76  
Cost-benefit analyses, 79  
Creep, 224  
Critical linkages, 29  
Critical rainfalls, 171, 183, 190  
Critical state, 232  
Cumulative risk, 27

## D

DACSAR, 240  
Damages of highway bridges, 195  
Debris flows, 178, 184, 187, 197  
Debris tanks, 189  
Decision making, 72  
Demolition, xiii  
Depth of the engineering bedrock, 155  
Design charts, 16  
Design life, 82  
Dike construction, 119  
Disaster mitigation, 13  
Disasters, 57, 115

Dissipated energy, 231, 233  
 Diversion tunnel, 83  
 Dynamics, 5

## E

Earthquake catalogs, 135  
 Earthquake characteristics, 156  
 Earthquake hazard, 153–154  
 Earthquakes, 46–47  
 Ecological footprints, 3, 43  
 Economic activity, 54  
 Economic independence, xi  
 Elastic limit, 232  
*Elastic state*, 238  
*Elasto-plastic state*, 238  
 Embankment, 63  
 Embodied energy, 60  
 Embodied Energy Intensity (EEI), 64  
 Emergency response, 22  
 Empirical procedure, 158  
 Energy efficiency, 67  
 Energy infrastructure, 81  
 Energy resource depletion, 60  
 Environment, 43  
 Environmental impacts, 60  
 Equivalent intensity factor, 25  
 Equivalent shear wave velocity, 152  
 Evaporation, 108  
 Excavation, 101  
 Exponential contractancy model, 241, 243  
 Exposure, 46  
 Extended Sekiguchi-Ohta models, 246–247  
 External loading, 211  
 Extreme events, 7  
 Extreme natural hazards, 191

## F

Failure modes, 13  
 Feature frequencies, 208  
 Fire following earthquake, 50  
 Flooding, 82  
 Footprint, 76  
 Fragility curve, 8  
 Freefall, 220  
 Frequency dependent characteristics, 157  
 Fuel consumption, 65  
 Functional units, 29  
 Future of the earth, ix

## G

Geographical Information Systems (GIS),  
 145, 196  
 Geo-hydraulic characteristics, 112  
 Geomats, 119

Geotextile Mat, 117  
 Glass-crete, xiii  
 Global climate change, 212  
 Global influence, 41  
 Global warming, x, 59  
 Ground deformation, 216  
 Ground motion suites, 24  
 Ground response analysis, 139  
 Ground shaking intensity, 152  
 Ground shaking microzonation, 162  
 Grouted geotextile mattress, 121

## H

Hazard curve, 8  
 Hazard maps, 131  
 Hazards, 38  
 Health Monitoring, 205  
 Highway bridge failures, 192  
 Horizontal expansion, 101  
 Horizontal flow, 108  
 Human exploitation, ix  
 Human-powered, xi  
 Hydraulic characteristics, 112

## I

Incremental dynamic analysis, 26  
 Industrial revolution, x  
 Industry transformation, 87  
 Infrastructure, 37, 79  
 Infrastructure damages, 192  
 Infrastructure networks, 29  
 Infrastructure Planning Commission (IPC), 86  
 Initial yield surface, 236  
 Innovation cycle, 77, 87  
 Installation energy, 64  
 Intelligent safety monitoring system, 193  
 Inter-agency coordination, 53  
 Interdependent, 44  
 Interdependent systems, 56  
 Internal energy, 233

## J

John Muir, ix  
 Justice, x

## L

Landslides, 169, 175  
 Laterite, 93  
 Leading technology users, 77  
 Life-cycle cost, 9  
 Lifeline systems, 43  
 Lifestyle, 75  
 Limits to Growth, 2–3  
 Liquefaction, 141  
 Local economies, xi

Logarithmic contractancy model, 241, 243  
 Los Angeles, 44  
 Loss of functionality, 30  
 Low carbon construction industry, 85  
 Low carbon economy, 79–80

## M

Manufacturing energy, 64  
 Material energy, 64  
 Megacities, 37  
 Mega-system, 43  
 Micro-gravity environment, 219  
 Microzonation, 139, 152, 175  
 Milky Way, viii  
 Mitigation alternatives, 53  
 Mitigation measure, 227  
 Modified Cam Clay, 231  
 Moral, ix  
 Mud bricks, xii  
 Multi-system integration, 44  
 Municipalities, 45

## N

Natural disasters, xi, 7, 22  
 Natural fibres, xiii  
 Negative dilatancy (or contractancy), 231  
 Negative spiraling sequence, 7  
 Niigata Airport, 225  
 Non-structural items, 30

## O

Overarching target (summary), 80  
 Over-scale floods, 200

## P

Paint-crete, xiii  
 $P'$ -constant drained shear, 231  
 Peak spectral accelerations, 162  
 Performance, 13–14, 19  
 Performance based design, 33  
 Performance-based engineering, 23  
 Performance requirements, 28  
 PGA, 162  
 PGV, 162  
 Pile-slab, 61  
 Pitfall, 97, 113  
 Political drivers, 78  
 Population, 1, 39  
 Positive spiral, 7  
 Post-disaster decisions, 23  
 Post-disaster simulator, 36  
 Post-earthquake functionality, 31  
 Post-earthquake situation, 22  
 Poverty, xii

Practical, ix  
 Prasat Suor Prat (Tower of Rope Dancer), 93  
 Prefabricated caisson, 122  
 Prevention of scour, 125  
 Probabilistic hazard, 147  
 Prudence, x  
 Pumping station, 106

## Q

Quality of life, 75

## R

Rainfall, 170  
 Rainfall intensity, 183  
 Rammed earth, xiii  
 Rate dependency, 217  
 Raw materials, 69  
 Recover, 54  
 Recycle, xii  
 Regional economy, 52  
 Regional sustainability, 5  
 Reinforced adobe, xiii  
 Remote sensing techniques, 5  
 Resilient, 38  
 Response spectrum, 206  
 Retrofit, 33  
 Retrofit methods, 23  
 Risk analysis, 204  
 Risk assessment, 11  
 Risk management, 22  
 Risks, 46  
 Robustness, 18  
 Rubber dams, 118

## S

Safety monitoring and warning, 205  
 San Andreas Fault, 47  
 Scour, 203, 207  
 Scouring, 191  
 Seismic microzonation, 139  
 Seismic performance, 215  
 Seismic risk, 33  
 Sekiguchi-Ohta models, 241  
 Service, 19  
 Serviceability, 212  
 Sewers, 83  
 ShakeOut Scenario, 47  
 Shared humanity, xi  
 Shear wave velocity, 155  
 Shibata's coefficient D, 240  
 Shi-Tzou Bridge, 207  
 Siem Reap, 111  
 Simulation, 49  
 Site response analyses, 131, 152

Site-specific, 13  
 Slope instability, 183  
 Slopes, 173  
 Slope stabilization, 189  
 Smart infrastructure, 55  
 Socio-economic impacts, 53  
 Soil-structure system, 13  
 Spectral acceleration, 133  
 Spectral hazard maps, 131  
 Spoil, 69  
 Stabilization works, 187, 190  
 State boundary surface, 232  
 Stream bed, 183  
 Streams, 175  
 Structural behavior, 211  
 Subduction zones, 134  
 Suction caisson, 126  
 Sumatran fault, 134  
 Sumatran fault zone, 135  
 Sustainability, x, 22  
 Sustainable, 38  
 Sustainable development, xi, 2  
 Swelling wall, 232  
 Systems, 38  
 System serviceability, 49

**T**

Technological innovation, 2  
 Thames Barrier, 82  
 Threshold limit, 11  
 Time to stabilization, 33  
 Tolerable drift, 27  
 Transformation in performance, 87  
 Transportation energy, 64  
 Transportation units, 29  
 Transport fuels, x  
 Travel time, 32

Trenched section, 97, 112  
 Tsunami, 17  
 Tsunami hazard, 133, 143  
 Tsunami hazard assessment, 147  
 Tsunami inundation, 144  
 Tsunamis, 141  
 Tunnel, 61  
 Typhoon Morakot, 191

**U**

Uncertainties, 8, 12  
 Undeveloped, xii  
 Unreinforced adobe, xii  
 Urbanization, 39  
 Urban sprawl, 41

**V**

Vibration characteristics, 206  
 Vibration tests, 207  
 View of the earth from near space, viii  
 Viscous model, 216  
 Vulnerability, 7, 17–18, 46

**W**

Warning systems, 212  
 Water balance, 101  
 Water levels, 101  
 Water resources, 101  
 Water supply, 45  
 Water system restorations, 51  
 Water systems, 46  
 Wordsworth, ix

**Y**

Yield locus, 232  
 Yodo River Levee, 216